Annual Report

2007

7

40th

ANNIVERSARY - 1967/2007

Institut Laue-Langevin

ill

NEUTRONS
FOR SCIENCE

The Institut Laue-Langevin

NEUTRONS FOR SCIENCE

The Institut Laue-Langevin (ILL) is an international research centre where neutrons are used to probe the microscopic structure and dynamics of a broad range of materials from the molecular, atomic and nuclear point of view. The ILL is owned and operated by three founding countries - France, Germany and the United Kingdom.

The three Associate countries contributed a total of 58 M€ to the Institute in 2007, a sum enhanced by significant contributions from the ILL's Scientific Member countries, Austria, Belgium, the Czech Republic, Hungary, Italy, Poland, Spain, Sweden and Switzerland. ILL's overall budget in 2007 amounted to approximately 75 M€.

The ILL was founded to provide scientific communities in its member countries with a unique flux of slow neutrons and a matching suite of experimental facilities (some 40 instruments) for use in fields as varied as solid-state physics, materials science, chemistry, the biosciences and the earth sciences as well as nuclear physics and engineering.

… an exceptional centre of excellence and a fine example of successful co-operation in Europe

The Institute has ever since been an exceptional centre of excellence and a fine example of successful co-operation in Europe, a prototype of the European Research Area. It operates the most intense neutron source in the world. About 2000 visiting scientists, performing a total of 750 experiments each year and the output in high impact journals, bear witness to the scientific success of the facility.

High intense neutron source

Multidisciplinary science

International user community

Leading instruments

Technical innovations

Research partnerships and networks

Training future scientists

Contents

NEUTRONS
FOR SCIENCE

Director's foreword

2007 was indeed a remarkable year for the ILL. It started off in style with the Institute's 40th Anniversary celebrations, attended by over 500 external guests and former staff members, including a number of directors and heads of division from the Institute's past. The ceremony graced by brilliant piano performances of Rachmaninov, Chopin and Ginastera – was a splendid tribute to the success the ILL has achieved over the years and the quality of its present endeavours and ambitions for the future.

As part of these anniversary celebrations many of our staff members and their families will have fond memories of the ILL Open Day in June. This cheerful event held under clear blue skies was organised for our staff members as a token of our appreciation for their levels of motivation, creativity and ingenuity, and for the excellent services they have consistently provided to ILL's broad user community.

The projects under the first phase of the Millennium Programme – Phase M0 – are progressing very well and are due to be completed by the end of 2008. The upgrade of 5 instruments and the commissioning of 6 new instruments and related infrastructure has already boosted the average efficiency of ILL's instrument suite by a factor of more than 14. This is double the target aimed at when the Millennium Programme was launched back in 2000! It is particularly rewarding for the Institute's nine Scientific Member countries, who together contribute some 18% of the ILL's budget and are therefore now well set to harvest considerably more science for every euro invested. Our Scientific Members contribute not only to the ILL's budget but also, and most significantly, to the Institute's scientific life and output. In 2007 at least two of the events held at the ILL, the Italian Society of Neutron Spectroscopy's *4th Neutron school* and the joint Belgian-ILL workshop on *nuclear physics under extreme conditions: Exotic Nuclei and Nuclear Astrophysics*, very successfully illustrated this. I am also delighted to recall in this context the ceremony held later in the year in Madrid, to commemorate the 20th anniversary of the most fruitful scientific cooperation between the ILL and Spain, ILL's very first Scientific Member.

In July 2007, after comprehensive discussions with our Scientific Council and final approval by ILL's Steering Committee, Phase M1 of the Millennium Programme was officially kicked off. Nine instruments, together with the neutron infrastructure and sample environments they require, are on the drawing board for construction or upgrade. A 52 million € budget has been allocated and a 2007-2013 timeline. Seven of the existing instruments no longer at the height of their art will be decommissioned. The Millennium Programme's second phase will help secure the ILL's place at the forefront of neutron science well beyond the next decade; it will also have a significant impact on the quality of research infrastructure in Europe. In October 2007 Brussels awarded the ILL a European grant of 4.7 million € for the programme, which has been given an important place on the ESFRI Roadmap. This was indeed good news!

' The Millennium Programme's second phase will help secure the ILL's place at the forefront of neutron science well beyond the next decade '

In 2007 the Seismic Refit Programme was officially signed off by the French nuclear safety authorities. This marked the end of almost six years of intensive renovation that placed a heavy burden on both staff and users. Our neutron facilities and the neighbouring environment and population are therefore better protected today than they ever

have been from the very low-probability, but nevertheless serious, possibility of a seismic event. I want to pay a tribute to all our staff members who have contributed admirably to meet this tremendous challenge!

Under the Refit Programme the non-destructive examination of several key reactor components confirmed the complete integrity of the reactor system after 35 years of operation. This provided further evidence that from a technical viewpoint the operating horizon of our neutron source extends well beyond the year 2030. The ILL Steering Committee received the news of such great perspectives with real satisfaction.
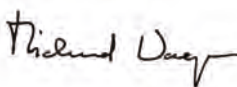
Curiosity, we know, comes bundled in the genes of our children. ILL's continuing outreach activities are helping science teachers in Europe to build on this inherent potential, encouraging children to develop their interest in science as they grow up. The ILL and the ESRF organized *Science on Stage* in 2007 with sponsorship from the seven members of the EIROforum and the EU. The festival was quite an attraction, drawing over 500 science teachers from 29 countries to Grenoble for an exchange of innovative and successful teaching methods and materials. ILL was honoured on this occasion by the visit to the Institute of the European Commissioner for Science and Research, Mr Janez Potočnik.

' the ILL's fortieth birthday … a major milestone on the road to an equally splendid future '

2007 was also a year of change for ILL's management team. Christian Vettier left his post as French Director and Head of the Science Division. His place has been taken by Dr José Luis Martínez Peña from Spain. José Luis took over the Projects & Techniques Division from Andrew Harrison, who is now leading the Science Division. Christian Vettier's eight years of service at the Institute made him the ILL's longest-serving director. He has indeed left his mark. Together with his fellow directors he was not only a significant force in the shaping of the Millennium Programme but also successfully promoted the creation of support laboratories and thriving scientific partnerships on the ILL-ESRF-EMBL campus. Christian put a great deal of effort into our relations with the local and regional authorities, successfully attracting external funding for the development of our site. It was just after his departure that we were informed that his tremendous endeavours are finally paying off: we were very grateful to hear that the new *CPER*, the regional development plan signed by Rhône-Alpes and the French State, includes a 15 million € award to help us transform our site over the next 6 years into a recognised centre of scientific excellence for European scientists.

Given the good news and achievements of 2007 the ILL's fortieth birthday was clearly more than an occasion to look back on a most successful past; it should also be seen as a major milestone on the road to an equally splendid future.

Richard Wagner
Director of the ILL

Why neutrons

Neutron beams have the power, when used as a probe of small samples of materials, to reveal what is invisible using other radiations. Neutrons can appear to behave either as particles or as waves or as microscopic magnetic dipoles and it is these specific properties which enable them to uncover information which is often impossible to access using other techniques.

• Electrically Neutral

Neutrons are non-destructive and can penetrate deep into matter making them an ideal probe for e.g. biological materials and samples under extreme conditions of pressure, temperature, magnetic field or within chemical reaction vessels.

• Microscopically Magnetic

They possess a magnetic dipole moment which makes them sensitive to magnetic fields generated by unpaired electrons in materials. Precise details of the magnetic behaviour of materials at the atomic level can be investigated. In addition, the scattering power of a neutron by an atomic nucleus depends on the orientation of the spin of both the neutron and the atomic nuclei in a sample thereby providing a powerful tool to detect the nuclear spin order.

• Wavelengths of Ångstroms

Their wavelengths range from 0.1 Å (10^{-2} nm) to 1000 Å making them an ideal probe of atomic and molecular structures ranging from those consisting of single atomic species to complex biopolymers.

• Energies of millielectronvolts

Their energies are of the same magnitude as the diffusive motions of atoms and molecules in solids and liquids, the coherent waves in single crystals (phonons and magnons) and the vibrational modes in molecules. An energy exchange between the incoming neutron and the sample of between 1 μeV (even 1 neV with spin-echo) and 1eV can readily be detected.

• Randomly sensitive

The variation of scattering power from nucleus to nucleus in a sample varies in a quasi-random manner even in different isotopes of the same atom. This means that light atoms are visible in the presence of heavy atoms and atoms neighbouring in the periodic table may be distinguished from each other. In addition, isotopic substitution (for example D for H, or one nickel isotope for another) can allow contrast to be varied in certain samples thereby highlighting specific structural features. The neutron is particularly sensitive to hydrogen atoms and therefore is a powerful probe of hydrogen storage materials, organic molecular materials, and biomolecular samples or polymers.

What is the ILL ?

Formally, ILL is a non profit-making French company under civil law, which is governed by an International Convention signed at Foreign Ministry level by three countries - France, Germany and the United Kingdom. Our Associates - the CNRS and the CEA representing France, the FZ Jülich representing Germany and the STFC representing the United Kingdom - own and administer the Institute. They are also responsible for all liabilities and eventual decommissioning costs.

Although the ILL is an international organisation, its staff are not paid tax-free salaries, but instead they are enveloped within the French tax, employment and social security systems, which has marked advantages but also marked disadvantages from whichever point of view you look at it. The Institute is answerable to French legal bodies and to French security authorities. We exist and operate within the French Labour law (Code du Travail). Our staff representative bodies, as laid down by French law, are a significant presence in the ILL's daily life. We have strong links to the Mairie of Grenoble and surrounding communities, to the Préfecture of the Isère and to the Council of the Rhône-Alpes Region.

Whilst our Associates own the facility and contribute the largest amount to the almost 74 M€ annual operating costs, the ILL also benefits from the scientific partnerships of nine other nations - Austria, Belgium, the Czech Republic, Hungary, Italy, Poland, Spain, Sweden and Switzerland – who together contribute about 17% of the operational and investment costs of the Institute. All nine partner countries in addition can and do contribute to capital projects at the Institute, within the Institute's priorities but according to their own priorities also.

Our governing body is the Steering Committee, which meets twice-yearly and is made up of representatives of the Associates and the Scientific Partners together with Directors and Staff Representatives. Within the framework of the International Convention, the Steering Committee has the ultimate responsibility for determining operational and investment strategies for the Institute.

The Institute has a Director and two Associate Directors, representing each of the Associate countries, appointed on short-term contracts normally of five years. The Director's role is generally taken alternately by the German and British appointee. The two Associate Directors are responsible for the Science Division and the Projects and Techniques Division respectively. The Head of the Administration Division is also appointed on a short-term contract, whereas the Head of the Reactor Division is a permanent ILL employee. These five people together constitute the Management Board of the Institute and are responsible for its day-to-day operation.

The scientific life of the Institute is guided by the Directors, with input from the ILL's ten scientific colleges. A Scientific Council, comprising external scientists from the member countries, advises the Directors on scientific directions for the Institute, on the evolution of the instrument suite and technical infrastructure to best meet the needs of the user research programme, and to assess the scientific output of the Institute. It is helped in this process by the Instrument Sub-Committee and by the Chairmen of the nine Scientific Sub-Committees who twice-yearly peer review the experiment proposals.

The ILL is composed of four Divisions, each with its distinct role and, it is true to say, its own culture.

The Science Division staffs the instruments and delivers the science; the Projects and Techniques Division designs and builds new instruments, develops new concepts and maintains beamlines and instruments operational; the Reactor Division delivers the neutrons, operates and mans the reactor 24 hours during 4 cycles of 50 days each per year and has responsibility for all aspects of security; the Administration Division deals with Personnel matters with particular responsibility for interactions with staff representative bodies, with Purchasing, with Finance and with Site and Building maintenance; and the Director's Services deal with Radiological safety, with conventional safety, with Health and Working Practices and with Public Relations.

The ILL's neutron source is the finest in the world, being based on a single element 58.3 MW nuclear reactor designed for high brightness. The main moderator is the ambient D_2O coolant surrounding the core which delivers intense beams of thermal neutrons to 11 beamlines and to four neutron guides. A graphite hot source operating at 2400 K delivers hot neutrons – energies up to 1 eV and wavelengths down to 0.3 Å – to 3 beamlines. A renewal project has resulted in the installation of a new hot source and beam tubes during 2003. Two liquid deuterium cold sources at 25 K deliver cold neutrons – energies down to 200 μeV and wavelengths up to 20 Å – to some 17 instruments. An ultra-cold neutron source fed from the top of one of the cold sources delivers neutrons vertically through the reactor pool to 5 instruments on the operational floor of the reactor.

In all there are more than 50 measuring stations, 27 of which have full public access. In addition, the ILL provides a framework in which Collaborative Research Groups (CRGs) can build and manage instruments to carry out their own research programmes. There are at present ten CRGs at the ILL.

The ILL's neutron source is the finest in the world, being based on a single element 58.3 MW nuclear reactor designed for high brightness

Our community of users is world-wide with scientists from non-partner nations also having a chance to apply for beamtime with outstanding research proposals. This broader community of users enriches the scientific life of the Institute.

In 2000, the ILL launched an ambitious modernisation programme of instruments and infrastructure called the ILL Millennium Programme (Phase M0: 2000-2008; Phase M1: 2007-2013) whose aim is to optimise the ILL's instrument suite, and thereby maintaining the Institute's world-leading position for another 20 years.

The ILL monitors the papers published as a result of the use of our facilities. This gives a figure of more than 500 papers per year. With a total annual budget of 74 M€, the cost per published paper is less than 150 k€. We pay particular attention to papers published in high impact journals. About 80 such papers per year are published from data taken on ILL instruments which, interestingly, is equivalent to the output of ESRF, and a factor of two higher than the second most productive neutron source in the world.

Beam days delivered for science during four reactor cycles amount to 5505 in 2007. The cost per beam day of science therefore stands at a very cost effective 13.4 k€ per day.

Scientific highlights

Magnetism
Chemistry and crystallography
Materials
Soft matter
Liquids and glasses
Biology
Nuclear and particle physics
Spectroscopy, modelling and theory

Throughout its 40 years of existence the Institut Laue-Langevin has continuously strived to provide the best facilities for neutron science in the world. That tradition is being carried forward through the Millennium Programme, whose benefits are all already apparent, as illustrated by several of the scientific highlights that follow. However, the scope of the science we aim to serve changes too. One need only to consider the subjects of a couple of the scientific talks at our 40th Anniversary celebrations in January 2007 - high-temperature superconductivity, and the structure of membranes - to see how the applications of neutrons have evolved. Although high-T_c materials were far from conception in 1967, the use of neutrons to probe their magnetic correlations would have been regarded as core business; however, the study of soft condensed matter by neutrons was in its infancy. One of our challenges therefore is to anticipate or stimulate such growth, and to this end the ILL has also invested in interface laboratories, and thought hard about new methods of access that might suit a different type of user better.

Among the interface laboratories, our pioneering deuteration facility - the D-Lab, a key component of the Partnership for Structural Biology - has been so successful that it is being copied worldwide and it is now implicated in about 40% of experiments at ILL on biological systems. FaME38, the facility to aid engineering experiments at ILL and ESRF, as well as the C-Lab, which provides a broad range of computational support, both underpin an increasing number of measurements. Our next venture of this sort is the Partnership for Soft Condensed Matter, for which the first step has been to appoint Giovanna Fragneto as an ILL Senior Fellow to set it up in partnership with ESRF.

Access to ILL facilities has also changed: the Block Allocation Group system of organising small-angle experiments in biology has led to collaborations with new user groups, and it has greatly increased the efficiency of use of beamtime and we intend to expand its scope. We will also explore ways to encourage users to bring development projects and new investment to ILL through allocations of small but extended periods of beamtime - provided, of course, that the outcome is valuable and freely available to the wider user community.

the ILL has also invested in interface laboratories, and thought hard about new methods of access

Last, but by no means least, tribute should be paid to Christian Vettier, who for the past eight years has driven many of the innovations that will support new science at ILL. In his report last year he presented a vision of a science campus on the site we share with ESRF and EMBL, and his work to secure substantial funding to take us closer to that vision has paid off as we anticipate significant funding from the Rhône-Alpes region and the city of Grenoble in 2008.
We look forward to an exciting future in which the science conducted at ILL continues to evolve and grow yet stronger.
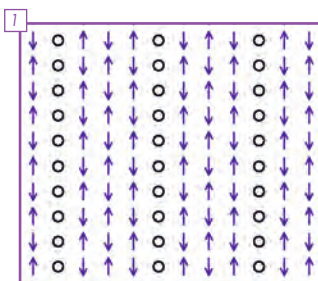
Andrew Harrison
Associate Director

Magnetism

Once again, in 2007, about a third of the experiments carried out at the ILL were related to magnetism. The magnetism community has produced several outstanding highlights in 2007, 5 of which are presented in this Annual Report.

We have seen a renewed interest in molecular magnetism, as shown in the study of Cr_7Ni rings (Guidi et al.). Such systems could give rise to great technological advances in quantum computing. This particular experiment takes us a step further in understanding how a potential component of such a device works.

The many aspects of superconductivity are still actively studied, as shown in several highlights by Boothroyd et al. (magnetic structure in $La_{2-x}Sr_xCuO_4$, using polarised neutron diffraction), Hinkov et al. (excitations in $YBa_2Cu_3O_{6.6}$, using three-axis spectroscopy), or Eskilden et al. (vortices in $TmNi_2B_2C$, using small-angle scattering).
The electronic phase in the vicinity of the anomalous 1/8 doping state of the cuprates $La_{2-x}Sr_xCuO_4$ has been probed on IN20 with polarisation analysis. The results show that the superconducting state coexists either with one-dimensional stripe correlations or, possibly, with an intriguing two-dimensional electronic phase with non-collinear spin correlations.
Further understanding of the high T_c state comes from a spectroscopic study on the archetypal high T_c superconductor $YBa_2Cu_3O_{6.6}$ in which there are indications for the existence of an extra phase competing with the superconducting state.
In addition to diffraction and spectroscopy, small-angle neutron scattering is increasingly important in the elucidation of nano-scale order such as vortex lattices created via the antagonistic interplay between superconductivity and magnetism. In $TmNi_2B_2C$, the conduction electron paramagnetic moments, induced by the exchange interaction, are shown to accumulate exclusively around the vortex cores, creating nanotubes of magnetisation associated with Tm and maintaining the field distribution contrast of the vortex lattice.

Continued efforts towards the understanding of quantum criticality in exotic materials have been made through a study of $Sr_3Ru_2O_7$ (Ramos et al.). Using the *FlatCone* option on IN14 it was possible to characterise the spin fluctuations around the quantum critical region of $Sr_3Ru_2O_7$ over a large area of reciprocal space. Further investigations revealed incommensurate fluctuations, indicating a most unusual second quantum criticality in addition to a quantum critical metamagnetic state.

These latter measurements were made feasible through the implementation of the multiplexed secondary spectrometer *FlatCone*, on IN14, allowing much faster mapping of the Brillouin zone. Significant improvements to instrument performance have also been seen on the diffuse scattering spectrometer D7, whose upgrade has led to an increase in detected flux by a factor of 80.

These highlights reflect the great diversity of subjects within the magnetic community and show the necessity for continuous improvements to the instruments. In the coming years we shall see upgrades on IN4 and IN5 and the development of new instruments such as WASP, THALES and D33. These will greatly enhance our suite of instruments to study magnetism.

Anne Stunault, College 5B Secretary
http://www.ill.eu/college5B/
Pascale Deen, College 4 Secretary
http://www.ill.eu/college4/

Chemistry and crystallography
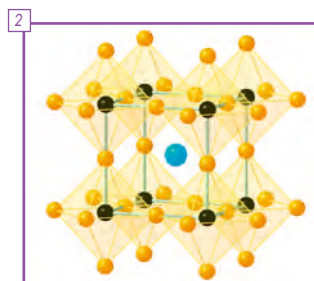
Once again, the activities of College 5A covered very diverse aspects of the science underpinning the atomic structure of materials. One trend observed in the proposal committee is an increasing interest in high pressure, especially above 3GPa. We anticipate exciting results from these experiments in the very near future. In the meantime, the three highlights chosen below show the breadth of research done with the assistance of the ILL and whose success is due to combining modern neutron diffraction methods with other experimental techniques, as well as modelling.

The study of materials with unusual or useful properties – for example high ion mobility – continues to be particularly active and centred around transition metal oxides. A good example of such work is provided by Y. Tsujimoto et al. who have used complementary synchrotron X-ray and neutron measurements to show that a mixed-metal oxide containing iron and strontium is isostructural with the 'infinite layer' cupric oxides. The complete structure is composed of sheets which order antiferromagnetically at low temperature. This first observation of such square-planar coordination around Fe^{2+} was possible thanks to the new opportunities offered by low-temperature solid-state chemical reactions and the recently discovered use of calcium hydride as a reducing agent. By contrast with classical liquid and/or high-temperature reactions, this method allows controlled removal of oxygen from oxides, while still preserving the initial atomic structure of the metal ions. This novel solid-state chemical path for transition metals offers very new possibilities to synthesise materials previously impossible to obtain by reaction in solution.

The understanding of the processes that occur in batteries is particularly topical at present with heightened interest in 'greener' methods of producing or storing energy. M. Casas-Cabanas et al. have made a significant contribution to this field by deciphering the structural transformations which take place during nickel oxyhydroxide electrode operation. Combining X-ray and neutron powder diffraction and high resolution transmission electron microscopy, it was shown that the positive electrode material β-NiOOH, used in the nickel-based batteries, undergoes reversible structural transformations during oxidation and reduction processes. The simultaneous consideration of structural and microstructural models in the Rietveld refinement was decisive in interpreting the poor diffraction patterns and in understanding how proton insertion/extraction affects the structure at the atomic level during the reduction/oxidation processes.

Molecular switching is a very important topic, with much recent interest in photo-control of electronic multistability. In this field, Goujon et al have investigated the light-induced spin transition in a model organometallic complex, $[Fe(ptz)_6][BF_4]_2$, for which the spin crossover takes place between a diamagnetic low-spin state at low temperature and a paramagnetic high-spin one, stabilised at high temperature by entropy effects. The instrument VIVALDI is particularly well adapted for such a kinetic investigation on a single crystal, allowing fast acquisition of Laue patterns as a function of light exposure time. After the determination at 2K of the different possible structures (ground state, quenched low-spin phase, and photo-excited high-spin phase), they have shown that the kinetic structural changes from one phase to another were continuous, without any phase separation, despite the cooperative character of the spin-crossover system.

Marie-Hélène Lemée-Cailleau, College 5A Secretary
http://www.ill.eu/college5a/

NEUTRONS FOR SCIENCE
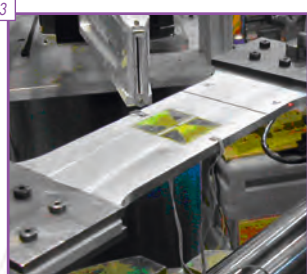
Materials

The ILL provides an extensive set of tools to study material science, especially metallurgy, strain/texture measurements as well as smart materials, ceramics and polymers related to industrial applications, and archaeology. The instruments at ILL involved in such work include mainly the strain scanner SALSA, the diffractometers D1B and D20, and the small-angle spectrometers D11 and D22. Complementary techniques such as microstructural characterisation, sample metrology, sample positioning and alignment (including the SALSA hexapod), and up to 50 kN test rigs are available at the joint ILL/ESRF FaME38 facility. In addition, the chemistry laboratory provides furnaces, optical microscopes, UV/VIS and IR spectrometers, and DSC equipment to facilitate experimental work in this field further.

Understanding and improving welding techniques is essential for industry to optimise the production and life-cycle of engineering components. This is especially important for the aerospace and automotive industry which require structures to withstand extreme fatigue and stress. The SALSA strain scanning diffractometer is dedicated to mapping the stress inside materials, especially around welds and machined areas. These measurements are then used to validate simulation models. Liljedah *et al.* present a typical experiment with in situ fatigue loading of large aluminium welded structures for the aerospace industry, which can be achieved within a week.

Shape memory alloys are smart materials used, for example, in medicine, robotics and the aerospace industry. Feuchtwanger *et al.* have measured the behaviour of ferromagnetic shape memory alloy/polymer composites under load. In these materials, the motion of twinning boundaries during pseudo-plastic deformation can dissipate large amounts of mechanical energy by internal friction. This type of material can then be used in very efficient, light-weight dampers. Last but not least of the three highlights, Seydel *et al.* have recorded *in situ* structural and dynamical changes of silkworm silk when applying a tensile force. They have shown that most of the deformation of the silk fibres takes place in the amorphous regions of the material. Moreover, no change is observed in the molecular vibrational or reorientational response, in agreement with a rubber entropy elasticity model.

Emmanuel Farhi, College 1 Secretary
http://www.ill.eu/college1/

Soft matter

2007 was a very promising year for soft condensed matter research at ILL. The strong commitment to this field was underlined by the appointment of Giovanna Fragneto as ILL Senior Fellow for soft condensed matter. A key role for her in this new post will be to promote the founding of the Partnership for Soft Condensed Matter on the ILL/ESRF site. Additionally, she will oversee the extension of the existing sample preparation and characterisation laboratories, as well as installing new rheometry, calorimetry, and light scattering instruments to aid sample characterization before and during ILL experiments. The Scientific Council also supported our community by giving highest priority to upgrading and developing sample environments specifically used for soft matter and biological studies.

The Millennium programme will provide several new, or upgraded instruments for the soft condensed matter user community. At the time of writing the D11 small-angle scattering instrument is being upgraded from its guide all the way through to a larger area detector. The new FIGARO liquid surface reflectometer's installation has also just started. Further, the Scientific Council has approved the selection of new instruments which will be built by 2013. Among them several are of great interest to soft matter scientists: the new IN16B back-scattering spectrometer which will succeed IN16; WASP, the new wide-angle spin-echo instrument, will be the successor of IN11; and finally a third small-angle machine D33 will be built, reducing the high demand for the existing SANS machines.

Despite the high demand for dynamic studies, the highlights in this Annual Report are all results from small-angle scattering measurements. These reports explore three different ways of inducing structural changes in materials - namely they utilise pressure changes, illumination with light and finally mechanical shear to impose order on soft matter. The size of the molecules studied ranges from the very small and chemically simple carbon dioxide via gelatin and short chain surfactants to the long chain block co-polymers. All three demonstrate that innovative sample environments are as important as improvements to neutron flux to study the kinetics of soft matter.
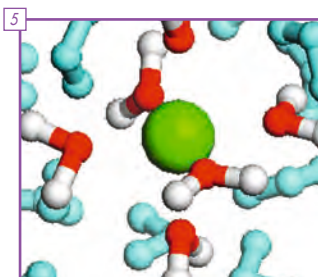
Péter Falus, College 9 Secretary
http://www.ill.eu/college9/

3

Liquids and glasses

Disordered systems have been the subject of intense study with neutrons over the years. Dealing with these complex systems, generally requires a wide variety of experimental techniques and computer simulations. Although the majority of proposals submitted to College 6 are in the research area of molecular liquids and glasses, an increasing interest has been observed,

during the last few years, in the study of confinement of liquids and polymeric glasses, quantum liquids, ionic liquids and liquid alloys, covering structural and dynamical studies. On the other hand the new perspectives on sample environment offered at the ILL open the possibility of experiments carried out under extreme conditions. The three highlights selected this year illustrate the diversity of topics explored in College 6.

The first highlight is the experiment carried out by S. Klotz et al. to measure the density of states of ice under pressure on the time-of-flight spectrometer IN6. This experiment was made feasible thanks to the new Paris-Edinburgh pressure cell that can reach pressures of up to 10 GPa in the temperature range 3.5-300°K. The purpose was to study the microscopic mechanisms that cause the melt of ice at high pressure and their relation to the transition to an amorphous state under pressure.

The second highlight is an example of the new approach to the analysis of the measured dynamic structure factor $S(Q,\omega)$ on the liquid deuteromethane (CD_4) measured on the thermal three-axis spectrometer IN3 by E. Guarini et al. The results of this study have shown that the combination of inelastic neutron scattering and molecular dynamics simulations provide a new method to discern the dimer geometry that is favoured in the dynamical behaviour of a molecular liquid.

The last highlight belongs to an area that is of growing interest - the Environmental Sciences. In particular the work of G. Cuello et al. is focused on the study of the hydration of divalent mercury in aqueous solution. This work is particularly significant because mercury is one of the most hazardous pollutants and water is the main medium for Hg^{2+} transport and interaction with biological objects. The water coordination of Hg^{2+} was studied by using the diffractometer for liquids D4C in order to understand the behaviour of this ion in natural systems.

Monica Jimenez, College 6 Secretary
http://www.ill.eu/college6/

Biology

These are exciting times for biological activity at the ILL, two years after moving the Deuteration Laboratory into dedicated new premises, the Carl-Ivar Brändén Building (CIBB)- where it became a platform in the Partnership for Structural Biology (PSB). The impact of the involvement of the ILL in the Centre for Integrated Structural Biology has been very positive, reflec-

ted in the increasing quality and enlarged scope of beamtime proposals.
In this context, initiatives such as the new Small-Angle Scattering (SAS) platform are only natural. This PSB platform includes the small-angle X-ray facilities of the ESRF (ID2) and the small-angle neutron facilities of the ILL (D11 and D22). It involves bringing together instrumentation, software and expertise for a more efficient use of the facilities. The combination of the SAS platform with the Block Allocation Group (BAG) proposal system, put in place last spring, will no doubt provide increased scheduling flexibility. The BAG system has been a success and it has now expanded into five types of proposal groups: solvent interactions, structure of membrane proteins, protein complexes, medical group and deuteration.

The College 8 scientific activities are also benefiting from the impressive improvements at the high resolution quasi-Laue diffractometer LADI-3; this instrument was installed at the LADI-1 position, at the end of the cold guide H142, and has now been commissioned. An increase in detector quantum efficiency of 25%, compared to LADI-1, translates into the possibility to use smaller crystals, with larger unit cells. More complex biological systems are now in the reach of high resolution neutron crystallography with reduced data collection times at the ILL.

As College 8 secretary I was also very pleased to witness the strengthening of the training programme for our biophysics Ph.D. students. The ILL lectures are now integrated into the doctoral programme of the Université Joseph Fourier (UJF) and included in the credit system. ILL biophysics students also have access to training in principles and techniques of structural biology organised by those working in the CIBB.

The biological highlights in this report are good examples of collaborative efforts where the careful design of the experiments was a key to successful results. The highlights both concern a scientific problem at the very core of biology: the need to understand the interactions between water and living organisms. Even the search for extraterrestrial life has been strategically focused on the essential equation that we have only begun to understand: Water = Life.
Is water really a pre-requisite for life? How does life adapt to extreme conditions? While our understanding of the interactions between water and living organisms at the molecular level remains poor, one thing is certain: neutrons are a unique probe into the function and dynamics of water in biological systems. The importance of the questions raised and the potential impact of the results determined my choice for two biological highlights where neutron scattering is used to study water in biological systems, at high salt concentration (Tehei et al.) and low temperature (Haertlein et al.) conditions.

Susana Teixeira, College 8 Secretary
http://www.ill.eu/college8/

Nuclear and particle physics

The 2007 vintage of NPP experiments and publications was characterised by the hunt for 'exotic' particles and the search for new worlds.

The first unexpected effects observed at LOHENGRIN were unfortunately not of a scientific nature, but related to the installation of a new high-voltage system to replace its 35 year old predecessor whose maintenance had become too demanding. After a prolonged commissioning phase that required numerous interventions on the high-voltage system, experiments were resumed with the observation of the decay of the most neutron-rich isomer beyond ^{132}Sn observed to date. Despite the extreme ratio of neutrons to protons in ^{136}Sb, its nuclear structure can be well described with established parameters of the nuclear shell model. This is in contradiction to theoretical predictions of a '*weakening of shells*' for very neutron-rich nuclei.

The PERKEO II experiment at PF1B studied the neutrino asymmetry parameter B in the free neutron decay. The result can be perfectly described by a pure exchange of *left-handed W bosons* as predicted by the standard model of particle physics and allows one to infer that a possible *right-handed W boson* is at least 310 times heavier than the neutron. So far, high-energy physics experiments at particle accelerators (e.g. CERN) have not been able to find this elusive particle that has been predicted by some theoreticians. Direct detection is very difficult since a right-handed particle would only interact very rarely with the left-handed particles that make up our world.

In our world *matter* (e.g. neutrinos) is *left-handed* while *antimatter* (e.g. antineutrinos) is *right-handed*. Due to the large excess of matter over antimatter our world is dominantly left-handed. Many particle physicists feel unsatisfied with a world that is purely left-handed without obvious reason. To restore the overall symmetry, a right-handed 'mirror world' has been predicted. Certain theorists even predicted that neutrons could oscillate quickly on a timescale of the order of seconds between our world and a mirror world with important consequences for particle physics and astrophysics. Two experiments at PF2 have now shown that neutrons do not disappear in measurable quantities from our world.
The situation of left- and right-handed elementary particles that show little mutual interaction can be illustrated using an elusive animal populating the mountains around Grenoble: The *dahu* (Le dahu, P.Leroy, Ed.Du Mont, 2000) - akin to the *wild haggis* (http://www.undiscoveredscotland.co.uk/usfeatures/haggis/wildhaggis.html) in the Scottish Highlands and the *Wolpertinger* (Wolpertinger und ihre Verwandschaft, H.J. Gregor, 1996) in the Bavarian Alps - is a goat-like species that has shorter legs on one side of its body than on the other. This enables it to walk upright on the steep slopes of its mountain environment. Two species exist: the *left-handed dahu* (which has shorter legs on the left side, and thus goes around the mountain counter-clockwise) and the *right-handed dahu* (which has shorter legs on the right side, and thus goes around the mountain clockwise), see figure. For obvious topological reasons these creatures seldom interbreed.

Finally, another experiment at PF2 demonstrated a wavelength-shifting effect when neutrons traverse accelerated matter. This effect is universal for all kinds of waves. For light the change is too small to be detected even by high-resolution laser spectroscopy, but now it has been observed for the first time with neutrons.

Ulli Köster, College 3 Secretary
http://www.ill.eu/college3/

Spectroscopy, modelling and theory
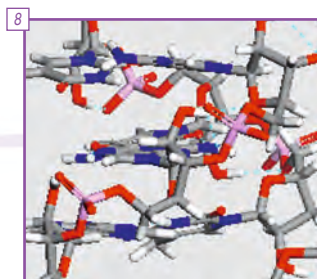
In this year's Annual Report, there are six contributions from spectroscopy, modelling and theory covering superconductivity and magnetism in 'hard matter' and biological systems and polymers in 'soft matter'.

Spectroscopy in 'soft matter' concerns the biological systems, DNA (Merzel *et al.*) and a membrane protein, bacteriorhodopsin (Wood *et al.*). In these cases, the experimental data are better understood with the aid of atomistic, energy-based simulations. Phonon calculations for DNA reveal enhanced opening of base-pair hydrogen atoms by vibrations with higher frequencies than previously thought. These dynamics underpin biophysical processes such as transcription, replication and melting. For bacteriorhodopsin, molecular dynamics simulations coupled with experiments on partially deuterated samples demonstrate the dynamical heterogeneity of the protein in its membrane. On a longer length scale, the physical properties of polymers, namely the formation of globules in core-shell structures in aqueous solution, have been investigated in the Theory Group using Monte Carlo calculations and analytical mean field methods (Yoshinga *et al.*).

In 'hard matter', first principles (density functional theory) calculations have been used to complement comprehensive experimental studies of a frustrated magnetic system (Simonet *et al.*). Frustration occurs for triangular configurations of anti-ferromagnetically coupled spins, here, on a short length-scale, within clusters of nine copper atoms and, on a longer length-scale, between clusters. Samples have a small amount of vanadium in the copper clusters and total energy calculations help to identify the most likely vanadium sites and characterise the magnetic interactions. Inelastic neutron scattering data is particularly helpful in understanding the magnetic states of the clusters containing vanadium. Again on a longer length-scale, a theoretical approach allows the effect of chemical doping in CMR manganite materials to be investigated (Bouzerar *et al.*). The model predicts that local disorder is not fully random and that spatial correlations tend to favour inhomogenous charge distributions and nano-scale magnetic structures. Finally, theoretical methods based on a cluster extension of dynamical mean field theory have been applied to the on-going debate concerning the mechanism of high-temperature superconductivity (Civelli *et al.*). These calculations predict the existence of two energy gaps in cuprate-based superconductors and their distinct behaviour as a function of chemical doping.

Stéphane Rols, College 7 Secretary
http://www.ill.eu/college7/
Marcello Civelli, College 2 Secretary
http://www.ill.eu/college2/
Mark Johnson, Leader of Computing for Science
http://www.ill.eu/computing/

Pauli paramagnetic effects on vortices in superconducting TmNi$_2$B$_2$C

3

For more than half a century the phenomenological Ginzburg-Landau theory, based on the concept of field-independent characteristic length scales, has provided a surprisingly good description of the mixed state in superconductors subjected to an applied magnetic field. However, in a system containing localised magnetic moments that are strongly coupled to the superfluid condensate, such a description is no longer adequate. We report on small-angle neutron scattering studies of the vortex lattice in TmNi$_2$B$_2$C, which show how the induced paramagnetic moments around the vortex cores act to maintain the field contrast probed by the neutrons.

When a superconductor is placed in a magnetic field, it is threaded by 'whirlpools' of electric current known as vortices, and which provide a unique probe into the nature of the host superconductor. We have used studies of the vortices to investigate the interplay between superconductivity and local magnetic moments, which is a fascinating problem with relevance to a number of important unresolved questions such as the detailed nature of high-T_c as well as heavy-fermion superconductivity.

The antiferromagnetic members of the intermetallic nickelborocarbide superconductors RNi$_2$B$_2$C (R = Ho, Er, or Tm), have proved especially rich vehicles for studies of the interplay between superconductivity and magnetism. In these materials, as well as other magnetic superconductors, the exchange interaction between the $4f$ localised moment and the conduction electron spin is important for understanding systematic changes of both superconducting and magnetic transition temperatures. Importantly, even in the paramagnetic state above the antiferromagnetic ordering temperature, T_N, the conduction electrons are subjected to an exchange field due to the field induced $4f$ moments. Here we report small-angle neutron scattering (SANS) studies of the vortex lattice (VL) in TmNi$_2$B$_2$C at several temperatures above T_N = 1.5 K, investigating specifically how the magnetic field profile around the vortices is influenced by the paramagnetic state.

At all fields and temperatures we observe a rhombic VL, as shown in the insets of **figure 1**.

Figure 1: *Measured internal magnetic field (B) versus applied field (μ_oH) at 1.6 K for TmNi$_2$B$_2$C (squares) and non-magnetic LuNi$_2$B$_2$C (circles). At 1.6 K the upper critical field for TmNi$_2$B$_2$C is ~ 0.75 T. The upper inset shows a VL diffraction pattern obtained at 1.6 K and 0.2 T. The lower inset shows a schematic of the diffraction pattern, indicating the scattering vectors q_1 and q_2. Here open and solid circles represent first order VL Bragg peaks belonging to different domain orientations, while the crosses denote higher order reflections.*

Authors

M.R. Eskildsen and L. DeBeer-Schmitt
(University of Notre Dame, USA)
N. Jenkins *(University of Geneva, Switzerland)*
C.D. Dewhurst *(ILL)*
M. Ichioka and K. Machida
(Okayama University, Japan)
S.L. Bud'ko and P.C. Canfield
(Ames Laboratory/Iowa State University, USA)

The opening angle, β, was found to decrease with increasing field, indicating a continuous transition from a distorted square to a distorted hexagonal VL. As a consequence of having a non-square VL pinned to an underlying square crystalline lattice, two VL domains were observed at all measured fields and temperatures. A direct measure of the magnetic induction, B, can be obtained by $B = (\phi_0/4\pi^2) |q_1 \times q_2|$, using two scattering vectors, q_1 and q_2, belonging to the same domain. In **figure 1** we show the measured induction in $TmNi_2B_2C$ as a function of applied field, compared to that of non-magnetic $LuNi_2B_2C$. For $TmNi_2B_2C$ we find that $B > \mu_0H$ for the entire measured field range, indicating a significant paramagnetic contribution to the induction. Below 0.55 T the measured B is in excellent agreement with magnetisation

measurements [1]. It is presently not clear what causes B to approach μ_0H at H_{c2}.

From the absolute scattered intensity of the VL Bragg peaks we are able to determine the vortex form factor $|F(q)|^2$ [2], which is the Fourier transform of the magnetic-field profile around a vortex and is determined by the two characteristic length scales: the penetration depth, λ, and the coherence length, ξ. Since the scattering vector depends on the vortex density and consequently the applied magnetic field, we are able to measure the form factor continuously over a wide q-range. In **figure 2** we show the measured form factor in $TmNi_2B_2C$ as a function of magnetic field at 1.6 K. The measured $|F(q)|^2$ is in striking contrast to the essentially exponential field dependence of the form factor, calculated

from the Ginzburg-Landau (GL) model [3] using constant values for λ and ξ and shown by the dashed line. Instead the vortex form factor in $TmNi_2B_2C$ remains approximately constant or even increases slightly at low fields, followed by a sudden drop above roughly 0.6 H_{c2}.

The form factor data for vortices in $TmNi_2B_2C$ are described well by calculations, shown by the solid line in **figure 2**, which take into account the paramagnetic spin susceptibility due to localised magnetic moments as well as the resulting Pauli paramagnetic breaking of the Cooper pairs. To visualise the contribution from the paramagnetic moments around the vortex cores, the insets to **figure 2** show the spatial structure of the internal field $B(r)$ in the VL unit cell both for the nonmagnetic case (a) and with the parameters used to fit the measured form factor (b). This shows how the paramagnetic component is confined at the vortex center, resulting in an enhancement of the internal field. The physical picture that emerges is that the conduction electron paramagnetic moments, induced by the exchange interaction, accumulate exclusively around the vortex cores, creating nanotubes of Tm magnetisation and maintaining the field distribution contrast of the VL.

Further details concerning both the measurements and the theoretical model can be found in reference [4].

Figure 2: Field dependence of the vortex form factor in $TmNi_2B_2C$ at 1.6 K. The dashed line shows the form factor calculated using constant ($\xi = 210$ Å and $\lambda = 780$ Å) values for the characteristic length scales. The solid line is calculated using the model by M. Ichioka and K. Machida [4]. The insets show the spatial structure of the internal field, B(r), around a vortex, both without (upper inset) and including (lower inset) Pauli paramagnetic effects.

References

[1] B.K. Cho et al., Phys. Rev. B 52 (1995) 3676

[2] D.K. Christen et al., Phys. Rev. B 15 (1977) 4506

[3] J. Clem, J. Low Temp. Phys. 18, (1975) 427

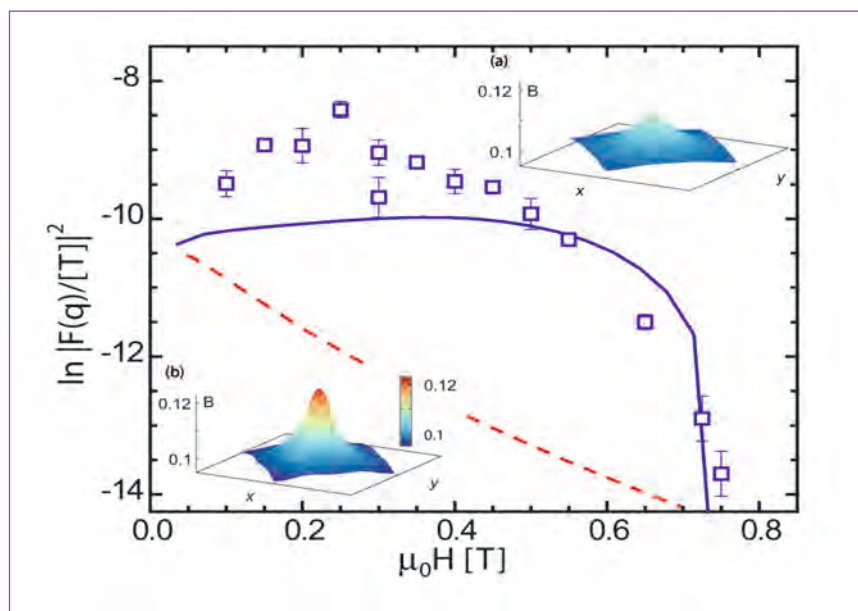**[4]** L. DeBeer-Schmitt et al., Phys. Rev. Lett. 99 (2007) 167001

Quantum oscillations of the total spin in a heterometallic antiferromagnetic ring

The identification of systems displaying quantum coherence at the mesoscopic scale is of great interest, both from a fundamental scientific perspective, and in the context of potential technological applications in the field of quantum computation. Antiferromagnetic molecular rings are very interesting in this respect. Using inelastic neutron scattering (INS), with applied magnetic fields B up to 15 T, we have studied the spin dynamics of an important member of this class of materials, Cr_7Ni. We demonstrate that several avoided crossings (ACs), involving states with different total-spin quantum numbers, occur with increasing B. This corresponds physically to quantum oscillations of the total spin of the ring.

Authors

T. Guidi (HMI, Berlin, Germany)
S. Carretta, P. Santini and G. Amoretti
(University of Parma, Italy)
R. Caciuffo
(EC, JRC-ITU, Karlsruhe, Germany)
A. Hiess (ILL)
J.R.D. Copley and Y. Qiu
(NIST Center for Neutron Research, USA)
G. Timco and R.E.P. Winpenny
(University of Manchester, UK)

Antiferromagnetic (AF) molecular rings are cyclic clusters with dominant nearest neighbour AF coupling. When organised in a crystal lattice, they provide an ensemble of identical, almost non-interacting magnetic units [1] and represent very promising systems for the observation of quantum coherent phenomena.
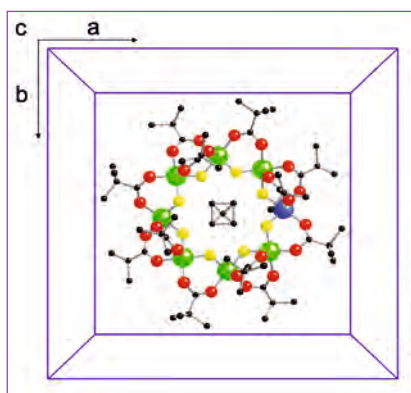

Figure 1: Schematic view of the Cr_7Ni molecular structure in the unit cell (view direction parallel to the crystallographic c axis). Cr: green spheres, F: yellow, O: red, C: black; Ni, blue, disordered over the 8 sites of the ring. H atoms are omitted for clarity. The experiment on IN14 was performed with the magnetic field lying in the plane of the ring.

Among the wide class of AF rings synthesised so far, the Cr_7Ni heterometallic ring has been identified as a model system for the implementation of qubits [2]. This cyclic cluster has a $S=1/2$ doublet ground state, resulting from the dominant AF exchange interaction between seven Cr(III) ions (s=3/2) and one Ni(II) ion (s=1) (**figure 1**).

A doublet ground state, well separated from the first excited level, is one of the prerequisites for a system to be suitable for encoding a qubit. Another crucial condition is the persistence of quantum coherence during the time needed for the elementary computational operations to be performed. It is thus important to know in great detail the quantum spin dynamics of these systems to better understand to what extent their properties match the desired ones.

The application of an external magnetic field B enables the energies and the composition of the eigenstates from the ring's Hamiltonian to be tuned. In particular, in Cr_7Ni several "avoided crossings" (AC) between different spin states are induced by a field with appropriate value and direction. When AC conditions are met, two different spin states are superimposed, and the total spin of each ring oscillates in time between S and S+1 [3].
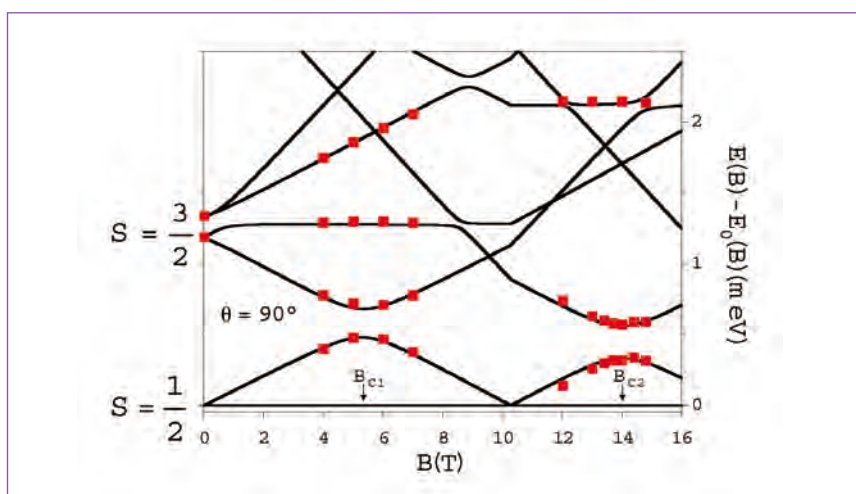

Figure 2: Calculated field-dependence of the low-lying energy levels of Cr_7Ni, relative to the ground-state energy, for an angle $\theta = 90°$ between the applied magnetic field and the anisotropy axis c. Points indicate the positions of the observed INS peaks. AC conditions occur in correspondence of magnetic field amplitudes B_{C1} and B_{C2} (arrows).
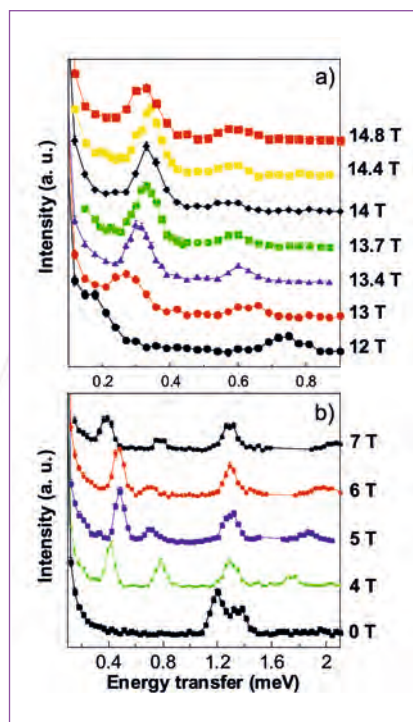
Figure 3: Constant **Q** scans for **Q** =(4.5, 0, 0) r.l.u. (reciprocal lattice units), varying the incident energy (fixed $k_F = 1.15$ Å^{-1}) at different magnetic fields near the AC conditions (T=1.5 K). The data are vertically offset for clarity. The modulus of **Q** was chosen close to the value where the magnetic intensity has its maximum [3].
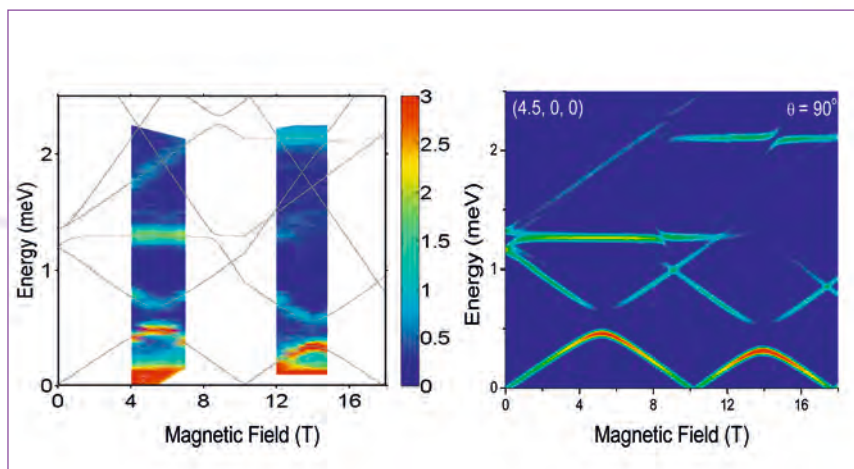

Figure 4: Intensity plot showing energy and field dependence of the measured (left) and calculated (right) INS cross sections for $\Theta = 90°$ and **Q**=(4.5, 0, 0) r.l.u.; T=1.5 K.

Using the Disk Chopper Spectrometer at NIST, we have observed this phenomenon around an AC that involves the spin ground state [3].

The three-axis spectrometer IN14 was then used to study the spin dynamics at AC conditions involving excited spin states, and to investigate the effects of the AC on the composition of the spin wavefunctions.

For this experiment, we used a 0.4 g single crystal sealed in a preservative THF/MeCN(1:2) atmosphere within an aluminum sample holder. A 15 Tesla vertical-field cryomagnet was used to apply a magnetic field parallel to the ring plane (figure 1). With fixed final neutron wave vector $k_F = 1.15$Å^{-1}, and a base temperature of 1.5 K, we collected inelastic constant Q scans, at different magnetic fields around the ACs.

The modulus of Q was chosen close to the value corresponding to the maximum of the magnetic intensity as a function of Q [4].

In **figure 2** the energies of the observed excitations are compared against the calculated energy level scheme as a function of the magnetic field. The occurrence of ACs between the first and second excited spin states at B_{C1}=5.3 T and B_{C2}=14 T is evidenced by the field dependence of the observed excitations and by the very good agreement with the theoretical calculations.

The spectrum at 0 T in **figure 3b** shows the transition from the S=1/2 ground state to the S=3/2 first excited state, split by anisotropic spin-spin-interactions and uniaxial local crystal fields. Increasing the field, we were able to follow the Zeeman shift of the low temperature excitations in the field interval corresponding to the AC fields B_{C1} (**figure 3b**) and B_{C2} (**figure 3a**).

The mixing of different spin states at the AC condition also affects the intensities of the observed excitations. **Figure 4** shows a plot of the INS cross section as a function of magnetic field and energy transfer. For magnetic fields approaching B_{C1} and B_{C2}, a redistribution of the INS intensity is observed, providing additional insight into the readjustment of the spin wavefunctions in the vicinity of the AC condition.

In conclusion, high field INS measurements on a Cr$_7$Ni single crystal have demonstrated the occurrence of avoided crossings involving states with different total-spin quantum numbers. The INS cross section shows an enhancement of the effect of the superposition of different states at the AC condition, where quantum oscillations of the total spin of the molecule take place. The very good agreement for the positions and intensities of the observed excitations with calculations gives us confidence in the validity of the model spin Hamiltonian and permits further speculations and predictions as to the feasibility of quantum information processing using this class of molecules.

References

[1] F.K. Larsen et al., Angew. Chem. Int. Ed 42, 101 (2003). R.H. Laye et al., Chem. Commun. 1125 (2005). M. Affronte, et al., Chem. Commun., 1789 (2007) and references therein

[2] F. Meier, J. Levy and D. Loss, Phys. Rev. Lett. 90 (2003) 47901; F. Troiani et al., Phys. Rev. Lett. 94 (2005) 207208

[3] S. Carretta at al., Phys. Rev. Lett. 98 (2007) 167401 and references therein

[4] R. Caciuffo et al., Phys. Rev. B 71 (2005) 174407

Magnetism in a charge-ordered superconductor

In recent years, the nature of the spin and charge order found in certain copper oxide superconductors has been hotly debated. We used polarised neutron diffraction to test a number of magnetic models proposed for superconductors doped with 1/8 hole per copper site. The results show that the superconducting state near 1/8 doping coexists either with one-dimensional stripe correlations or, possibly, with an intriguing two-dimensional electronic phase with non-collinear spin correlations.

Authors

A.T. Boothroyd and R.A. Ewings
(Oxford University, UK)
N.B. Christensen
(PSI Zurich, Switzerland and Risø National Laboratory, Denmark)
H.M. Rønnow
(EPFL Lausanne and PSI Zurich, Switzerland)
J. Mesot
(PSI Zurich, Switzerland)
D.F. McMorrow
(UCL London and ISIS Facility, UK)
N. Momono, M. Oda and M. Ido
(Hokkaido University, Japan)
M. Enderle *(ILL)*

Since their discovery in 1986 [1], many observations have confirmed that the copper oxide high-T_c superconductors display fundamentally new types of behaviour not found in conventional metals. The work highlighted here [2] relates to one of the most intriguing phenomena found in these materials, the presence of spin and charge inhomogeneities on the doped copper-oxide layers.

Static spin and charge order has been observed in several superconducting cuprates, such as $La_{2-x}Ba_xCuO_4$ (LBCO) whose phase diagram is shown schematically in **figure 1**. At zero doping ($x = 0$), the Cu spins on the cuprate layers order near room temperature into a simple antiferromagnetic pattern characterised by an in-plane wavevector $Q_{AF} = (½, ½)$. Upon doping, Néel order is suppressed and a glassy phase with incommensurate spin fluctuations appears which coexists with superconductivity at doping levels beyond $x \approx 0.05$. At optimal doping (i.e. highest T_c) magnetic order disappears entirely, leaving only dynamic spin fluctuations.

Glancing at **figure 1** one is struck by the anomalous suppression of superconductivity in a narrow range around $x = 1/8$. This so-called '1/8 anomaly' coincides with the appearance of static incommensurate magnetic satellites around Q_{AF} with accompanying second order harmonics around the structural Bragg peaks. The implication is that near $x = 1/8$ a complex ordered phase competes with superconductivity.
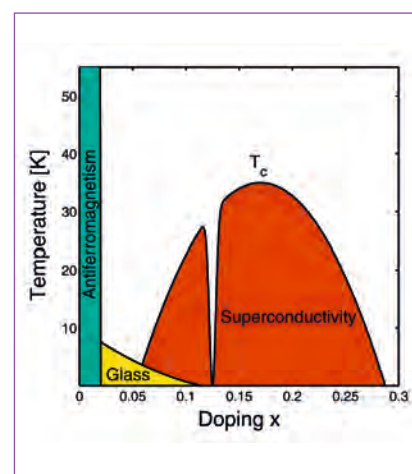

Figure 1: Simplified phase diagram of La-based superconducting cuprates such as LBCO as a function of hole doping x, showing the dramatic reduction in T_c at x = 1/8.
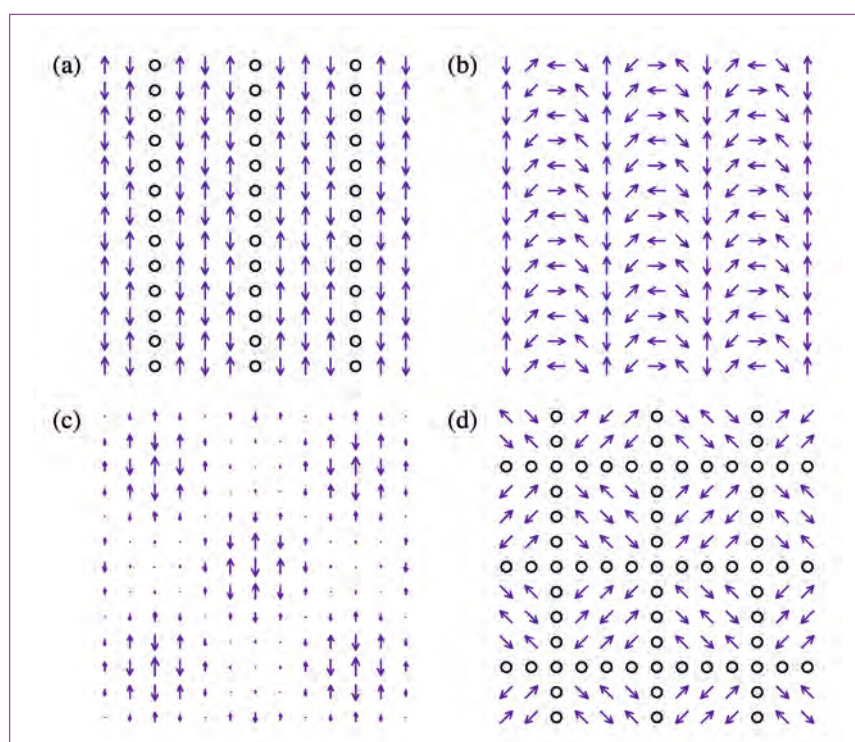

Figure 2: *Models for the magnetic order in La-based cuprates at a doping x = 1/8. (a) and (d) are consistent with the present results, (b) and (c) are not.*
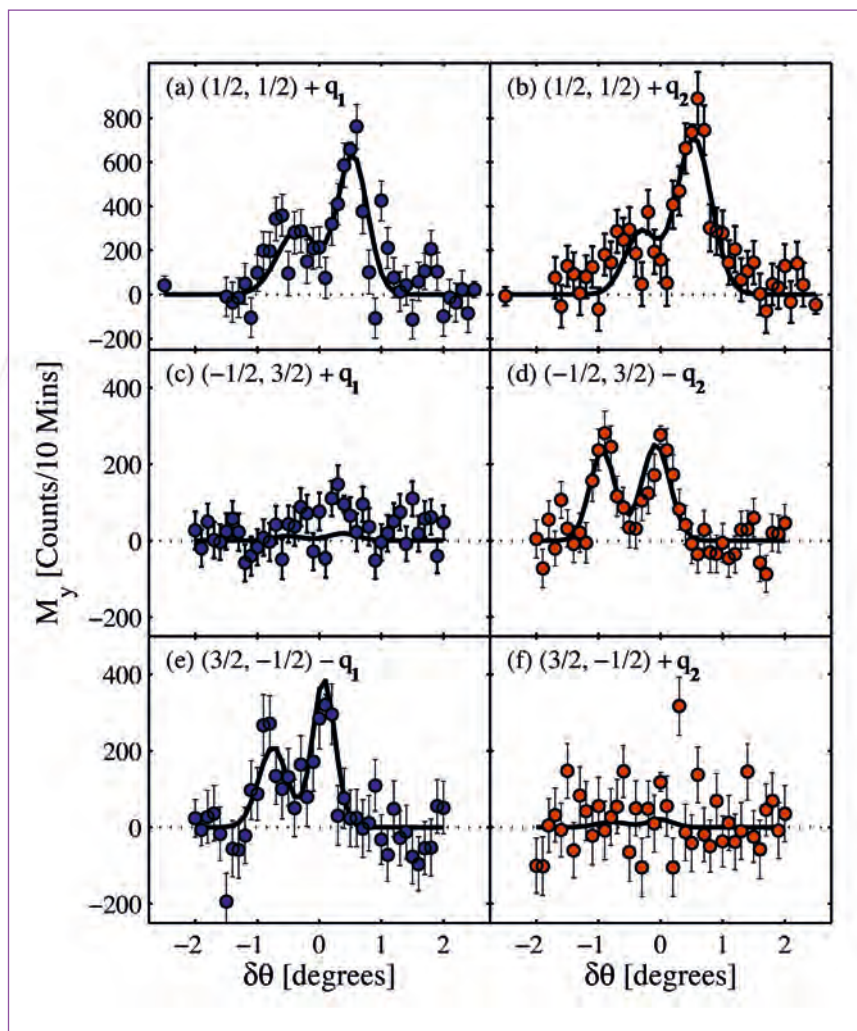
Figure 3: Polarised neutron diffraction showing M_y, the in-plane component of the magnetic cross section perpendicular to Q in the vicinity of three equivalent Q_{AF} positions, as a function of the rocking angle $\delta\theta$. The incommensurate satellite positions are $q_1 = (1/8,0)$ and $q_2 = (0,1/8)$.

the ordered spins in this model have no favoured in-plane direction. This is inconsistent with the data in **figure** (**3c**) and (**3e**). The model shown in **figure** (**2c**) is a two-q structure and consequently the q_1 and q_2 satellites of any given Q_{AF} should be almost the same size. This is clearly not the case for the $(-1/2, 3/2)$ or the $(3/2, -1/2)$ positions, **figures** (**3c**)–(**3f**).

By contrast, the data are consistent with the model in **figure** (**2a**), which is a representation of the 'stripe' model in which the doped holes segregate into one-dimensional charge stripes that form anti-phase boundaries in the Néel order [3]. The crystal structure makes it natural for the stripes run in orthogonal directions in adjacent layers, giving an equal number of layers with vertical (q_1) and horizontal (q_2) stripes.

Interestingly, the data are also consistent with the unusual two-q structure shown in **figure** (**2d**), which is derived from a coherent superposition of two orthogonal stripe domains. The charge order in this model forms a two-dimensional grid reminiscent of patterns observed by scanning tunnelling microscopy in several materials [4]. Our results impose the noncollinear spin arrangement shown in **figure** (**2d**) over any such grid.

What we can conclude from this work, therefore, is that the magnetic order in the spin-charge-ordered cuprate studied here is either modulated in 1D only or takes the form of a previously unconsidered non-collinear two-q structure. In the former case, it is reasonable to conclude that associated charge order is also one-dimensional, consistent with the stripe model.

What is the nature of the order in this phase? **Figure 2** shows four models of spin and charge order which yield diffraction patterns consistent with experiment, assuming equal populations of equivalent domains. Each model has principal Fourier components $Q_{AF} \pm q_1$ and $Q_{AF} \pm q_2$, where $q_1 = (1/8,0)$ and $q_2 = (0,1/8)$, as observed in LBCO at $x = 1/8$.

To distinguish between these models we used the instrument IN20 to make polarised neutron diffraction measurements on a crystal of Nd-doped $La_{2-x}Sr_xCuO_4$, which is structurally identical to LBCO and exhibits the same spin–charge ordered phase. **Figure 3** shows a series of sample rotation scans through

q_1- and q_2-type magnetic Bragg peaks surrounding three equivalent Q_{AF} positions. The quantity plotted (M_y) is the magnetic diffraction from in-plane spin components perpendicular to Q deduced from longitudinal polarisation analysis. The q_1 and q_2 satellites close to $(1/2, 1/2)$ are seen to have roughly equal intensity. Near $(-1/2, 3/2)$, however, the q_1 peak is clearly weaker than the q_2 peak, while the situation is reversed near $(3/2, -1/2)$.

These data conclusively rule out the models shown in **figure** (**2b**) and (**2c**). The reasoning is as follows. The model in **figure** (**2b**) predicts that the q_1 peaks near $(-1/2, 3/2)$ and $(3/2, -1/2)$ should be the same size because

References

[1] J.G. Bednorz and K.A. Müller, Z. Phys. B 64 (1986) 189

[2] N.B. Christensen et al., Phys. Rev. Lett. 98 (2007) 197003

[3] J.M. Tranquada et al., Nature 375 (1995) 561

[4] J.E. Hoffman et al., Science 295 (2002) 466; T. Hanaguri et al., Nature 430 (2004) 1001

The spin excitation spectrum in the pseudo-gap phase of a high-transition-temperature superconductor

Figure 1: Left panel: photograph of the (001)-surface of a twinned $YBa_2Cu_3O_{6+x}$ crystal taken with a polarisation microscope. There are four twin domains (two in each of the two regions), however they are pair-wise equally oriented: bright stripes in region I have the same orientation of the crystallographic axes a and b as bright stripes in region II. The same holds for the dark stripes, in which a and b are orthogonal to their counterparts in the bright stripes. Right panel: photograph of a detwinned crystal consisting of only one domain.

A lot can be learned about the microscopic arrangement and the correlations of the spins (magnetic dipoles) from the dispersion, i.e. the energy- and momentum-dependence of the spin excitations. We demonstrate that these quantities are fundamentally different below and above the superconducting transition temperature of the high-temperature super-conductor $YBa_2Cu_3O_{6.6}$ and that a different phase competes with superconductivity. From the geometry of the spin excitations we infer that this phase spontaneously breaks the rotational symmetry of the system, e.g. by exhibiting a Fermi surface deformation or by the establishment of a fluctuating stripe phase, consisting of an arrangement of one-dimensional domains of spin-rich and charge-rich regions.
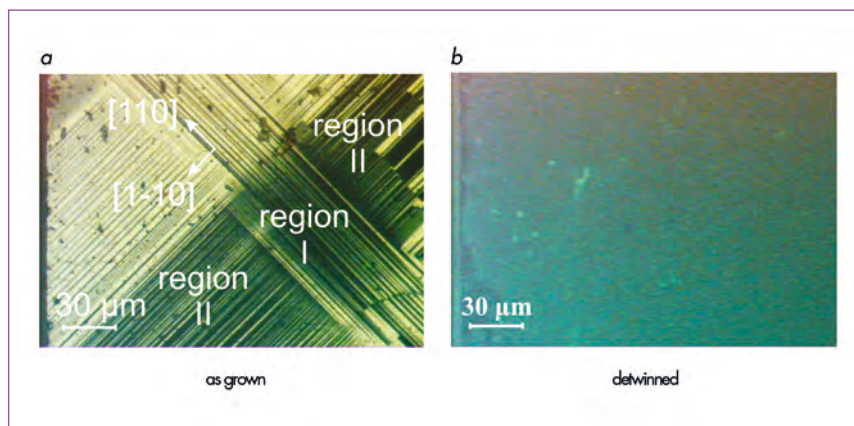
Authors

V. Hinkov, C.T. Lin, D.P. Chen, B. Keimer
(MPI-FKF, Stuttgart, Germany)
P. Bourges, S. Pailhès, Y. Sidis
(LLB, Saclay, France)
A. Ivanov *(ILL)*

High-transition-temperature superconductors such as $YBa_2Cu_3O_{6+x}$ exhibit a variety of phases depending on charge carrier concentration ("doping") and temperature, among which the superconducting (SC) phase is not even the most puzzling one. The underdoped region of the phase diagram, i.e. the region in which the carrier doping is below the one at which the maximal transition temperature of $T_c = 92$ K is reached for $YBa_2Cu_3O_{6.95}$, is dominated by the so-called pseudogap (PG) phase. This is characterised by the partial depletion of low-energy states already above T_c and is observed by many methods sensitive to the single-particle state occupation such as photo emission, ellipsometry or NMR. Since this depletion bears some similarity to the superconducting gap opening below T_c, some researchers believe that the PG is related to superconductivity and might even constitute a "precursor" phase, in which charge carriers already form Cooper pairs, which then, below T_c, condense to the well-known superconducting condensate. Other researchers, however, believe that the PG is unrelated to superconductivity and might even compete with it, though the superconductivity wins below T_c.

We have investigated the spin-excitation spectrum of a mosaic of 180 small, high-quality individually detwinned crystals (total volume of 0.450 cm^3) of underdoped $YBa_2Cu_3O_{6.6}$ with a T_c of 61 K using inelastic neutron scattering [1]. The result of the detwinning procedure is illustrated in **figure 1**.

The most prominent manifestation of the PG phase is a pile-up of intensity below a temperature of $T^* \sim 200$ K at moderate energies of up to 50 meV, while the presence of low-energy depletion remains debated and might be only present at comparatively high doping. In the **figure 2** we compare the spin excitations in the SC and the PG phases along the main

in-plane crystallographic axes *a* and *b* for the most relevant range of excitation energies. In the SC state we observe the hour-glass dispersion already reported for $YBa_2Cu_3O_{6+x}$ [2] and $La_{2-x}Ba_xCuO_4$ [3]. It exhibits an anomaly around 40 meV, the so-called resonance peak: the intensity is significantly higher than at other energies and the signal narrows down in the momentum direction (*H*, *K*) forming the hour-glass 'neck'.

In contrast, in the PG phase the anomaly has disappeared: there is no sharp resonance peak at 40 meV and the hour-glass neck has disappeared. The spin excitations exhibit a vertical or 'Y'-shaped dispersion. In addition, the difference between the *a*- and the *b*-direction is much more pronounced in the PG phase: the 'leg' of the Y-shaped dispersion is almost 50% broader along *a* than along *b* (**figure 2**, panels c,d). While there are also differences between *a* and *b* in the SC phase, the observed anisotropy is considerably smaller. From the pronounced change of the spin excitations across T_c, i.e. when going from the PG to the SC state, we conclude that the scenario in which the pseudogap competes with superconductivity is the more likely one.

What can we say about the nature of the pseudogap phase? The observed *a-b*-anisotropy of nearly 50% is most unusual, when we consider that the structural *a-b*-anisotropy is only of the order of 1%. Thus, there is a mechanism enhancing the tiny structural anisotropy by more than an order of magnitude. Such behaviour is frequently observed when a phase which spontaneously breaks orientational symmetry is involved, as found in ferromagnets (the spins have a tendency to point in the same direction) or nematic liquid crystals (the anisotropic molecules tend to be aligned in the same direction). A weak magnetic or electric external field will define a preferential direction for the spontaneously symmetry-broken phase. In our case, the slight structural anisotropy plays the role of the weak external field.
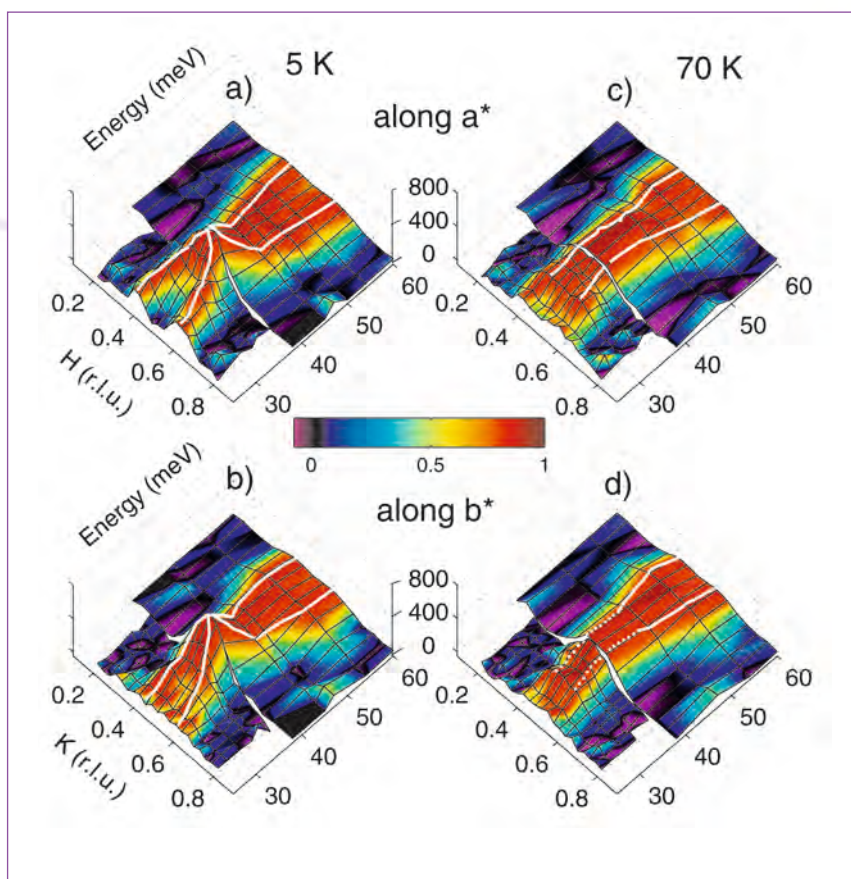
Figure 2: The magnetic intensity obtained from triple-axis scans performed on the spectrometer IN8. Panels a), b) show the superconducting state, panels c), d) the pseudogap state. At each individual energy, the colour scale was normalised to the peak intensity of the scan, allowing a better comparison of the variation with Q at different energies.

Two archetypes of phases breaking orientational symmetry are conceivable: (i) fluctuating stripe phases, which break the symmetry in real space [4]; (ii) a Fermi surface deformation, which breaks the symmetry in reciprocal space [5].

References

[1] V. Hinkov et al., Nature Physics 3 (2007) 780

[2] S.M. Hayden et al.,
Nature 429 (2004) 531

[3] J.M. Tranquada et al.,
Nature 429 (2004) 534

[4] S. Kivelson et al., Rev. Mod. Phys.
75 (2003) 1201

[5] H. Yamase and W. Metzner, Phys. Rev.
B 73 (2006) 214517

Quantum critical metamagnetism in Sr₃Ru₂O₇

Quantum criticality is the source of many new phenomena. One recent example is $Sr_3Ru_2O_7$, the first material with a quantum critical end-point and a candidate for electronic nematic order. Inelastic neutron scattering measurements show the signature of the critical point. At the same time, they provide new information about the spin dynamics (such as a strong anisotropic response in an applied field) that indicate an electronic behaviour even richer than originally expected.

Authors

S. Ramos, E.M. Forgan, C. Bowell, A.J. Schofield, and M. Laver
(University of Birmingham, UK)
S.M. Hayden and E.A. Yelland
(University of Bristol, UK)
A. Hiess, J. Kulda and A. Wildes *(ILL)*
R.S. Perry
(University of St. Andrews, UK)
Y. Maeno
(Kyoto University, Japan)
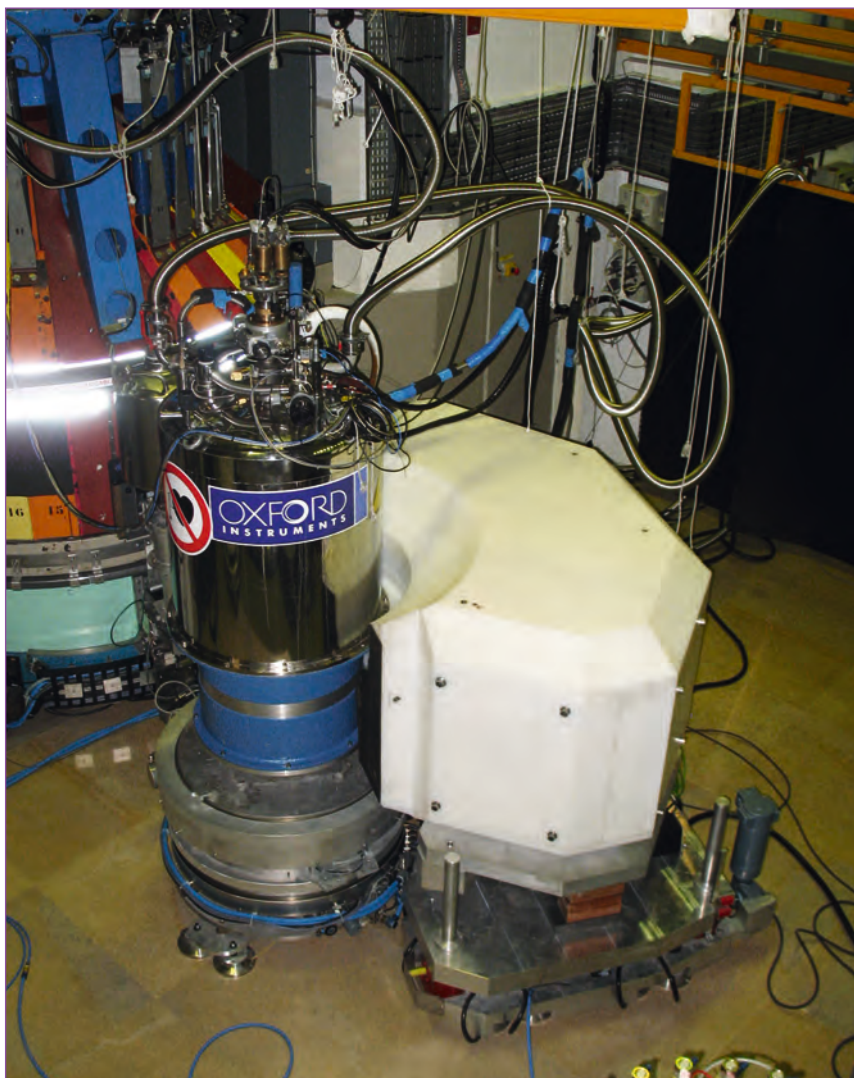
Figure 1: The FlatCone multianalyser installed on the cold neutron three-axis spectrometer IN14.

The layered perovskites and heavy fermion materials provide several fascinating examples of systems whose unusual superconducting and magnetic properties are the consequence of the presence of a quantum critical point in their phase diagram [1]. The bilayer ruthenate $Sr_3Ru_2O_7$ (SRO327) has become a highly topical material following the discovery of a new type of quantum critical point in its phase diagram: the quantum critical end-point. Regular quantum critical points are generated by second order phase transitions suppressed to absolute zero by changing a control parameter (e.g. sample composition or pressure). Unexpectedly, the critical end-point of a first order (metamagnetic) transition in SRO327 can be driven to 0 K by the application of

a ~ 8 T magnetic field along the c-axis of single crystals of ultra-high purity. The reason why this is an important discovery derives from the different nature of first order and second order phase transitions. While in a second order phase transition there is a symmetry of the system that is spontaneously broken, a first order transition can occur while keeping all symmetries the same [2]. This fundamental difference has a practical consequence that distinguishes this material from others with quantum critical points: in SRO327, there is no long-range-ordered magnetism or any other symmetry change at the critical point.

In addition, low-temperature measurements have found that below 1 K a new non-superconducting phase develops close to the critical point

in crystals with a residual resistivity better than 1 $\mu\Omega$cm. The new phase is characterised by strong anisotropy in the magnetoresistance and suggests an anisotropic ground state for the electrons. A scenario proposed to explain the experimental data is that the ground state has nematic electronic order, that is, an anisotropic electronic ground state that does not originate in the asymmetries of the crystalline lattice. The idea is that this electronic ground state, characterised by reduced rotational symmetry just like in a nematic liquid crystal, generates the anisotropic response in transport measurements [3]. One important question is: what is the origin of this anisotropy?
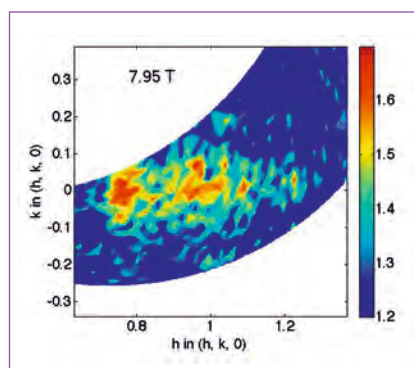

Figure 2: *Inelastic response of the bilayered ruthenate $Sr_3Ru_2O_7$ at 40 mK and at a constant energy transfer ΔE of 0.8 meV. At the critical metamagnetic field of 7.95 T, scattering in the (1 0 0) region shows the presence of ferromagnetic fluctuations. Of similar intensity is the signal found at the incommensurate positions (0.77 0 0) and (1.23 0 0).*
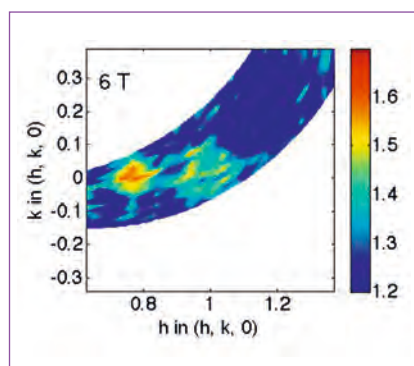

Figure 3: *Inelastic response of the bilayered ruthenate $Sr_3Ru_2O_7$ at 40 mK and $\Delta E = 0.8$ meV as above, but at an applied field of 6 T, well below the critical value. The incommensurate signal at (0.77 0 0) now dominates the spin dynamics.*

Most data currently available about this exciting material have been obtained using bulk and averaging probes such as magnetotransport and NMR. Inelastic neutron scattering (INS) is the ideal tool to obtain crucial and complementary information about microscopic electronic properties by looking at the spin dynamics. As the energies involved in quantum phase transitions are very low, we have used the cold neutron spectrometer IN14 to investigate SRO327.

During 2007, the newly-developed multiplexed secondary spectrometer *FlatCone* (**figure 1**) has been made available to users [4]. It is built with 31 individual analyser-detector units covering an angular range of 75°. When used on IN14, the final neutron wave-number for all channels is fixed to 1.4 Å^{-1}. This set-up enables the simultaneous exploration of a wide range in momentum space with a constant energy transfer. We have used it to map sectors of interest in reciprocal space and find out what characterises the spin fluctuations in the quantum-critical region.

Figure 2 shows the inelastic scattering at 40 mK and at the metamagnetic critical field (7.95 T for our sample) with an energy transfer of 0.8 meV. Significant intensity is visible at two momentum space positions: one corresponds to incommensurate fluctuations at (0.77 0 0) and (1.23 0 0); the other to ferromagnetic fluctuations at (1 0 0). Three important results are represented in this map. Firstly, the results show a signature of a metamagnetic critical point. The thermodynamic behaviour at a metamagnetic transition is a superlinear rise in the magnetisation, becoming a divergence of the susceptibility at a critical point. This would be reflected in the inelastic scattering spectrum by low-energy ferromagnetic fluctuations of the spins. The development of a peak in the (1 0 0) position in reciprocal space at the metamagnetic field signals precisely this type of fluctuation. This peak is missing in measurements at fields lower than the critical value, as can be seen in **figure 3**. The figure shows a fraction of reciprocal space measured at the same temperature, same energy transfer and a lower field of 6 T, away from the metamagnetic transition. In this case, the incommensurate fluctuations dominate the scattering, while only a very weak signal is found *around* (1 0 0).

The second important result is that there is a dramatic asymmetry in the scattering from the incommensurate fluctuations in an applied magnetic field. In the absence of a field, the incommensurate fluctuations are found at

(0.75 0 0), (1.25 0 0), (1 0.25 0) and (1 -0.25 0), with 4-fold symmetry around (1 0 0) [5]. Under an applied field, the incommensurate fluctuations are only present at (0.77 0 0) and (1.23 0 0) and missing from the other two positions (see **figure 2**). This implies that in a magnetic field, the low energy spin fluctuations are confined to particular directions in the layers of this ruthenate material. The origin of the anisotropy is still to be explained but it could hold the key to understanding the anisotropy in the new low temperature phase.

Finally, measurements of the intensity of both the ferromagnetic and incommensurate fluctuations as a function of the energy of the excitation provide compelling evidence of the involvement of the incommensurate fluctuations in the quantum critical behaviour. Theoretical predictions about the nature of the metamagnetic quantum critical point say that it is the ferromagnetic fluctuations only that should drive the transition [6]. Our measurements thus imply that the physics of SRO327 is more than just metamagnetic quantum criticality.

In summary, we have used the new developments in the detection system of the ILL three-axis spectrometers to study the quantum critical behaviour of the bilayer ruthenate $Sr_3Ru_2O_7$. The inelastic neutron scattering measurements have provided microscopic evidence of metamagnetism near the quantum critical point in this system. In addition, the strong anisotropy in the incommensurate signal and the involvement of these fluctuations in the quantum criticality provide evidence of electronic behaviour that is even more interesting than originally thought.

References

[1] P. Coleman, A.J. Schofield,
Nature 433 (2005) 226

[2] S.A. Grigera et al,
Science 294 (2001) 329

[3] R.A. Borzi et al., Science 315 (2007) 214

[4] M. Kempa, B. Janousova, J. Šaroun,
P. Flores, M. Boehm, F. Demmel and J. Kulda,
Physica B 385-386 (2006) 1080

[5] L. Capogna et al.,
Phys. Rev. B 67 (2003) 012504

[6] A.J. Millis et al.,
Phys.Rev.Lett. 88 (2002) 217204

SrFeO$_2$: the first infinite layer iron oxide with a square-planar coordination obtained by low-temperature synthesis

Iron, one of the most widespread elements in the Earth, forms an enormous number of oxides, some of which have been widely used in industry as low cost ferrite magnets or pigments. In almost all of them, iron atoms are tetrahedrally or octahedrally coordinated, few examples are known where iron adopts pyramidal coordination. Thus iron can be considered as a chemical chameleon, as it is able to switch easily to different coordination and valence states in a given structural framework. A prominent example is the SrFeO$_{3-x}$ perovskite system. Variation of the oxygen stoichiometry leads to several distinct phases which can be described as a series of Sr$_n$Fe$_n$O$_{3n-1}$ with n = ∞, 8, 4 and 2 [2]. The respective stoichiometries lead to the simple formula of SrFeO$_3$ with the cubic perovskite structure and Fe (IV) in an exclusively octahedral

Solid state reactions carried out at high-temperatures naturally limit the control of coordination polyhedra in transition-metal oxides to only those obtainable within the bounds of known coordination geometries for a given transition metal. It has been shown recently that binary metal hydrides can act as reducing agents already at low temperature, allowing access to unprecedented structures.

In this way the reaction of the oxygen deficient perovskite SrFeO$_{3-x}$ with CaH$_2$ yields for the first time SrFeO$_2$ with square-planar oxygen coordination around Fe(II). SrFeO$_2$ is isostructural with the "infinite layer" cupric oxides, and exhibits antiferromagnetic order below T$_N$= 473 K [1].

Authors

Y. Tsujimoto, T. Watanabe, H. Kageyama, K. Yoshimura and N. Hayashi
(Kyoto University, Japan)
C. Tassel
(Kyoto University, Japan and University of Rennes 1, France)
M. Takano
(Kyoto University and Kyoto Research Institute for Production Development, Japan)
M. Ceretti and W. Paulus
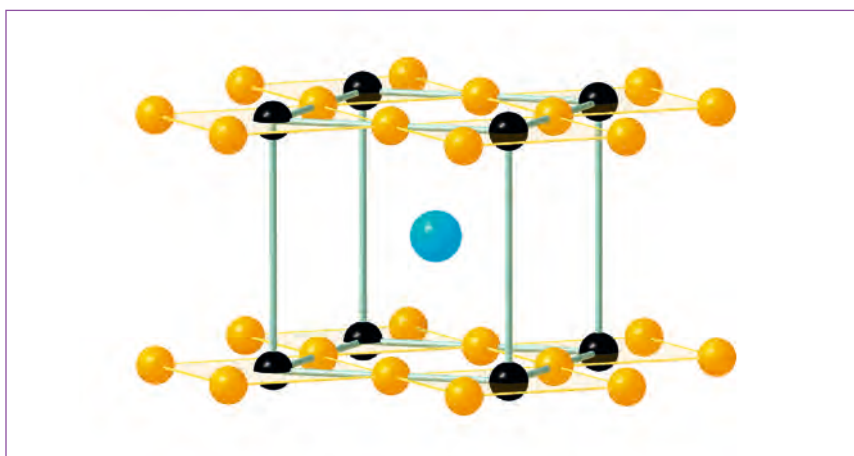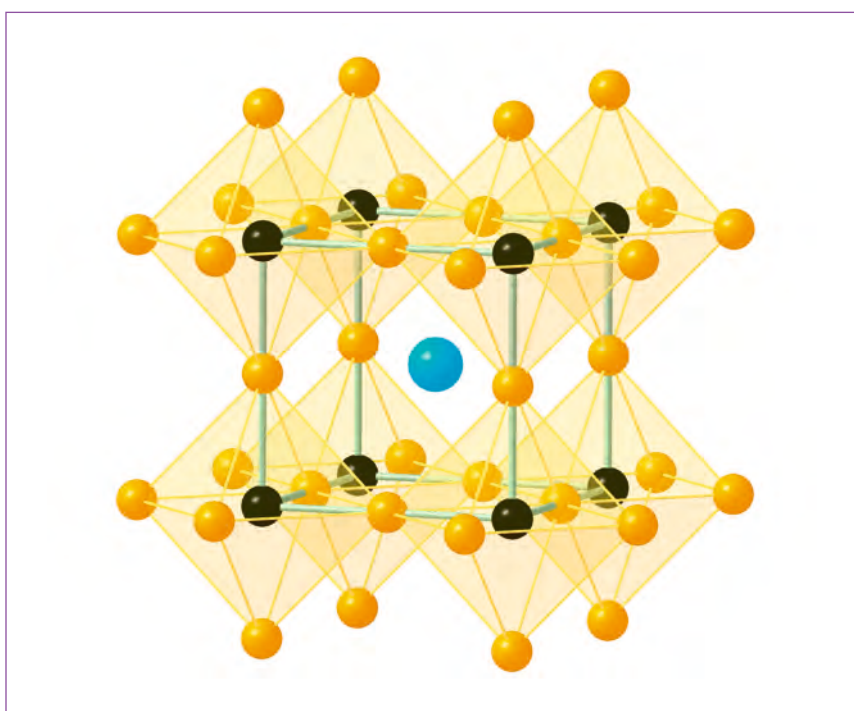*(University of Rennes 1, France)*
C. Ritter *(ILL)*

Figure 1: *Structural evolution of the SrFeO$_3$ Perovskite phase towards SrFeO$_2$ consisting of infinite layers of (FeO$_2$)$_\infty$ units.*
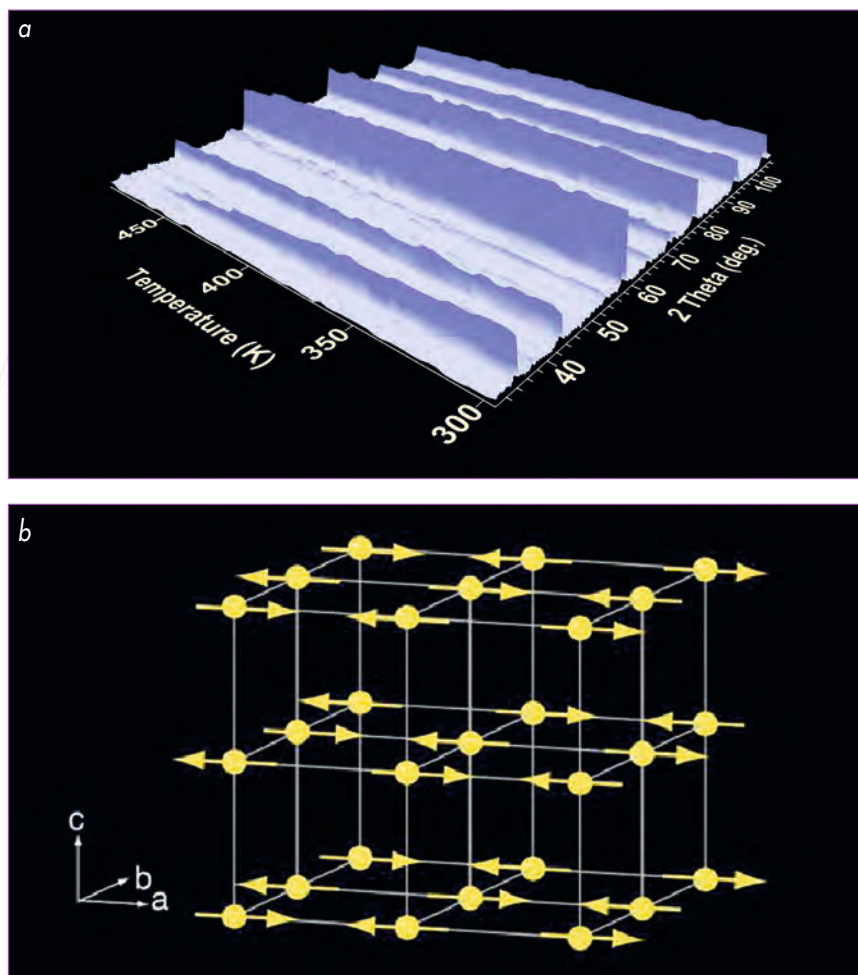
Figure 2: (a) Evolution of the NPD patterns of SrFeO₂ with temperature, obtained on D1B from a pure sample of 200 mg only. The reflection at low angles is the purely magnetic (½ ½ ½) reflection with respect to the nuclear cell. From its intensity T_N was determined to 473 K. (b) Orientation of the magnetic moments.

environment; the other phases correspond to $SrFeO_{2.875}$ and $SrFeO_{2.75}$ with iron in octahedral and pyramidal coordination as well as equally distributed octahedral and tetrahedral coordination in $SrFeO_{2.5}$ with a Brownmillerite type structure and only Fe(III). The latter compound has long been considered as the end member with the lowest oxygen stoichiometry, as extensive experimental efforts to control the oxygen content, including synthesis at high temperature with oxygen partial pressures ranging from 10^{-9} to 100 MPa, electrochemical reaction in aqueous solution at room temperature, as well as reduction in hydrogen atmosphere failed to create additional oxygen vacancies.

In this sense it is rather surprising to note that $SrFeO_2$ (**figure 1**) can be obtained via a low temperature reaction from $SrFeO_{3-x}$ (x ≈ 0.12) at ≈ 280°C using CaH_2 as reducing agent. $SrFeO_2$, the first solid oxide showing Fe in square planar coordination, shows an infinite layer structure consisting of $(FeO_2)_\infty$ slabs. Structural data obtained from neutron powder diffraction (NPD) at 10K on D1A, are summarised in **Table 1**. $SrFeO_2$ presents a new modification with n = 1 in the $Sr_nFe_nO3_{n-1}$ series. NPD on D1B (**figure 2a**) also revealed the presence of (π,π,π) antiferromagnetic order, where the magnetic moments are directed perpendicularly to the c axis (**figure 2b**), much

as found in the undoped, antiferromagnetically ordered parent phase of high-T_c cupper oxide superconductors. In $SrFeO_2$, Fe(II) atoms are in a high-spin state $(d_{yz}, d_{zx})^3 (d_{xy})^1 (d_{z2})^1 (d_{x^2-y^2})^1$ with S = 2. From temperature dependent NPD studies on D1B and Mössbauer measurement, the Néel temperature was determined to be T_N = 473 K, which is quite high considering the 2D character.

Surprisingly $SrFeO_2$ is stable in an ambient condition but it is extremely reactive towards oxidation on heating under oxygen atmosphere already below 373 K. This makes it a promising candidate to serve as an oxygen absorber even at rather low temperatures, with potential applications e.g. in the field of gas purification with respect to oxygen contamination.

The synthetic approach to reduce conventional oxides via CaH_2 at moderate temperatures is far from being exploited, and we might expect that, especially in the case of iron oxides, a variety of phases with interesting magnetic properties and unusual coordination chemistry are still to be discovered.

atom	x	y	z	b_{iso}	occ.
Sr	½	½	½	0.47(5)	1
Fe	0	0	0	0.47(4)	1
O	½	0	0	0.79(5)	0.99(1)

Table 1: SrFeO2 structural data at 10K obtained from NPD on D1A with λ = 1.91 Å.

Space group: P4/mmm, a = 3.985(1) Å, c = 3.458(1) Å, vol. = 54.92(2) Å³, R_p= 3.82%, R_{wp} = 4.70%, χ^2 = 5.52, R_{Bragg} = 3.61%, R_{mag} = 6.77%. The magnetic moment at 10K has been refined to be 3.6 μ_B/Fe perpendicular to the c axis

References

[1] Y. Tsujimoto, C. Tassel, N. Hayashi, T. Watanabe, H. Kageyama, K. Yoshimura, M. Takano, M. Ceretti, C. Ritter & W. Paulus, Nature 450 (2007) 1062-1065

[2] J.P. Hodges, S. Short, and J.D. Jorgensen, X. Xiong, B. Dabrowski, S.M. Mini, and C.W. Kimball, Journal of Solid State Chemistry 151 (2000) 190-209

Crystal structure of the oxidised positive electrode in nickel batteries

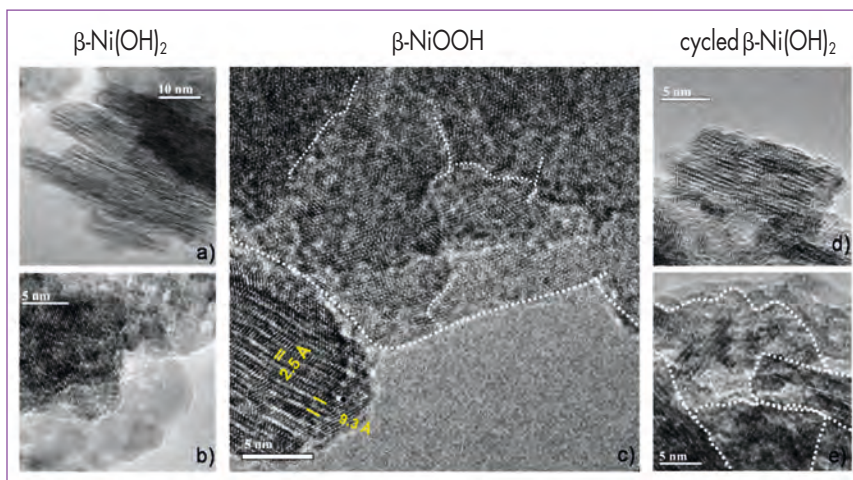**Figure 1:** *HRTEM images corresponding to pristine β-Ni(OH)₂, β-NiOOH and chemically cycled β-Ni(OH)₂. (a) and (b) correspond to pristine β-Ni(OH)₂ particles aligned along and perpendicular to the c-axis respectively, revealing rather coherent and crystalline domains. (c) shows a typical image of different β-NiOOH particles where the c-axis is doubled upon oxidation and a mosaic strained microstructure appears. (d) and (e) are images of chemically cycled β-Ni(OH)₂ exhibiting the original stacking sequence along the c-axis with retention of the mosaic texture.*

A combination of X-ray and neutron powder diffraction and high resolution transmission electron microscopy (HRTEM) has been used to demonstrate that the nickel battery positive electrode material β-NiOOH undergoes reversible structural transformations upon oxidation and reduction processes. With the implementation of models taking into account microstructural features, it was possible to refine the structure of the oxidised phase, with intrinsic low crystallinity. Contrary to what was believed, it is not isostructural with reduced β-Ni(OH)₂. This discovery represents an important step towards a full understanding of the operation mechanism of the positive electrode in all nickel based batteries at the atomic level.

Authors

**M. Casas-Cabanas,
J. Canales-Vázquez and M.R. Palacín**
(Materials Science Institute of Barcelona CSIC, Spain)
J. Rodríguez-Carvajal *(ILL)*

Nickel based batteries using nickel hydroxide as the active material in the positive electrode are still extensively used although the first patents were published more than one hundred years ago. Different technologies have been developed using a range of negative electrode materials such as either Ni/H₂ or Ni/MH, but the positive electrode material remains unchanged, i.e. β-Ni(OH)₂ in the discharged (reduced) state and β-NiOOH in the charged (oxidised) state.

β-Ni(OH)₂ crystallises in a brucite type structure (space group $P\bar{3}m1$) that can be described as a hexagonal close packed structure of hydroxyl ions (*AB* oxygen packing) with Ni(II) occupying octahedral interstices in one plane out of two. The unit cell parameters are a = 3.126 Å and c = 4.593 Å [1], although the complete structural characterisation of β-NiOOH had not been achieved to date due to its poor crystallinity. However, there was general agreement that no major modifications take place in the brucite layered structure upon oxidation; in other words, that no substantial structural changes occur in the positive nickel electrode under working conditions, with the exception of an irreversible microstructural transformation that produces a mosaic texture during the first oxidation of β-Ni(OH)₂ [2]. This process involves the formation of several slightly misoriented domains within each crystallite, caused by the relaxation of the microstrains that appear when half the hydrogen atoms from the hydroxide are extracted.

In order to carry out a complete study of the structural and microstructural evolution of the positive active material upon battery operation, pure phases were chemically prepared to mimic the electrochemical processes occurring upon battery charge/discharge. The samples were studied using a combination of HRTEM (**figure 1**) and X-ray and neutron diffraction techniques. The latter were carried out at the ILL on the instrument D1A.

The as-received β-Ni(OH)₂ used in this study consisted of small monolithic hexagonal platelet-shaped particles with an average diameter of approximately 30 nm (**figures 1a** and **1b**). β-NiOOH particles exhibit mosaic texture and consist of 5-10 nm domains with a large concentration of microstrains, resulting in slightly misoriented subdomains covering a few unit cells (**figure 1c**). However, the most striking feature of β-NiOOH is the doubling of the c axis compared to β-Ni(OH)₂ that is consistent with previous reports describing a weak reflection observed at d~9.3 Å in the corresponding XRD patterns [3]
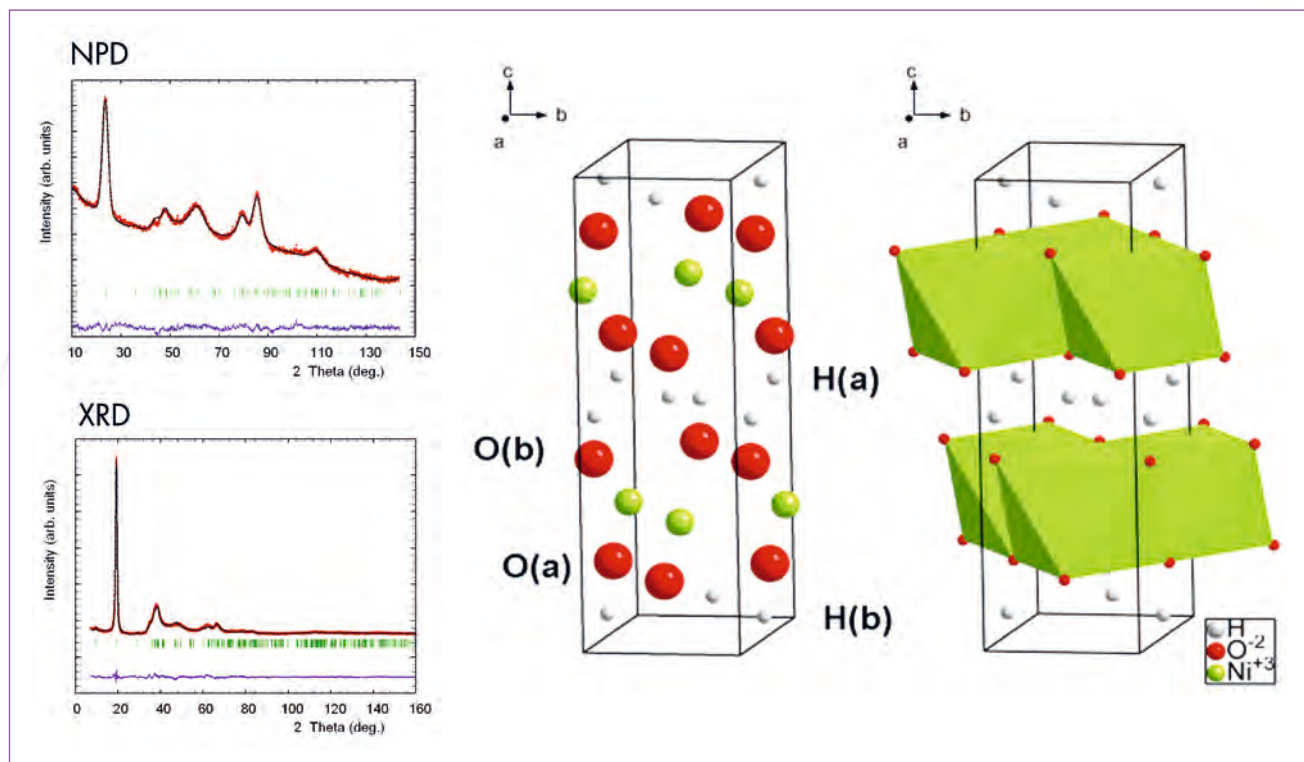
Figure 2: X-ray and neutron powder diffraction patterns (small circles) showing the final Rietveld fit (solid line) with difference pattern below, together with the refined β-NiOOH unit cell in atomic and polyhedral representations corresponding to an oxygen ABCA stacking sequence.

and though this was regarded as compatible with a larger unit cell, it was mostly assigned to impurities without further comment. In β-Ni(OH)$_2$ obtained by further reduction of β-NiOOH the d-spacing corresponding to the c-axis is approximately 4.6 Å, which indicates that despite the mosaic texture being retained, the structure reverts to the original layer stacking sequence after proton insertion during reduction (figures 1d and 1e).

Although the complex microstructure of β-NiOOH dramatically broadens the diffraction peaks, a combined X-ray and neutron Rietveld refinement was attempted using the FullProf program [4]. With the assumption that the Ni-O bonds in the NiO$_6$ layers do not break upon oxidation of β-Ni(OH)$_2$ and that only a shearing of the layers occurs, *ABCA* is the only candidate stacking sequence compatible with the observed doubling of the unit cell. In addition, a rough indexing suggests that an ortho-hexagonal cell derived from β-Ni(OH)$_2$ reproduces the position

of the main peaks, including the low-intensity peak at d = 9.3 Å, the most likely space group being C2/m. Finally, realistic models considering the anisotropic broadening of the diffraction peaks in β-NiOOH due to both the very small platelet-shaped crystallites and the presence of strong anisotropic microstrains were taken into account. The best results were obtained treating the former through the use of a quadratic form in reciprocal space considering ellipsoidal crystallite morphology and the latter with a limited development (seven terms) of spherical harmonics. The microstructural information extracted from the diffraction line profile is in very good agreement with HRTEM and the resulting average crystal structure is shown in **figure 2** together with a plot of the experimental and calculated diffraction patterns. The refined cell parameters are a = 4.883(5) Å, b = 2.920(8) Å, c = 9.24(1) Å and β = 88.8 (1).

In conclusion, we have been able to determine the crystal structure of β-NiOOH and hence

demonstrate that severe but reversible structural changes happen in nickel battery positive electrodes upon operation [5]. Critical to the success of this task was the simultaneous consideration of structural and microstructural models in the Rietveld refinement.

References

[1] *C. Greaves and M.A. Thomas, Acta Crystall. B-Stru. 42 (1986) 51*

[2] *A. Delahaye-Vidal, B. Beaudoin and M. Figlarz, React. Solid. 2 (1986) 223*

[3] *H. Bode, K. Dehmelt and J. Witte, Z. Anorg. Chem. 366 (1969) 1*

[4] *J. Rodríguez-Carvajal, Physica B 192 (1993) 55*

[5] *M. Casas-Cabanas, J. Canales-Váquez, J. Rodríguez-Carvajal and M.R. Palacín, J. Am. Chem. Soc 129 (2007) 5840*

Neutron Laue diffraction on the spin-crossover crystal [Fe(ptz)$_6$](BF$_4$)$_2$ showing continuous photo-induced transformation

The structural aspects of photo-induced phase transitions in spin-crossover compounds were investigated by neutron Laue diffraction.
The structures of the ground state and of the metastable LIESST state of the Fe(II) spin transition compound [Fe(ptz)$_6$](BF$_4$)$_2$], in the quenched rhombohedric phase, were determined at 2K. The structural changes were observed to be continuous, despite the cooperative character of the spin-crossover system, and their kinetics were followed during the photo-excitation at 2K [1].

The solid-state aspects of the photo-excitation process in spin-crossover compounds were recently studied by X-ray diffraction [2]. The existence of like-spin domains, i.e. domains of high-spin molecules or low-spin molecules was evidenced both at the thermal and photo-induced transitions, in pure spin-crossover solids, and in Prussian Blue analogues, which exhibit charge-transfer-induced spin transition. Indeed the phase separation into like-spin domains was already suggested in previous experimental works in the light-induced instability of spin-crossover compounds under light in the temperature range where self-accelerated relaxation efficiently competes against the photo-excitation process [3]. Structural differences between the photo-induced and thermally induced high-spin phases have been reported in some cases, and are presently a 'hot topic' in the field of molecular switchable solids.

We report here the first study using neutron Laue diffraction to investige the structural aspects of the photo-induced spin transition in [Fe(ptz)$_6$](BF$_4$)$_2$ (ptz = 1-n-propyltetrazole). This compound is the most prominent member of this class of spin-crossover compounds. Upon slow cooling, the spin transition is normally accompanied by a crystallographic phase transition ($R\overline{3}$ to P$\overline{1}$) with hysteresis of 7K (T$_c$↓=128K and T$_c$↑=135K), but this phase transition can be suppressed by quenching the sample in liquid nitrogen [4]. The spin transition is then abrupt with crystal turning from colourless in the HS phase to purple in the LS one. The LIESST (LS→HS) effect is generated by continuous laser sources in the 450-550 nm range. At 2K, the lifetime of the photo-induced state is several weeks and irradiation can be switched off when photo-excitation has been completed. On increasing temperature, relaxation of the
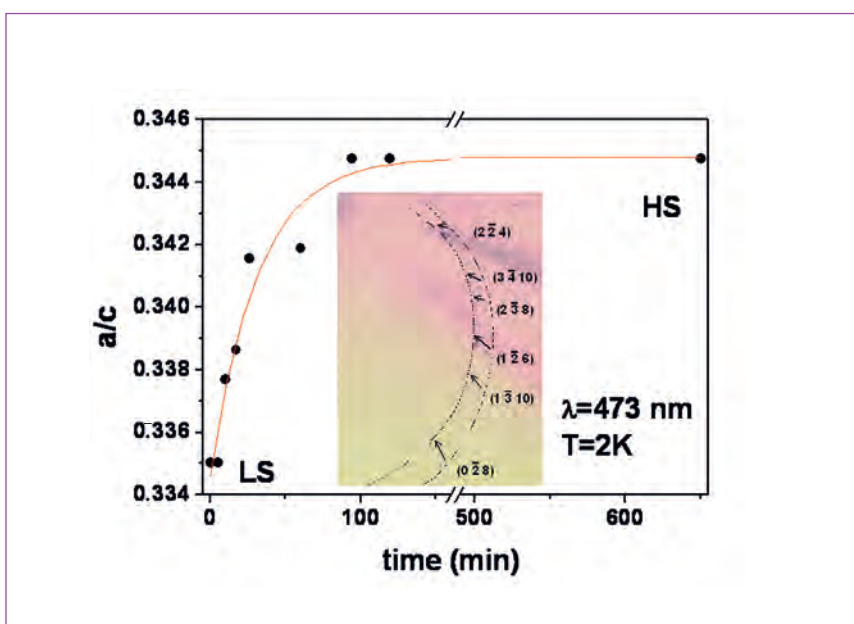
Figure 1: Kinetics of the photo-excitation of [Fe(ptz)$_6$](BF$_4$)$_2$ at 473 nm, 2 K followed through the cell parameter ratio a/c. Data are tentatively fitted by a single exponential function.
Insert: partial view of a superposition of two Laue patterns of [Fe(ptz)$_6$](BF$_4$)$_2$ at 2K, before and after illumination (473 nm, 2 mW/cm², 2 h), showing the shift of the Bragg spots upon photo-transformation.

Authors

A. Goujon, B. Gillon and A. Cousson
(LLB, France)
G.J. McIntyre
(ILL)
F. Varret
(CNRS-Université de Versailles, France)
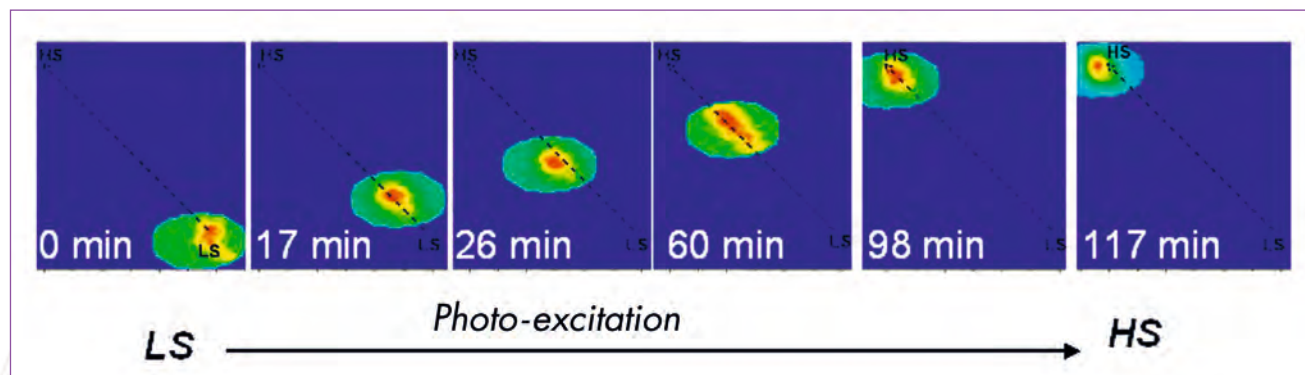
Figure 2: *Shift of the (0 −2 8) reflection of [Fe(ptz)₆](BF₄)₂ upon photo-excitation at 473 nm, 2 K [1].*

metastable HS state becomes sizeable. In the presence of light, the spin equilibrium is governed by the competition between relaxation and photo-excitation. Above 50 K relaxation dominates photo-excitation, and the lifetime of the photo-excited HS state can drop down to zero, which totally hinders the photo-excitation effect.

A photocrystallographic experimental set-up has been installed on VIVALDI [1]. A [Fe(ptz)₆](BF₄)₂ single crystal, with a hexagonal platelet $2 \times 2 \times 0.1 \, mm^3$ [5], was mounted on the diffractometer. The sample was cooled down to 4.2K, within ~5 minutes, and the expected rhombohedric LS phase was (indeed) observed. The sample was subjected to a low intensity of $2 \, mW/cm^2$ coming from the laser source (473 nm, 30 mW).

In order to follow the kinetics of the photoexcitation process at 2K, a series of Laue patterns were recorded, after different irradiation times, with the light switched off and a neutron exposure-time of 20 minutes. Saturation was reached after about 2 hours of light irradiation. The shift of the diffraction spots is shown in **figure 1**, and agrees with the expected volume increase across the LS→HS transition. The kinetics of the photo-switching is in good agreement with the previous photo-magnetic data, once the differences in the specific intensities and wavelengths are accounted for.

Phase separation during spin transitions is still a pending question since the earliest works which evidenced the coexistence of high-spin (HS) and low-spin (LS) peaks in X-ray diffraction patterns in the temperature range of the spin transition. The question of phase separation also applies to all solids undergoing photo-induced phase transitions. Recently, several structural investigations of the light-induced spin transition of single crystals have shown phase separation [2]. The evolution of the (0,-2, 8) Laue spot, as a function of the total irradiation time is displayed on **figure 2**.

The observed continuous shift clearly rules out a mechanism of nucleation and growth of like-spin domains during the phase transformation. It also shows the basically homogeneous character of the photo-excitation process, which requires that the penetration depth of light greatly exceeds the crystal size at all stages of irradiation, i.e. irrespective of the bleaching process which facilitates the complete photo-excitation. The absence of like-spin domains in the present cooperative spin-crossover system can be understood by considering the nature of the driving force for the nucleation and growth process. In the mean-field approach we developed in previous works [3], demixtion is driven by the bistability of the photo-stationary states due to competition between photo-excitation and self-accelerated relaxation rates.

We concluded that the presence of cooperative interactions was not a sufficient condition for the phase separation to occur, and pointed out that nucleation and growth of like-spin domains certainly require a thermodynamic driving force and (presumably) the thermal diffusion of the spin state. A further investigation of the compound in the vicinity of the light-induced instability is in progress. Emphasis is given to the profiles of the spots in order to obtain quantitative information on the phase separation.

References

[1] A. Goujon et al.,
Phys. Rev B 73 (2006) 104413

[2] Y. Morimoto et al.,
Phys. Rev B 73, 060408(R) (2006)

[3] A. Desaix et al., Eur. Phys. J. B 6 (1998) 183

[4] G.J. McIntyre, M.-H. Lemée-Cailleau,
and C. Wilkinson, Physica B 385-386 (2006) 1055

[5] Kindly provided by Prof. Jelena Jeftic,
ENSCR, Université de Rennes, France

Dynamic determination of twin-boundary motion in Ni—Mn—Ga/polymer composites

The motion of twin boundaries in the metallic filler of a Ni—Mn—Ga/ polymer composite was observed during a mechanical deformation cycle by measuring *in situ* the neutron diffraction pattern of the composite in stroboscopic mode. By looking at the change in area ratio of two peaks corresponding to the short and the long *a* axes of the martensite cell, the motion of the twin boundaries can be compared with the macroscopic stress and strain in the sample.

Ferromagnetic shape memory alloys (FSMAs) are a relatively new class of active materials that combine the large maximum amplitude of displacement obtainable from thermo-elastic shape memory alloys (SMAs) and the higher bandwidth of magneto-strictive materials. Like conventional SMAs in the tetragonal martensite phase the material can pseudo-plastically deform by the motion of twin boundaries: additionally, FSMAs have a magnetic moment, strongly coupled to the unique axis of the martensite cell [1].

Like plastic deformation, the motion of twin boundaries during pseudo-plastic deformation can dissipate large amounts of mechanical energy. This makes them attractive as mechanical dampers, but single crystals make a poor choice, because they are brittle, heavy and expensive. However the strong magnetic anisotropy of these alloys can be used to make composite materials that would have a strong crystallographic texture, retaining most of the ability to dissipate energy, but would be lighter and less expensive. The only requirement would be that the twin boundaries in the FSMA filler particles could be moved repeatedly back and forth in the composite by an external stress. Previous X-ray experiments did show a slight change in the peak intensity for an applied static strain [2]. However, the diffractometer D20 at the ILL is uniquely suited to show the motion of the twin boundaries in real time and how that tracks with the load applied to the composite.

The samples used for the experiment were made by first mixing particles of Ni—Mn—Ga made by spark erosion from a master alloy, and ranging in size from 25 to 75 μm in diameter with a commercial polyurethane. The composite was cured in a 1 T magnetic field parallel to its long direction in order to align the magnetic particles.

For the measurement an Instron mechanical testing machine was placed inside the sample cavity of the D20 diffractometer. The mechanical testing machine was driven under strain control, and the strain output signal was used to synchronize the neutron diffraction data acquisition.
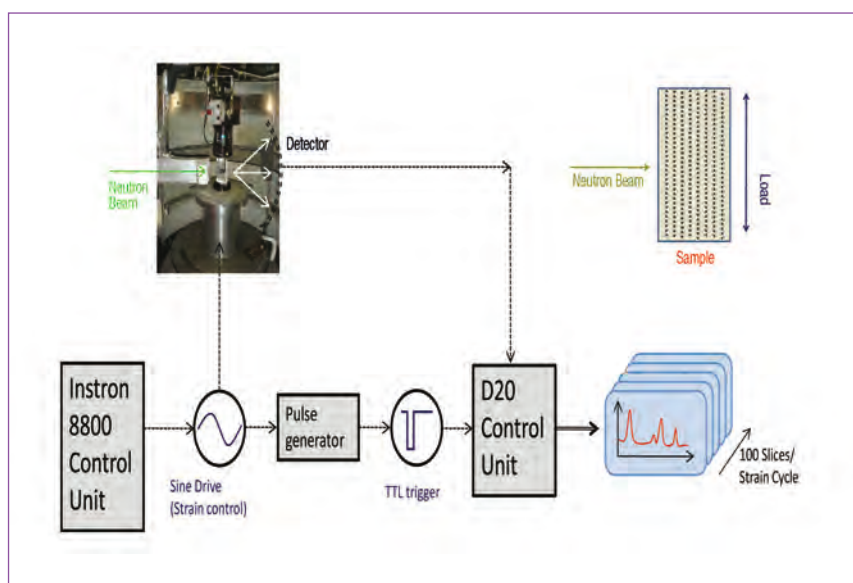

Figure 1: *Schematic of the diffraction experiment set-up.*

Authors

**J. Feuchtwanger, P. Lázpita,
N. Vidal, J.M. Barandiaran
and J. Gutiérrez**
(Universidad del Pais Vasco, Bilbao, Spain)
T. Hansen and M. Peel
(ILL)
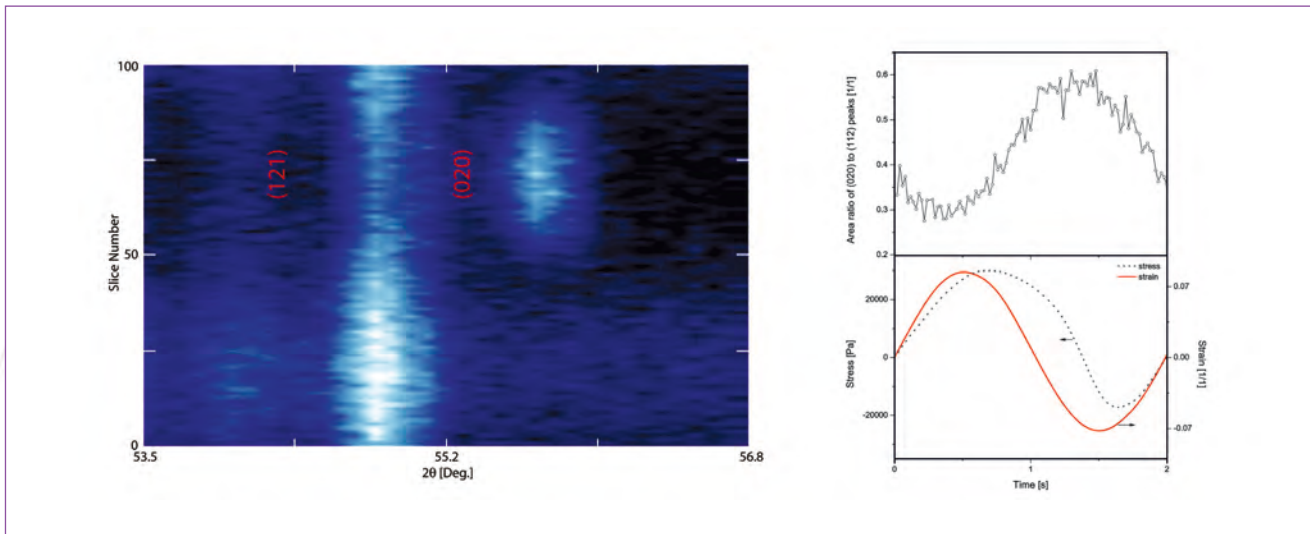**C. Mondelli**
(CNR-INFM and ILL)

Figure 2: Left: diffraction peaks' intensity. Right top: Area ratio of the (112) to (020) peak. Right bottom: Stress and strain on the sample.

The rising edge of the 0.5 Hz sinusoidal drive strain was used as a trigger for the diffractometer, which was operated in stroboscopic mode, so that 100 slices of 20 ms each were taken over each cycle of mechanical deformation. A schematic of the experimental setup is shown in **figure 1**. The mechanical load was applied along the long direction of the sample, while the neutron beam was directed normal to the applied stress.

The left panel of **figure 2** shows the diffraction peak intensity along the deformation cycle. The area ratio of the (112) to the (020) peak was calculated by fitting the peaks to Lorentzians with a linear background subtracted for each slice. The curves shown in the right panel of **figure 2** are the result of adding up the accounts of all corresponding slices from the approximately 2000 mechanical deformation cycles. The ratio of the two peaks varies over the deformation cycle in a sinusoidal-like fashion that follows the stress and the strain on the sample, also shown in **figure 2**. While the strain on the sample is forced to follow a 0.5 Hz sine wave the resulting stress deviates quite strongly from a sine wave.

The variation in the area ratio of the (112) to the (020) peak indicates the existence of mobile twin boundaries in the composite, because these two peaks are the result of the splitting of the (220) higher temperature, cubic 'austenite' parent phase peak[1]. The change in their relative areas indicates that the number of short axes in the metallic filler particles parallel to the neutron beam varies during the stress cycle, something that can be explained by only twin motion since it would be very unlikely that spherical particles would consistently rotate as a function of the applied load over 2000 cycles [3]. The departure from a sine wave also indicates a non-linear modulus of the particles, indicative of twin boundary motion.

Such materials use the internal friction of the particles when they deform pseudo-plastically to dissipate the mechanical energy applied to the composite. Even though they are not designed to replace conventional shape memory alloys, due to their fragility, they can be used as damping materials where weight is critical and higher losses than those obtainable with polymers are needed.

1) *The terms 'austenite' and 'martensite' are mostly used for historical reasons since the phase transformation observed in shape memory alloys are analogous to those observed in steels. Both terms are not strictly correct and may be replaced by 'cubic' or 'tetragonal', respectively. The austenite phase is named after Sir William Chandler Roberts-Austen and the martensite phase after Adolf Martens.*

References

[1] *S.J. Murray, M.A. Marioni, A.M. Kukla, J. Robinson, R.C. O'Handley and S.M. Allen, J. Appl. Phys. 87 (2000) 5774–5776*

[2] *J. Feuchtwanger, PhD thesis, Massachusetts Institute of Technology, February 2006*

[3] *J. Feuchtwanger, P. Lazpita, N. Vidal, J.M. Barandiaran, J. Gutierrez, T. Hansen, M. Peel, C. Mondelli, R.C. O'Handley and S.M. Allen, Journal of Physics: Condensed Matter, 20 (2008) 104247*

Evolution of weld residual stresses with *in situ* fatigue loading and crack growth

The strain diffractometer SALSA has been used to measure the evolution of the residual stresses in a welded airframe aluminium alloy with fatigue loading and consequent crack growth. Fatigue crack growth (FCG) was performed *in situ* on SALSA and strain measurements were carried out along the crack path. The unique data acquired gives an enhanced understanding of the evolution of residual stresses with FCG, their interaction with the structure's fatigue behaviour, and their overall effect on its structural integrity.

The constraints of cost and increased service life of aerospace structures have changed the way new materials are introduced in the design cycle of new products. It has moved from a purely performance driven approach to a customer driven approach [1]. The objectives are to improve performance, to extend the life and to reduce the environmental impact.

The use of large integral structural sections in the design of aerospace components can significantly reduce the weight of the final assembly. However, an inherent inconvenience with welded integral structures is the residual stresses caused by the intense local heating. These stresses can significantly influence the crack initiation and growth rate in engineering components. Civil fixed wing jet aircraft are certified under damage tolerance regulations and hence the fatigue crack growth rate determines the inspection intervals [2]. Large safety factors are hence imposed if the effect of these residual stresses on the fatigue behavior are not fully understood and documented. This reduces the competitiveness of integral structures.

Linear elastic fracture mechanics is the most frequently employed approach to account for the effect of an existing residual stress field on fatigue crack growth behaviour. It is assumed that the applied and the residual stresses are additive, and that residual stresses act in the same way as externally applied stresses.

Detailed knowledge of the evolution of residual stresses with fatigue crack growth therefore has to be determined in order to be able to assess the validity of these assumptions. Several researchers have attempted to measure the residual stress relaxation that occurs with crack growth [3, 4]. However, in these works the 'crack' was extended by machining a notch in the specimen.
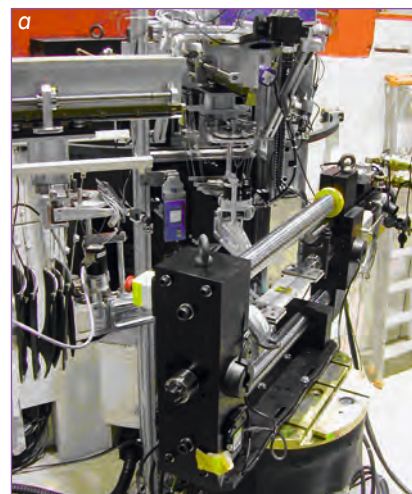
Figure 1: Experimental set-up at SALSA for measurement of the stress in a welded plate under fatigue crack growth, measuring a) in the transverse direction and b) in the longitudinal direction.

Authors

C.D.M. Liljedahl, O. Zanellato and M.E. Fitzpatrick
(Department of Materials Engineering, The Open University, Walton Hall, UK)
L. Edwards
(Department of Materials Engineering, The Open University, Walton Hall, UK and Australian Nuclear Science and Technology Organisation, Australia)
D.J. Hughes
(ILL)

Under these circumstances elastic redistribution of the stress is certain since the slot produced does not have the plasticity associated with a fatigue crack. It has been suggested that one of the reasons for the difficulty in predicting the fatigue life in the presence of a strong residual stress field is the interaction between the fatigue induced plastic strains and original misfit strains that gave rise to the residual stress field in the component.

Neutron diffraction has been used for measurement of residual stresses in various types of materials and industrial components. The method has been extensively applied to measure residual stresses in welds as the stresses are usually high, the gauge volume typically used is small compared with the weld and the penetration depth is large. The neutron technique is non-destructive and so is ideal for the monitoring of residual stress fields in fatigued samples.

Metal inert gas (MIG) welding was used to manufacture 2024 aluminium alloy middle tension specimens. The measurements were carried out on the SALSA diffractometer. The evolution of the residual stresses with fatigue crack growth was hence measured by fatigue testing the specimen *in situ* on the diffractometer. This was achieved by fixing a 50 kN Instron hydraulic stress rig on the SALSA sample table (**figure 1**).

The measured residual stresses were seen to increase with crack length and then a decrease at long crack length (**figure 2**). A finite element (FE) simulation of the elastic re-distribution of the initial residual stresses field showed the same characteristics (**figure 3**) and a good correlation was found between the experimental results and the FE prediction.

This work hence indicates that the evolution of the residual stresses at this level of resolution is indeed governed by elastic re-distribution. It shows that linear elastic fracture mechanics can be used successfully in the assessment of the fatigue behaviour if the initial residual stress field in the component is known. It is likely that previous inaccuracies in life assessment have been due to incomplete knowledge of the initial residual stress profile. It has further been shown that the ILL engineering instrument SALSA can be used as an excellent tool in the assessment of the understanding of residual stress interactions and models for structural integrity predictions.

Figure 2: *Measured evolution of the residual stresses with fatigue crack growth.*
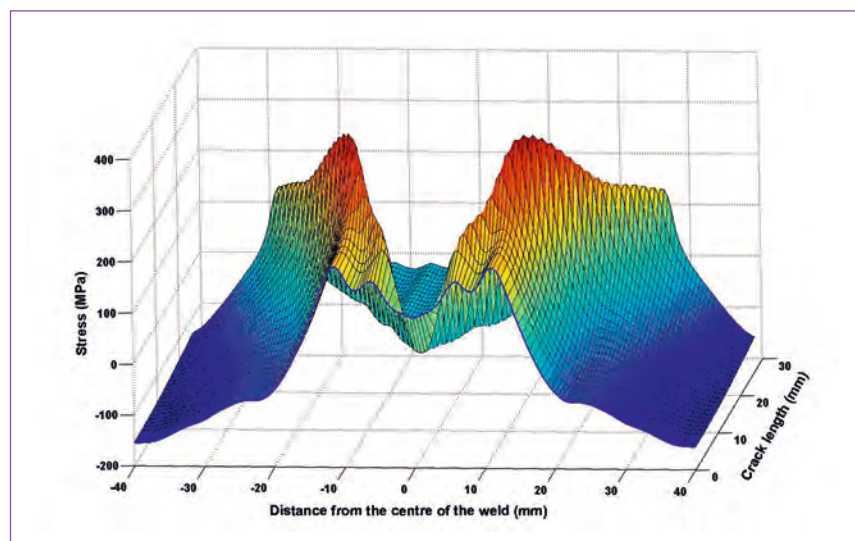
Figure 3: *Elastic finite element simulation of the evolution of the residual stresses with crack extension.*

References

[1] *J.C. Willams and E.A. Starke, Acta. Mater 51 (2003) 5775*

[2] *U. Goranson, Damage tolerance: Facts and Fiction, International Conference on Damage Tolerance (September 2007), Delft, Netherlands*

[3] *R. Galatolo and R. Lanciotti, Int. J. Fatigue 40 (1997) 43*

[4] *Y. Lee, C. Chung and Y. Park, Int. J. Fatigue 20 (1998) 565*

Silkworm silk under tensile strain investigated by synchrotron X-ray diffraction and neutron spectroscopy

In order to test models of the mechanical properties of silk fibres, we have exposed silkworm silk fibre bundles *in situ* to tensile forces sufficient to reach and exceed the yield point of plastic deformation whilst recording X-ray microbeam diffraction patterns and neutron time-of-flight spectra, respectively. The X-ray studies confirm the assumption that most of the deformation upon extension of the fibres has to happen in the amorphous regions of the silk. The neutron results indicate that the externally applied force is not reflected by any noticeable effect in the molecular vibrations or translational/reorientational diffusion. This observation of unaffected molecular dynamics is in agreement with a model of entropy elasticity.

Considerable interest has existed for a long time in mimicking biological high-performance polymers for their extraordinary mechanical properties. Silk fibres, including those with the most outstanding mechanical properties such as spider dragline, consist of a protein composite structure made out of crystalline and amorphous regions. Spider and silkworm silk fibres are morphologically very similar, and the superior mechanical properties of spider dragline are assigned to a 'higher quality' spinning process [1].

We have carried out complementary experiments to address the question how the mechanical properties of dry silkworm silk are governed by the amorphous regions and whether they can be explained by a model related to entropy elasticity that is well-established for rubber [2].
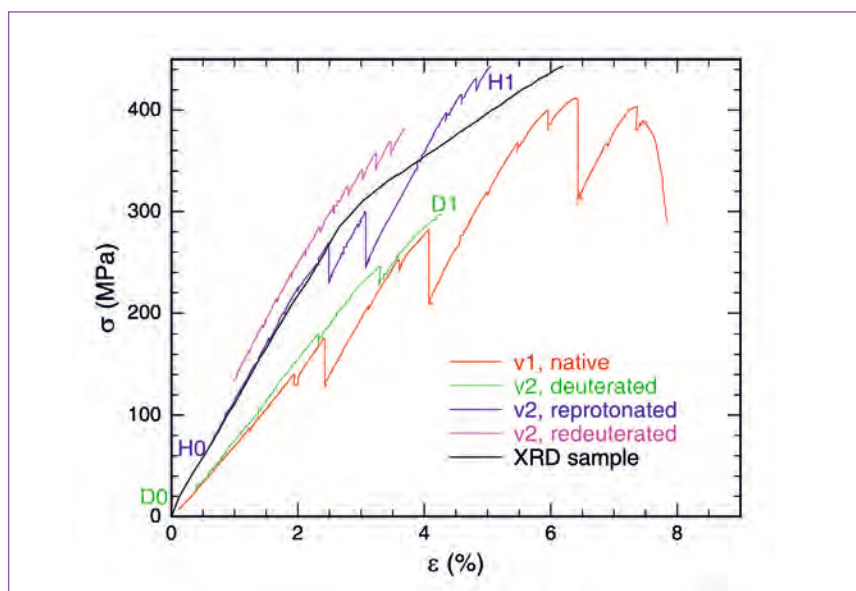
Figure 1: Stress (tensile force per cross section area) σ of the Bombyx mori silk fibre bundles measured in situ, using two samples v1 and v2, during the neutron scattering experiments at IN6 plotted versus the strain (relative elongation) ε. For comparison, the stress-strain curve of the X-ray diffraction experiment (XRD sample) on 3 double strand bundles is displayed as well. The sample v2 was deuterated, subsequently protonated ('reprotonated'), and again deuterated ('redeuterated') in the course of the experiment. The data displayed in figure 2 were recorded at the positions marked D0,D1 on the deuterated sample and H0,H1 on the reprotonated sample.

Authors

T. Seydel and M. Koza
(ILL)
**K. Kölln, I. Krasnov, I. Diddens,
N. Hauptmann, G. Helms,
M. Ogurreck, S.-G. Kang
and M. Müller**
(IEAP, University of Kiel, Germany)
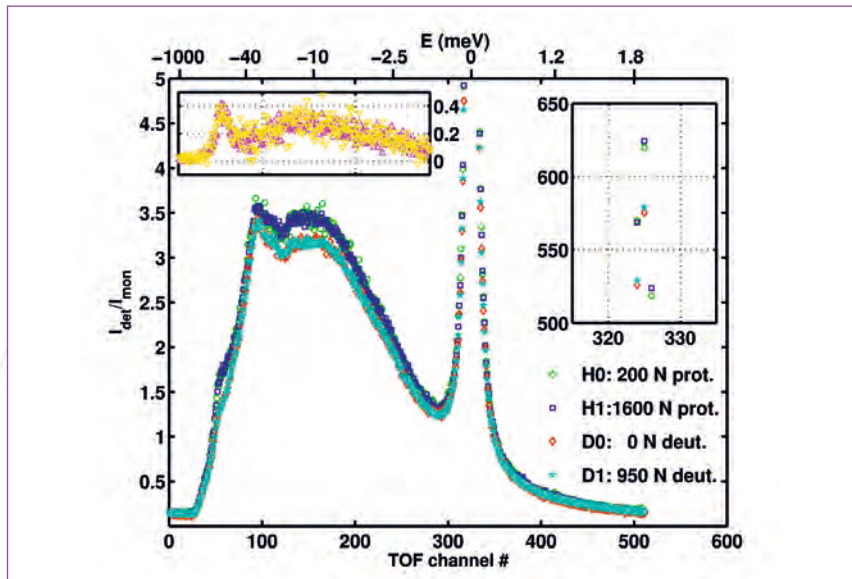
Figure 2: *Time-of-flight spectra of Bombyx mori silk recorded on IN6 (λ=5.1Å) plotted versus the time-of-flight channel number (corresponding energy transfer as top axis). Right inset: elastic peak maxima using the same axis units as in the main figure. Left inset: difference spectra from the protonated and deuterated sample using the same time-of-flight and energy axis as in the main part of the figure; Δ-symbols: difference between the protonated sample at 1600 N and the deuterated sample at 950 N (H1-D1); ∇-symbols: difference between the reprotonated sample at 200 N and the deuterated sample at 0 N (H0-D0).*

This central question translates into the experimentally accessible question whether or not an externally induced strain has a measurable effect on chemical bonds in the amorphous regions. The absence of such an effect would be an argument for the model of entropy elasticity even in dry silk. An adequate method to address this question by probing the predominant hydrogen bonds in silk fibres is provided by neutron time-of-flight spectroscopy. This method gives information on vibrational modes in the meV energy transfer range. In addition, a diffraction pattern is recorded *in situ* and reveals any structural changes as a function of tensile strain. In the particular case of silks, predominantly only the amorphous regions are accessible to guest molecules such as water. A selective residual deuteration of these regions has thus been obtained in our experiment by immersing the

samples in heavy water and a subsequent drying process. The neutron spectroscopy experiment has been complemented by *in situ* synchrotron X-ray diffraction measurements on silk fibre bundles upon tensile strain. The X-ray experiment provides information on the structural changes in the silk fibre upon the externally applied strain. In particular, the morphological changes in the crystalline regions can thus be quantified with a high accuracy, and indirect conclusions on the disordered regions can be drawn.

In the neutron spectroscopy part of our study [3], we have used two **Bombyx mori** silkworm silk samples, namely v1 and v2, with masses of the order of 300mg each, which we have spun on steel hooks attached to a computer-controlled tensile machine. This machine enabled a tensile force of up to 2500 N to be applied to the

sample *in situ* during the acquisition of the neutron spectra, with the direction of the force being vertical, i.e. perpendicular to the scattering plane of IN6. The corresponding stress-strain history recorded on our samples is displayed in **figure 1**. We have recorded spectra on both protonated and deuterated samples at nearly no tensile force (H0, D0) as well as at a tensile force near or beyond the yield point of plastic deformation (H1, D1). These spectra are displayed in **figure 2** after a normalisation to the incident beam flux and illuminated sample volume, taking into account the change of this volume due to the different fibre extension upon the externally applied stress. The intensities recorded in all detectors within the equatorial plane have been summed up. The essential observation is that only the deuteration alters the spectra, whilst there is no difference between the spectra with or without applied force (**figure 2**).

From our experiments we conclude that the amorphous regions of silk fibres are of major importance for the mechanical properties. In particular, the X-ray diffraction results [3] show that they account for most of the extensibility of silk fibres. By selective deuteration of the water-accessible regions of silk, which we could identify with the amorphous parts, their response to tensile stress was measured with neutron spectroscopy. According to our results the molecular vibrational or reorientational response in the silk fibres is independent of the externally applied stress, in agreement with the phenomenon of rubber elasticity.

References

[1] *Z. Shao and F. Vollrath,
Nature 418 (2002) 741*

[2] *J.M. Gosline, M.W. Denny
and M.E. DeMont, Nature 309 (1984) 551*

[3] *T. Seydel et al.,
Macromolecules 40 (2007) 1035*

Order causes quasi-forbidden Bragg peaks in soft materials

Scattering techniques are one of the most powerful experimental tools in soft condensed matter. It was noted [1] early that soft materials that had been ordered and aligned in external fields exhibited Bragg peaks which could not be indexed assuming a single homogeneous crystal structure. Their origin was attributed to changes in the crystal structure induced by the external field. Such structural defects comprise changes in layer stacking, phase coexistence, twinning, unit cell distortions, specific multi-grain arrangements or multiple diffraction. Field-induced structural defects would seriously limit the use of external fields to generate ordered soft materials for applications where homogeneous order and orientation are critical such as in the preparation of photonic crystals or nanostructured magnetic or semiconducting materials.

Highly ordered soft materials exhibit Bragg peaks that are difficult to index assuming homogeneous crystal structures. Their origin had been attributed to changes in the crystal structure induced by the ordering process. We demonstrate that these Bragg peaks are an inherent property of homogeneous ordered soft materials related to the finite coherence of their crystalline lattice. This consideration allows a detailed and quantitative analysis of the diffraction patterns of seemingly unrelated materials such as lyotropic liquid crystalline phases, mesoporous materials, colloidal dispersions, block copolymers, electro-rheological fluids, and photonic crystals.
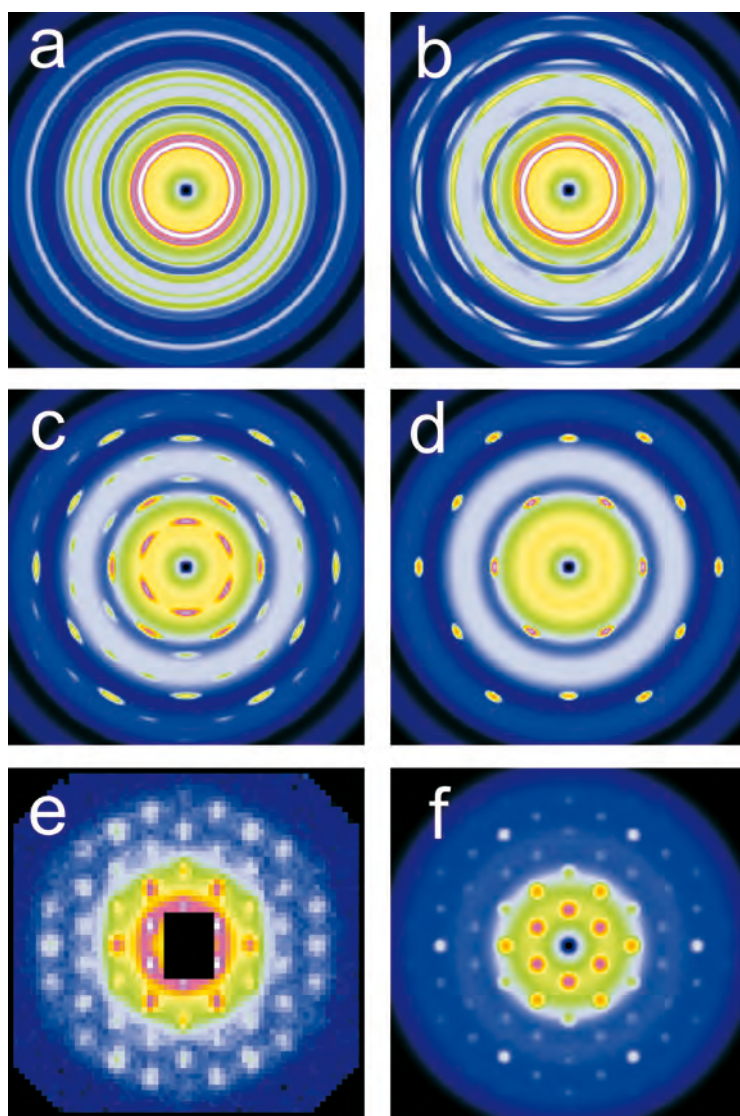
Figure 1: Evolution of Debye-Scherrer rings (**a**), into Bragg peaks (**d**) upon increasing the orientational and translational order of an fcc-lattice with unit cell dimension of $a = 42.5\,nm$ (**a**: $l_t = 0.1\,nm \rightarrow$ **b**: $l_t = 30\,nm \rightarrow$ **c**: $l_t = 80\,nm \rightarrow$ **d**: $l_t = 150\,nm$). At intermediate states of order (**b**, **c**) the diffraction patterns show a large number of allowed and quasi-forbidden Bragg peaks. (**e**) shows a small-angle neutron scattering pattern typical for the intermediate state measured at D11 together with a theoretical calculation (**f**).

Authors

**C. Schellbach, A. Timmann,
A. Frömsdorf and S. Förster**
(University of Hamburg, Germany)
P. Lindner
(ILL)
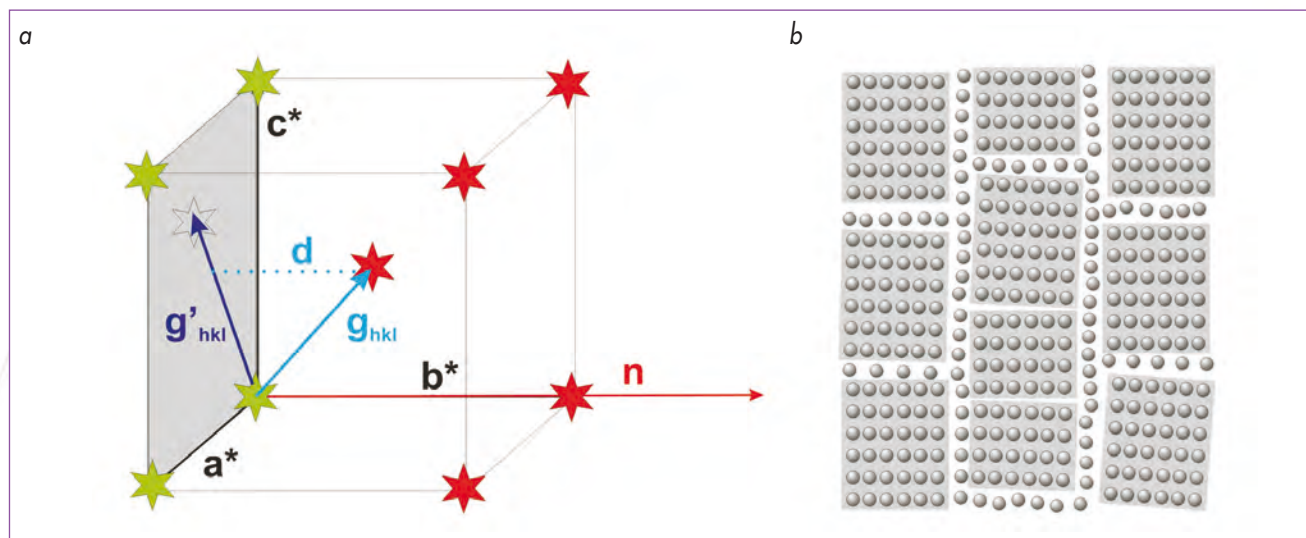
Figure 2: (a) Ewald plane construction to illustrate the origin of quasi-forbidden Bragg peaks. The incoming beam direction n is parallel to the b*-axis of the reciprocal unit cell. All reciprocal lattice points (green) located on the (a*,c*)-plane (Ewald plane) fulfill the Bragg condition and lead to allowed Bragg peaks. All other reciprocal lattice points (red) do not fulfill the Bragg condition, but can lead to quasi-forbidden Bragg peaks if their peak width is of the order of the distance d to the Ewald plane. (b) Schematic model of a mosaic-like assembly of tilted crystalline domains with phase-destroying defects at their boundaries. The finite dimension and angular tilt of the domains leads to a finite coherence resulting in broadening of the Bragg peaks.

We demonstrate that such unexpected Bragg peaks are characteristic for ordered homogeneous, macroscopically oriented soft materials. Their origin is related to the softness of the interaction potential, which on one hand allows spontaneous ordering by tolerating imperfections of the constituent structures, but on the other hand also tolerates imperfections that limit the coherence of the crystalline lattice. This is shown by a combination of scattering experiments (neutron and synchrotron X-ray diffraction), direct imaging (scanning electron microscopy), and model calculations. It explains the presence of unexpected Bragg peaks in seemingly unrelated materials such as lyotropic liquid crystalline phases, mesoporous materials, colloidal dispersions, block copolymers, electrorheological fluids, and photonic crystals since these materials are either soft or have been prepared from soft material precursors [2].

The effect of finite lattice coherence is related to the fundamental question of how Debye-Scherrer rings transform into Bragg peaks if an originally isotropic multi-domain structure is oriented in a particular direction. Intuitively, one would expect Debye-Scherrer rings that correspond to (hkl)-lattice planes which are forbidden in this direction to gradually disappear, whereas Debye-Scherrer rings that correspond to (hkl)-lattice planes that are allowed are expected to gradually develop Bragg peaks. Eventually, all Debye-Scherrer rings would disappear and only allowed Bragg peaks would remain. The calculations show, however, that there exists a broad intermediate state, where all Debye-Scherrer rings – even those that correspond to forbidden (hkl)-lattice planes – develop Bragg peaks (figure 1a-c). Eventually, at higher orientations the Bragg peaks that belong to forbidden (hkl)-lattice planes lose intensity and disappear (figure 1d).

At the ILL the lattice structure of soft materials has been investigated by shear alignment experiments, using the specialised Bohlin CVO rheometer with the Searle type shear cell at the small-angle neutron scattering (SANS) instrument D11. As a prototype soft material a lyotropic liquid-crystalline fcc phase of block co-polymer micelles (PI-PEO at a concentration of 17 %wt in D_2O) was used. Before shear orientation the sample was isotropic, showing a scattering pattern with a series of Debye-Scherrer rings (similar to the ones showed in figure 1a). Above a shear rate of 100 s^{-1}, the sample shear-oriented and developed a diffraction pattern typical for the intermediate state (see figure 1e) which agrees very well with theoretical calculations (figure 1f).

The origin of the quasi-forbidden Bragg peaks can be explained by using the Ewald sphere construction. For a particular Bragg peak the observed peak intensity depends on the peak position and the peak width relative to the Ewald sphere, which for small-angle diffraction can be well approximated by a plane such as shown in figure 2. All reciprocal lattice points that are located on this plane fulfill the Bragg condition and give rise to allowed Bragg peaks. All other reciprocal lattice points located at distances d away from the plane do not fulfill the Bragg condition. If, however, the peak width δ of the peaks related to these lattice points are of the order of the distance d, then these reciprocal lattice points will (partly) fulfill the Bragg-condition leading to quasi-forbidden Bragg peaks. With increasing order and decreasing peak width, these Bragg peaks will decrease in intensity and will eventually disappear, as seen in figure 1.

The consideration of lattice coherence and peak width allowed us for the first time to quantitatively interpret diffraction patterns from shear ordered soft matter.

References

[1] B.J. Ackerson, J.B. Hayter, N.A. Clark and L. Cotter, J.Chem.Phys. 84 (1986) 2344

[2] S. Förster, A.Timmann, C. Schellbach, A. Frömsdorf, A. Kornowski, H. Weller, S.V. Roth and P. Lindner, Nature Materials 6 (2007) 888

Photosensitive gelatin

Employing photodestructible surfactants in gelatin-based aqueous gels presents novel possibilities for controlling colloidal and aggregation properties. Light-triggered breakdown of the gelatin-bound photosurfactant aggregates causes dramatic changes in viscosity and aggregation.

Gelatin is a commodity chemical owing to low-cost, gel-forming, film-forming and surface-active properties. Amongst other applications in food and formulations, gelatin is an important component of photographic emulsions. In such complex systems surfactants are also added, and these interact with gelatin forming surfactant-gelatin complexes (SGCs), which influence surface tension and rheology during coating and wetting processes. As such SGCs have received considerable attention because of their ability to impart significant changes to interfacial, rheological and physiochemical properties [1,2].

Surfactant-gelatin complexes are stabilized by strong electrostatic interactions between anionic surfactant headgroups and cationic residues on the gelatin strands. Physical cross-linking of gelatin strands by micelles has been used to explain significant increases in viscosity over pure gelatin solutions [1,2]. The system composition, as well as temperature, strongly influences the rheological and aggregation behaviour.

Here it is shown that SGCs can be made light-sensitive by introducing a photodestructible surfactant, and then incident UV light can be used to control viscosity and aggregation. Breakdown of the photo-degradable surfactant sodium 4-hexylphenylazosulfonate (C6PAS) via UV has been shown to affect colloid and interface properties [3], since two non-surface active photoproducts are formed.

After UV irradiation the physical appearance of the C6PAS-containing SGCs changed: samples turned from yellow to brown owing to the photochemistry of C6PAS, and there was an obvious reduction in viscosity (**figure 1**) [4].

Viscometry and small-angle neutron scattering (SANS) on D22 (**figure 2**, **table 1**) analyses have been employed to study changes in viscosity and aggregation properties of the photosensitive SGCs [4].

Figure 1: Physical appearance of 10 wt% gelatin plus 0.03M C6PAS samples at 41°C before (lower sample) and after irradiation (top).

Authors

A. Vesperinas and J. Eastoe
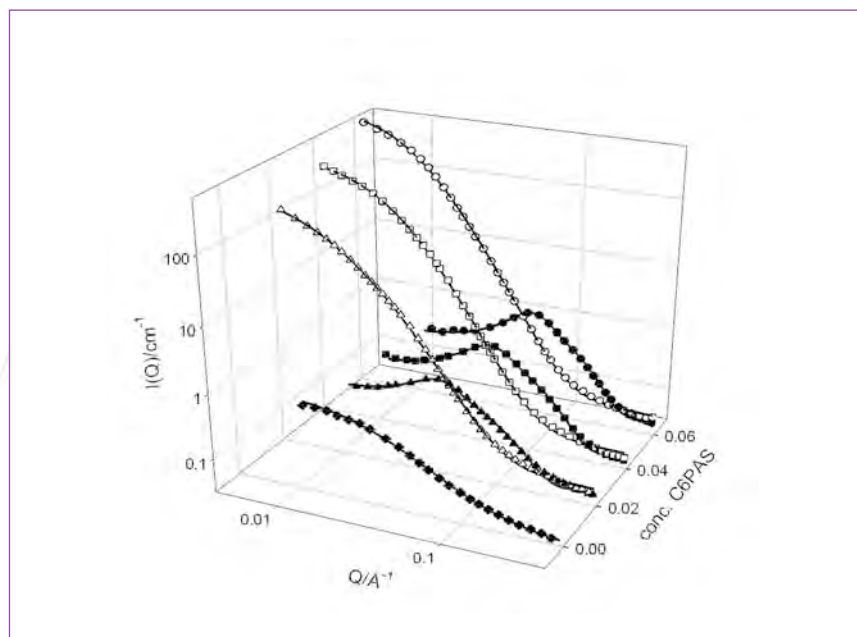(University of Bristol, UK)
I. Grillo
(ILL)

Figure 2: *SANS data from D22 and model fitting analyses for 5% gelatin (♦) and a series of C6PAS-SGCs in D₂O. Before irradiation filled, and after irradiation empty markers.*

Non-irradiated			
C6PAS Conc	R_1 (Å)	R_2 (Å)	Micelle charge
0.02	17	82	30
0.04	16	62	17
0.06	15	54	16

UV irradiated		
C6PAS Conc	t (Å)	
0.02	110	
0.04	180	
0.06	290	

Table 1: *Fitted parameters for SANS from 5 wt% gelatin C6PAS SGCs. R_1 and R_2 are ellipsoid radii and t is the sheet thickness.*

As shown in **figure 2**, in the presence of C6PAS the initial scattering at low Q seen for gelatin alone (♦) disappeared, which suggests that gelatin has undergone a dramatic change in configuration on complexation with the photosurfactant. Prior to irradiation the scattering profile changes progressively with increasing surfactant concentration, and these pre-UV data could be fitted as charged ellipsoidal micelles [4].

There are two distinct micellar environments in SGCs: micelles bound on the gelatin strands and free aggregates in the background solvent [1,2]. Hence, the ratio of free to bound micelles depends on the surfactant concentration. The apparent increase in micelle size with decreasing surfactant concentration is due to surfactant micelle binding to gelatin. However, in the most concentrated sample there are no obvious contributions of gelatin to the overall scattering. This is consistent with a saturation of the gelatin network and as consequence more C6PAS is present as background equilibrium micelles in the water.

After irradiation the aggregation increases and the changes are consistent with a transition from ellipsoidal charged micelles to extended sheet-like aggregates. For the post-irradiated C6PAS-SGCs strong logarithmic scattering is observed, which may be accounted for by a model for monodisperse, randomly-oriented lamellar stacks. As shown in **table1** there is apparently a growth in stack thickness with concentration.

A novel approach to control rheological and aggregation properties of aqueous gelatin-containing systems has been presented. The use of UV as a rheo-structural trigger means the transitions can be induced externally, without need for gross changes in thermodynamic or internal composition variables. Photodegradation of C6PAS in gelatin presents a novel approach to controlling aqueous gel properties with possible applications requiring rheological switches. Further details can be found in reference [4].

References

[1] J. Greener, B.A. Contestable and M.D. Bale, *Macromolecules* 20 (1987) 2490

[2] T. Cosgrove, S.J. White and A. Zarbakhsh, *Langmuir* 11 (1995) 744

[3] J. Eastoe and A. Vesperinas, *Soft Matter* 1 (2005) 338

[4] A.Vesperinas, J. Eastoe, P. Wyatt, I. Grillo and R.K. Heenan, *ChemComm.* (2006) 4407

Supercritical carbon dioxide - microemulsions as precursors for nano-foams: study of microstructure

We studied the microstructure of supercritical carbon dioxide ($scCO_2$) microemulsions, i.e. thermodynamically stable, nano-structured, but macroscopically homogeneous mixtures of water, surfactant and $scCO_2$. These $scCO_2$-microemulsions can be used as starting material for the production of polymer foams with nanometre-sized pores, which are expected to be good thermal insulators because the convection of the gas that fills the pores is suppressed (Knudsen effect). Until now such nano-foams can only be produced by an elaborate sol-gel process yielding nano-structured, but expensive aerogels.

Figure 1: Picture of an inorganic nano-foam: an aerogel (source: NASA).

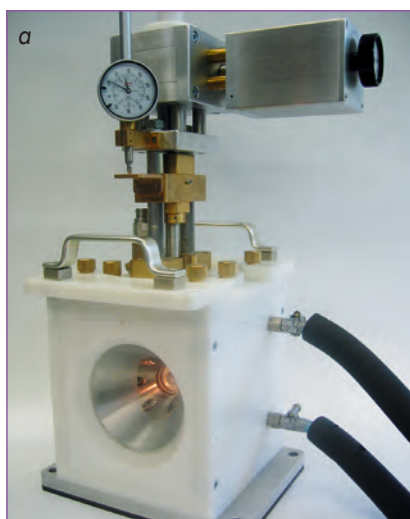Figure 2: (a) The high-pressure SANS sample holder (volume: 10 cm³, temperature range: 0 - 80°C, pressure range: 1 - 300 bar). (b) The cell is dismounted from the neutron beam of D11 for preparing a new sample. The pivot-mounted holder for the high-pressure cell is shown in the foreground.
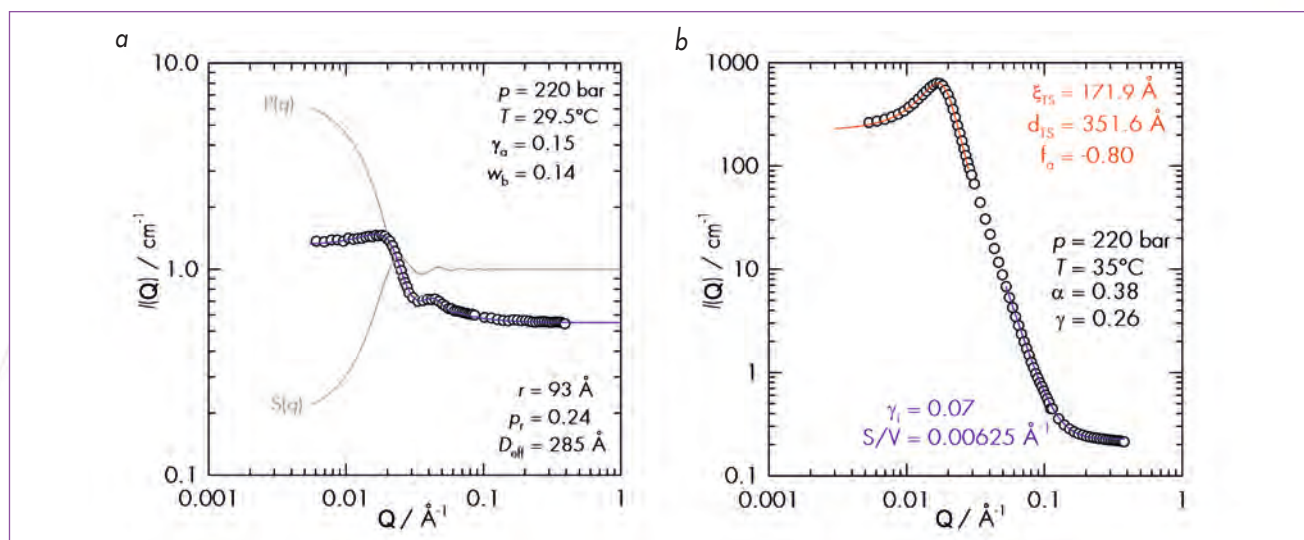
Authors

**L. Kramer, T. Sottmann
and R. Strey**
(University of Cologne, Germany)
P. Lindner and R. Schweins
(ILL)

Figure 3: (a) Scattering curve of a water-rich microemulsion of the type $D_2O/NaCl$ - CO_2 - Lutensol XL60/Zonyl FSN-100 at the CO_2efb. The shape of the curve points to the existence of spherical droplets. P(Q) and S(Q) are the form and structure factors fitted to the scattering curve. (b) Scattering curve of a microemulsion of the type $D_2O/NaCl$ - $scCO_2$ - Zonyl FSN-100/Zonyl FSH containing equal volumes of D_2O and $scCO_2$.

To improve this situation, i.e. to produce low-cost, nano-structured polymer foams, Strey and coworkers have proposed the 'Principle Of Supercritical Microemulsion Expansion (POSME)' [1]. The starting point of this approach is the formulation of microemulsions that contain nano-sized spherical micelles swollen by a supercritical fluid in a water/monomer mixture (number density up to 10^{19} cm^{-3}). For the formation of the foam, the polymerisation of the monomers will be initiated, and the mixture will be expanded. Having chosen supercritical conditions, the density of the expanding supercritical fluid decreases continuously from a liquid-like to gas-like density. Consequently the nucleation of bubbles and a rupture of the nano-porous structure of the curing polymer are avoided, conserving the microstructure of the microemulsion during the formation of the foam. Carbon dioxide was used as supercritical fluid because it is nontoxic, non flammable, cheap and has convenient values of the critical temperature and pressure, T_c = 31.6° C, p_c = 71 bar.

The aim of the SANS experiments was to prove the existence of the nanometre-scaled structure of the $scCO_2$-microemulsion. To perform these experiments we developed a new high pressure cell with variable cell volume with the instrument team of D11, to ensure that the cell is compatible with the geometry of D11 and D22 (figure 2).

This stainless-steel cell is equipped with two large sapphire windows (diameter 16 mm, thickness 12 mm), for observing the phase behaviour of the samples. Pressures of up to 300 bar can be applied, while the temperature can be varied within the range 0 to 80 °C.
Several SANS experiments on water-in-$scCO_2$ microemulsions have been performed by Eastoe and co-workers [2]. However, this newly developed high-pressure SANS sample holder allows for the first time the proof of bicontinuous structured $scCO_2$-microemulsions. Furthermore, we could record the spectra of $scCO_2$-droplets-in-water microemulsions.
Figure (3a) shows the film contrast scattering curve of a sample containing nearly-$scCO_2$ (14 wt.%), the hydrophilic components $H_2O,D_2O,NaCl$ (71 wt.%) and the surfactants Lutensol XL60, Zonyl FSN-100 (15 wt.%) at p = 220 bar and T = 29.5 °C. The scattering curve exhibits the typical features observed in spectra of polydisperse spherical shells. Consequently, the scattering curve was analysed using the form factor of polydisperse spherical shells P(Q) and the Percus-Yevick structure factor of hard spheres S(Q) [3]. The analysis points to the existence of slightly polydisperse $scCO_2$-nanodroplets (polydispersity index p_r = 0.24) with a radius of r = 93 Å.

Figure (3b) shows the bulk contrast scattering curve of a sample containing $scCO_2$ (38 wt.%), the hydrophilic components $D_2O/NaCl$ (36 wt.%) and the surfactants Zonyl FSH, Zonyl FSN-100 (26 wt.%) at p = 220 bar and T = 35 °C. The scattering curve exhibits the typical features observed in spectra of bicontinuous structured samples. Analysing the peak of the scattering curve revealed the average 'diameter' of $scCO_2$ domains to be $d_{TS}/2$ = 176 Å [4]. The mass fraction γ_i = 0.07 of surfactant molecules in the internal interface was determined by analysing the large-Q part of the scattering curve [5]. This means that 2/3 of the applied surfactant is dissolved in $scCO_2$ in monomeric form and is thus not available for forming the internal interface between water and $scCO_2$.

References

[1] R. Strey, T. Sottmann and M. Schwan, Patent No. WO2004058386 (2002)

[2] J. Eastoe, A. Dupont and D. C. Steytler, Curr. Opin. Coll. Int. Sci. 8 (2003) 267

[3] J. K. Percus and G. J. Yevick, Phys. Rev. 110 (1957) 1

[4] M. Teubner and R. Strey, J. Chem. Phys. 87 (1987) 3195

[5] G. Porod, in Small-Angle X-ray Scattering, O. Glatter and O. Kratky Eds., Academic Press (1982) 18

How ice melts under pressure

We all know that the melting curve of ice is odd: under pressure it decreases, reaching -25 °C at 2 kbar. New measurements on the time-of-flight instrument IN6 shed light on the microscopic origin of this anomaly – and its relation to what happens at very low temperature under pressure, i.e. the transition to an amorphous state under pressure.
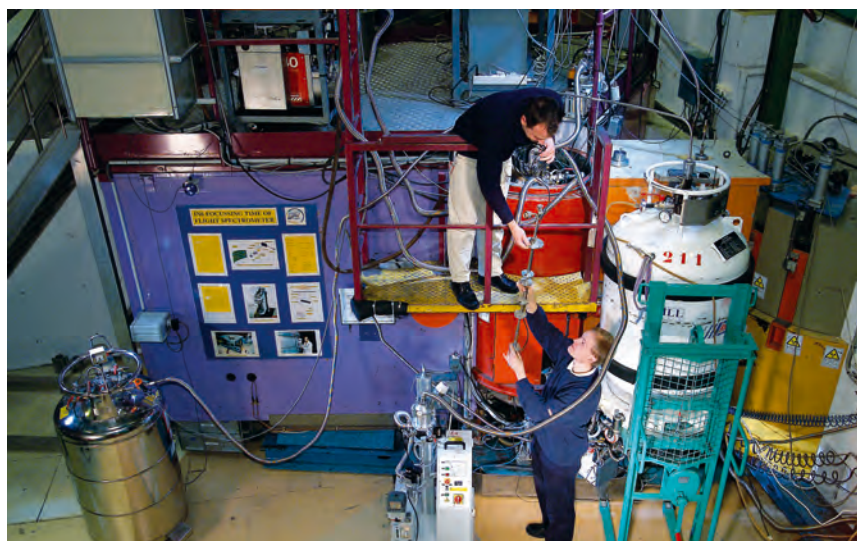
The time-of-flight instrument IN6.
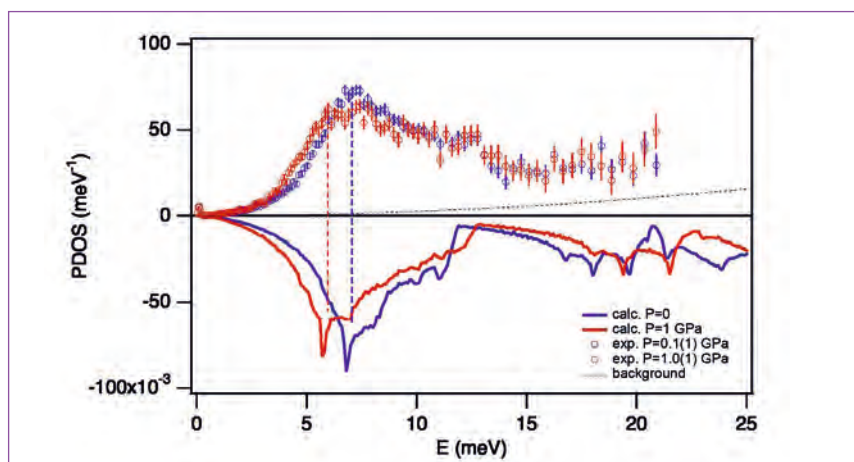
Figure 1: Phonon density of states (PDOS) measured at IN6 (circles) at low and high pressure (0 and 1 GPa), respectively. The lower curves are predictions from a lattice dynamical model derived from phonon dispersion measurements under pressure to 0.5 GPa. Note the pressure-induced shift to lower energies for phonons below 12 meV.

Authors

S. Klotz and G. Hamel
*(IMPMC, CNRS-UMR 7590,
Université P.& M. Curie, Paris, France)*
T. Strässle
*(LNS, ETH Zurich
and PSI Villigen, Switzerland)*
M.M. Koza and H. Schober
(ILL)

One of the curious properties of ice is that it floats on its liquid, or, expressed in another way, that its melting line *decreases* under pressure. Indeed, at 2 kbar, ice melts at -25° C. Since melting occurs when the thermal motion of the molecules exceeds a certain fraction of the interatomic distance (the so-called 'Lindemann criterion' [1]), a negative melting line means that the thermal motion in ice *increases* under pressure. This is highly anomalous; a normal solid becomes 'stiffer' under pressure, i.e. the thermal displacements *decrease*. Since the thermal displacements are dominated by the contribution from acoustic phonons, it was predicted that the increase in thermal motion should show up in a red-shift of the entire phonon density of states (PDOS) below ~ 12 meV.

Recent measurements on IN6 at 80 K using the newly available Paris-Edinburgh pressure cell confirm this prediction and provide a vibrational spectrum which is close to predictions obtained by a Born-von Kármán model (**figure 1**) [2]. Such experiments were up to now not feasible since they require high pressure equipment which allows the compression of ice *in situ* at low temperature, and to high pressure to at least 1.5 GPa (15 kbar, **figure 2**).

These data are a direct signature of the increase of the thermal parameters in ice with pressure, and application of the Lindemann criterion indeed gives a negative melting line which is close to the measured one [1]. For pressures beyond ~ 1.2 GPa, ice transforms into high-density amorphous ice (HDA), and the data show that the phonon density of states returns to normal behaviour, i.e. the low-energy tail is shifted to higher energy under pressure.

The data also reveal another interesting detail: if the temperature is sufficiently low, melting by an increase of thermal motion (thermal melting) is governed by a different mechanism of breakdown of the crystal structure. In fact, the red-shift of the PDOS is caused by the softening of various transverse acoustic phonons, and hence some elastic constants. To maintain a crystal stable, certain elastic constants or a combination of them have to fulfil specific conditions, the famous Born stability criteria [3].

Figure 2: Picture of the ILL Paris-Edinburgh press attached to its dedicated CCR. The systems allow measurements up to 10 GPa in the temperature range 3.5-300 K.

It turns out that in ice at temperatures below ~ 100 K, the crystal structure does no longer disintegrate because the pressure-induced thermal motion becomes too large, but because Born's stability criteria are no longer fulfilled. Moreover, an entire transverse acoustic phonon branch is found to become uniformly soft, leading to a frustrated lattice instability and so-called 'mechanical melting'.

There seems therefore to be a crossover between thermal ('normal') melting at high temperatures and mechanical melting at low temperatures in ice under pressure. The disordered solids obtained in each case are likely to be different, since they arise through different mechanisms. Amorphous ice obtained by compression at low temperatures (77 K) is therefore expected to be inherently defective. Strong relaxation effects are indeed observed and well documented, when as-prepared amorphous ice is warmed under pressure to above the crossover temperatures.

The IN6 study therefore provides a comprehensive understanding of these phenomena.

References

[1] F.A. Lindemann, Phys. Z. 14 (1910) 609

[2] Th. Strässle et al., Phys. Rev. Lett. 99 (2007) 175501

[3] M. Born and K. Huang, Dynamical Theory of Crystal Lattices (Clarendon, Oxford, 1954)

Hydration of divalent mercury in aqueous solution

3

Mercury is one of the most hazardous pollutants: exposure to mercury-containing toxic compounds leads to severe poisoning. Mercury is a cumulative heavy metal poison which can occur as elemental mercury, inorganic salts and complexes (Hg^{2+}, $HgCl_2$, $Hg(OH)_2$) or as organomercury compounds (like mono-and di-methyl mercury). Neutron diffraction with isotopic substitution (on the diffractometer D4) allows us to study the coordination of Hg^{2+} by water and to understand its behaviour in natural systems.
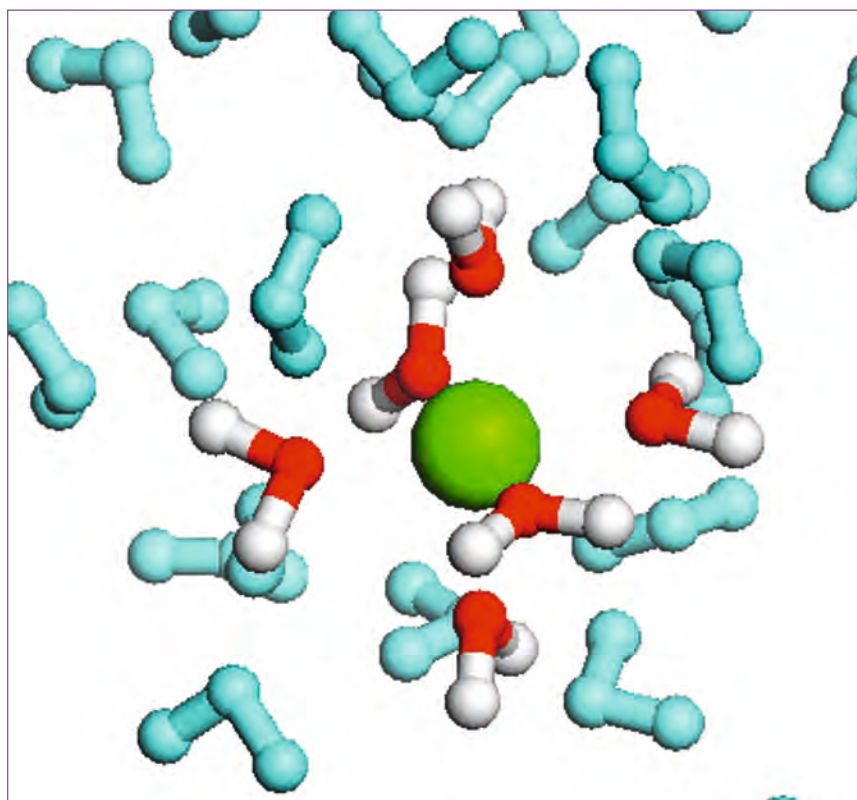
Figure 1: Schematic of water coordination of Hg^{2+}, showing 6-fold hydration.

The effect of exposure to elemental mercury or some of its compounds depends on their absorption and metabolism [1]. However, with sufficient exposure all mercury-based toxins damage the central nervous system and other organs or systems such as the liver or the gastrointestinal tract.

The majority of mercury pollution comes from industrial emission, which has steadily increased since the 19th century, especially from the burning of fossil fuels – particularly high-sulphur coal. Other industrial sources include mercury mining and smelting, chloralkali process plants, and organic mercurial pesticides. Improper disposal of mercury-based waste can also lead to mercury exposure, e.g., after an elemental mercury spill in military sites or following improper disposal of fluorescent light bulbs. Other sources of mercury vapour include crematoriums, waste incinerators, and volcanoes.

Mercury exposure can also occur by ingestion of contaminated food. The consumption of fish is by far the most significant source of ingestion-related mercury exposure in humans, due to the magnification of methyl mercury in the food chain. Plants and livestock may also contain mercury due to uptake from soil, water and atmosphere, and due to ingestion of other mercury-containing organisms.

Mercury and many of its chemical compounds, especially organomercury compounds, can also be readily absorbed through direct contact with bare skin, or in some cases (such as di-methyl mercury) insufficiently protected skin. Mercury and its compounds are commonly used in chemical laboratories, hospitals, dental clinics, and facilities involved in the production of items such as fluorescent light bulbs, batteries, and explosives.

Authors

G.J. Cuello (ILL)
O. Sobolev and L. Charlet
(LGIT, University of Grenoble and CNRS, France)
G. Román-Ross
(University of Girona, Spain)
N.T. Skipper
(University College London, UK)
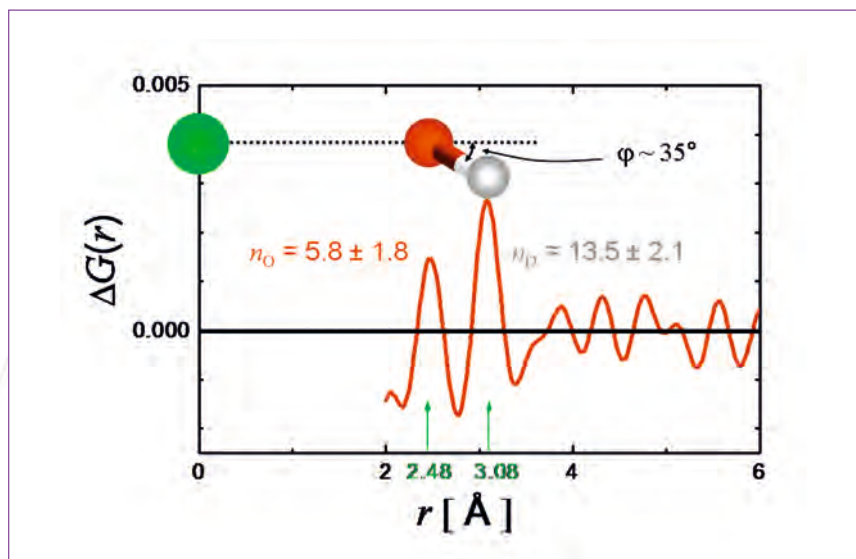
Figure 2: *The pair correlation function ΔG(r) centred at the Hg^{2+} ion (green circle). The water molecule position is shown, as well as the tilt angle.*

Salts of Hg^{2+} are much more common and stable in the environment than Hg^+ salts and water is the main medium for Hg^{2+} transport and interaction with biological objects. Taking into account the neurotoxic effect of mercury, the study of the interaction between divalent mercury and water molecules becomes important. Indeed, the function of the nervous system is based on electric signals caused by ions moving in and out through the ion channels in cell membranes. The ion channels are able to admit only certain ions, i.e. only those for which the distance to the oxygen atoms in the ion channel is the same as in hydration shell of the cation tailored to the channel (e.g. Ca^{2+}) [2]. Thus, it is important to compare parameters of hydration of mercury with other divalent ions like Ca^{2+}, in order to understand how mercury can penetrate living nerve cells.

The structural parameters of Hg^{2+} hydration have previously been studied by different experimental methods [3], and most of these methods give a water coordination of 6 molecules (**figure 1**). However, there is significant uncertainty about the Hg–O distance, with the experimental results varying in the range 2.33 – 2.42 Å.

Furthermore, no experimental data are available on the Hg–H correlation, which is crucial for determining the orientation of water molecules around Hg, and also for detailed comparison with other divalent cations. Neutrons are particularly useful to study the ion–hydrogen correlation.

With the aim of exploring the water coordination around the Hg^{2+} ion we have conducted neutron diffraction experiments at the D4 diffractometer at room temperature [4]. Two samples with ^{nat}Hg and ^{199}Hg (0.225 mol/L solutions) were prepared from HgO in 1M solution of DNO_3 in D_2O.

The isotopic substitution of Hg allows determination of the pair correlation function $\Delta G(r)$, which is a measure of the probability of finding any atom at a distance r from the Hg atom (**figure 2**). The first two peaks of the $\Delta G(r)$ are attributed to the Hg – O and Hg – D correlations in the first hydration shell of Hg^{2+}. Integration of $\Delta G(r)$ under these peaks gives the number of oxygen and hydrogen atoms around Hg, as shown in figure 2. The combination of n_O and n_D gives the number 6 ± 1 of water molecules

in the first hydration shell of the Hg^{2+} cation. The centres of the first two peaks of the $\Delta G(r)$ correspond to the distances Hg – O and Hg – D. The Hg – O distance observed in the neutron diffraction experiment is larger by about 0.1 Å than that obtained by X-ray diffraction [3]. This difference is caused by the shift of electronic shell of the oxygen towards the mercury cation, since X-rays are scattered by the electronic clouds of atoms and neutrons are only by atomic nuclei; thus the latter find the O atom in a slightly different position relative to the Hg atom. This shift of the electronic density means that the Hg–O interaction is not simply electrostatic, but it is partially covalent.

The parameters obtained for the hydration sphere can be compared with those for Ca^{2+} and Ni^{2+} [3] cations. The angle between the plane of the water molecule and cation–water oxygen axis, which can be calculated from the observed cation–oxygen and cation–hydrogen distances, is approximately the same for Hg^{2+} and the above two ions (around 35°). The Hg–O and Hg–H distances are very close to those obtained for Ca^{2+} cations (2.40 and 3.03 Å for Ca–O and Ca–H, respectively) [5]. This is a key result for the understanding the mercury toxicity: mimicking the Ca^{2+} hydration allows the Hg^{2+} ion to penetrate cell membranes through the Ca^{2+} ionic channels.

References

[1] L.I. Sweet and J.T. Zelikoff, J. Toxicol. Environm. Health 4 (2001) 161

[2] J.J.R. Fraústo da Silva and R. J. P. Williams, The biological chemistry of the elements, Oxford University Press Inc., New York, 2001

[3] H. Ohtaki and T. Radnai, Chem. Rev. 93 (1993) 1157

[4] O. Sobolev, G.J. Cuello, G. Román-Ross, L. Charlet and N.T. Skipper, J. Phys. Chem. A 111 (2007) 5123

[5] Y.S. Badyal, A.C. Barnes, G.J. Cuello and J.M. Simonson, J. Phys. Chem. A 108 (2004) 11819

Neutrons for a dynamical access to mutual arrangement and interactions in molecular liquids

In-depth knowledge of the interactions ruling the dynamics of molecular liquids is crucial to understand their nano-scale properties, also relevant to active fields as biology and alternative-fuel engineering. A dynamical approach to the interactions in polyatomic fluids long remained unattempted. An unconventional use of inelastic neutron scattering and simulations shows how sensitively anisotropic potentials can be discerned, and further reveals the molecular-pair geometry favouring the observed dynamics: a technique, first applied to methane, acting as a prototypical dynamical nanoscope of molecular liquids.

Authors

E. Guarini, F. Barocchi, M. Sampoli and G. Venturi
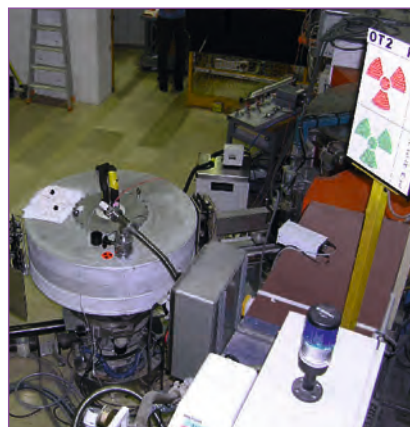*(University of Florence, Italy)*
U. Bafile
(CNR-ISC, Florence, Italy)
F. Formisano
(CNR-INFM/OGG, Grenoble, France)
F. Demmel
(ILL, presently RAL, UK)

Neutron experiments in rare-gas fluids and liquid metals, combined with computer simulations and/or theory, clearly showed that many, even weak, interaction properties (short- and long-range, two and three-body) can be probed by exploiting structural and dynamical data. In the more complex case of molecular liquids, inelastic neutron scattering access to the interaction law has never been attempted. Indeed, existing studies of the dynamic structure factor $S(Q,\omega)$ of polyatomic fluids typically focus on the collective properties alone. Thus, the important opportunity to draw deeper information on the interactions in molecular liquids from the dynamical spectra is still to be seized.

A dynamical approach can be much more incisively probing than a static study, since spectral shapes supply more stringent tests of trial potential models employed in molecular dynamics (MD) simulations. Increased power of readily available computers combined with improved performance of neutron spectrometers now make in-depth studies of the totally unexplored 'interaction sensitivity' of $S(Q,\omega)$ of molecular liquids possible. We thus combined these two methods to investigate, for the first time, the interaction properties of a simple fluid: liquid methane.

Methane eminently illustrates the complexity of the interaction problem in molecular systems: even for this simple classical fluid of non-polar high-symmetry molecules, several, rather different, site-site potentials are available.

This variety reflects the lack of well-established criteria for model-potential construction already at the level of the simplest molecules.

We thus probed the dynamics of liquid deuteromethane (CD_4) through parallel inelastic neutron scattering measurements on the IN3 spectrometer of the ILL [1], and MD simulations, the latter performed using four different methane potentials, i.e. those of Tsuzuki, Uchimaru and Tanabe (TUT), of Righini, Maki and Klein (RMK), of Strauss *et al.* (SA) and of Rowley and Pakkanen (RP) [2] .

From **figure 1**, showing the neutron and MD spectra of CD_4 at particular Q values, the selective power of $S(Q,\omega)$ neutron data is impressive. Clearly, only the TUT model successfully accounts for the measured spectra, while the RMK potential is very inefficient. The RP and SA results show opposite tendencies with varying Q: RP does not account for the low-Q spectra, while SA, though predicting the low-Q dynamics quite well, increasingly deviates from experiment as Q grows. In fact, experimental and MD data indicate some equivalence between TUT and SA at low Q, and between TUT and RP at high Q.

Our innovative approach is to look for a unique explanation of such results in the features of the various potentials, analyzed for different dimer configurations. **Figure 2** shows the potential-energy curves in three significant CD_4-CD_4 geometries: base-vertex, base-base, and vertex-vertex. The conclusion that only base-vertex pairs produce potential curves compatible with the results of **figure 1** is quite straightforward. Indeed, only the base-vertex case displays the close resemblance of TUT with SA at medium-range, and of TUT with RP in the hard-core region, as witnessed by the Q evolution of the spectra.

These findings not only highlight the joint use of inelastic neutron spectroscopy and simulations as an invaluable and sensitive selection method among anisotropic model-potentials for polyatomic systems, but also represent the embryo of a new nanoscopic technique capable even of discerning which dimer geometry is favoured in the dynamical behaviour of a molecular liquid.
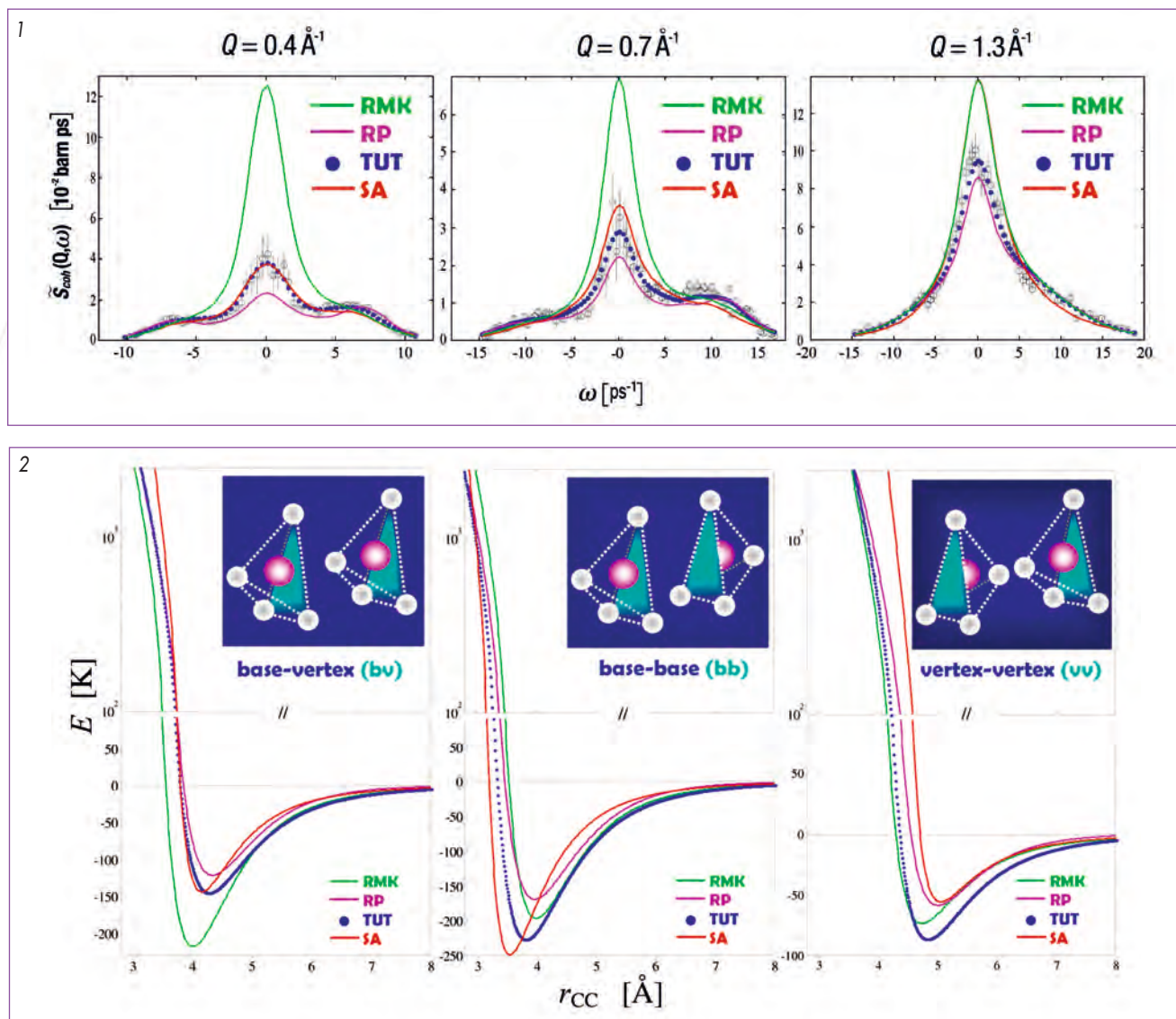
Figure 1: Coherent dynamic structure factor of liquid CD_4 at selected Q values. Neutron data (black circles with error bars) are compared with the corresponding MD results for the SA (red line), RMK (green line), TUT (blue dots) and RP (pink line) potentials. In the right frame, the SA and RMK central peaks coincide.

Figure 2: Three significant configurations of methane pairs (mutual orientation of the methane tetrahedra are sketched in the insets) and corresponding CD_4-CD_4 potential energy, in units of the Boltzmann constant. Different curves refer to the RMK (green), TUT (blue), RP (pink), and SA (red) models, plotted as a function of the carbon-carbon (CC) distance. Different energy scales are adopted to enhance, simultaneously, all the details of the attractive well and of the hard-core region: a linear scale is used for the former, and a logarithmic scale for the latter.

References

[1] E. Guarini, U. Bafile, F. Barocchi, F. Demmel, F. Formisano, M. Sampoli and G. Venturi, Europhys. Lett. 72 (2005) 969-975

[2] E. Guarini, M. Sampoli, G. Venturi, U. Bafile and F. Barocchi, Phys. Rev. Lett. 99 (2007) 167801, 1-4

Large crystals of a perdeuterated protein that inhibits the formation of ice crystals

Arctic fish can swim in waters colder than the freezing point of their blood thanks to the presence of anti-freeze proteins, a class of polypeptides produced by certain vertebrates, plants, fungi and bacteria. This highlight concerns an ongoing high-resolution neutron protein crystallography study of the solvent environment and the anti-freezing mechanism. Preliminary tests at the ILL new Laue diffractometer, LADI-3 show that a relatively small (0.13mm^3) perdeuterated crystal diffracts up to 2 Å resolution. A full neutron Laue data collection is planned and will be used in combination with ultrahigh resolution X-ray data collected at the ESRF.

Anti-freezing proteins (AFPs, also referred to as ISPs: ice structuring proteins) inhibit growth and re-crystallisation of ice that would otherwise be fatal to organisms that live in sub-zero environments. AFPs are hundreds of times more effective at lowering the freezing point than any other known water solute, such as salt.

Figure 1: The arctic fish, ocean pout (Macrozoarces americanus). Picture taken from: http://www.fishbase.org (R. Froese and D. Pauly, Eds.) - Picture credited to: D. Flescher, National Marine Fisheries Service Systematics Laboratory, Woods Hole, MA 02543, USA.
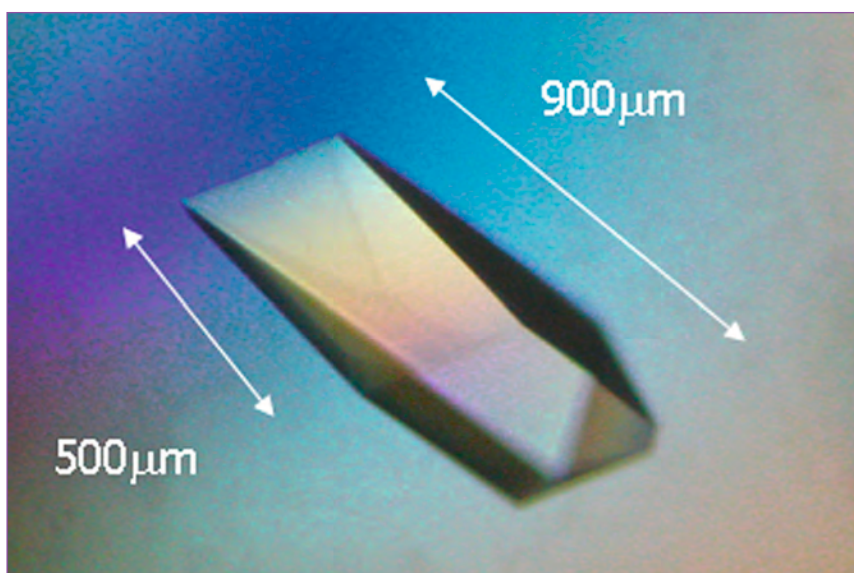
Figure 2: Picture of a perdeuterated AFP crystal taken under polarised light. The crystal volume is approximately 0.13 mm^3. The protein crystallises in space group $P2_12_12_1$ with cell constants a = 32.5 Å, b = 39.4 Å and c = 45.3 Å.

Authors

I. Haertlein, M.P. Blakeley and M. Haertlein
(ILL)
A. Podjarny, A. Mitschler and I. Hazemann
(Institut de Génétique et de Biologie Moléculaire et Cellulaire, Strasbourg, France)
E. Howard
(IFLYSIB, La Plata, Argentina)
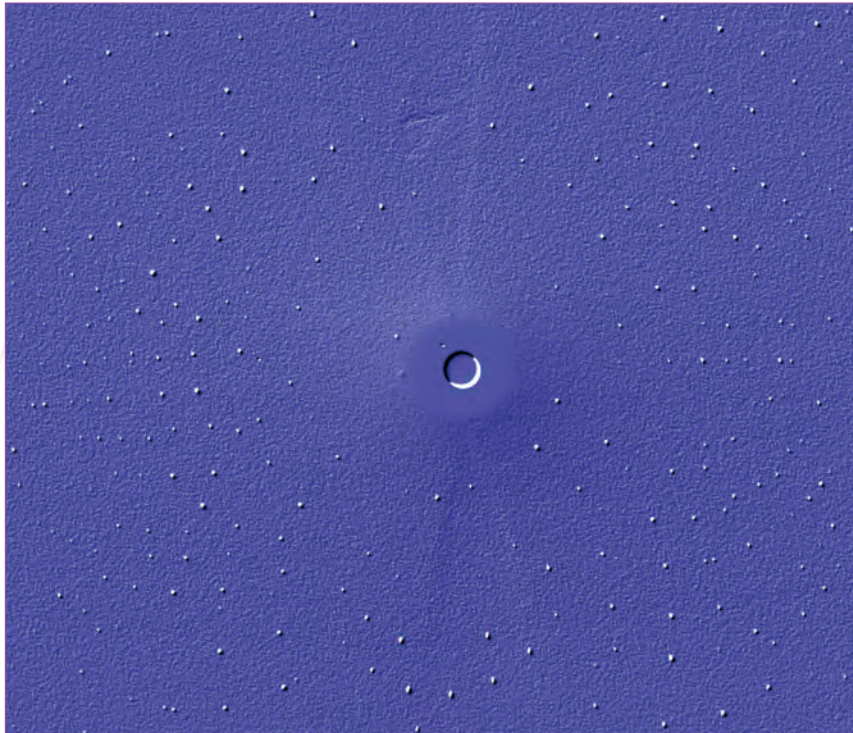
Figure 3: Centre section of a neutron Laue diffraction pattern from perdeuterated AFP using LADI-3.

For example, the ocean pout - *Macrozoarces americanus* (**figure 1**), is an arctic fish which produces AFPs (5-10 mg/ml) that lower the freezing temperature of its blood fluids without decreasing its melting temperature [1].

AFPs work by binding to ice crystal nuclei and inhibiting their further growth. A flat 'Ice Binding Surface' (IBS) has been identified as the possible binder to the ice crystals. Both hydrophobic interactions [2] and specific hydrogen bonds [3] have been suggested to explain this binding. To gain further insight, we intend to use neutron diffraction data to study the protonation states of the residues at the IBS and the orientation of the water molecules in contact with it in fish Type-III AFP.

At the ILL-EMBL Deuteration Laboratory, purified perdeuterated and amino acid-specifically reverse labelled anti-freeze protein has been produced. *M. americanus* AFP has been overexpressed in *E.coli* and crystals of perdeuterated protein have been grown to a volume of 0.13 mm^3 (**figure 2**). In parallel, protocols have been developed for amino acid specific reverselabelling and validated by mass spectrometry analysis at the IBS [4].

Preliminary tests on the new Laue diffractometer, LADI-3, show that the crystal diffracts to 2 Å with 24 h exposures (**figure 3**). By harnessing the improved neutron detection of LADI-3 we can collect data to higher resolution, using shorter exposure times and smaller crystal volumes than previously possible. This is a critical advance for neutron protein crystallography. The technique has become more accessible to the structural biology community by extending the size and complexity of systems that can be studied while lowering the sample volumes required. Ultrahigh resolution X-ray diffraction data (1.05 Å) have been collected at room temperature at the ESRF and will be used in a joint structural refinement with the neutron Laue data.

There is a strong commercial interest in AFPs due to their potential applications, ranging from simply increasing freeze tolerance of crop plants and extending the harvest season in cooler climates to improving cryosurgery. With the study described here we therefore hope to contribute to a better understanding of the anti-freezing mechanism and support the engineering of medical and other applications of AFPs.

These studies also form part of an international collaboration (H. Hauptman, N. Niimura, A. Podjarny) funded by the Human Frontiers Science Program, with the aim to develop new mathematical methods for phasing neutron diffraction data [5]. The AFP samples will be used to study the application of isomorphous replacement methods for the phasing of high resolution neutron scattering data from macromolecular structures.

References

[1] A.C. DeVries, Annu. Rev. Physiol. 45 (1983) 245–260

[2] A. Jorov, B.S. Zhorov, D.S. Yang: Protein Sci. 2004, 13:1524-1537

[3] N. Prabhu, K. Sharp: Chem. Rev. 2006, 106:1616 -1623

[4] http://www.ibs.fr/content/ibs_eng/presentation/platform/Facilities/spectro_masse.htm

[5] H.A. Hauptman, D.A. Langs: Acta Cryst A. 2003, 59:250-254

Neutron scattering reveals cell water dynamics in living organisms

Experiments carried out at the ILL led to the discovery of a new type of water behaviour within the cells of ancient organisms that live in the saturated salt waters of the Dead Sea. These 'salt-loving' cells, called halophiles, are a class of extremophiles, i.e. organisms that require extreme conditions in order to thrive. The study of such extremophiles can teach us a great deal about the properties of certain bio-organisms and their enzymes and the ability of living organisms to adapt to extreme conditions on earth. It may even help us in our search for signs of life on another planet.

Figure 1: The Madaba map is a 6th century floor map from the Church of Madaba, Jordan ('The Madaba Mosaic map' by Michael Avi-Yonah, Israel Exploration Society, Jerusalem 1954). A small part of the map shows a boat on the Dead Sea at the point of junction with the river Jordan. The lumps on the boat represent salt obtained by evaporation from Dead Sea water.

Authors

M. Tehei and G. Zaccai
(IBS Grenoble and ILL)
M. Jasnin
(IBS Grenoble)

Early this year, work by Tehei and co-workers [1] made the cover of the *Proceedings of the National Academy of Sciences of the United States of America* journal, with a picture of a Jordanian 6th century mosaic depicting the Dead Sea (**figure 1**). Laboratories in France, Germany and Israel have developed a collaboration to study the water behaviour within cells of *Haloarcula marismortui*, an ancient organism that lives in the Dead Sea.

This archaeal extreme halophile shows a very high selectivity for K^+, which can be retained within a cell with high permeability for over 24 hours in the absence of metabolism. It is thought that this is possible through the formation of a tertiary system of ordered water molecules, KCl and cell proteins. Cell pellets of native (hydrogenated) and deuterated *H. marismortui* were studied by neutron scattering, in order to investigate intracellular water dynamics in this organism. Water is a key component of all living organisms as well as of the chemical reactions that create and regulate our environment on earth. The presence of liquid water is the first thing that scientists look for when exploring the Universe for signs of extra-terrestrial life. Despite all this, we still know very little about the molecular properties of water and how it influences fundamental biological molecules, such as proteins and DNA.

The QENS technique

Neutron scattering is an ideal tool for probing the dynamic behaviour of water molecules under different conditions. The quasielastic neutron scattering (QENS) technique gives access to atomic motions of a few Ångstroms occurring in a time-range going from 10^{-12} to 10^{-9} s. The length- and time-scales of the accessible
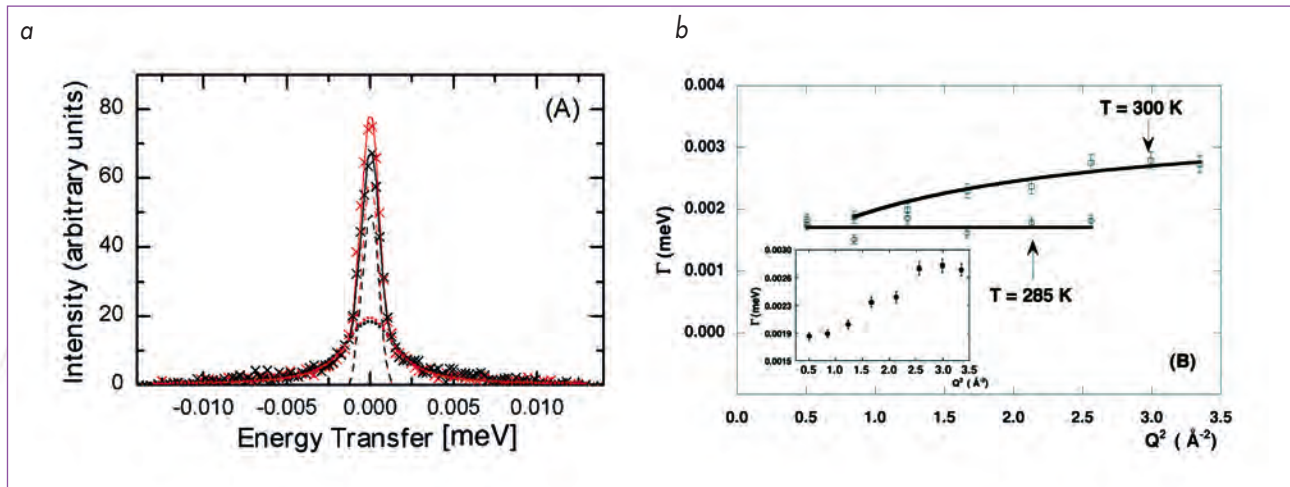
Figure 2: IN16 data. (**a**) Quasielastic spectra at T = 300 K and Q = 0.7 Å⁻¹: the crosses indicate the experimental data and the solid lines are the fitted curves obtained by using one elastic contribution and one Lorentzian, for deuterated cells in H_2O (black) and hydrogenated cells in H_2O (red) respectively. The fits of the quasielastic spectra were performed for - 0.013 < $\hbar\omega$ < 0.013 meV. The different components correspond to the elastic contribution (dashed line) and the Lorentzian (dotted line). (**b**) Half widths at half maximum of the Lorentzian Γ as a function of Q^2 at T = 285 K and T = 300 K. At 300 K, the bold solid line results from the fit using the restricted jump diffusion model of Hall and Ross [2]. (**Inset**) A zoom-in on the data obtained at 300 K.

motions are defined by the wave-vector transfer modulus, Q, and the energy resolution of the spectrometer, ΔE, respectively. The shape of the QENS peak and its Q variation contain information on the characteristic times and geometry associated with the motions. In the same way as diffraction by a structure is related to the structure itself by Fourier transformation in crystallography, the energy transfer scattering pattern of a moving particle is related to the time-dependence of its motion by Fourier transformation. Simple diffusion is described by an exponential decay function in time; the Fourier transform of such a function is a Lorentzian function, and it corresponds to the peak shape usually observed in QENS. By applying various models to fit the Lorentzian width as a function of Q, it is possible to calculate the diffusion coefficients, residence times and relaxation times of the motions (**figure 2**).

Neutron scattering experiments on selectively labelled samples

Dynamics information was derived from the analysis of the incoherent neutron scattering as a function of angle and energy change. The incoherent neutron scattering cross-section of hydrogen is 40 times larger than that of deuterium, so that D-labelling a chemical group significantly reduces its contribution to scattering. Selective deuterium labelling allowed thus for specific components of the cells to be examined.

From IN6 time-of-flight data (ΔE = 100 μeV), a translational diffusion constant of 1.3 10⁻⁵ cm² s⁻¹ was determined at 285 K for *H. marismortui* cells. This value is close to that found previously for other cells and close to that for bulk water, as well as that of the water in the 3.5 M NaCl solution bathing the cells. A very slow water component was discovered from the IN16 data (ΔE = 0.9 μeV; **figure 2**). At 285 K the water protons of this component display a residence time of 411 ps (compared with a few ps in bulk water). At 300 K, the residence time dropped to 243 ps and was associated with a translational diffusion of 9.3 10⁻⁸ cm² s⁻¹, or 250 times lower than that of bulk water. This slow water accounts for about 76 % of cell water in *H. marismortui*. No such water was found in the 'normal' bacteria *Escherichia coli* measured on BSS (ΔE = 0.9 μeV; Jülich Neutron Centre's backscattering instrument). It is hypothesised that the slow mobility of a large part of *H. marismortui* cell water indicates a specific water structure responsible for the large amount of K⁺ bound within these extreme halophilic cells.

Further experiments were recently performed on the IN6 spectrometer and the IRIS time-of-flight instrument at ISIS (UK) (ΔE = 17 μeV) to look into water dynamics in the cytoplasm of *Escherichia coli* [3]. The studies were performed on living deuterium labelled *E. coli* cells (prepared at the ILL-EMBL Deuteration Laboratory) containing

H_2O, in a wide range of time-scales to cover motions from those of pure to slow interfacial water. Contrary to the expectation that water is "tamed" by macromolecular confinement, the measurements established that water diffusion in the bacteria is pure-like at physiological temperature and hydration conditions.

The unique ability for *H. marismortui* to survive in high-salt environments and bind specifically potassium ions seems to be closely related to the low mobility of water in the cells, which can not simply be explained by hydration interactions with halophilic proteins. A mechanism of structured water around potassium ions similar to what was seen by R. MacKinnon (potassium channels, see [4]) has been suggested.

References

[1] M. Tehei, B. Franzetti, K. Wood, F. Gabel, E. Fabiani, M. Jasnin, M. Zamponi, D. Oesterhelt, G. Zaccai, M. Ginzburg and B.-Z. Ginzburg. PNAS U.S.A. 104 (2007) 3, 766-771

[2] P. L. Hall and D. K. Ross, Molecular Physics 42 (1981) 673-82

[3] M. Jasnin, M. Moulin, M. Haertlein, G. Zaccai and M. Tehei (2007). Accepted with minor corrections by EMBO rep. 2007

[4] R. MacKinnon, Nobel Lecture (2003), Stockholm University, Stockholm

A world behind the mirror? Search for dark matter with ultracold neutrons

The hypothesis that the dark matter in the Universe might be due to a 'parallel world' of mirror elementary particles has triggered recent experiments to search for neutron-to-mirror-neutron transitions. Two independent experiments, using ultracold neutrons at the ILL, improved the limit for the time constant of such a transition by more than two orders of magnitude.
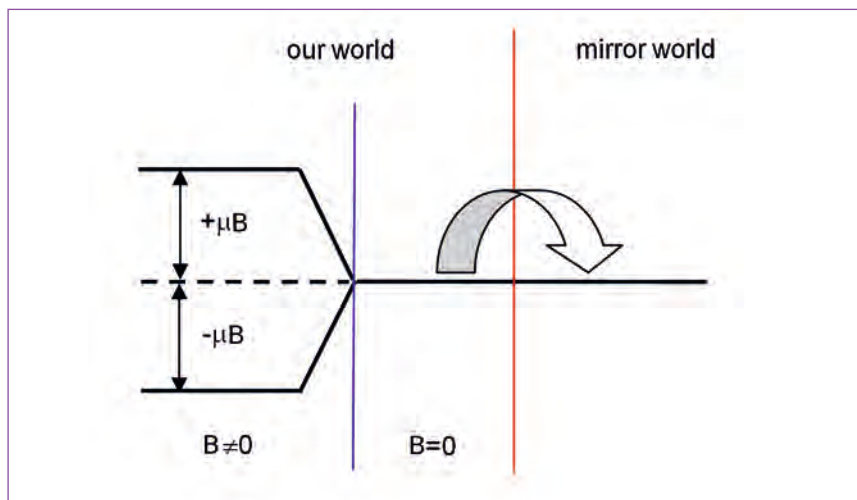
Figure 1: For zero magnetic field (B=0, and assuming the absence of mirror magnetic fields at the experimental site), ordinary and mirror neutron states are degenerate and transitions are possible. The magnetic field lifts the degeneracy and suppresses the transitions.

Our world can be distinguished from its mirror image because parity is violated. Consider for example an antineutrino that emerges from the neutron decay: its spin is always aligned antiparallel to its momentum hence it is labelled *right-handed*. Looking into a mirror, this antineutrino would face a *left-handed* counterpart. However, nature seems to prefer a particular handedness of particles and up to now only *right-handed* antineutrinos have been observed. Our world is asymmetric with respect to parity.

Many ideas were formulated since the discovery of parity violation to explain this situation. One idea could open the window to a 'world behind the mirror'. It describes a hidden sector of 'mirror particles' that might restore the symmetry of parity in a global sense. These particles would constitute an invisible parallel world, not interacting with our world by any known force except gravity. Mirror particles amongst themselves are supposed to behave like ordinary matter, but with opposite handedness of interactions. The right-handed antineutrino would thus have a left-handed counterpart in the mirror world, and mirror neutrons would decay into mirror particles with opposite sign of parity violation [1,2].

This hypothesis has regained recent interest as a viable candidate for dark matter in the Universe [3,4]. An interesting test can be performed by searching for transitions of neutral particles to corresponding mirror particles, which might occur due to mass mixing induced by a super-weak force. Ultracold neutrons (UCNs) are particularly well suited for this test, as they can be trapped in a bottle. Any mirror neutron n' that has undergone a transition from a neutron n during storage of a sample of UCN will leave the trap due to the absence of interaction with the trap walls. For observation of the effect it is necessary to minimize all external fields that may suppress the transitions, since the energy of particle interaction with the field (and mirror particle with an eventual mirror field) will lift the degeneracy of the two states. Therefore, good magnetic shielding is required to remove the magnetic field of the Earth. The effect would manifest itself as a difference of UCN storage time constants without, respectively, with application of a magnetic field (note that the presence of a transition-suppressing magnetic mirror field at the experimental site is extremely unlikely).

After a first dedicated attempt to observe nn' transitions with cold neutrons [5], two experiments with UCN were performed recently. The experiments took advantage of existing equipment for the search of the neutron electric dipole moment (EDM), sharing rather similar requirements with respect to magnetic field shielding and quality of UCN storage.

Authors

C. Plonka-Spehr, P. Geltenbort and O. Zimmer
(ILL)
D. Rebreyend
(LPSC, Grenoble, France)
K. Kirch
*(PSI, Villigen, Switzerland)*
A.P. Serebrov
(PNPI, Gatchina, Russia)
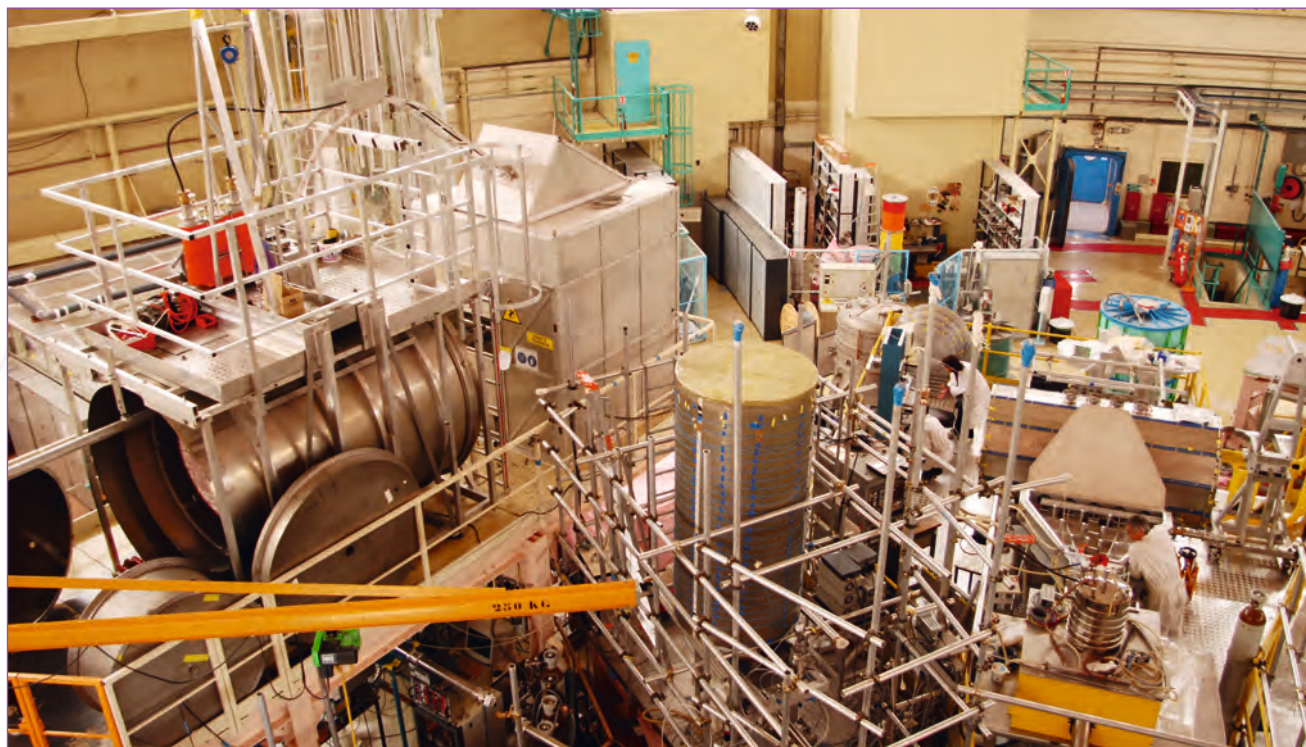
Figure 2: *Experimental installations to search for nn' transitions at the instrument PF2.*

The first one was performed by the nEDM collaboration that operates the former RAL/Sussex EDM experiment at the instrument PF2. The external magnetic fields were suppressed to a level below 50 nT. By comparing the number of UCN stored in a volume of 21 litres at different magnetic field configurations, the experiment provided a lower limit for the characteristic *nn'* transition time constant of 103 s (95% c.l.) [6]. This improved the previous indirect limit [4] by two orders of magnitude.

The second one was performed by a Russian collaboration. A big UCN storage vessel (190 litres) offers a large time of free flight for the UCN between wall collisions, which has a strong influence on the experimental sensitivity. The external magnetic fields were suppressed below 20 nT. A lower limit of 414 s (90% c.l.) was established [7], thus improving the previous result [6]. This limit is already not too far from the neutron lifetime but might still be too low to exclude a mechanism of appearance of high-energy protons above the GZK-cutoff in cosmic radiation due to *nn'* oscillations [4].

Still lacking a positive signal, the window to the mirror world is not open yet! The discussion about mirror particles and mirror matter has been going on for 50 years (see a recent review [8]). However, the search for dimensions beyond our visible world has inspired mankind for considerably longer, not least the monks of the monastery of the Chartreuse…

References

[1] I.Yu. Kobzarev, L.B. Okun and I.Ya. Pomeranchuk, Yad. Fiz. 3 (1966) 1154

[2] R. Foot, H. Lew and R.R. Volkas, Phys. Lett. B272 (1991) 67

[3] Z. Berezhiani, Int. J. Mod. Phys. A 19 (2004) 3775

[4] Z. Berezhiani and L. Bento, Phys. Rev. Lett. 96 (2006) 081801; Phys. Lett. B635 (2006) 253

[5] U. Schmidt et al., http://inpa.lbl.gov/~bl2007/talks.html

[6] G. Ban et al., Phys. Rev. Lett. 99, 161603 (2007)

[7] A.P. Serebrov et al. (2007); http://www.arxiv.org/pdf/0706.3600

[8] L.B. Okun, 'Mirror particles and mirror matter: 50 years of speculations and search', hep-ph/0606202, Uspekhi Fiz. Nauk 177 (2007) 397

New information on states below the microsecond isomer in ^{136}Sb

The very neutron-rich nucleus ^{136}Sb has been studied at the Lohengrin spectrometer. This is the most neutron-rich nucleus beyond the 82 neutron shell closure, close to the doubly magic ^{132}Sn for which spectroscopic information exists. State-of-the-art shell-model calculations are able to correctly reproduce the experimental measurements.

The study of very neutron-rich nuclei around the doubly magic ^{132}Sn (50 protons, 82 neutrons) is a subject of great interest, as it offers an opportunity to test the basic ingredients of nuclear shell-model calculations, in particular the nucleon-nucleon effective interaction, when moving towards the neutron drip line. In this context, a considerable effort is currently being made to gain information on exotic nuclei beyond the $N=82$ shell closure, with special attention focused on the Sb isotopes, which are most appropriate for testing the matrix elements of the proton-neutron interaction between valence nucleons in different major shells.

Recent beta-decay measurements of excited states ^{135}Sb performed at ISOLDE, CERN appeared to show a weakening of the shell-gap [1], as shell-model calculations were unable to correctly reproduce the energies of some states. These results have motivated both new theoretical and experimental efforts in this region. The Naples group has performed calculations in this region

using a different technique, "Q-box folded diagrams" to derive the two-body effective nucleon-nucleon interaction [2]. Using this interaction, shell-model calculations are able to correctly reproduce the level schemes of ^{134,135}Sb. In order to further test these calculations new data have been obtained on the very neutron-rich ^{136}Sb which was studied at the ILL's 'Lohengrin' fission-product spectrometer.

The nucleus ^{136}Sb, with an N/Z ratio of 1.67, is at present the most exotic open-shell nucleus beyond ^{132}Sn for which spectroscopic information is available. In an experiment at GSI [3] only one gamma ray, of energy 173 keV, was observed, which alone is insufficient to explain the origin of a μs isomer. Using the ILL's 'Lohengrin' fission-product spectrometer, recently upgraded for gamma-ray spectroscopy as part of the ILL's Millennium programme, conversion-electron and gamma-ray spectroscopic studies identified the energies and multipolarities
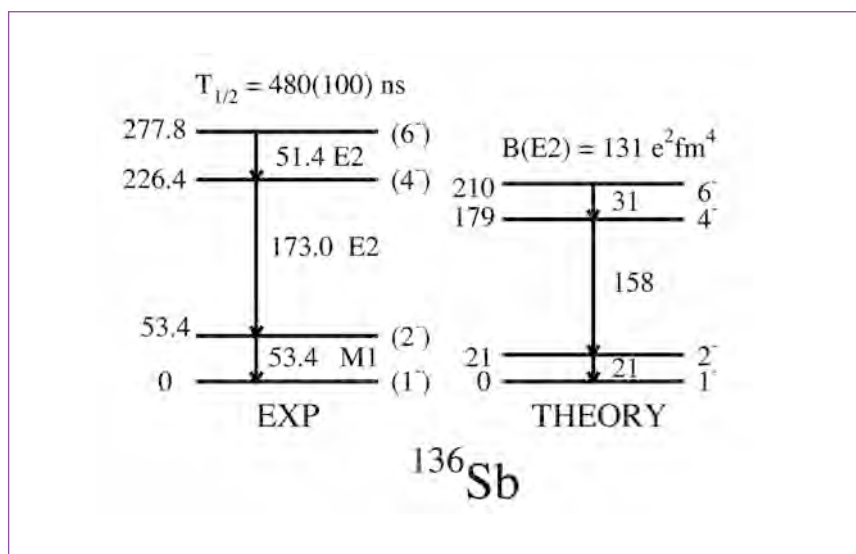

Figure 1: Comparison of experimental and theoretical decay schemes of ^{136}Sb.

Authors

**G. Simpson, J.-C. Angelique,
J. Genevey and J.-A. Pinston**
(LPSC, Grenoble, France)
U. Köster
(ILL)

(angular momentum and electromagnetic character) of two new transitions in this nucleus. The experimental level scheme was then compared to the state-of-the-art shell-model calculations performed by the Naples group.

As shown in **figure 1**, the theoretical calculations are able to correctly reproduce the main features of the level scheme, including the μs isomeric lifetime, from the B(E2) transition rate. This further supports the idea that the shell model calculations by the Naples group work correctly, in this region far from stability.

More experimental support for the Naples calculations comes from another experiment on ^{138}I [4], also performed at Lohengrin. These results were combined with data on the same nucleus from a spontaneous fission experiment. Some shell-model calculations predict energies which are too high for states containing the proton $d_{5/2}$ orbital, the same orbital responsible for the states seen in ^{134,135}Sb. Lowering the energy of this orbital 'by hand' then allows the experimental level scheme to be reproduced, as is the case of ^{134,135}Sb. As ^{138}I is not too far from stability it is unlikely that any shell-gap quenching is present here. It is thought that the problem of the energies of states involving the proton $d_{5/2}$ orbital arises from incorrect two-body matrix elements.

In addition to testing and improving nuclear-structure models there is also an astrophysical interest in these studies. The rapid neutron-capture nucleosynthesis process (*r-process*) in core collapse supernova explosions is thought to be responsible for the creation of around half the matter in the universe heavier than iron.

A possible path of the *r-process* is shown in **figure 2**. Nuclear-structure parameters are an important input into calculations attempting to
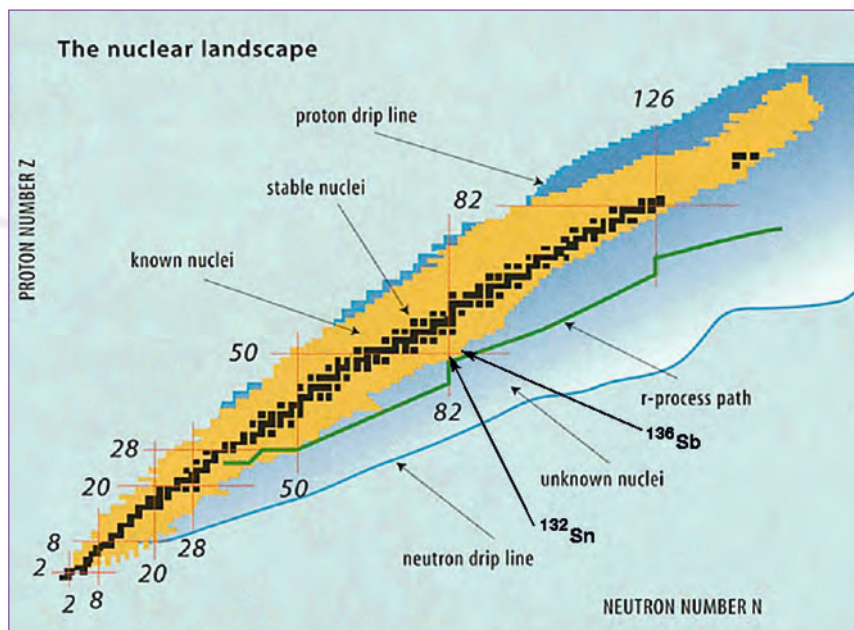
Figure 2: The nuclear landscape. Black squares represent stable nuclei, yellow show observed radioactive nuclei and dark blue are those as yet unobserved but predicted to be bound. Full proton and neutron shells, so-called 'magic' numbers, are also labelled. The anticipated path of the astrophysical process is shown too.

map the direction and speed of the *r-process*. The need to have accurate measurements and models of nuclear properties far from stability is therefore obvious. This is especially true around masses 120 to 130 where *r-process* calculations are unable to correctly reproduce the elemental abundances found on Earth.

One possible explanation for this effect, predicted by some nuclear theories, is a change in the strength of nucleon-nucleon interactions when a large excess of neutrons is present.

The work reported here and other recent measurements, such as spectroscopy of the singly magic (*N*=82) ^{130}Cd [5] performed very recently at GSI, show that the state-of-the-art shell-model calculations are valid far from stability

near ^{132}Sn without the need to invoke any corrections to the nucleon-nucleon effective interaction strength in spite of the large neutron excess.

References

[1] J. Shergur et al., Phys. Rev. C 65 (2002) 034313

[2] L. Coraggio et al., Phys. Rev. C 73, (2006) 031302(R)

[3] M. Mineva et al., Eur. Phys. J. A 11 (2001) 9

[4] T. Rzaca-Urban et al., Phys. Rev. C 75 (2007) 054319

[5] A. Jungclaus et al., Phys. Rev. Lett. 99 (2007) 132501

A precision measurement to test the Standard Model

Emission anisotropies of the decay products in neutron decay can be used to search for physics not described within the framework of the Standard Model, and to set limits on new theories. A new precise measurement of the neutrino asymmetry parameter B - yielding the smallest corrections so far - was performed at the cold neutron beam position PF1B using the spectrometer PERKEO II.
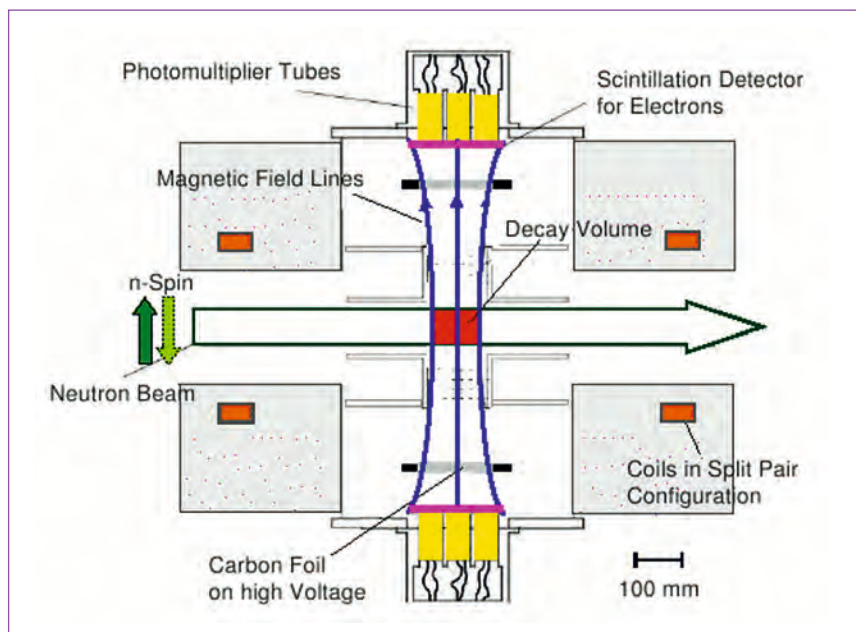
Figure 1: Sketch of the electron spectrometer PERKEO II. Transversally polarised neutrons pass the apparatus and a certain fraction decays in flight. In the decay volume, the magnetic field divides the full solid angle into two hemispheres – in and against spin direction – and guides the charged decay products onto the two detectors.

Authors

**M. Schumann, M. Deissenroth,
J. Krempel, B. Märkisch, D. Mund,
and H. Abele**
(University of Heidelberg, Germany)
**T. Soldner, M. Kreuz and
A. Petoukhov**
(ILL)
F. Glück
(University of Karlsruhe, Germany)

For many decades, the Standard Model of particle physics has proven its validity in innumerable experiments over all accessible energy scales. Up to now, no experimental result has been found that does not agree with the Standard Model (neutrino oscillations can be included by minor extensions of the model). However, many arguments make scientists believe that the Standard Model is only the low energy manifestation of a more fundamental theory. It leaves many parameters unpredicted, cannot explain the number of particle generations, the existence of dark matter and dark energy, and it does not include gravity. It also gives no explanation for the violation of parity in the weak interaction, where only left-handed neutrinos occur (i.e. spin and momentum anti-parallel).

One class of extensions of the Standard Model assumes a left-right symmetric world at very high energies. Parity violation, as observed today, is introduced by spontaneous symmetry breaking in the expanding and cooling Universe. Consequently, a right-handed weak interaction mediated by a heavy boson W_R should exist. Although it is overwhelmed by the left-handed weak interaction mediated by the much lighter boson W_L of the Standard Model, traces might be detected experimentally.

There are different attempts to find these traces of new physics. One is to go to the high energy frontier. Large accelerators like the LHC at CERN scheduled to start operation soon, collide particles with enormous energies in the TeV range. In these reactions new particles might be created directly. A different approach is to perform precision experiments at much lower energies where unknown particles like the boson W_R can be detected indirectly in deviations from the Standard Model predictions – even if their masses are largely above collider production thresholds.

The neutron decay into electron, proton, and electron-anti-neutrino (in the following called neutrino) constitutes a well suited laboratory for low-energy precision measurements. It is a rather simple system where theoretical corrections and uncertainties are small and well calculable. Prominent observables are the asymmetry parameters describing the correlation between the spin of the decaying neutron and the momentum of one of the decay particles: A stands for the electron asymmetry, B for that of the neutrino, and C for the proton asymmetry. All three parameters are non-zero, expressing the parity violation in the weak interaction. The asymmetries are important observables to measure

parameters of the Standard Model, but can also be used to probe this theory and to set limits on new physics.

In order to measure the neutrino asymmetry parameter B with high precision [1] and – very important for precision measurements – with only small corrections, the electron spectrometer PERKEO II was installed at the beam position PF1B. PF1B delivers an intense beam of cold neutrons, a necessary prerequisite to get sufficient statistics. The beam was spin polarised to $P=99.7(1)\%$ using two supermirror polarisers in X-SM geometry [2], a novel technique to achieve highest polarisation developed at the ILL. Several opaque ^{3}He cells were employed to measure polarisation and spin-flip efficiency, $F=100.0(1)\%$, to high precision. An evacuated beamline of several metres length housed a neutron collimation system and transported the polarised neutrons to the spectrometer.

PERKEO II (**figure 1**) consists of two large superconducting coils in split pair geometry. The magnetic field has a maximum of about 1 T and decreases slightly towards the two detectors that are installed next to the neutron beam. It guides electrons and protons from neutrons decaying in the spectrometer centre to one of the detectors, realising a full $2x2\pi$ solid angle coverage. The neutron spin was directed towards one of the detectors that could therefore be used to determine if a particle was emitted in or against neutron spin direction. Only about $2\cdot10^{-7}$ of

Figure 3: Photo of one of the two detector housings: the plastic scintillator was read out by six photomultipliers protected by a massive copper block.

Figure 2: Photo of the assembly used to measure electrons and protons with the same detector: the thin carbon foil in the foreground is set to negative potential (18 kV) to accelerate the protons created in the decay volume (behind the window in the background).
At the foil, the protons generate secondary electrons that can be detected with a plastic scintillator (removed for the picture).

the neutrons transversing PERKEO II actually decayed, all others were absorbed in a beamstop behind the experiment.

Due to its tiny interaction cross section, the neutrino cannot be detected directly. Its emission direction was derived from a coincident detection of electron and proton. When both were detected in the same hemisphere, energy and momentum conservation restrict the neutrino momentum to the other hemisphere. A sophisticated technique was developed in order to be able to detect both particles in the same detector (**figure 2**). The electrons (energy of up to 782 keV) were detected directly in a plastic scintillator. The protons (maximal energy 3 orders of magnitude lower) were accelerated onto a thin carbon foil on negative potential (18 kV). They then had enough energy and ionisation power to knock out secondary electrons from the foil that were again accelerated towards the plastic scintillator on ground potential. The electrons from the decay passed through the foil almost unperturbed.

The experimental neutrino asymmetry is defined as $B_{exp}(E) = (N^{++}-N^-)/(N^{++}+N^-)$, where $N^{ij}(E)$ is the number of events with electrons and protons emitted in (+) or against (-) neutron spin direction. E is the electron energy. From $B_{exp}(E)$ we obtained the correlation coefficient $B = 0.9802(50)$.

Due to the clean experimental set-up and the extremely high neutron polarisation, the corrections to this result are 0.5% only, almost one order of magnitude smaller than those of previous experiments. The new value agrees with all previous results and reduces the uncertainty of the new world mean value by 25%. Within the simplest left-right symmetric model, we derive a lower mass limit of $m>290.7$ GeV/c^2 (90% CL) for a heavy boson W_R. The new result can be employed in global analyses of neutron decay to set updated limits on various other theories beyond the Standard Model [3,4].

References

[1] M. Schumann et al., Phys. Rev. Lett. 99 (2007) 191803

[2] M. Kreuz et al., Nucl. Instr. and Meth. A 547 (2005) 583

[3] N. Severijns, M. Beck and O. Naviliat-Cuncic, Rev. Mod. Phys. 78 (2006) 991

[4] H. Abele, Prog. Part. Nucl. Phys. 60 (2008) 1

Experimental demonstration of a new optical effect with UCNs

It is theoretically predicted that when a wave of any nature passes through a medium moving with linear acceleration, a change of its wave frequency and corresponding energy occurs. This effect is universal and to our knowledge has not been verified experimentally. Using UCN we could carry out for the first time an experimental demonstration.

It is well known for any wave that the wave number k in a medium is related to its vacuum value k_0 by the index of refraction n. The generally accepted understanding is that when a wave returns the medium back to vacuum, the absolute value of its wave number is exactly equal to the incident wave number, although the propagation direction may be different. This statement is valid for all types of waves, but only for the case of a medium at rest or moving with constant velocity. In the latter case a sample movement may only result in the change of the phase of the transmitted wave due to the change of the effective length $\Delta l = v\tau$ of the sample. Here $\tau = L/nc$ is the passage time through the sample of length L, and c is the wave speed in vacuum.

However, it was predicted theoretically, that wave number and frequency change when the wave passes through an accelerating sample of a refractive medium. That was firstly shown by K. Tanaka [1] for the case of light optics. Later, the same result was derived for neutron waves [2,3]. More generally, a refractive index may be introduced for waves of any nature and the only requirement is the presence of scattering centers in the medium. Therefore, particles of any nature should change their energy passing through the bulk volume of the accelerating medium [4]. It is worth noting that the Tanaka effect is very small for waves propagating with the speed of light, that despite the extraordinary sensitivity of modern optical methods it has not been observed yet. However, the neutron-optics experiment of this kind appeared to be feasible and was performed recently.

If a neutron passes through a refractive sample, which is moving with acceleration a, it changes its energy by $E = [(1-n)/n] maL$. The use of Ultra Cold Neutrons (UCN) limits the sample thickness L due to the strong absorption in matter. However, this disadvantage is compensated by two factors:

i) In the case of UCNs the factor $(1-n)/n$ is rather high and its value may be as large as 0.5. For cold neutrons with wavelength, for instance, 2 nm, this value is of the order of 10^{-3};

ii) UCN spectrometry methods, based on neutron Fabri-Perot interferometers, have extraordinary sensitivity.
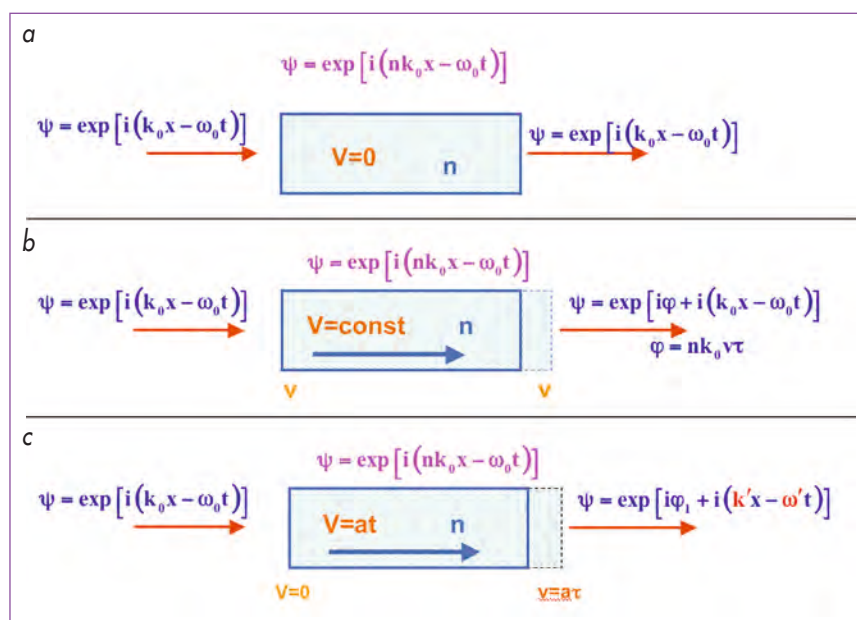
Figure 1: When the sample is at rest (a) or moving with constant velocity (b) the wave vector and frequency of the transmitted wave are the same as for the initial wave. The motion of the sample with constant acceleration c) causes the change of the wave frequency and of the corresponding wave number. In the case of the matter wave the particle energy $E' = \hbar\omega'$ also differs from the initial value $E_0 = \hbar\omega_0$.

Authors

A.I. Frank and G.V. Kulin
(Frank Laboratory of Neutron Physics, Dubna, Russia)
D.V. Kustov
(Frank Laboratory of Neutron Physics, Dubna, Russia and Institute for Nuclear Research, Kiev, Ukraine)
P. Geltenbort and M. Jentschel
(ILL)
V.G. Nosov and A.N. Strepetov
(Kurchatov Institute, Moscow, Russia)

Nuclear and particle physics
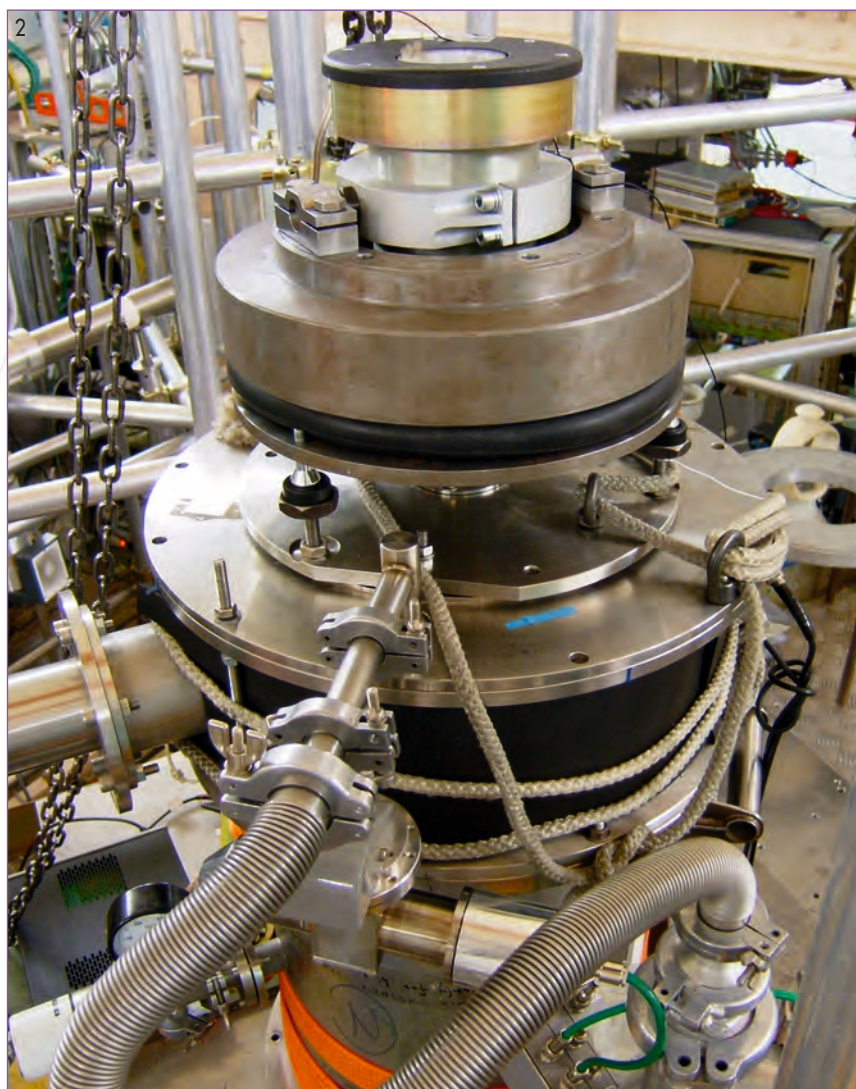
Such a spectrometer based on two Fabry-Perot wavelength filters (see e.g. [5]) was used for detecting the effect of an accelerating medium in neutron optics. Samples of silicon wafers of thickness 0.6 mm and 1.85 mm were placed between the two filters. The Si-Samples were oscillated with frequencies 40 Hz and 60 Hz, which gave a periodically modulated acceleration achieving maximum values of about 10 g (g – free fall acceleration).

The value of energy change to be detected was about 0.2 to 0.6 neV. The periodical modulation of the acceleration imposes a periodical change of neutron energy. Due to the narrow band pass properties of the spectrometer, this should lead to an oscillation of the neutron count rate. Additionally, the total neutron count rate is influenced by other effects.

However, measuring the phase of the count rate oscillation provided the unambiguous way to separate the effect of the accelerating medium from other systematical effects. **Figure 3** shows results of one of these measurements. These results are in quite good agreement with theoretical predictions and are in dramatic contradiction to simulations assuming the absence of the effect. In conclusion, using UCN gave us the possibility to show a new optical effect that is of universal nature.

Figure 2: Gravity UCN spectrometer. An electro-magnet driver inducing a harmonical motion to the sample is installed at the upper flange.

Figure 3: Phase of the count rate oscillation as a function of the distance between the two Fabry-Perot interferometers. Blue points – experimental results. Red curve – theoretical prediction. The brown straight line is the result of a simulation assuming the absence of the accelerating matter effect.
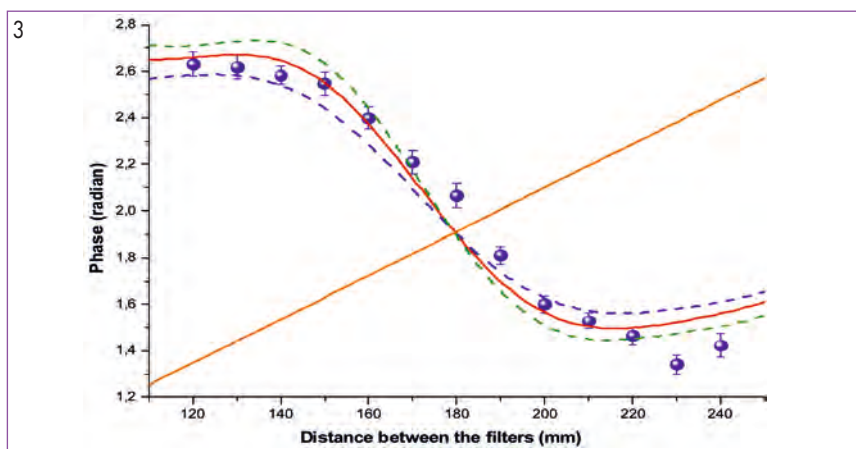
References

[1] K. Tanaka, Phys. Rev. A 25 (1982) 385

[2] F.V. Kowalski, Phys. Lett. A 182 (1993) 335

[3] V.G. Nosov and A.I. Frank, Phys. of Atomic Nuclei. 61 (1998) 613

[4] A.I. Frank, P. Geltenbort, G.V. Kulin, D.V. Kustov, V.G. Nosov and A.N. Strepetov, JETP Letters. 84 (2006) 363

[5] I.V. Bondarenko et al., ILL Annual Report 1999

Dynamical heterogeneity of specific amino acids in bacteriorhodopsin

The dynamics of biological macromolecules is essential for their function, but their characterisation remains challenging. Coupling neutron scattering to isotope labelling has allowed us to explore the dynamics of specific amino acids within bacteriorhodopsin as a function of temperature. The study reveals differences in the dynamics of two very similar amino acid types, which has been further explored by performing molecular dynamics simulations.

Figure 1: Comparison of atomic mean square displacements extracted from neutron scattering measurements and molecular dynamics simulations. In both figures the unlabelled purple membrane data are represented, as a linear fit for the neutron measurements, and as crosses for the simulation points.
a) Leucine dynamics (deuterated purple membrane with hydrogenated leucine residues)
b) Isoleucine dynamics (deuterated purple membrane with hydrogenated isoleucine residues).

Authors

K. Wood
(MPI für Biochemie, Martinsried, Germany, IBS and ILL)
S. Grudinin
(INB-2, Jülich, Germany)
M. Weik
(IBS, Grenoble)
B. Kessler and D. Oesterhelt
(MPI für Biochemie, Martinsried, Germany)
R. Ghosh, M. Johnson and G. Zaccai
(ILL)

Biological macromolecules are dynamical entities, being animated by motions occurring over a wide-range of time and space scales. Understanding which motions are essential for specific biological functions remains a challenge for the future. A first step towards this goal is the characterisation of the underlying dynamical heterogeneity, to explore if different parts of a system have different dynamics.

Neutrons have a unique role to play in this field, since they directly probe the thermal fluctuations corresponding to the forces stabilising biological structures. Here we have used neutron spectroscopy to measure atomic mean square displace-

ments as a function of temperature. Temperature dependent data is of importance for theoretical modelling of protein motions [1].

Bacteriorhodopsin is a protein which acts as a nano-machine, harnessing light energy to pump protons. It has provided biophysicists with an exceptional model that has attracted much experimental activity over the last ten years. Bacteriorhodopsin is the main constituent of the purple membrane, which remains one of the best characterised natural membranes. The dynamics of the purple membrane under different conditions has been well studied by neutron scattering, reviewed in [2]. Neutron spectroscopy

on bio-molecules is dominated by hydrogen scattering and generally provides average information on the whole sample. It is possible to concentrate on one part of a complex system, by using labelling techniques consisting in a selective substitution of a hydrogen atom by a deuterium atom. The hydrogenated part dominates the signal, and the deuterated part is effectively masked. Using this technique, the dynamical heterogeneity of bacteriorhodopsin has already been shown, with the core of the protein having different dynamics compared to the average membrane [3].

In order to go further into the dynamical mapping of the membrane, we have investigated the dynamics of specific amino acids in bacteriorhodopsin. We have prepared 150 mg of specifically labelled purple membrane samples by 'feeding' the archae-bacteria (from which it is produced) with the right mix of deuterated and hydrogenated media. The results obtained from two different samples are discussed in this paper: the first sample consists of a deuterated purple membrane with hydrogenated leucines and the second is made of deuterated purple membrane with hydrogenated isoleucines. Therefore, the signal will be dominated by leucine and isoleucine dynamics for the first and second sample respectively, while for a normal (unlabelled) purple membrane, the average dynamics of the membrane will dominate the signal. Note that isoleucine and leucine residues are hydrophobic residues with similar structure, differing only in the positioning of a methyl group along the side-chain.

The atomic mean square displacements (labelled $<u^2>$) measured on the IN16 backscattering spectrometer for both samples are compared to a 'normal' unlabelled purple membrane in **figure 1a**. The data reveal that the leucine residues show a dynamical behaviour similar to that of the global membrane in the entire temperature range studied (**figure 1a**). In contrast, the isoleucine residues have their $<u^2>$ increased with respect to the average purple membrane above 120 K (see **figure 1b**).

In order to further explore the dynamical differences observed in leucine and isoleucine residues, we performed molecular dynamics simulations
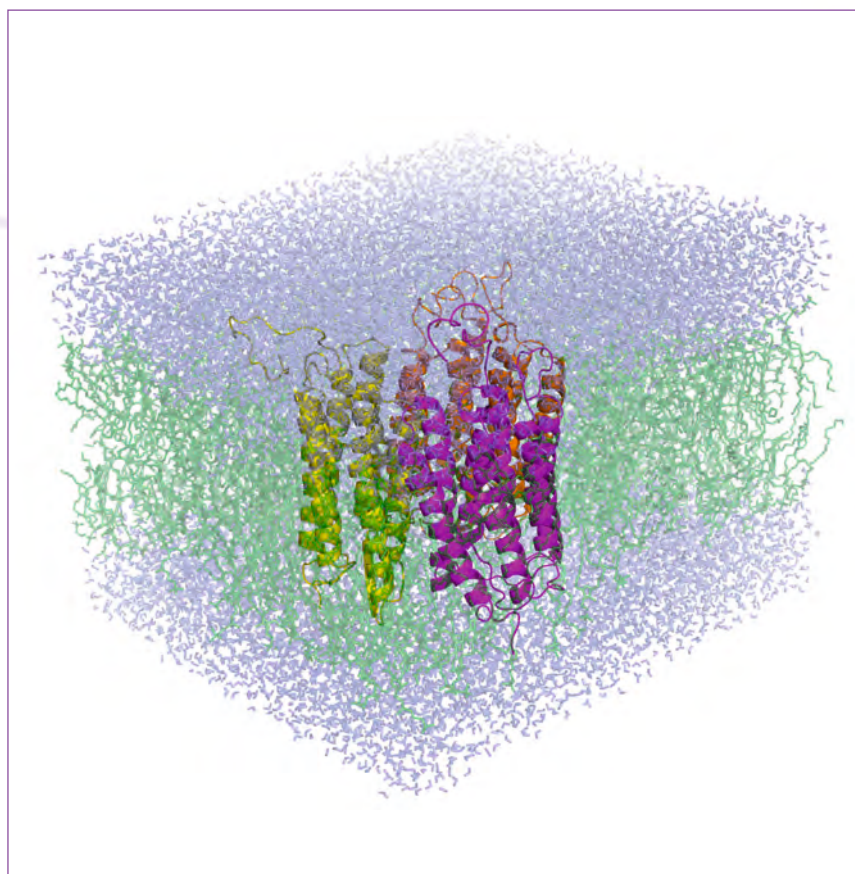
Figure 2: Simulated system, made up of three bacteriorhodopsin molecules, embedded in a lipid bilayer (green), with a water layer (blue). The total number of atoms is 88 867.

using AMBER on a purple membrane model. A snap-shot of the simulated system, comprising almost 90,000 atoms, is given in **figure 2**. The simulations were performed at five temperatures and the resulting mean square displacements are presented in **figure 1a** and **1b** for comparison with neutron scattering data. The simulation reproduces extremely well the similar dynamics of leucine residues to the global membrane, and the increased dynamics of isoleucines, showing the precision of current force fields. The quantitative agreement validates the simulation, and has allowed a site-specific investigation of the dynamics.

Combining isotope labelling, neutron scattering and molecular dynamics simulations has proved particularly well-suited to the establishment of a

'dynamical map' of purple membrane heterogeneity. Analysis of the molecular dynamics results reveals that it is a mixture of both environment and residue type that defines the dynamics of an amino acid.

References

[1] P.W. Fenimore, H. Frauenfelder, B.H. McMahon and R.D. Young, Proc. Natl. Acad. Sci. USA (2004) 101, 14408-13

[2] G. Zaccai, Biophys. Chem. 86 (2000) 249-57

[3] V.Reat, H. Patzelt, M. Ferrand, C. Pfister, D. Oesterhelt, and G. Zaccai, Proc. Natl. Acad. Sci. USA 95 (1998) 4970-5

Formation and coupling of collective spins in an array of frustrated nano-magnets: experiment and simulation

Figure 1: 9-spin and 8-spin clusters from electronic structure calculation (Cu, V and O are in blue, yellow and red respectively).

Magnetisation measurements, elastic and inelastic neutron scattering, DFT calculations of electronic structure and exact diagonalisation of model Hamiltonians, reveal that the oxide $La_3Cu_2VO_9$ exhibits arrays of weakly interacting frustrated nanomagnets. On decreasing the temperature, a 10-fold degenerate collective spin $S=1/2$ is formed on 2/3 of these clusters and a collective singlet $S=0$ on the remaining 1/3. At the lowest temperature the collective spins start to get coupled, but condense into a non-trivial, non-Néel phase

Figure 2: Electronic density map obtained from DFT spin polarised calculation without Cu/V substitution.

The $La_3Cu_2VO_9$ lamellar oxide is constituted of Cu^{2+} planar kagomé clusters made of 4 corner-sharing triangles. The Cu^{2+} ions carry a spin $s=\frac{1}{2}$ and are the only magnetic ions. These interact antiferromagnetically through O-mediated superexchange but the triangular based geometry prevents all pairs of spins from simultaneously satisfying the interactions, resulting in geometric frustration. The superexchange paths between the clusters either are longer than inside the clusters or involve more than one O ion bridge, suggesting that the inter-cluster interactions are much weaker than the intra-cluster interactions.

The $La_3Cu_2VO_9$ compound thus provides an interesting example of an array of nanoscopic quantum frustrated magnets. The inter-cluster interactions can favour correlations within the Cu planes, subject to geometrical frustration on a longer length scale and with smaller exchange energy since the clusters are at the vertices of a triangular superlattice, or from plane to plane, in which case they exhibit spin tubes.

A substitution of non-magnetic V^{5+} ions for 1/27 Cu^{2+} ions occur for reasons of electric neutrality. Powder neutron scattering on D2B

Authors

J. Robert, V. Simonet, B. Canals and R. Ballou
(Institut Néel, CNRS/UJF, Grenoble, France)
M. Johnson, M. Zbiri, B. Ouladdiaf, J. Ollivier and P. Deen
ILL)

combined with DFT electronic structure calculation suggests that there should be no more than one substitution per kagomé cluster, which leads to a population of 1/3 clusters with 8 spins s=½ and 2/3 clusters with 9 spins s=½. Moreover the V^{5+} ion r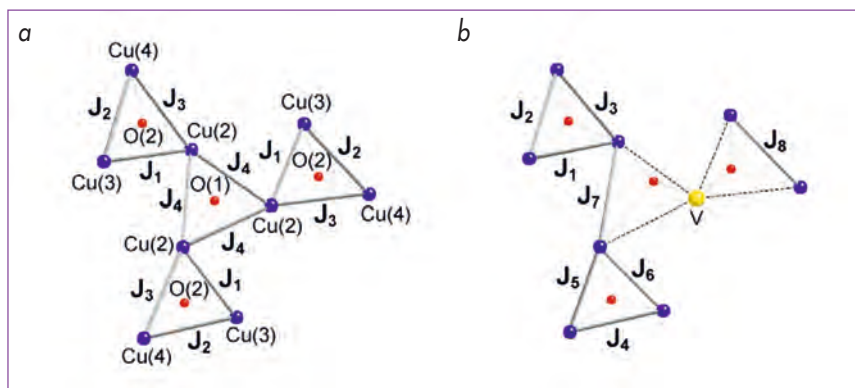esides preferentially on the central triangle of the cluster where it produces strong structural distortions, which drastically lowers the related J_7 and J_8 superexchange interactions (see **figure 1**).

The small size of the kagomé clusters allows for the exact diagonalisation of magnetic exchange models and the calculation of the quantities to be confronted with the experiments: magnetisation plateau measured under high magnetic fields, characteristic shape of the inverse susceptibility, cluster energy levels probed via specific heat and inelastic neutron scattering (see **figures 3** and **4**). A sensible choice, although not unique, constrains the variation of the exchange parameters to a few percent in the 9-spin cluster and to around 75 % in the 8-spin clusters, and is found to reproduce all the experimental data. Analysis of the quantum states reveals the formation below about 15 K of collective spins S=1/2 in the 9-spin clusters and S=0 in the 8-spin clusters out of the individual Cu^{2+} spins s=1/2.

The S=1/2 collective state can be described in terms of singlet dimer coverings and a dangling spin totally or partially delocalised on the whole cluster, depending on fine details of the exchange distribution in the 9-spin cluster. Spin-polarised DFT calculations on the 9-spin cluster (see **figure 2**) confirm that all four interactions are antiferromagnetic with an average value of 280 K, in reasonable agreement with the experimentally determined value of 445 K. These calculations also show that the inter-cluster interaction is an order of magnitude smaller. Further calculations are underway to investigate the experimentally predicted weakening of J_7 and J_8 in the presence of V in the 8-spin clusters.

The onset of magnetic correlations between the collective spins is revealed by a marked anomaly in the specific heat and magnetic susceptibility at about 2 K (see **figure 3**).
A scattering experiment using polarised neutrons with tri-axial polarisation analysis confirmed the presence of collective spins above 2 K and revealed no magnetic long-range order below 2 K.

The exact nature of the low temperature phase is under active investigation.
It is of considerable interest to determine whether the system stabilises a valence bond crystal of mesoscopic spins on triangular nets, suspected in the case of dominant in-plane correlations, or novel phases associated with mesoscopic spins correlated in tubes.
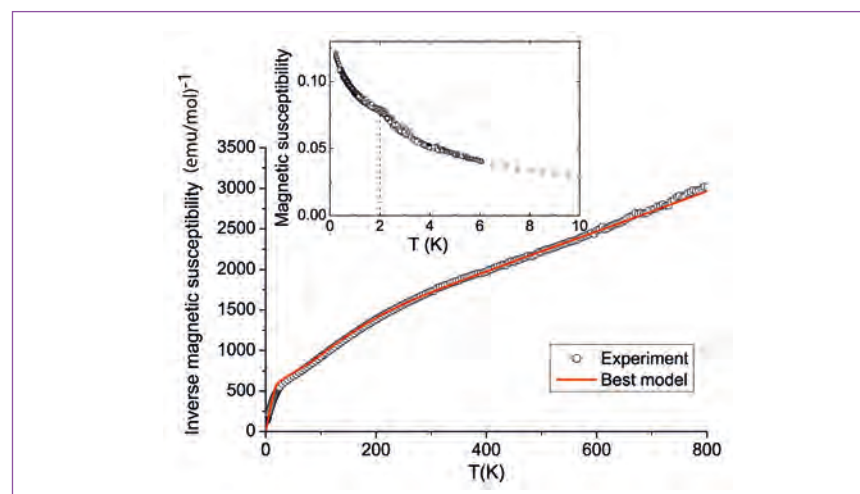
*Figure 3: Calculated and measured inverse magnetic susceptibility in the collective spins regime. **Inset:** 2 K anomaly in the susceptibility revealing inter-cluster correlations.*
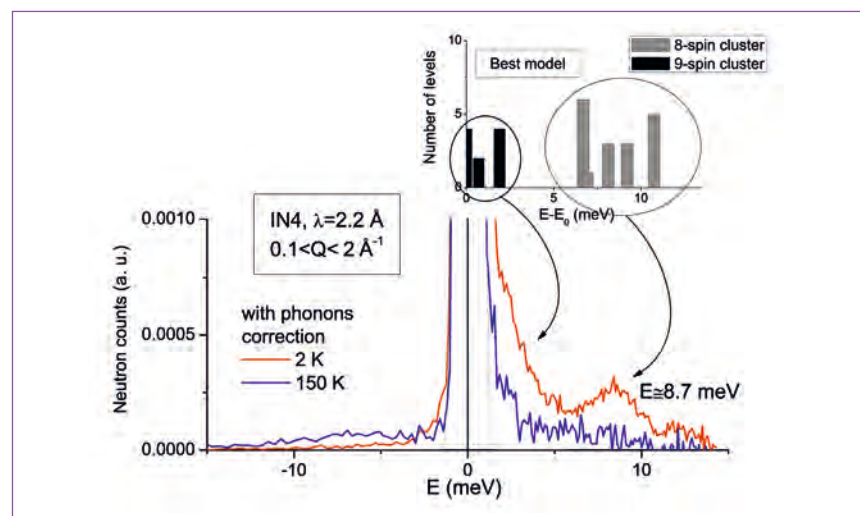
Figure 4: Inelastic neutron scattering probing the clusters energy levels compared to the calculated ones.

References

[1] D.A. Vander Griend, S. Malo, S. J. Barry, N. M. Dabbousch, K. R. Poeppelmeier, and V. P. Dravid, Solid State Sci. 3, 569 (2001)

[2] J. Robert, B. Canals, V. Simonet, R. Ballou, C. Darie, B. Ouladdiaf, and M. Johnson, J. Phys.: Cond. Matt. 19 145280 (2007)

[3] J. Robert, V. Simonet, B. Canals, R. Ballou, E. Lhotel, C. Darie, P. Bordet, B. Ouladdiaf, M. Johnson, J. Ollivier, D. Braithewaite , H. Rakoto, and S. de Brion, Phys. Rev. B vol. 77 (2008) 054421

Base-pair opening and the energy gap in DNA melting

DNA melts at temperatures around 100° C (370 K) depending on the base-pair composition. Vibrational modes, which increase the separation between base molecules, are thought to play an important role but these are typically assigned frequencies around 10 meV (120 K). Understanding DNA melting and related biological processes requires this apparent energy gap of more than 200 K to be understood. We have performed atomistic molecular simulations which enable us to reconcile this energy difference between cause and effect

(Original article: Phys Rev E 76, 31917, 2007)

Authors

F. Merzel
(National Institute of Chemistry, Ljubljana, Slovenia)
F. Fontaine-Vive and M.R. Johnson
(ILL)
G.J. Kearley
(Bragg Institute, ANSTO, Menai, Australia)
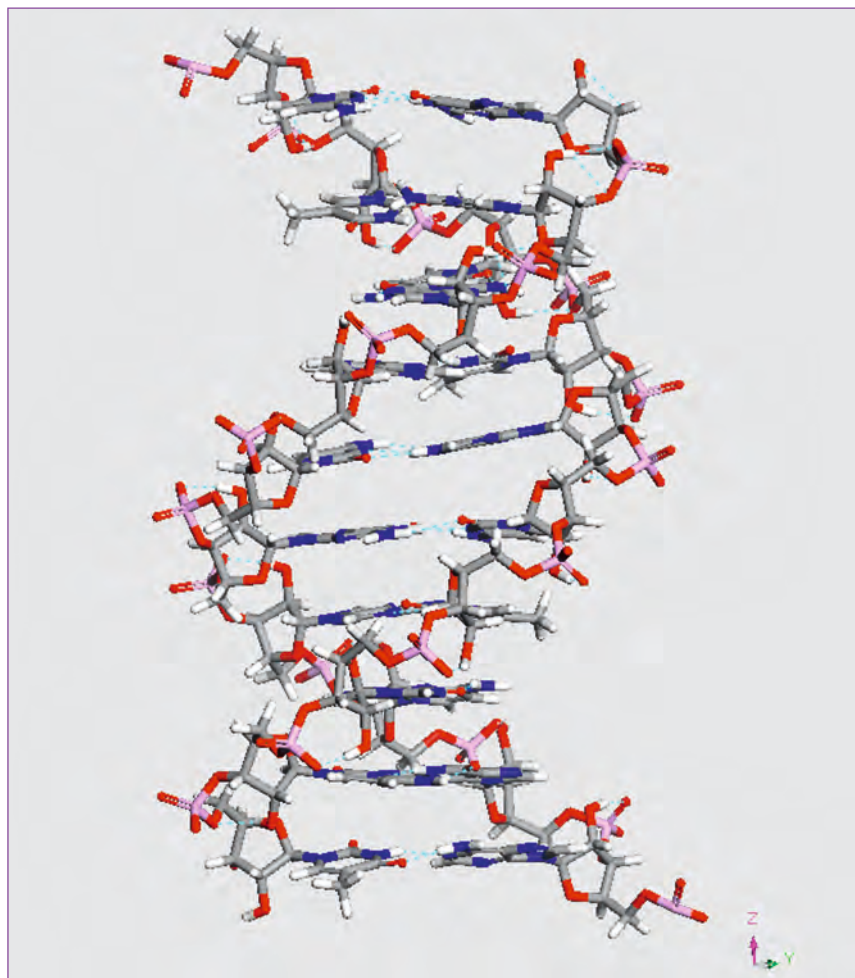
Figure 1: B-DNA model used in this work (water molecules, counter ions and periodic simulation box not shown)

Understanding the function of biological molecules requires a knowledge of their dynamics. In the case of deoxyribonucleic acid (DNA), a key point of interest is base-pair opening as such dynamics play a key role in replication, transcription and melting [1]. These processes all involve the splitting of the double helix into single strands, which is initiated locally by the breaking of inter-base hydrogen bonds and the formation of bubbles spanning several base-pairs. Although these processes often involve proteins, they are thought to be driven by the dynamics of DNA itself.

Experimentally, the dynamics of DNA has attracted considerable attention. A strongly dispersive mode was measured by inelastic neutron scattering (INS) in the vicinity (~20 nm^{-1}) of the base pair Bragg peak [2]. The same dispersive mode has recently been measured by inelastic X-ray scattering (IXS) close to the gamma point in a range of DNA samples [3]. The combined result of these INS and IXS measurements is of an acoustic-type phonon that has a maximum frequency of ~12.5 meV at ~10 nm^{-1}, a minimum of 2-4 meV at ~20 nm^{-1}. At higher Q the phonon is strongly damped and can no longer be measured.

Numerical and theoretical models are also essential for a detailed understanding. Mesoscale models have been developed, in which DNA is typically represented by a one-dimensional chain of effective atoms with a Morse potential
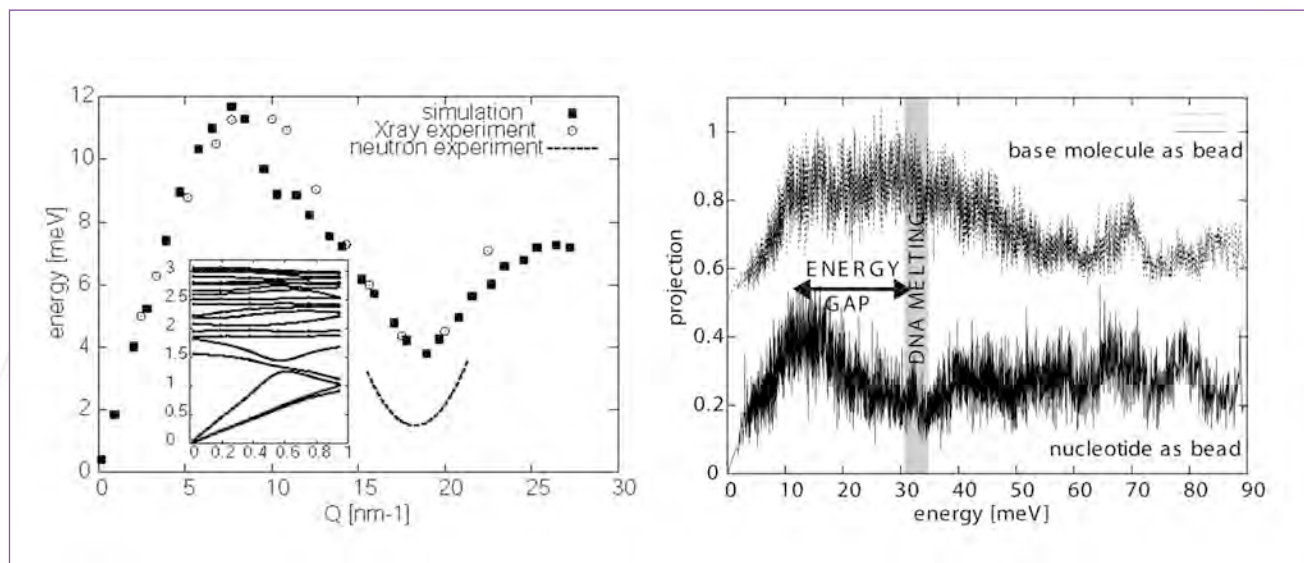
Figure 2: Left panel: calculated and measured spectral dispersion. Inset: dispersion curves in the first Brillouin zone of the helix. Right panel: base-pair opening character of vibrations analysed in terms of nucleotides (bottom curve) and molecules (top curve).

describing the hydrogen-bonding between the base-pair molecules. The Peyrard-Bishop-Dauxois model [4] has been parameterized to reproduce denaturation curves and describes base-pair opening frequencies at 5 meV and 10 meV for adenine-thymine (A-T) and guanine-cytosine (G-C) pairs respectively. Early atomistic models predict base-pair opening frequencies between 7.3 and 10.4 meV for A-T and between 11.8 and 15.4 meV for G-C [5].

We have used the CHARMM force field and molecular simulation package to calculate phonons in terms of all atomistic degrees of freedom which can be analysed at different levels of coarse graining [6]. A DNA structure in the B form (10 base-pairs per helical pitch, length 32 Å) was obtained from the Protein Data Bank (sequence CTCTGCTACT for 1 strand) and the simulation box was filled with 20 Lithium counter ions and almost 1000 water molecules (**figure 1**). MD simulations at 300 K, followed by a quench were used to generate the equilibrium structure.

Figure 2 (left panel, inset) shows the dispersion relations for the first 20 modes in the direction of the helix axis. The acoustic phonons have a maximum frequency of 1 meV at the Brillouin zone boundary. At higher frequencies,

optic modes with limited dispersion are found. Calculating the spectral intensities for all modes for coherent IXS and INS for wave-vectors up to 30 nm^{-1} gives total spectral profiles. These are well-fitted with a simple Gaussian, which enables the characteristic frequency and width of the spectra to be determined for each wave-vector. The dispersion curve obtained in this way (**figure 2**, left panel) agrees well with the experimental data in terms of frequency and width. The experimental signal is not a direct measurement of the acoustic phonons but it is the projection of spectral intensity over a large number of mainly optic modes.

Concerning the base-pair opening modes, the projection of the atomic displacement vectors summed over individual nucleotides on to the corresponding inter-nucleotide vectors, shows a maximum at 10-15 meV (**figure 2**, right panel). This is consistent with previous work, and the frequencies of these vibrations in bead models, but the vibration-melting energy gap is still not explained. However, redefining beads as base, sugar and phosphate molecules in our analysis gives a projection operator with a continuous plateau up to ~40 meV, indicating that base-pair opening modes exist up to frequencies that match the melting temperature of DNA. Base-pair opening occurs over about four nucleotide

pairs in low frequency modes and only over one or two nucleotide pairs at higher frequencies. Bubble formation due to low frequency modes is therefore enhanced by more localized modes close to the melting point.

INS spectra at higher frequency will be used to assess the accuracy of the CHARMM force field. Highly crystalline, oriented samples are prepared on the wet-spinning machine at ILL. These samples are also being used to directly investigate the melting of DNA by Andrew Wildes and co-workers using neutron scattering techniques.

References

[1] M. Peyrard, Nature Physics 2 (2006) 13

[2] H. Grimm et al., Phys. Rev. Lett 83 (1987) 5972

[3] M. Krisch et al., Phys. Rev. E 73 (2006) 61909

[4] M. Peyrard and A.R. Bishop, Phys. Rev. Lett. 62 (1989) 2755

[5] J. M. Eyster et al., Biopolymers 13 (1974) 2505

[6] F. Merzel et al., Comp. Phys. Comm. 177 (2007) 530

Dynamic core-shell structures in two-state models of neutral water-soluble polymers

We perform Monte Carlo simulation of annealed copolymers of solvophobic/solvophilic monomers. Our results show collapsed globular states having dynamic core-shell structures. In these, the core is mostly solvophobic while the core boundary contains an excess of solvophilic monomers.
The simulation results are rationalised in the framework of a simple mean-field model. This two-state model, where each monomer undergoes interconversion between solvophobic and solvophilic state, is a minimal version of models of neutral water soluble polymers.
The core-shell structures may explain the stability of PNIPAM globules as observed in the experiments. The statistics of the monomeric states along the chain vary with the degree of chain swelling. They differ from those of quenched copolymers designed to create water soluble globules though both systems involve core-shell structures.

Macromolecules of amphiphilic polymers contain both hydrophobic and hydrophilic groups possessing different affinity to water and polar solvents. Many synthetic and biological polymers, like proteins and phospholipids belong to this class. Studying theoretical models of amphiphilic polymers leads to a better understanding of important protein and enzyme properties, e.g. transition phenomena in proteins. Water solubility is a characteristic feature of these systems. In our work we discuss a distinctive mechanism operative in water soluble polymers. Namely, the monomers are assumed to interconvert between two states, a hydrophilic state (P) that is favoured at low temperatures, and a hydrophobic (H) state that is preferred at high temperatures.

The collapse of neutral water soluble polymers in aqueous media involves additional ingredients associated with the existence of an upper critical solution temperature. We consider [1] some of these ingredients with view to rationalising experimental results on the collapse behaviour of poly(N-isopropylacrylamide) PNIPAM in water.

We focus on the observations of thermodynamically stable collapsed globules of PNIPAM as reported in [2].

We use an off-lattice Monte Carlo simulation of a minimal version of the two-state models. This involves chains whose monomers undergo a unimolecular interconversion between two-states. The polymers are modeled as freely jointed chain of Lennard-Jones (LJ) particles. The monomers within this bead-spring model interact via a LJ potential. Such core-shell structures can qualitatively affect the binodal curve by lowering the surface tension of collapsed globules. This possibility is supported by experimental observations concerning the collapse behaviour of PNIPAM in water [2]. These structures are also of interest because introducing internal degrees of freedom, as exemplified by the two-state assumption, enlarges the scope of the possible configurational statistics of polymers. Its outcome imitates the amino acid residues sequence of natural proteins yielding guidelines for the synthesis of polymers capable of forming dense, water-soluble globules.
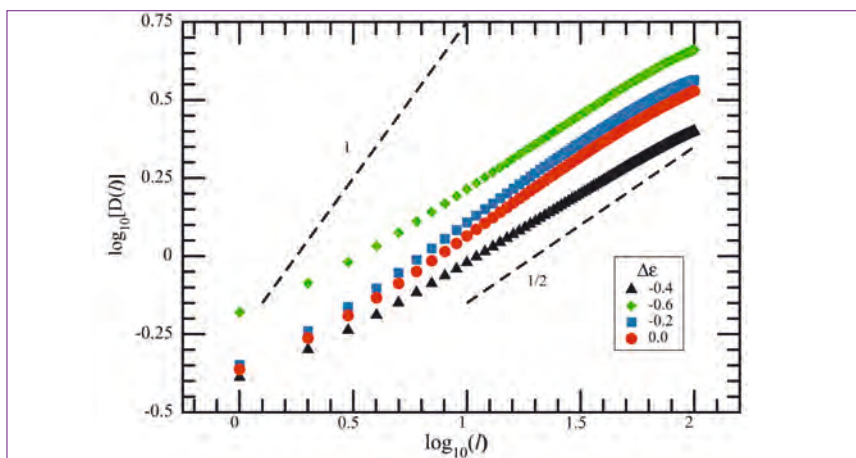
Figure 1: Log D(l) versus log l plots of swollen ($\Delta\varepsilon = -0.6$), collapsed core-shell ($\Delta\varepsilon = -0.2$) and intermediate conformations ($\Delta\varepsilon$ specifies the difference in chemical potential between noninteracting H and P monomers).

Authors

N. Yoshinaga
(Kyoto University, Japan)
D.J. Bicout
(ILL and ENVL Lyon, France)
E.I. Kats *(ILL)*
A. Halperin *(CEA-Grenoble, France)*
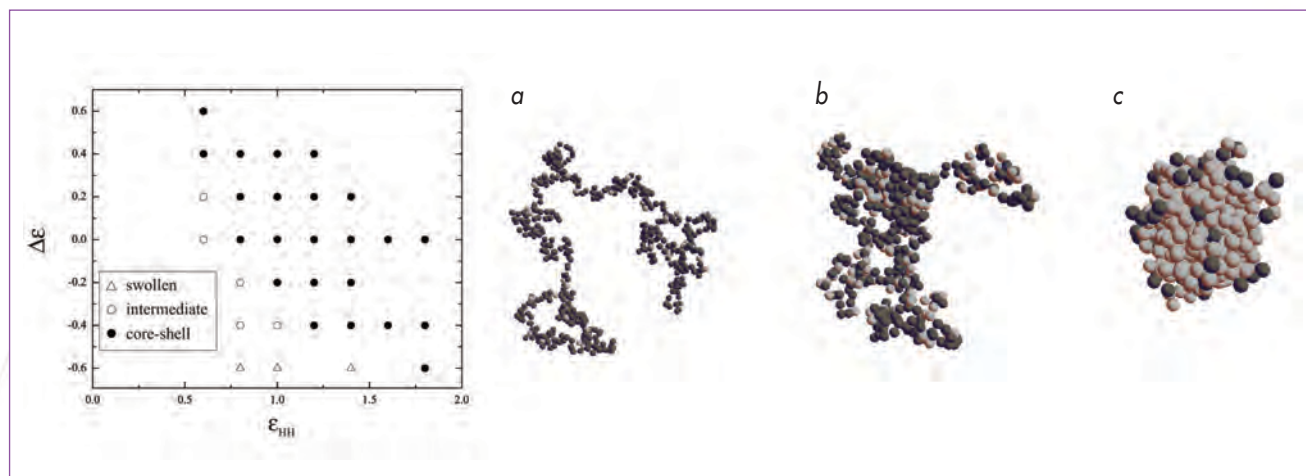
Figure 2: Model phase diagram and snapshots of swollen (**a**), intermediate (**b**) and collapsed (**c**) globules. The P monomers are coloured in dark gray and ε_{HH} is the pair interaction energy between H monomers.

The *PH* sequence and the configurations of the backbone are, in general, coupled. In principle two types of collapsed configurations are possible: dense globules with and without a fringe. The fringe consists of dilute or semidilute loops anchored to the surface of the globule. It is a form of coexistence between dilute and concentrated monomer phases as modified by the chain's connectivity. Our simple heuristic argument suggests however that a core-shell with a *P* rich exterior requires a fringe. To this end we consider a dense globule with a majority of *H* with an exterior shell comprising a binary mixture monolayer of *P* and *H*. Two ingredients distinguish such a shell from the dense core:

(i) One is the missing exterior neighbour. Within this simplified model, the interfacial layer experiences interactions with the dense *H* core substrate. In contrast, the next layer, at higher distance *R* from the centre, is vacant. As a result, the interaction energy now involves a smaller number of neighbours.

(ii) The second ingredient is the possibility of incomplete occupation of the interfacial layer.

Quenched, protein-like, *PH* copolymers form static core-shell structures that are somewhat reminiscent of the dynamic core-shell structures in homopolymers whose monomers interconvert between two states *PH*. In this last case the homopolymers may be considered as annealed copolymers.

Not surprisingly, the sequences corresponding to the two core-shell structures exhibit different statistics. In order to prove this, we generate a non-random walk corresponding to the *HP* sequence by assigning all monomers along the chain with steps $u(H) = 1$ and $u(P) = -1$. The correlations within the sequence are then characterised by the *l* dependence of the dispersion

$$D(l)^2 = \sum_{i,j=k}^{k+l} \left[<u_i u_j> - <u_i><u_j> \right].$$

A random sequence exhibits $D(l) \alpha\, l^{1/2}$ irrespective of the interval considered, while correlations are signalled by $D(l) \alpha\, l^{\alpha}$ with $\alpha \neq 1/2$. We find that in our case the swollen state of the annealed *PH*

copolymers exhibits $\alpha = 1/2$ scaling corresponding to a random copolymer. In contrast, the sequences associated with the dynamic core-shell structures deviate from $\alpha = 1/2$ and do not approach the ballistic case $\alpha \approx 1$ for small *l* (**figure 1**). This is because the interconversion of *PH* opposes block structure.

We found various equilibrium structures in our study, illustrated in **figure 2** along with the model phase diagram.

Our results illustrate how it is possible to profoundly change macroscopic behaviour by changing physical properties on a nanometric scale.

References

[1] N. Yoshinaga, D. Bicout, E. Kats and A. Halperin, *Macromolecules* 40 (2007) 2201

[2] C. Wu and X. Wang, *Phys. Rev. Lett.* 80 (1998) 4092

Correlated disorder and magnetic properties of colossal magneto-resistive materials

Figure 1: The inhomogeneous structures are the consequence of a (short-range) correlated disorder created by the replacement of a R^{3+} ion by a A^{2+} ion. (a) to (c): pictures of the calculated Mn-Mn couplings (or the local kinetic energy of the carriers) on the bonds of the crystal (high energy in dark) on one layer for three different carrier concentrations 0.1, 0.3, 0.5.

In colossal magneto-resistive materials, a realistic model for the disorder induced by the chemical doping refutes the idea that the Curie temperature of the ferromagnetic phase and the spin stiffness are controlled by the averaged magnetic coupling. A chemical dopant surrounded by neighbouring ions perturbs its environment in a way that respects the local symmetry. The local disorder is then not fully random (as in the Anderson disorder) but does maintain some degree of 'correlations' in space. We have found that such correlations tend to favour *inhomogeneous* charge and magnetic nano-scale structures with long-tailed distributions. We show that such inhomogeneous structures enhance the Curie temperature and decrease the spin stiffness, and could explain large deviations from the physics of clean systems.

Authors

G. Bouzerar
(Institut Néel, Grenoble and ILL)
O. Cépas
(LPTMC, Paris and ILL)

Manganese oxides of the family $R_{1-x} A_x MnO_3$ have fascinating electric and magnetic properties, the most well-known phenomenon being the colossal magnetoresistance: a magnetic field of a few tesla strongly suppresses the sample resistance. This occurs at temperatures of about 200 K, close to the border between a paramagnetic insulating and a ferromagnetic metallic phase.

The alignment of the localised spins of the Mn^{3+} ions allows the conduction electrons with the same spin to move more easily thanks to the Hund's coupling: this is the mechanism of double-exchange of Zener which has triggered interest in the search for spintronics. The amplitude of the phenomenon is, however, a major challenge: a few tesla changes the resistivity by an order of magnitude.

This raises the immediate question: what causes the strong variations of resistivity of these samples at the transition? Can disordered spins alone be at the origin of this effect? Is the chemical disorder (the substitution of a cation R by A induces a local disorder) a crucial ingredient or is the disorder 'self-induced' by a fraction of electrons [1]? All these questions remain at the centre of the discussion of the colossal magnetoresistance effect but a definite answer has not yet emerged.

In order to better appreciate to what extent the disorder is important we have studied its signatures in the magnetic properties. Indeed, (i) the magnetic excitations do not follow the simple cosine law of magnons in a ferromagnet, but are broadened; (ii) the spin stiffness is no longer

related to the critical temperature by a coefficient that depends only on the lattice structure but covers a wide range [2]. Basically, it is observed that the departure from the clean case is larger when the impurities in the sample are dilute: the spin stiffness over Curie temperature ratio of a sample with 10% of impurities is 5 times smaller than that with nearly 50% of impurities. Similarly in the 10-20% range of impurity concentration, phases that are known as Griffiths phases have been identified [3,4] (anomalies in the magnetic susceptibility) above the Curie temperature.

In such highly disordered phases, large (rare) clusters give singular contributions to the thermodynamic properties. It is actually highly debated whether the Griffiths phase is a prerequisite or not for the colossal magnetoresistance phenomenon [3,5].

We have shown that these experimental features can be explained by a simple model of 'correlated' disorder. In 1960, (together with the explanation of the spin-canted phase of the low-doped manganese oxides) P.-G. de Gennes [6] has discussed the influence of local 'colour-centers' resulting from the substitution of a R^{3+} ion by a A^{2+} ion. They create a Coulombic potential on the 8 neighbouring sites and a local orbit for the carriers which reinforces the local ferromagnetism. This is in essence, the local object that Nagaev called a 'ferron'. It is important to stress that it is a very different way to model the disorder as compared to the random uncorrelated potentials of the 'Anderson' model of disorder which is often considered in the literature. Now when a finite density of impurities is
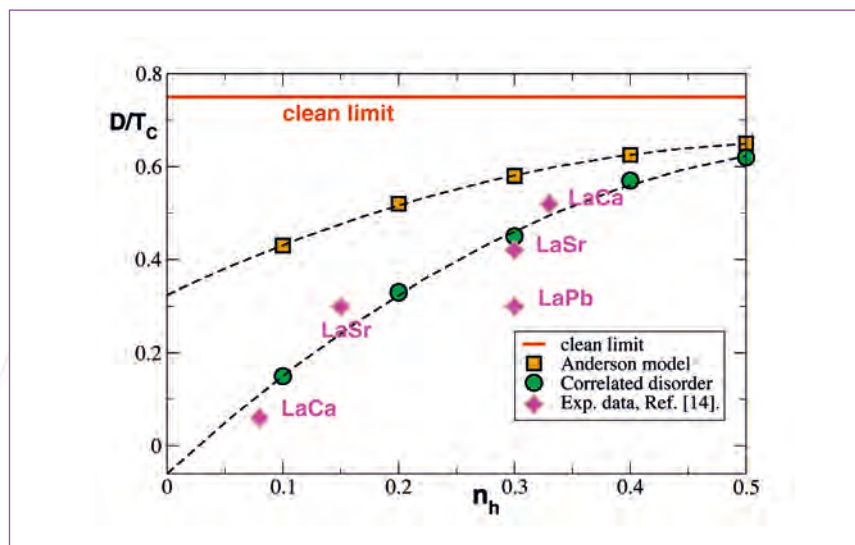
Figure 2: Ratio D/T_C as a function of hole concentration (Theory [circles] and Experiments [diamonds], see Ref. [2]). D is the spin stiffness (the lattice constant is a = 1) and T_C the Curie temperature. Anderson form of disorder cannot account for the amplitude of the reduction [squares].

present, we have found quite a different situation [7]. Instead of clear localised ferrons, the ferromagnetism is reinforced along paths of 'least action' for the carriers: large inhomogeneous structures emerge (figure 1), similar in fact to what has been seen by scanning tunneling microscopy.

In **figure 1**, we show the local kinetic energy of the carriers (the darker the stronger). According to the mechanism of double exchange this provides a direct picture of the nearest neighbour Mn-Mn spin couplings. In **figure 1a** (low carrier concentration) we clearly see nano-scale inhomogeneities where the couplings deviate strongly from the averaged value. When the concentration of carrier is increased (from left to right) such structures tend to disappear and the system becomes overall more homogeneous. All these features are direct consequences of the presence of short range correlation in the disorder. In contrast when a standard Anderson model (uncorrelated) is considered no such structures are observed.

Ferromagnetic Phase

The question of the influence of such inhomogeneous structures on both transport and magnetic properties is of great interest. We have found that the ratio of spin stiffness

to the Curie temperature was strongly affected by the presence of inhomogeneous structures. Indeed, at low carrier concentration the deviation from the clean case or from that obtained with the Anderson form of disorder (uncorrelated) is strongly enhanced. Note that, this ratio has been calculated including both thermal fluctuations within the random phase approximation and the disorder (localisation effects) was treated exactly [8]. Very low ratios for D/T_C were found in the low density regime (down to 0.1, see **figure 2**). They can be explained quite simply: T_C and D are not controlled by the same characteristic couplings. Roughly T_C is governed by an average associated to the strong coupling regions and couplings between them (thermal fluctuations have to destroy the magnetisation everywhere!) whereas D is governed by the weak coupling of the hole poor regions to allow the propagation of the long wavelength excitations in these regions. At half filling where the system is much more homogeneous (**figure 1c**) we found that the ratio gets closer to that expected for a model with no disorder (0.75 for a cubic lattice in the clean limit) and is almost similar to that obtained for the Anderson model. This clearly shows that the more inhomogeneous a sample, the smaller the ratio D/T_C.

This effect seems to account for the general trend of manganese oxides as shown in **figure 2**.

Griffiths Phase

At large temperature (T larger than T_C), although the phase is paramagnetic, some (non percolating) clusters have not yet reached their 'local' Curie temperature and behave as large magnetic moments.

This is made possible because the correlated disorder leads to long tails in the distribution of exchange couplings and allows the existence of regions with very strong couplings. We could estimate the maximum 'local' Curie temperature and compare it with the Griffiths temperature T_G identified with the anomalies in the experimentally measured susceptibility. We have found that the calculated T_G is weakly dependent on the carrier concentration and that the Griffith phase region (region between T_C and T_G) increases strongly as we decrease the carrier concentration. These features agree qualitatively well with the experimental observations.

We have shown that the present model Hamiltonian with 'color-centers' captures essential features of manganese oxides pretty well: large inhomogeneous structures (**figure 1a**), low spin stiffness, large Curie temperature (**figure 2**) and Griffiths phases. Consequently the present model makes a perfect candidate to study transport properties of manganese oxides!

References

[1] T.V. Ramakrishnan et al., Phys. Rev. Lett. 92 (2004) 157203

[2] T. Chatterji et al., J. Alloys Compd. 326 (2001) 15

[3] M.B. Salamon, et al., Phys. Rev. Lett. 88 (2002) 197203

[4] J. Deisenhofer et al., Phys. Rev. Lett. 95 (2005) 257202

[5] W. Jiang et al., Phys. Rev. Lett. 99, 177203 (2007)

[6] P.-G. de Gennes, Phys. Rev. B 118 (1960) 141

[7] G. Bouzerar and O. Cépas, Phys. Rev. B 76, (R) (2007) 020401

[8] The calculated T_C agree very well with the Monte Carlo simulations for both the clean case and for the Anderson model

Nodal/antinodal dichotomy and the two gaps of a superconducting doped mott insulator

Figure 1: Spectral function A(k,ω) for different doping δ. Panel A: nodal quasiparticle peak; Panel B: normal component (set $\Sigma_{ano}=0$) of the antinodal quasiparticle peaks; Panel C: nodal and antinodal quasiparticle weights. The inset shows the k_x-positions of the nodal and antinodal points in momentum space; Panel D: spectra at the antinodes.

We study the superconducting state of the hole-doped two-dimensional Hubbard model using Cellular Dynamical Mean Field Theory. In the under-doped regime, we find a natural decomposition of the one-particle (photoemission) energy-gap into two components. The gap in the nodal regions, stemming from the anomalous self-energy, decreases with decreasing doping. The antinodal gap has an additional contribution from the normal component of the self-energy, inherited from the normal-state pseudogap, and it increases as the Mott insulating phase is approached.

Authors

M. Civelli *(ILL)*
M. Capone
(SMC, CNR-INFM and University of Rome, Italy)
A. Georges
(CPhT and CNRS, Ecole Polytechnique, France)
K. Haule and G. Kotliar
(Rutgers University, NJ, USA)
O. Parcollet
(CEA and CNRS-Saclay, France)
T.D. Stanescu
(University of Maryland, USA)

Superconductivity in the high-T_C cuprates has been the subject of intensive research for more than twenty years (for a review see for example reference [1]). Low-energy descriptions in terms of quasiparticles interacting with bosonic modes (such as phonons or spin fluctuations) have been widely studied starting from the weak correlation limit. A different approach views the essence of the high-T_C phenomenon as deriving from doping with holes a Mott insulator [2]. The strong correlation viewpoint has not been yet developed into a fully quantitative theory and whether the weak- and strong-coupling pictures are qualitatively or only quantitatively different is an important open issue.

The development of Dynamical Mean Field Theory (DMFT) and its cluster extensions [3] provide a new path to investigate strongly correlated systems. These methods construct a mean-field theory for Hubbard-like models using a cluster of sites embedded in a self-consistent bath.

In this work we use Cellular DMFT (CDMFT) to explore the nature of the energy gap in the one-particle spectra of the superconducting state when correlations are strong. The goal is to identify qualitative aspects describing the approach to the Mott transition in the light of recent experimental studies on the superconducting state of under-doped cuprates (see for example [4] and references therein), which report the presence of two energy scales associated with nodal and antinodal regions.

We therefore consider the two-dimensional Hubbard Model:

$$H = -\sum_{ij\sigma} t_{ij}\, c^{\dagger}_{i\sigma}\, c_{j\sigma} + U\sum_i n_{i\uparrow}\, n_{i\downarrow}$$

Where $c_{i\sigma}$ destroys an electron with spin $\sigma=\downarrow,\uparrow$ on site i, $n_{i\sigma}=c^{\dagger}_{i\sigma}\, c_{i\sigma}$ is the number operator and $t_{ii}\equiv\mu$ is the chemical potential. Only next-neighbour t and nearest-next-neighbour $t'=-0.3t$
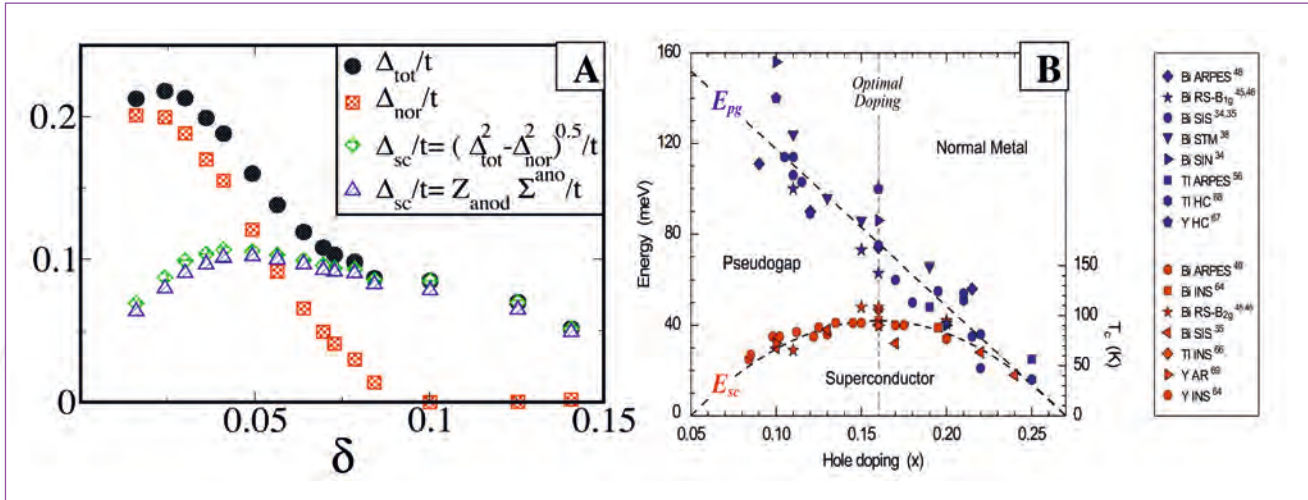
Figure 2: : Panel A: energy-gaps from CDMFT results. We show as a function of doping δ the antinodal energy gap Δ_{tot} (circles), obtained from the spectra of panel D in figure 1, decomposed in a normal contribution Δ_{nor} (squares), obtained from panel B in figure 1, and in a superconducting contribution Δ_{nor} (diamonds). Panel B: the two energy-gaps E_{sc} (superconducting) and E_{pg} (pseudogap) from different experiments (figure taken from reference [4]).

hoppings are considered. The on-site repulsion is set at $U=12t$. We implement CDMFT with the Lanczos method on a $2\cdot2$ plaquette, which allows study of a d-wave superconducting state.

Our main result is the presence of two energy-scales on the under-doped side of the phase diagram. This can be shown directly from an analysis of quantities defined inside the $2\cdot2$ cluster, which are the output of the CDMFT procedure [5]. However, in order to make contact with experimental observables, we extract the momentum-resolved Green's function $G_\sigma(k,t)=-i<c_{\sigma k}(t)\ c^\dagger_{\sigma k}>$ from the local cluster quantities. For this we employ a periodisation procedure, which restores the translational invariance of the lattice [5]. The imaginary part of the time-energy Fourier Transform $\int e^{i\omega t}\ ImG_\sigma(k,t)\ dt$ yields the spectral function $A(k,\omega)$, which is measured in photoemission spectroscopy. In order to physically interpret our results as compared with experiments, we first disentangle the normal from the superconducting contribution in $A(k,\omega)$ (which is possible within our scheme by simply setting the anomalous self-energy $\Sigma_{ano}=0$). $A(k,\omega)$ is shown in **figure 1**. The k-points along the nodal and antinodal directions are operatively defined as those where the highest peak is observed in $A(k,\omega)$. Their actual values are shown in the inset of panel C of **figure 1**. Near the nodal point (panel A) a quasiparticle peak is well defined at the Fermi level ($\omega=0$) and decreases by decreasing doping. In the anti-

nodal region (panel B), a quasiparticle peak is also found at the Fermi level for doping $\delta>0.08$. For $\delta<0.08$, however, the spectral weight shifts to negative energies signaling the opening of a pseudogap, whose size increases as $\delta\to0$. The approach to the Mott transition is characterised by a strong reduction in the area of the nodal spectral peak Z_{nod}, which is plotted in panel C (green circles). We also plot the area of the antinodal peak Z_{anod}, which shows a constant value upon the opening of the pseudogap. In panel D, we restore $\Sigma_{ano}\neq0$, and examine the actual superconducting solution. The superconducting gap opens in the antinodal region (the nodal region is practically unaffected). For doping $\delta>0.08$ the spectra are almost symmetric around the Fermi level, as in a standard superconductor.

In contrast, close to the Mott transition the pseudogap, which originates from the normal component, is superimposed on the superconducting gap, resulting in asymmetric spectra.

We finally turn to the superconducting energy-gap in **figure 2** (panel A). We evaluate the antinodal gap in the superconducting state Δ_{tot} by measuring the distance from the Fermi level ($\omega=0$) at which spectral peaks are located in panel D of **figure 1**. The normal contribution Δ_{nor} is extracted from panel B of **figure 1**. We also display the anomalous contribution to the antinodal gap $\Delta^2_{sc}=\Delta^2_{tot}-\Delta^2_{nor}$. The appearance of Δ_{nor} coincides with a downturn in Δ_{sc}. We interpret

Δ_{tot} as the monotonically increasing antinodal gap observed in cuprates superconductors, while the superconducting gap Δ_{sc} is decreasing in approaching the Mott transition.

The concept of two energy gaps with distinct doping dependence in the cuprates has recently been brought into focus from an analysis of Raman spectroscopy, and photoemission experiments [4], which have revived experimental and theoretical debate (see also panel B of **figure 2**). Our theoretical dynamical mean-field study of superconductivity near the Mott transition establishes the remarkable coexistence of a pseudogap, stemming from the normal self-energy, with superconducting gap, stemming from the anomalous self-energy. The two gaps present opposite trends with decreasing doping.

References

[1] K.H. Bennemann and J. B. Ketterson, Physics of Superconductors II, Springer-Verlag Berlin Heidelberg New York (2004)

[2] P.W. Anderson, Science 235 (1987) 1196

[3] G. Kotliar et al., Rev. of Mod. Phys. 78 (2006) 000865

[4] S. Huefner et al., arXiv:0706.4282

[5] M. Civelli et al., Phys. Rev. Lett. 100, 046402 (2008)

**On 17 January 2007
the ILL celebrated its 40th anniversary!**

The ILL was founded on 19 January 1967 with the signing of an agreement between the French Republic and the Federal Republic of Germany. It was the friendship between Louis Néel and Heinz Maier-Leibnitz and the influence they were able to wield that brought the project to its fruition in Grenoble.

The ILL was conceived as a service institute, an innovative status at the time. It was to offer the scientific community the world's leading facilities in neutron science and technology - a large cold neutron source and ten neutron guides, each capable of serving three or four instruments with a very high-intensity neutron flux.

The construction of the Institute and its high-flux reactor in Grenoble represented an investment of 335 million francs and was a joint venture by France and Germany. The reactor went critical in August 1971 and reached full power (57 MW) a few months later in December. Actual experiments began in 1972.

In January 1973 the United Kingdom decided to join the ILL. It became the Institute's third Associate member when it signed the Intergovernmental Convention of 19 July 1974.

The following ten countries have since signed Scientific Membership agreements with the ILL: Spain (1987), Switzerland (1988), Austria (1990), Russia (1996), Italy (1997), the Czech Republic (1999), Sweden and Hungary (2005), Belgium and Poland (2006).

Over the years, the ILL has firmly established itself as a leader in neutron science and technology. The Institute offers an exceptional centre of excellence, a fine example of successful co-operation in Europe, and a prototype of the European Research Area.

A lot has happened at the ILL since the 10-year Millennium Programme was first launched in 2000. The result is that our instruments can deliver 14 times as much high-quality data as they did in 1999. Today, our principal ambition is to keep the ILL at the forefront of neutron science for the next 20 years.

With its 40 years of experience the Institute can boast not only a most successful past but also the prospect of a splendid future.
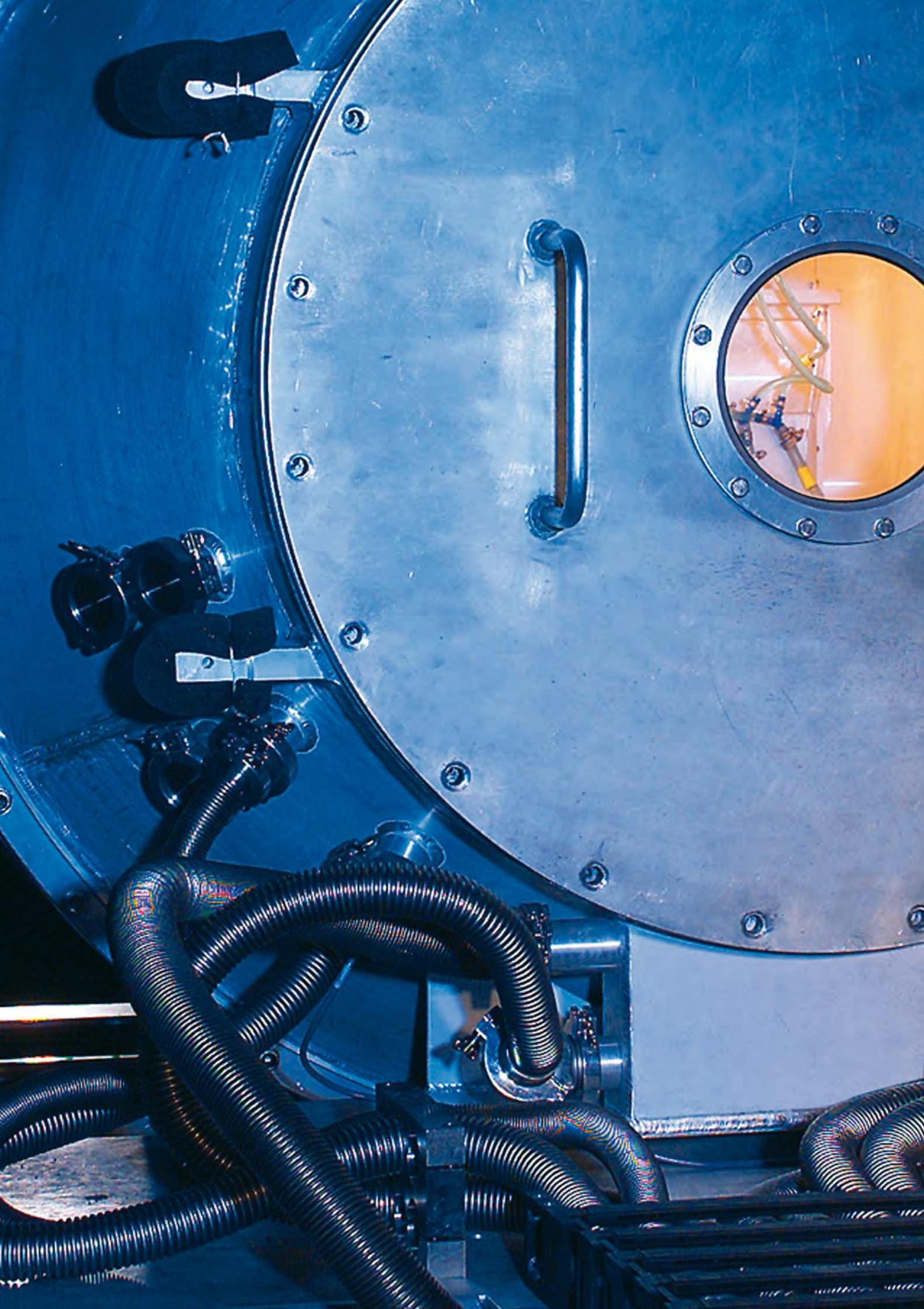
Millennium programme and technical developments

Millennium programme
Technical and computing developments
New experimental techniques

The ILL is a mature and vibrant institution changing and adapting to new challenges. It has proved itself as a research facility for both external users and ILL staff. The continuous evolution of the Institute is exemplified by the Millennium Programme, which is now well established as a one of the Institute's continuous technical development activities.
By the end of 2008 its initial M0 phase will have provided us with brand new instruments such as IN5B and FIGARO and will have evolved into its M1 phase for the 2008-2013 period.

The continuous evolution of the Institute is exemplified by the Millennium programme

Under M1 we will be focusing on five new instruments and their neutron infrastructure. Four different instruments will be re-sited at more suitable positions with increased neutron flux. The size of the official instrument suite will be maintained with the decommissioning of seven older instruments. Major changes are also planned for our sample environment facilities and ancillary equipment, the introduction of new cryostats and superconducting magnets in particular. Four instruments will be upgraded for improved performance at moderate cost. Detailed plans for some of these projects have not yet been signed and sealed; collaboration with our external partners remains on the agenda, for this has always been one of the strengths of the ILL's scientific and technical programme.

Initial discussions have already begun on a further phase of the programme: phase M2 will run from 2013-2016 and promises exciting new possibilities. The vision of a new cold source or a partnership on very high magnetic fields with our neighbours on the Polygone Louis Néel site could open up major innovations in the years to come.

The development of new instrumentation whilst simultaneously furnishing quality technical services under the user programme is an exacting art.
To ensure optimum performance, a full-fledged management system was introduced for the Millennium Programme. The projects all share identical and transparent project management procedures (for both scientific and technical aspects), with well defined steps, clear deliverables and reports at each milestone. This ensures that the scientific programme maintains its momentum and that we optimise the allocation of our necessarily limited human and financial resources.

There are a number of other projects outside the Millennium Programme that contribute to the continuous development of the ILL instrument suite.
We are currently working on the new CCD alignment camera and beam monitors, a new generation of neutron detectors, polarimetric neutron techniques, neutron optics design, neutron guide alignment techniques and instrument control software.
It is such continuity in development that underlies the ILL's strength in its field.

2007 was a year of intense activity and rigorous planning. The results of these endeavours are now beginning to feed through.

José Luis Martinez
Associate Director

The Millennium Programme

4

The Millennium programme passed an important milestone in 2007 with the formal approval by the Steering Committee of the ILL of its plans for the future. As the current ('M0') phase comes to an end, momentum will be maintained through the launch of a second ('M1') phase. This will furnish ILL with 5 new and 4 upgraded instruments over the next 6 years.
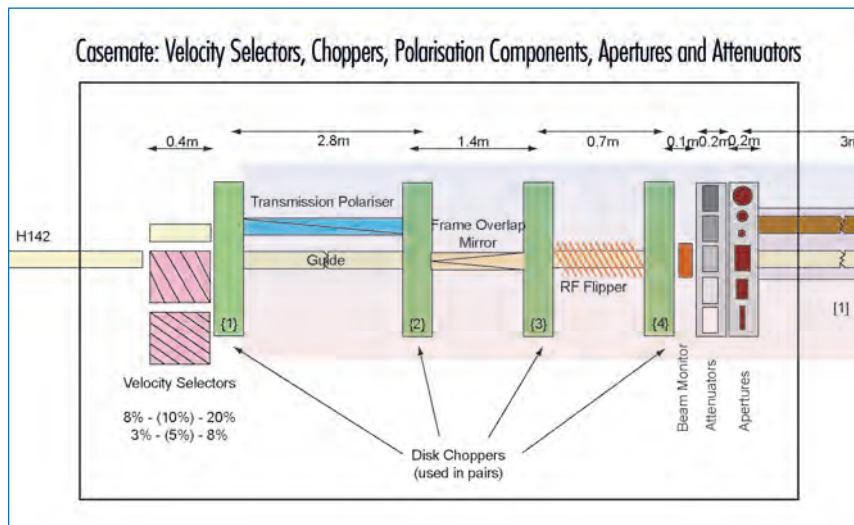
Figure 1: The polarisation components of the new small-angle scattering instrument D33.

The second phase of the ILL Millennium Programme foresees the construction of five new instruments: **D33** (**figure 1**) – a small-angle scattering instrument optimised for materials science and magnetism; **IN16B** (**figure 2**) – a backscattering spectrometer with a high-efficiency phase space transformer; **ThALES** (**figure 3**) – a cold neutron triple-axis spectrometer with a wide kinematic range; **WASP** – a high intensity, wide angle spin-echo spectrometer; **SuperADAM** - a polarised reflectometer and a German-Swedish CRG.

The first four of these instruments will occupy end positions of **new guides**, some of which will also service and enhance the flux of other instruments. Several upgrades will also be made.
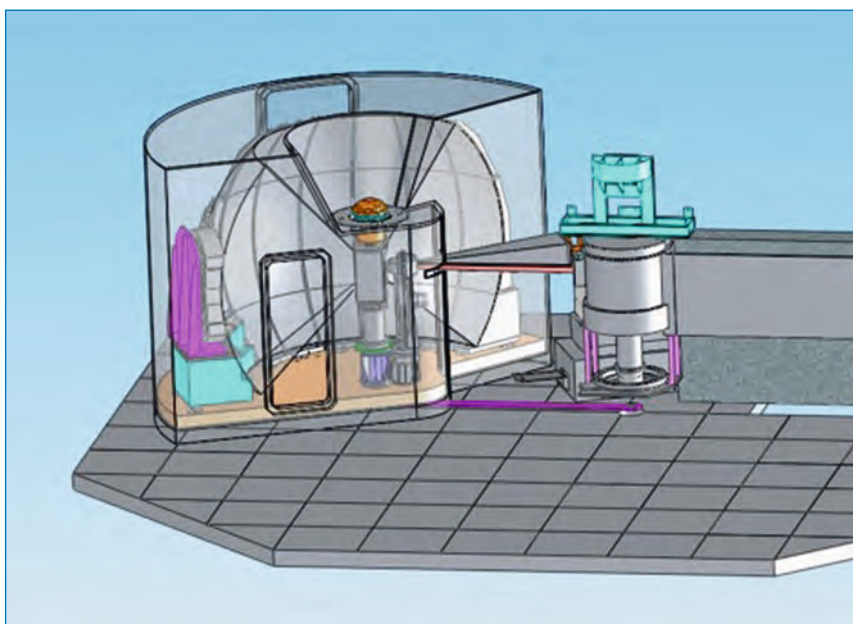
Figure 2: IN16B, a new back-scattering spectrometer with a high-efficiency phase-space transformer.

Author

A. Harrison
(ILL)

The beryllium-filter of **IN1** will be replaced by a new generation analyser that will provide unprecedented angular acceptance (2.5 sterrad) with a significantly improved energy resolution and a signal-to-noise ratio boosted by two orders of magnitude in the **LAGRANGE** project.

A key feature of an upgrade to **D17** will be higher detected flux – particularly for smaller samples – and the facility for polarised time-of-flight measurements; **IN4** will receive essential maintenance to maintain an important range of Q and ω within the ILL instrument suite.
These developments will require extensions to both guidehalls – **ILL7** and **ILL22** – to accommodate new, large instruments.

Finally, sample environment will be boosted, primarily through the provision of new magnets, furnaces and cryostats.

Many of the new instruments supersede older machines which will be decommissioned: the next few years will see the withdrawal of D1A, DB21, IN10, IN3, IN14, IN16, IN11 and ADAM. A long reactor shut-down is scheduled for 2011 while work on the in-pile section of new guides for ILL22 and ThALES takes place.

2007 has also seen the completion or commissioning of several M0 phase instruments. The thermal neutron diffractometer **D19** has been a fully-scheduled instrument from October 2007 but still continues to improve through refinement of the data analysis software, crucial to large-area multidetector instruments of this type.

The first stages of commissioning of **LADI-3** – a new Laue diffractometer for protein crystallography - have shown an increase by a factor of 2-3 in the efficiency of readout of the image plate relative to the system used in the original LADI-1 instrument.

The upgrade of the high-resolution two-axis diffractometer **D2B** has been completed through the installation of the new sample environment changer which can automatically move not only multiple cassettes of sample cans, but also entire pieces of equipment, including a new, dedicated 6T magnet, a cryofurnace, or a displex chiller.
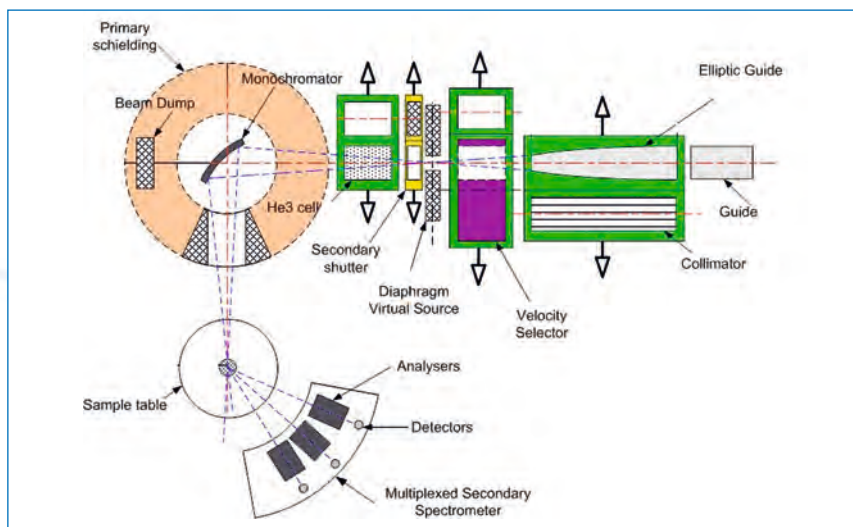
Figure 3: ThALES, the next generation cold three-axis spectrometer using state-of-the-art optics.

Figure 4: The multiplexed secondary spectrometer FlatCone operating on IN20.
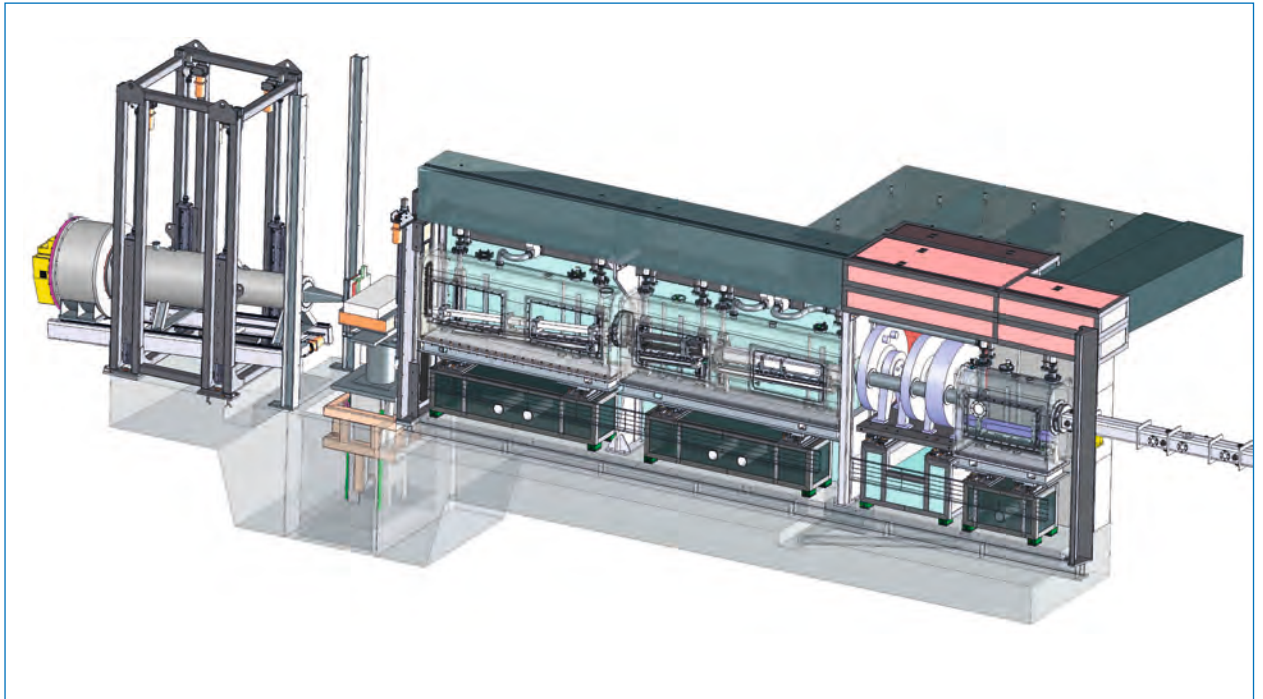
Figure 5: FIGARO, a new horizontal reflectometer to investigate fluid interfaces.

D7 – a diffuse scattering spectrometer with polarisation analysis – received the final analyser/detector bank in January 2007, marking the completion of the project one year ahead of schedule; the revamped instrument enjoys an increase by more than a factor of 70 in effective counting rate, together with an improved energy resolution – from $\Delta E/E_1$ = 11% to 4 % - provided by a new chopper and slit.

FlatCone – a versatile multiplexed secondary spectrometer for TAS instruments is now delivering impressive results as a fully-scheduled instrument, having successfully demonstrated that the tilting options works well both in terms of mechanical control and the optics of the instrument for such extended geometries. (**figure 4**)

There are also ongoing projects that will come to fruition in 2008.
Much of the guide for the new horizontal reflectometer **FIGARO** (**figure 5**) was installed during the summer of 2007, while space was made for the instrument through the relocation of D16 to ILL 22. Most of the key components of FIGARO such as the choppers and prototype detector have been successfully tested, and the instrument and the rest of the guide is on course for completion and commissioning over the first two reactor cycles of 2008.

FIGARO requires a wide but shallow beam which is taken from the lower part of the H17 beam port; the upper part is channeled through a separate guide

that will supply two instruments in level C of the reactor: **GRANIT**, intended to explore gravitational states, and **CryoEDM**, a CRG instrument designed to search for, or set an upper limit on the electric dipole moment of the neutron, and which will be moved from its current position in ILL 22 when WASP is installed.

The upgrade of the small-angle scattering instrument **D11** is also set to be finished during 2008, involving a complete refurbishment from the guide through the tank to the detector and its electronics; a USANS option that has the potential to go down to Q = 1 x 10^{-5} Å^{-1} is being developed at ILL and in collaboration within a joint research activity funded by FP6 (NMI3 project).

Figure 6: *IN5 secondary spectrometer flight chamber with the inset showing one of the cassettes of the 3m position-sensitive detectors.*

The third project due to be completed in 2008 is the upgrade of the secondary spectrometer of time-of-flight spectrometer **IN5** (**figure 6**). The massive - 17 ton - time-of-flight vacuum chamber for the secondary spectrometer was delivered in three sections and assembled on stands in the 'Hall d'Essais' workshop to test its vacuum seals and also the mounting of 12 cassettes of linear PSD detectors whose in-house fabrication was completed this year (**figure 7**);

this will give an increase by a factor of 6 to the detected flux on this instrument.

The Millennium Programme has also seen great progress with respect to infrastructure. The **world record in polarisation of** ^{3}**He spin filters** on an instrument continues to rise, now hovering at 80% on the Tyrex station equipped with zero-field 'magic box' devices for carrying filled cells to where they are used. The range

of **cryogen-free cryostats** continues to broaden, with new, rapid-cooling devices for Eulerian cradles that are available for diffractometers D9, D10 and D15, as well as relatively high-power devices for a 10 T asymmetric magnet.

Work on **NOMAD**, the instrument control software that provides the same framework across ILL, is focusing on ensuring that it is as stable as possible on the instruments on which it is currently installed; we anticipate an increasing implementation over the following few years, during which time the older system, MAD, will continue to be supported.

Figure 7: *Installation of the detector cassettes inside the flight chamber of the IN5 secondary spectrometer.*

Renaissance of the IN5 time-of-flight spectrometer

The year 2007 has seen the completion of key parts of the IN5 new secondary spectrometer. The manufacture and tests of the Position Sensitive Detector (PSD) panels have been completed and the time-of-flight vacuum chamber that will host the detectors has been delivered to the ILL. Pre-assembling and various tests will now run up to the installation at the instrument position by early 2008.

The IN5 high-precision direct-geometry spectrometer located on the H16 cold neutron guide has been undergoing upgrading for almost 10 years. Following the primary spectrometer (neutron guide and disk chopper) completed at the end of 2002, the secondary spectrometer (from the sample to the detectors) will mark a new milestone in the life of this 30 year old instrument.

The primary spectrometer upgrade gave a notable increase of the neutron flux at the sample, enlarged the accessible resolution range and improved the reliability of the instrument. The new secondary spectrometer promises a breakthrough in the cold neutron time-of-flight technique.

Combined with the increase of the effective detection solid angle, the qualitative novelty will be a position sensitive detector (PSD) array in a vacuum time-of-flight chamber. This improvement in detection aims at allowing single crystal studies in addition to conventional spectroscopy.

The secondary spectrometer

PSD technology has already been applied on time-of-flight instruments but IN5 will be the first cold-neutron spectrometer equipped with such detectors. This will allow probing of the high-resolution energy range covered by *cold neutrons* complementing the thermal instruments using such detectors. Progress in electronics has relaxed the constraints on the detector length. The required spatial resolution on IN5 will be achieved with 3 metre-length detectors.

An array made of such long tubes modifies the shape of the detector assembly which is now no longer tangent to a sphere but cylinder-shaped. Despite some disadvantages, the cylindrical shape allows simplifications of the design of the secondary spectrometer, e.g. detector mounting.

The position sensitive detectors

The PSDs will cover the inner back surface the chamber 4 m from the sample (**see figures 1 and 2**). The total detection area will be six times larger than before and will boost the neutron count-rate by the same amount.
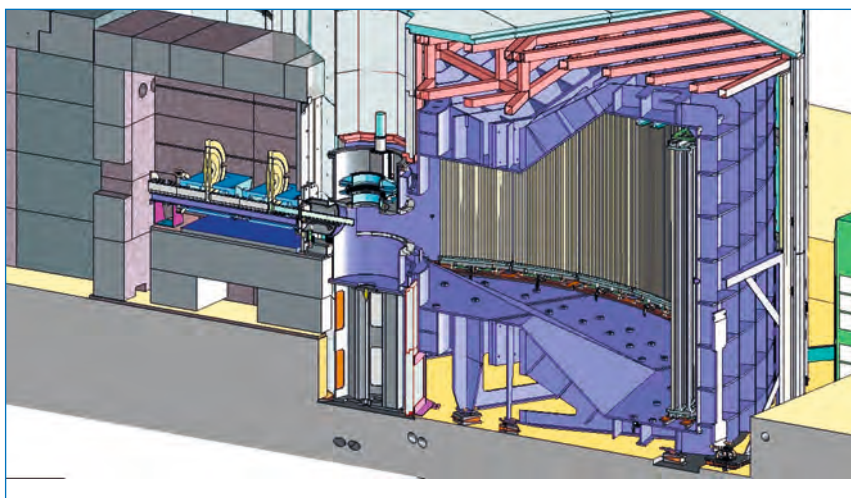
Figure 1: Vertical slice along the beam axis showing the last choppers, the sample chamber, the detector array, the flight chamber and the detector shielding (Image courtesy of B. Grenappin).
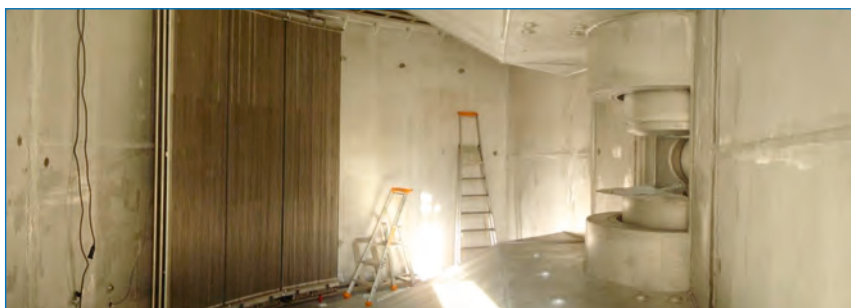

Figure 2: Three detector units mounted inside the time-of-flight chamber. The inner chamber height at detector position is 3.5 m; the detector unit full height is 3.2 m.

Authors

J. Ollivier, L. Didier and H. Mutka
(ILL, on behalf of the IN5 project team)

32 detector tubes are grouped in a single panel defining a detector unit sharing the same volume of gas. This unique design has been patented by the ILL Detector Group. Positioning of the units in the flight chamber has been optimised for minimal distances between panels in order to maximise the effective detector area and to avoid gaps in the experimental spectra.

The gas pressure results in 80% detection efficiency at IN5's maximum flux. Such efficiency is suitable for the needs of low-energy scattering, limiting the quantity of ^{3}He to be used. The low pressure also allows the thickness of the tube walls to be reduced to a minimum without compromising on security. Design and manufacturing of the PSDs have been realised in-house by the ILL Detector Group with the help of a subcontractor. Production of the 13 units (12 in operation and one spare) has taken a full year and was finished at the end of June 2007.

The time-of-flight chamber

In order to obtain a seamless and homogeneous detector surface from scattering angles as low as $2°$ to up to $140°$, the chamber is designed to withstand a primary vacuum. The massive vacuum-tight chamber is made of aluminium giving a fully nonmagnetic environment around the sample area.

The large detector solid angle as seen from the sample, is the reason for the absence of a window between the sample and the flight chamber. This should not interfere with the frequent changes of sample environment on IN5 (cryostats, furnaces, magnets...) since, with a properly designed pumping system, the nominal vacuum can be achieved in less than 2 hours despite the large volume to evacuate. Manufacturing of the chamber by a British subcontractor near Cambridge took nearly 15 months, under the tight control of the ILL design office.

The background protection (detector shielding)

In order for the combination of the detectors and flight chamber to perform appropriately the neutron background must be as low as possible.

According to previous measurements, within the available space, weight and cost limitations, a layered structure made of a high-density polyethylene neutron moderator, with an inner lining of 5 mm of B_4C-charged polyurethane was installed in spring 2006 (**see figure 3**). The new shielding that encloses the present unitary detectors has reduced the background by an estimated factor of four when compared to the former shielding. A comparison with the

*Figure 3: IN5 with its new neutron shielding as seen from above (**a**). The inside of the protection shows the aluminium frame and the neutron absorber (**b**). The windows will allow direct access to the detector electronics mounted on the back of the flight chamber.*

neighbouring IN6 instrument as well as with the new time-of-flight TOFTOF in Munich has shown that IN5 achieves a similar signal-to-noise ratio as these instruments.

The first milestone: the temporary secondary spectrometer

A first milestone was the reopening of the instrument to users after replacement of the detector shielding and the digging of a recess in the floor in order to accept the new larger flight chamber. It was also necessary to reinforce the floor because of the weight of the new secondary spectrometer. This operation did not affect scheduled users since all the work was carried out during the long shutdown required for the ILL refit programme.

Installation, commissioning and future

Started in 2004, the secondary spectrometer project is expected to be completed before commissioning of the new instrument during the second reactor cycle of 2008. 2008 will see the renaissance of IN5, which started with the primary spectrometer project 10 years ago.

The new IN5 will have nothing in common with the former 30 year old instrument, opening up new fields of physics. Indeed, in addition to the
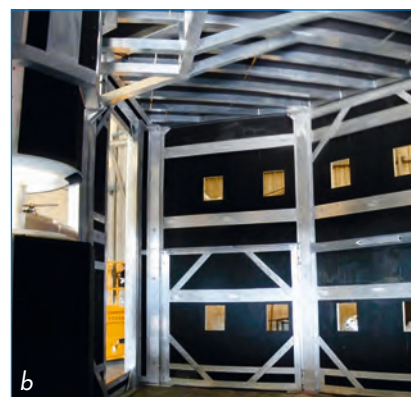
new detectors, every effort has been made to allow the installation of a wide range of sample environments. The non-magnetic chambers will allow high magnetic fields. A specific compensated coil with an asymmetric opening in order to cover a maximum detector area is to be developed in the future.

Furthermore, the size of the sample chamber will enable a polarisation device (^{3}He polariser, flippers and XYZ coils) to be installed. A beam polariser and a hyper-focusing nose guide for concentrating the beam on tiny single crystals have also been foreseen.

The remarkable relation between neutronics and picnics, and how wasps can help

rspb-images.com

Artificial intelligence tools, based on biological processes in nature, provide the means of designing and improving complex neutron instrumentation and optics, often exceeding the design capabilities of human beings by a significant margin. Applying software techniques modelled on the searching behaviour of insects, birds and fish, we have developed a focusing multi-channel guide system, the design of which could be rapidly customised to fit a particular instrument's needs, enabling experiments on small samples.

Anyone who enjoys picnics will have noticed the ability of wasps and ants to find exactly where you have placed your cakes, wine and beer. And, once the tasty snacks have been discovered, the number of uninvited guests rapidly increases. Simple algorithms can easily replicate this efficient searching behaviour, tolerant of noise caused by sampling statistics, and local optima (not everything that smells nice provides food!).

There is a strong demand in the neutron community to increase the rate of data acquisition, i.e. the number of counted neutrons, reducing the time and/or minimum sample volume for an experiment. This can be achieved by building brighter sources, and a number of these are coming online at present. The ILL can remain competitive by making more efficient use of the available instrumentation: replacing aging components, and upgrading instruments to take advantage of progress in instrumentation.

Improving existing instrumentation often involves some kind of focusing. This works well in cases where a larger beam divergence (and hence worse angular resolution) is acceptable. For an instrument such as IN5, the 20 mm horizontal beam component can be efficiently focused for small samples using a simple parabolic guide. On the other hand, the vertical direction is not so easy, at 60 mm height and already with an $m = 4$ divergence. We have been developing massively-focusing beam optics based on multi-channel guide techniques, to focus the beam onto a 2 x 2 mm sample. The guide essentially consists of a vertical array of many curved, converging guides. The problem is that the

Authors

P.M. Bentley
(HMI, Berlin, Germany and ILL)
K.H. Andersen *(ILL)*

geometry of one guide channel affects the optimum geometry of the other channels. Simultaneously optimising all channels is a search of a noisy 47-dimensional parameter space, full of local optima.

This is where the social insects come in. We used particle swarm optimisation, borrowed from the artificial intelligence community, which exhibits machine learning, and is closely related to evolutionary algorithms. At the core is a population of agents ('insects') that are primitive, independent, and free to explore the parameter space. They remember where they have been, and they are able to communicate their findings to the group, just like wasps, honeybees and ants. When acting alone, their search is inefficient, but in

a group the collective intelligence emerges and the efficiency increases, in the absence of a centralised organisational structure. A similar genetic-algorithm approach has produced, for example, new jet-engine technology [1], but for neutron purposes we have shown that a particle swarm is more efficient than a genetic algorithm (*article in preparation*).

The agents search the parameter space for the maximum number of neutrons hitting the sample. For the first time, we attached a machine-learning algorithm to a heavily-benchmarked Monte Carlo neutron ray-tracing program. The swarm explores the topology of the parameter space by sampling it with a simulation of 1 million neutron trajectories. Making use of modern CPU technology and running swarms in parallel

on multiple cores, a design can be optimised for an instrument at a given wavelength within a few days.

The swarm was free to add or remove channels as necessary, and, for this particular IN5 model at 5Å, settled on a design with 5 channels, shown in **figure 1**. We expect a 9-fold increase of the data acquisition rate on an IN5-like instrument, with a vertical divergence of 10°. In comparison, at the same wavelength the best human design was able to achieve a gain factor of 6, and a single-channel doubly-parabolic guide gives a gain factor of 4.

In conclusion, we have demonstrated that by coupling current artificial-intelligence technology directly with state of the art Monte Carlo techniques, we are able to improve the design of complex neutron devices where traditional human design methods become unfeasible. There is no technical reason why this full simulation method cannot be used to design entire instruments, in light of recent successes in spin echo instrument design [2].
We aim to make this approach available to instrument designers as a routine tool for designing modern neutron instrumentation and optics in the immediate future.

Figure 1: A vertical cross-section through the multi-channel guide designed using particle swarm optimisation. White regions are empty space, red shaded regions are super-mirror coated mountings. The exit of the existing guide system is shown as a pair of black lines on the left. The 2x2 mm sample is shown as a green block on the right.

References

[1] D.J. Powell, S. Shing Tong, M.M. Skolnick, "EnGENEous domain independent, machine learning for design optimisation", *Proceedings of the third international conference on Genetic algorithms (George Mason University, USA, 1989).* See also http://www.geae.com/engines/commercial/ge90/

[2] R. Hölzel, P.M. Bentley, P. Fouquet, "Instrument design and optimisation using genetic algorithms", *Rev. Sci. Inst.* 77 (2006), 105107

An inexpensive CCD neutron alignment camera

Simple techniques are often the most effective. The neutron Polaroid camera is an excellent example of the use of an existing commercial device in an essential new role – to ensure that the sample is actually within the neutron beam! This has saved countless hours of lost beamtime since the first Polaroid cameras were constructed for most ILL instruments 30 years ago.

However new interlock systems, while improving safety, have made it more difficult to use a manual device such as the Polaroid camera. And commercial film cameras have been largely replaced by CCD cameras, with millions spent on development.

Two years ago, Bachir Ouladdiaf replaced the old wet-film crystal alignment camera with a new cooled image-intensified neutron CCD system, which is ten times more sensitive and much easier to operate. The resulting OrientExpress Laue diffractometer has been a huge success, and is now being marketed commercially by Photonic Science UK. An even more powerful machine (Cyclops) is under construction.

Cooled, image-intensified CCD cameras were developed by several laboratories long ago and at ILL by Toni Heidemann, Roland Gähler and others. They are important for neutron tomography, where the highest resolution and sensitivity are essential, but are still too large and expensive for our purposes. A search for the modern equivalent of the Polaroid camera turned up CCD cameras used for video surveillance and amateur astronomy, where high sensitivity is obtained by frame integration rather than image intensification. Such cameras are relatively cheap and do not need to be cooled for integration over a few seconds.

Figure 1: The compact version of the CCD neutron alignment camera with a nominal sensitive area of 80x60 mm, together with its optional 7" (18cm) TFT monitor, alternative USB-2 PC adapter, and electronic exposure controller.

Authors

A. Hewat (ILL, now retired)
P. Falus (ILL)
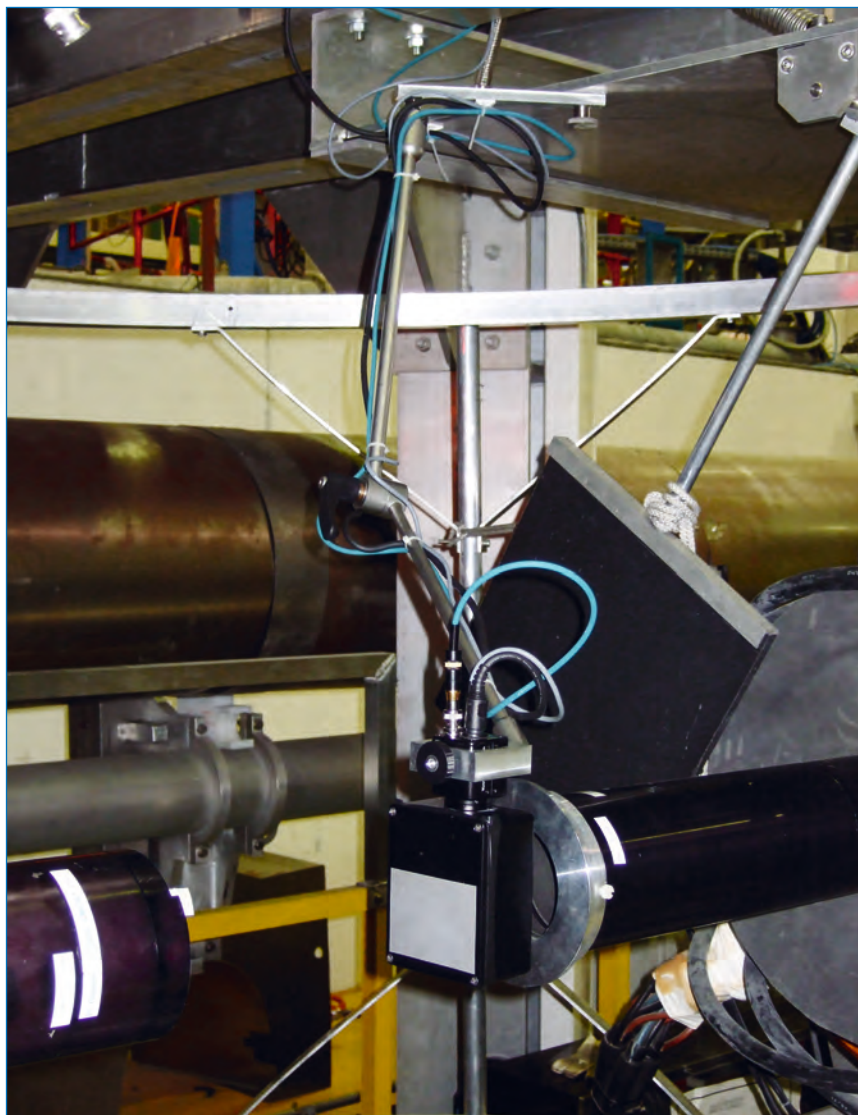
Figure 2: A compact CCD camera on an articulated arm on IN15.
The articulating arm is made of stainless steel and the 3 movable joints are simultaneously lockable by turning the black lever.

The CCD alignment camera (**figure 1**) is almost as compact as the old Polaroid camera, and has the great advantage that it can be operated remotely to give an almost real-time image of the neutron beam. Monitoring of the sample in the beam becomes a routine part of the experiment, not a manual procedure to be skipped by impatient users.

Figure 2 shows the new camera mounted on an articulated arm built by IN15 technician, Claude Gomez. To accommodate the various instrument configurations the camera was mounted on a triple jointed arm, based on a commercial product designed for holding micrometer dials. Using this arm the camera could be put in position with one hand and then locked in place with the other hand. The signal from the camera is sent through a video splitter to feed an LCD screen at the sample position for manual cryostat alignment, and it also feeds a frame grabber on the control computer to aid computerized positioning. It takes literally 5 seconds to position the camera or to stow it away, and there is always a screen to look at nearby. There is no excuse not to use this camera!

The low cost of this simple CCD camera has meant that over 30 examples have already been made for most instruments at ILL, with Jean-Claude Tribbia machining all of the aluminium camera boxes. A small company (NeutronOptics) has been set up to satisfy the demand from other laboratories. In collaboration with PSI Switzerland, new scintillators will be used on future cameras, and with the help of the Japanese maker of the CCD unit, an unlimited exposure model is being tested for weaker neutron beams.

Further details are available on ***http://www. neutronoptics.com.***

Hydrogen positions made easy

The determination of hydrogen positions in most inorganic materials or organometallics no longer requires sample deuteration or the growth of large single crystals. Hydrogenous materials studied on the D20 diffractometer, operating in optimised resolution mode, produce excellent quality diffraction data above the large, smooth, incoherent background. Profile analysis of these data, sometimes in combination with X-ray diffraction information, allows the precise and accurate determination of the hydrogen positions, including those in crystallographically-complex compounds.

Hydrogen is a key element whose functionality stretches from geochemical materials (e.g. clay minerals, cements), through key inorganic compounds (e.g. catalysts, organometallics [1], coordination complexes and hydroxides/hydrates) and materials [2] (e.g. polymers, ferroelectrics, hydrogen storage media, proton conductors/ fuel cell components) to supramolecular and framework systems (e.g. aluminosilicates, solvates and clathrates). Determining the role of hydrogen in the structures of these materials is thus of the utmost importance as it often controls their properties and, hence, derived applications.

Due to the weak scattering of X-rays by hydrogen, neutron diffraction is the obvious choice for locating it. However, the incoherent scattering of neutrons by the ^1H isotope normally leads to high backgrounds, very long counting times and noisy data sets using traditional powder neutron instrumentation, from which the extraction of hydrogen positions is so poor as to be not worthwhile. Certain problems can be overcome by sample deuteration or single crystal neutron studies but these techniques are of limited applicability due to the cost and time for deuteration or the impossibility of growing large single crystals. Deuteration may also affect the material's properties, e.g. in hydrogen-bonding and ferroelectricity.

The diffractometer D20, operating in its high takeoff-angle geometry with the variable vertical focusing Ge(113) monochromator, provides optimal resolution (~$\Delta d/d$ of 2×10^{-3}) across a large Q-range (0.1 - 9.5 $Å^{-1}$) for unit cells up to 1000 $Å^3$, larger in high symmetry cases. A very high count-rate is retained due to the combination of a high flux on the sample coupled with a large detector area and counting times depend on the structural complexity of the material (unit cell volume, space group and number of unique atoms) and sample volume, but it has been shown experimentally that high quality data can be collected in minutes to a few hours. Where data remain somewhat noisy, due to structural complexity or very high hydrogen content, useful information concerning
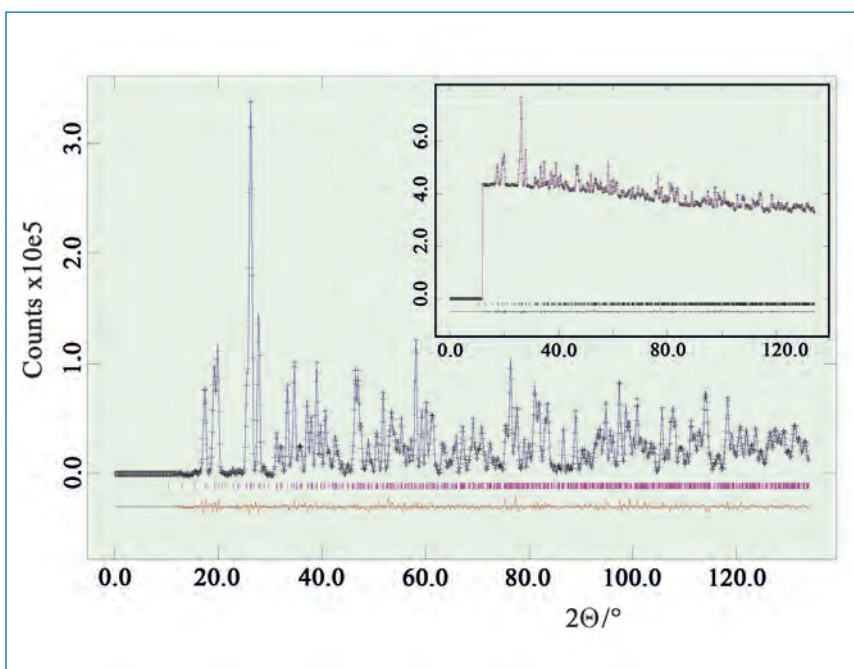
Figure 1: *The profile fit to data collected from Bi(NO₃)₃.5H₂O. Inset: pre-background subtraction showing the high incoherent scattering but a typical signal to noise ratio of 100,000:500*

Authors

M. Weller (University of Southampton, UK)
C. Wilson (University of Glasgow, UK)
P. Henry (ILL)
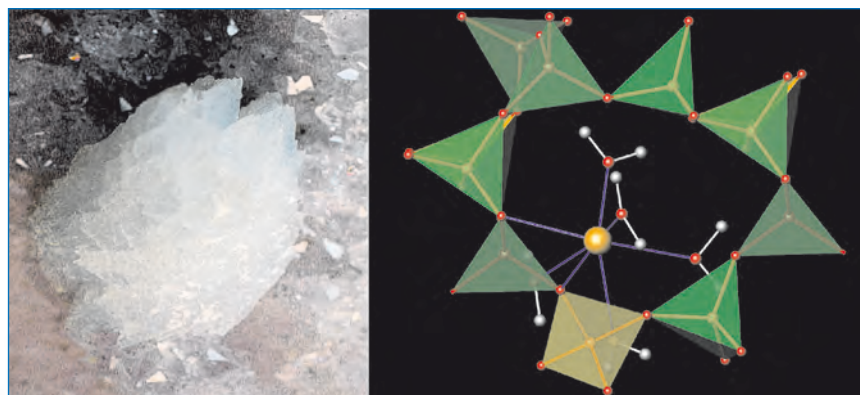
Figure 2: A polycrystalline mass of the rare natural zeolite goosecreekite (left). The structure of goosecreekite showing the full water positions, including precisely determined hydrogen, from D20 data (1h) (right). [4]
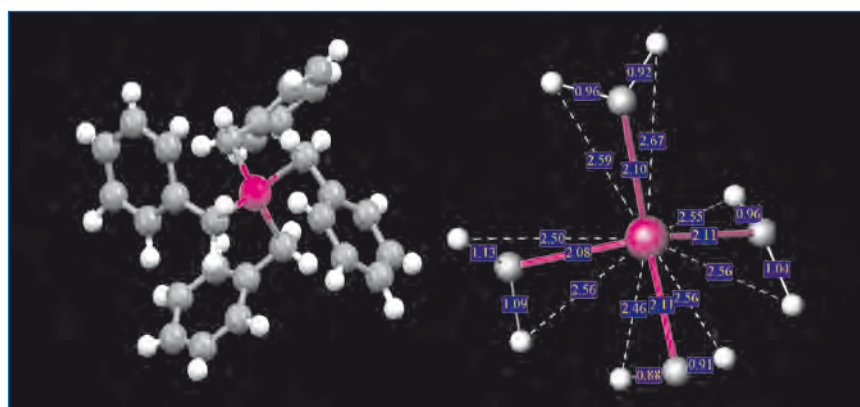
Figure 3: The structure of Ti$(C_6H_5CH_2)_4$ refined using a joint Powder Neutron Diffraction (PND) - Single Crystal X-ray Diffraction (SXD) analysis with unconstrained hydrogen positions (left). The titanium coordination environment showing no abnormally short Ti-H interactions and hence no agostic bonding in this compound (right).

hydrogen can still be extracted, particularly where the data set is analysed in conjunction with X-ray diffraction data. We have shown that the implementation and application of methodology now allows *routine* hydrogen position definition from *readily available* material, i.e. small easily synthesised quantities 1-2 g and in polycrystalline/small single crystal (≤50μm) form. Initial commis-sioning experiments have concerned a variety of important hydrogenous structure types.

Metal salts and coordination compounds

Metal salt hydrates play important roles in a number of chemical and geochemical areas.

A simple example, gypsum $CaSO_4.2H_2O$, was used as a test sample in this work to determine how quickly accurate and precise hydrogen positions could be extracted for a material containing 33 atom% hydrogen. This demonstrated that in under 30 minutes an optimised crystallographic model (as good as that determined from single crystal neutron diffraction data) could be refined.

Diffraction data from a 2g sample of $Bi(NO_3)_3.5H_2O$ were collected in 1 hour on D20 ($\lambda = 1.87$Å), **figure 1**. Profile fitting in GSAS and Fourier difference methods rapidly located the (previously unknown, [3]) positions of 10 unique hydrogen atoms. Full unconstrained

refinement allowed determination of hydrogen-bonding patterns and subtle effects such as elongation of OH distance and changes in O(D)-H....O(A) bond angles as a function of O(D)—O(A) distance.

Hydrated and adsorption complexes of zeolites

Zeolites are widely used in the chemical industry including applications in environmental pollution control (ion exchange), molecular adsorption (e.g. gas separation and solvent drying) and catalysis. A full understanding of their structures, including hydrogen positions of any adsorbed molecules, is therefore crucial in the optimization of these materials for their applications. A study of the naturally occurring goosecreekite [4] (GOO topology) has located the water molecules in the structure, **figure 2**, and an *in situ*, variable temperature decomposition study - possible with polycrystalline materials - has permitted changes in structure which occur as a function of water content to be determined.

Organometallics

Hydrogen atom positions in organometallic compounds are often central to controlling the bonding and properties including catalysis and C-H bond activation. Examples include different types of direct metal-hydrogen bonds and agostic hydrogen-bonding [1]. Studies of Zeiss's salt (KPt$(C_2H_4)Cl_3.H_2O$) and titanium tetrabenzyl Ti$(C_6H_5CH_2)_4$), **figure 3**, have shown that refined hydrogen positions can be extracted for these organometallics of reasonably high structural complexity (about 60 atoms in the asymmetric unit, 50 atom% hydrogen).

References

[1] W. Scherer and G.S. McGrady, Angew. Chem. Int. Ed. 43 (2004) 1782

[2] T. Steiner, Angew. Chem. Int. Ed. 41 (2002) 48

[3] TF. Lazarini, Acta Cryst. C41 (1985) 1144

[4] P.F. Henry, M.T. Weller, C.C. Wilson, Chem. Commun. (2008) DOI: 10.139/b719464a

A new high-resolution angular interferometer for gamma-ray spectroscopy

4

The kilogram is the only remaining fundamental unit within the SI system that is defined in terms of a material artefact. Therefore, one of the major tasks of modern metrology is the redefinition of the kilogram on the basis of a natural quantity or of a fundamental constant. The ILL gamma-ray spectrometer GAMS, with its new optical interferometer, can play a crucial role in this attempt.

Measuring picoradian angles

Two approaches are currently proposed in order to be able to link a new definition of the kilogram to a fundamental constant. The first project, the so called 'Watt-balance' [1], suggests linking the kilogram to Planck constant h. The second approach, the so called 'crystal density' [2], proposes to measure Avogadro constant N_A and define the kilogram via the mass of a free carbon atom: $1000/12 \cdot N_A \cdot Ar$ (^{12}C). Additionally one could also determine the energy equivalent to the mass of a ^{12}C atom, leading to the fundamental constant $N_A \cdot h$, but a direct measurement of the energy equivalent is difficult since small masses correspond to enormous energies. However, measuring the mass and energy balance in a thermal neutron capture reaction offers an attractive possibility to realise this concept. The ILL plays a fundamental role in this part of the project with the GAMS high-resolution gamma-ray spectrometer. The key difficulty in the experiment is a precise absolute determination of gamma-ray energies emitted after the thermal neutron capture reaction.

This is done by diffraction at perfect Si crystals measuring the very small diffraction angles in absolute terms. The goal uncertainty for the determination of $N_A \cdot h$ is 10^{-8}, which requires an adequate accuracy for the diffraction angles' measurement and the calibration of the apparatus.

A key step towards a new $N_A \cdot h$ measurement is a new optical interferometer with 10 prad precision and linearity over a total measurement range of 20° and high stability of about 0.1 nrad/hour (**figure 1**). The interferometer follows a Mach-Zehnder layout, which allows a strict separation in space between all beams. This avoids unwanted mixing, which would lead to non-linearity in the angle measurement. The interferometer is designed such that we have the possibility to measure the rotation of both spectrometer axes using a single set of optical elements. This highly symmetric layout increases the stability and the accuracy of the angle measurement by self compensating eventual drift of the apparatus. All the optical elements are high quality fused silica pieces
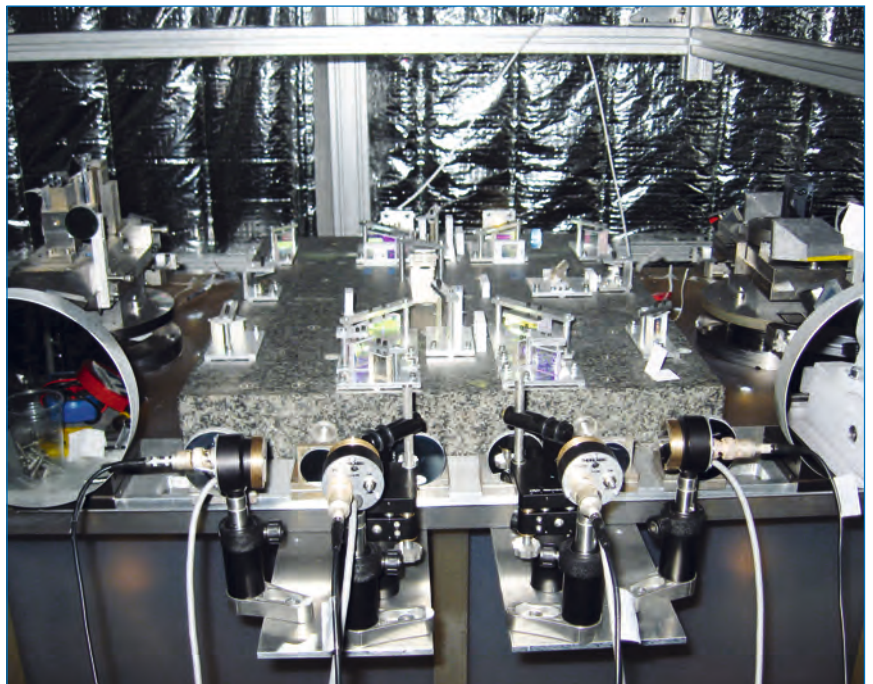
Figure 1: The prototype of the new interferometer mounted on the GAMS5 spectrometer for the functional tests.

Authors

P. Mutti, F. Cecillon, M. Jentschel, J. Krempel, T. Mary, G. Pigny, J. Ratel and F. Rey *(ILL)*

with custom made surface treatment. In the final version of the interferometer they will be chemically bonded [3] to the ZERODUR base of the spectrometer to avoid the use of glue. All the roof-prisms and retro-reflectors used in the realisation of the optical path are hollow since in solid elements the path length is not constant with respect to rotation [4].

New laser source for the interferometer

Classical interferometry allows displacement measurements of typically 10^{-2} of the optical wavelength. This resolution can be improved by a factor of 100 by using a different wave-length in each interferometer arm. This concept is realised in our new interferometer. Starting from a highly stabilised monodyne laser source, the single laser wavelength is split into two beams and each of them is frequency shifted. The two frequencies are obtained by mixing a difference signal of 100 kHz with a carrier frequency of 40 MHz. We have developed a Phase-Locked Loop (PLL) circuit which allows mixing the reference signal of a commercial lock-in amplifier with a signal of a precision signal generator. The two frequencies are transferred to the laser beam via Acousto-Optic Modulators (AOM). After frequency shifting, the laser beams are injected into the interfero-meter via glass fibres. The interference signal will be detected as a beat node modulation. The phase of this beat signal is proportional to the length variation of the interferometer paths originated by the rotation of the axis. The phase gets measured relative to a reference signal generated within the interferometer by newly developed phase measurement electronics.

Phase read-out and nano positioning electronics

The interferometer delivers for each of the two axes a measurement signal and reference signal. If one axis is rotated, the phase of the beating of the according signal changes with respect to its reference. The electronics has to measure the phase change and count integer periods (one period is equivalent to one opti-cal fringe or to an angle of about 0.5 µrad). To perform those tasks we have developed a VME based electronic module consisting
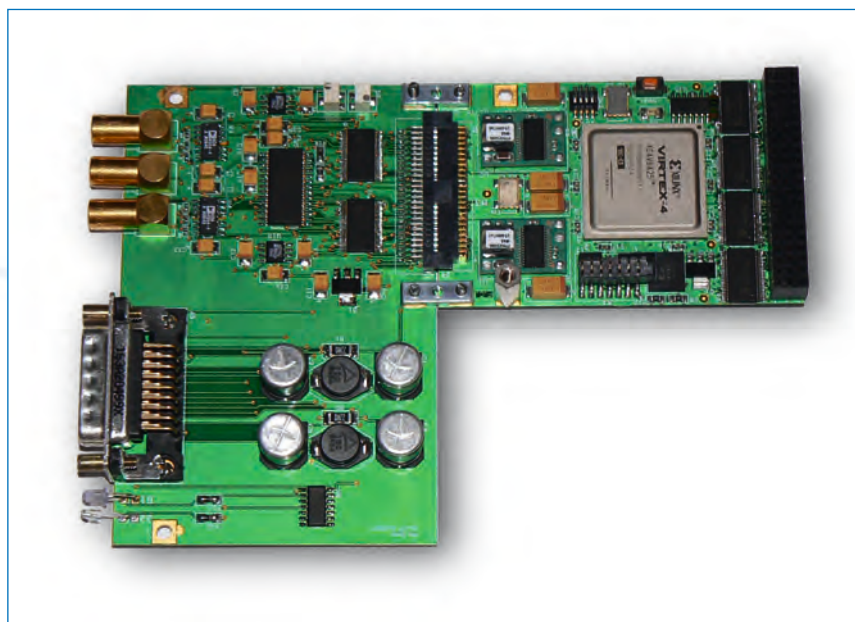
Figure 2: VIRTEX-4 FPGA module for phase read-out and positioning of the spectrometer axis.

of a VIRTEX-4 FPGA associated to an M-Module treating all signals from the interferometer. The beating signals are filtered and trans-ferred into square waves by high stability differential operational amplifiers. The phase is then measured by time interval counting. The module is driven by a master clock running at 100 MHz which allows the 100 kHz periods to be sampled with an accuracy of ± 10 nsec. This uncertainty is equivalent to 0.001 interfe-rometer fringes (50 prad). The count of integer fringes provides necessary information for the macroscopic positioning of the spectrometer axes using DC motors.

The axis fine positioning is achieved using a piezo element controlled by a voltage signal provided by a 14 bit DAC. We have achieved a positioning resolution of 0.01 fringes, being limited only by the amplitude of the residual vibrations transmitted to the axis. To remove any axis drift and to minimise those residual vibrations, the phase signal is used as feedback for a closed loop real-time regulation mechanism. This regulation is based on a hardware Proportional-Integral-Derivative (PID) controller which corrects for any deviation of the measured

phase from the desired one. The phase infor-mation is also recorded in coincidence with the gamma-ray signals from the HPGe detector in the acquisition card. This supplementary information is fundamental to correctly interpret the measured data since it allows removing the excess width, which is affecting the gamma-ray peaks due to the incorrect determination of the axis position during the data acquisition.

The new interferometer with its electronics represents a major component of the new GAMS6 spectrometer, which will be used for future $N_A \cdot h$ measurements.

References

[1] L.R. Steiner et al., Metrologia 42 (2005) 431

[2] P. Becker et al., Metrologia 40 (2003) 271

[3] US-Patent 6,284,085 B1 'Ultra Precision and Reliable Bonding Method'

[4] E.R. Peck, J. Opt. Soc. Am. Vol 38 No 12 (1948) 1015

Polarimetric neutron spin-echo demonstrated

The multifaceted dynamics of antiferromagnets and helimagnets ask for more than the classical Neutron Spin-Echo set-up (NSE). Indeed, the neutron beam polarisation is not necessarily flipped upon scattering. When the magnetic interaction vector is complex and/or when there are nuclear-magnetic interferences, the rotation of the incident polarisation can be of any angle around or toward a specific direction and it is impossible to distinguish between a simple depolarisation due to e.g. magnetic domains and a rotation of the polarisation vector.
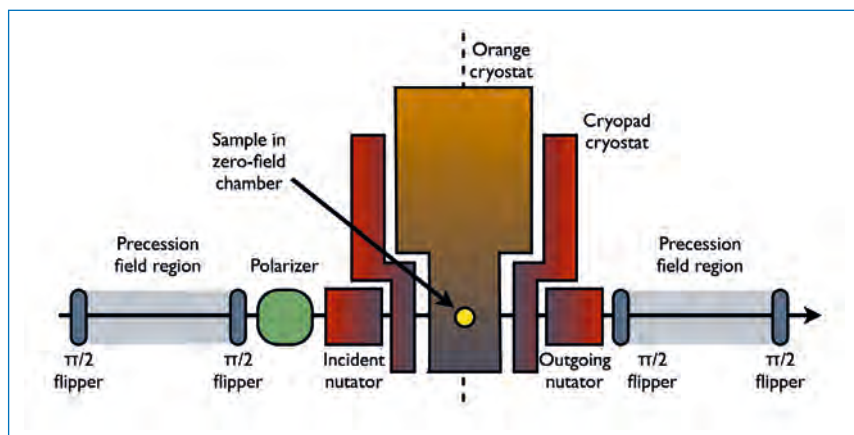
Figure 1: Schematic view of the instrument around the sample.

One way of overcoming these difficulties is to implement a zero-field polarimeter [1] on a NSE spectrometer [2]. Indeed, the only way to access the components of the scattered polarisation which are transverse to the incoming polarisation is to implement a zero-field area around the sample position. The first realisation of such a set-up has been accomplished using the third-generation Cryopad [3] and a modified version of the Intensity Modulated variant of NSE (IMNSE).

Cryopad is a zero-field polarimeter based on Meissner shields and μ-metal screens able to do the most generalised polarisation analysis experiments measuring all theoretically possible pair-correlation functions at any point of the reciprocal space. On the other side, IMNSE is a powerful technique that disconnects completely the sample area from the NSE measurement at the price of some intensity losses due to the addition of polariser and analyser devices [4].

To implement Polarimetric Spin-Echo (**figure 1**), we install two additional $\pi/2$ flippers located near the sample space. These flippers, combined with the other two $\pi/2$ flippers, define the Larmor precession regions before and after the sample position which are used to directly measure the energy transfer at the sample. Then, we add a solid-state polariser after the first Larmor precession region so that the beam is repolarised, which is necessary for handling the polarisation vector in Cryopad. The last step comprises the installation of the Cryopad cryostat (**figure 2**) with its two rotating nutators and the Orange cryostat used to cool down the sample.

The set-up finally consists of two high-field regions split by a zero-field one (≈ 2 mG). The increase of the field (of the spin-echo resolution) has obviously an impact on the zero-field chamber and therefore the precision with which the polarisation vector is handled in Cryopad. Hopefully, thanks to the combination of μ-metal and Meissner screens, the field screening is quite efficient and we can work at 50% of the nominal spin-echo resolution on the instruments SPAN at HMI with an uncertainty on the direction of the polarisation vector of the order of 1.7 degrees at 4.5 Å.

After some tuning, we can check the set-up with a Grafoil mounted in the zero-field chamber of Cryopad. In this case, an echo is obtained only

Authors

**E. Lelièvre-Berna, E. Bourgeat-Lami
and M. Thomas** (ILL)
**C. Pappas and P. Bentley
and E. Moskvin**
(Hahn-Meitner Institut, Berlin, Germany)
**S. Grigoriev, V. Dyadkin
and E. Moskvin**
(PNPI, Gatchina, Russia)
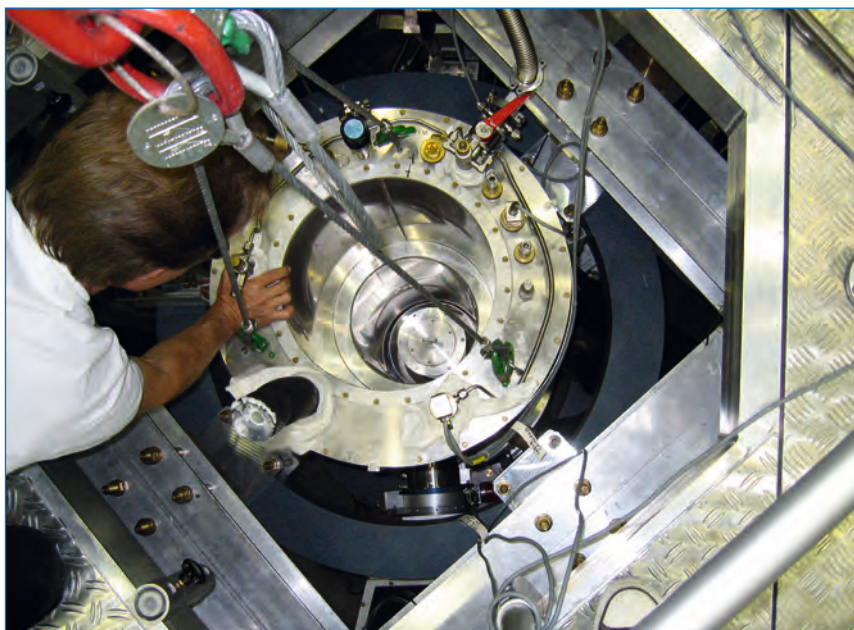
Figure 2: Installation of the Cryopad on SPAN at the HMI.
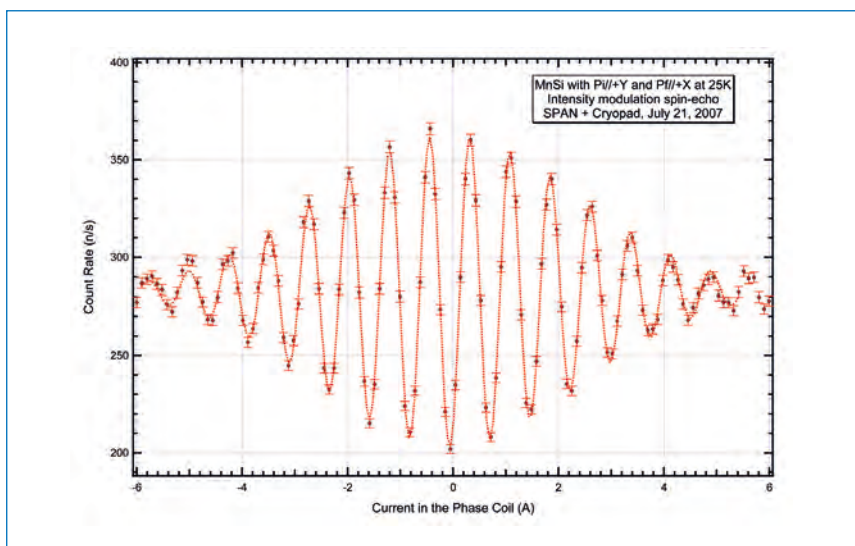
Figure 3: Spin-Echo Group recorded on the helimagnetic Bragg peak of MnSi with the incident polarisation perpendicular to Q and the scattered polarisation vector anti-parallel to Q.

for the components of the scattered polarisation parallel to the incident direction (null transverse components). With a magnetic sample for which the incident polarisation is rotated by 90° toward the scattering vector (e.g. MnSi), we have checked successfully that we can measure the spin-echo group on transverse components (**figure 3**).

After the successful development of this new technique on SPAN (*http://www.hmi.de/bensc/instrumentation/pdf_files/BENSC_V5.pdf*) at the HMI, the Cryopad was installed on IN15 (*http://www.ill.eu/in15/home/*) at the ILL with the help of P. Falus, B. Farago and C. Gomez, whom we expressly acknowledge here.

The measurements on IN15 completed the results on the relaxation of the excitations in MnSi and will be reported elsewhere. The polarimetric spin-echo option is now available on IN15, where the uncertainty on the direction of the polarisation vector is 3.5 degrees at 9 Å.

References

[1] *F. Tasset, Physica B 157 (1989) 627*

[2] *F. Mezei, Z. Phys. 255 (1972) 146; F. Mezei (ed.), Neutron Spin Echo, Lecture Notes in Physics Series, Vol. 128 (Springer, Heidelberg, 1980)*

[3] *E. Lelièvre-Berna, P.J. Brown, F. Tasset, K. Kakurai, M. Takeda, L.-P. Regnault, Physica B 397 (2007) 120-124*

[4] *B. Farago, F. Mezei, Physica B 136 (1986) 627*

The ILL member countries

- France
- Germany
- United Kingdom

- Austria
- Czech Republic
- Italy
- Spain
- Switzerland

- Belgium
- Hungary
- Poland
- Sweden

Experimental
and user programme

**At its own level,
the ILL too is extending its horizons.**

Over the last few years, for example, we have been joined by four new Scientific Members, Poland being the latest country to acquire ILL membership, after the recent accession of Sweden, Hungary, and Belgium.

As Europe grows, so too does the European Research Area (ERA). Europe's future competitiveness, as far as research is concerned, depends most probably on its ability to develop its scientific expertise through the processes of innovation and exchange.

User operation

The ILL User Support is there to assist all our users. If you are coming to the ILL to carry out experiments, the User Office is here to give you the organisational and administrative support you need for the successful operation of your experiments. Neutron beams and instrument facilities are free of charge for proposers of accepted experiments. Scientists affiliated to ILL member countries will also, in general, be assisted with necessary travel and daily subsistence for a limited period. The User Support Team makes all arrangements for accommodation and transport and will process claims for expenses after you have completed your experiment.

Extensive information about the ILL, its facilities and application for beamtime is available on our web-site (http://www.ill.eu/users).

The ILL Visitors Club

All administrative tools for our scientific visitors are grouped together and directly accessible on the web, thanks to the Visitors Club. All information is presented in a user friendly environment. After having logged in with your own personal identification, you will have direct access to all the available information which concerns you. Users with particular responsibilities have privileged access to other tools, according to their role. The ILL Visitors Club includes the electronic proposal and experimental reports submission procedures, and electronic peer review of proposals. Additional electronic services have also been put in place: acknowledgement of proposals, subcommittee results, invitation letters, user satisfaction forms and so on.

Prof. Hartmut Zabel (Bochum University) between Richard Wagner (left) and Andrew Harrison (right) is the new chairman of the ILL Scientific Council

Proposal submission

There are different ways of submitting a proposal to the ILL:

- Standard submission – twice a year – via the Electronic Proposal System (EPS).
- EASY access system (EASY) throughout the year.
- Director's discretion time (DDT) throughout the year.
- Special access for proprietary research and industrial users.

Submission of a standard research proposal

Applications for beamtime should be submitted electronically, via our Electronic Proposal Submission system (EPS), available on the Visitors Club web-site. Proposals can be submitted to the ILL twice a year, usually in February and in September. The web system is activated two months before each deadline. Submitted proposals are divided amongst the different colleges, (see indent) according to their main subject area.

The ILL scientific life is organised into 10 colleges:

College 1	- Applied Physics, Instrumentation and Techniques
College 2	- Theory
College 3	- Nuclear and Particles Physics
College 4	- Magnetic Excitations
College 5A	- Crystallography
College 5B	- Magnetic Structures
College 6	- Structure and Dynamics of Liquids and Glasses
College 7	- Spectroscopy in Solid State Physics & Chemistry
College 8	- Structure and Dynamics of Biological Systems
College 9	- Structure and Dynamics of Soft-condensed Matter

Proposals are judged by a Peer Review Committee of the Subcommittees of the ILL Scientific Council. Subcommittee members are specialists in relevant areas of each College and they evaluate the proposals for scientific merit, assigning priorities and beamtime to accepted proposals.

Before the meeting, the subcommittee receives a report on the technical feasibility and safety of a proposed experiment from the appropriate College at the ILL. Two proposal review rounds are held each year, approximately six weeks after the deadline for submission of applications. There are normally 4 reactor cycles a year, each of which lasts 50 days. Accepted proposals submitted by February will receive beamtime in the second half of the year and those submitted by September, in the first half of the next year. More detailed information on application for beamtime and deadlines are given on our website at:
http://www.ill.eu/users/proposal-submission/

Easy Access System

The Easy Access System (EASY) grants diffraction beamtime to scientists from ILL member countries, who need a rapid structural characterisation of samples and data analysis. Access is open all year long, and it does not go through the ILL standard proposal round and consequent peer review system.

The system offers one neutron day per cycle, on four instruments (D1A, D2B, VIVALDI and OrientExpress) to perform very short experiments (a maximum of 4h per cycle) at room temperature. The users will not be invited to the ILL, but will send their samples to one of two designated ILL scientists (one for powder and one for single-crystal experiments), who will be responsible for the measurements and sample radiological control. The ILL will ship back the sample once the measurement is finished. You can apply for EASY beamtime on the Visitors Club. More information is available at: *http://club.ill.eu/cvDocs/EASY_Guidelines.pdf*.

Submission of a proposal to the Director's Discretion Time

This option allows a researcher to obtain beamtime quickly, without going through the peer-review procedure. DDT is normally used for hot topics, new ideas, feasibility tests and to encourage new users. Applications for Director's Discretion Time can be submitted to the Head of the Science Division, Prof. Andrew Harrison, at any time.

Access for proprietary research and industrial users

The ILL's mission is to provide neutrons for both public and industrial research. Our Industrial Liaison and Consultancy Group (ILC) ensures rapid access and total confidentiality to industrial companies, and provides a specialised staff. The ILC Group is in fact composed of scientists with considerable experience and expertise in neutron techniques applied to industrial R&D, and it facilitates and co-ordinates all aspects of industrial R&D at the ILL: initial enquiries, contractual questions, planning, experimental operations. All industrial research programmes are confidential and can be organised at short notice. To apply for proprietary beamtime, please contact the ILC at *industry@ill.eu* or consult the web site under *http://www.ill.eu/industry/*.

Experimental reports

Users are asked to complete an experimental report on the outcome of their experiments. Following a recommendation of the ILL Scientific Council, the submission of an experimental report is now compulsory for every user who is granted ILL beamtime. Failure to do so may lead to rejection in case of application for beamtime for a continuation proposal.

All ILL Experimental Reports are software-archived and accessible via the web server as PDF files (*under http://club.ill.eu/cv/*). You can search for a report by experimental number, instrument, college, date of experiment, title, institute, experimental team or local contact.

Experimental reports for experiments performed in 2007 are included in the CD-ROM of this year's Annual Report.

Out of hours support

We have actively strengthened the level of technical support outside working hours. To date Out of Hours Support (OHS) has been implemented within the Instrument Control Service, the Detector Service and the Sample Environment Service.

Collaborative Research Group instruments

The ILL provides a framework in which Collaborating Research Groups (CRGs) can build and manage instruments on ILL beam lines to carry out their own research programmes. CRGs represent a particularly successful form of long-term international scientific collaboration.

CRGs are composed of scientists from one or two research disciplines, and often multinational, carrying out a joint research programme centred around a specific instrument. CRGs enjoy exclusive access to these instruments for at least half of the beamtime available. The CRGs provide their own scientific and technical support and cover the general operating costs of these instruments. If there is demand from the user community and the resources are available, the beamtime reserved for ILL can be made accessible to users via the subcommittees.

More than simply neutrons...

Deuteration Laboratory

A common ILL/EMBL deuteration laboratory is available to external users. The aim of the laboratory is to provide a focus for European scientists wishing to make their own deuterated materials for neutron scattering or NMR experiments. Information about the availability of this facility for external users is given at:
http://www.ill.eu/fileadmin/users_files/ Other_Sites/deuteration/index.htm.

Please contact the Head of the Deuteration Facility, Dr Michael Härtlein (haertlein@ill.eu) for further details.

Facility for Materials Engineering

The joint ILL-ESRF Facility for Materials Engineering (FaME38) provides a range of support to our users, from advice with experiment proposals to advanced sample metrology. In particular, FaME38 works with users to optimise the experimental methodology before the start of an experiment. This takes the form of standardised specimen mounting, digitisation of samples, definition of measurement macros and liaising with the instrument responsible. It is recommended that users arrive at the ILL a day or two prior to the start of an experiment to enable these off-line preparations to be performed. The extra subsistence costs may be available from the SCO if requested beforehand. More information about this support may be found on the FaME38 website *(http://www.ill.eu/filead-min/users_files/Other_Sites/FaME38/)*.

Partnership for Structural Biology

The Partnership for Structural Biology (PSB) is a collaboration between the ILL, ESRF, EMBL and the neighbouring *Institut de Biologie Structurale* (IBS). As a centre of excellence in the field of structural genomics, the PSB concentrates its research programmes on proteins and other biomolecules selected for their medical interest. It shares its office and laboratory space (located in the Carl-Ivar Bränden Building, CIBB) with the *Institut de Virologie Moléculaire et Structurale* (IVMS) of the Joseph Fourier University.

Partnership for Soft Condensed Matter

A Partnership for Soft Condensed Matter (PSCM) is now proposed, building upon the success of the CIBB. It will similarly allow our users to characterise samples before their experiments at both the ILL and ESRF, and to facilitate the performance of complementary *in situ* measurements. The partnership will also develop complex sample environments for carrying out advanced surface and solution science experiments. A working group of the ILL Scientific Council has concluded that the PCSM will greatly enhance the throughput, quality and scope of science in soft condensed matter performed on the ILL's instruments.

At the ILL Soft Matter User Meeting held in November 2006, users had the opportunity to discuss the idea of the Partnership and the outcome was very positive as summarised in the Neutron News report of the workshop *(http://www.ill.eu/fileadmin/users_files/ Other_Sites/softill2006/ILL_Soft_Matter_User_ Meeting/Homepage.html*

Experimental and user programme

Instrument Layout
December 2007

NEUTRONS
FOR SCIENCE
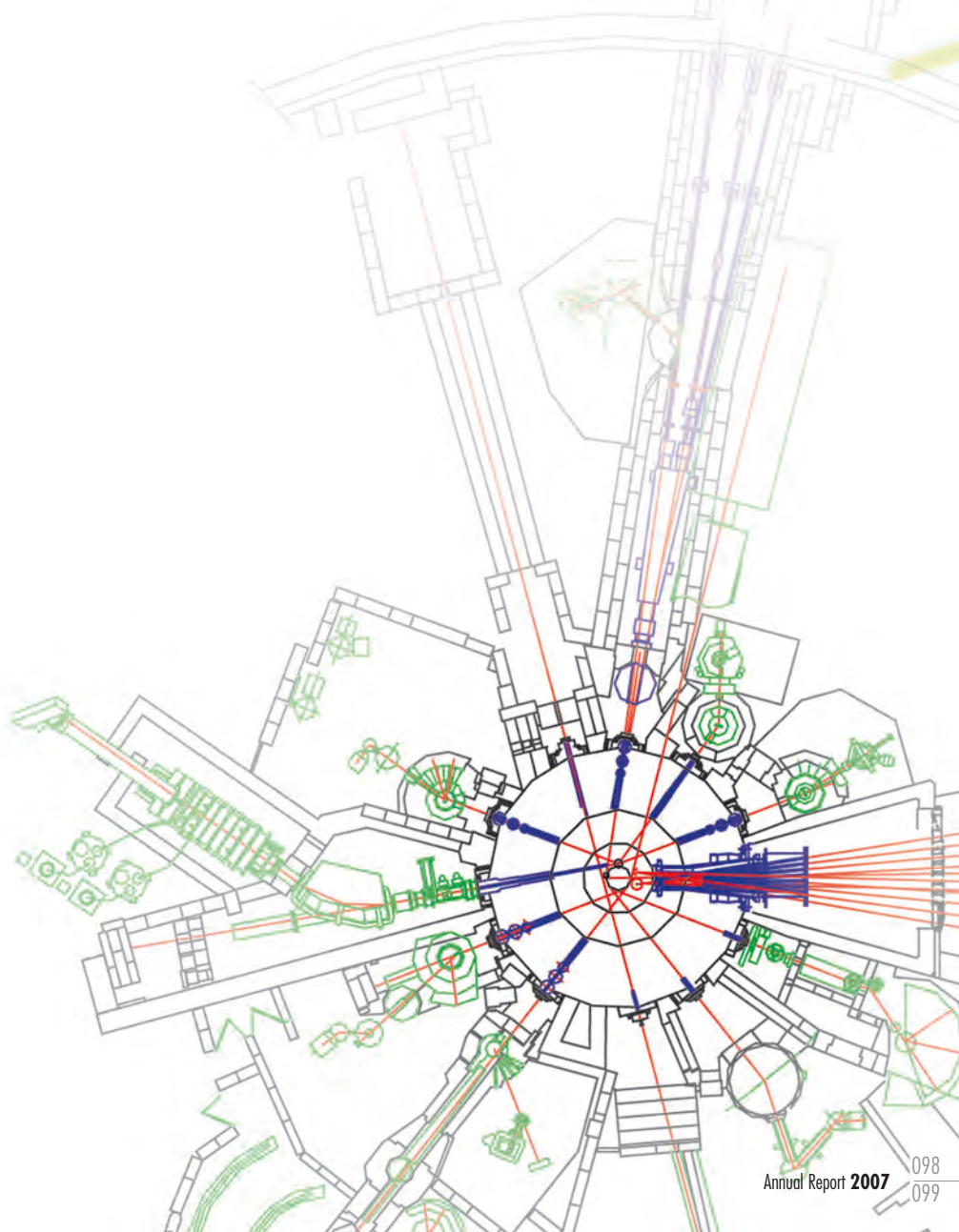
Instrument Layout in 2013

ILL instruments

D1A (50%)	powder diffractometer	operational
D2B	powder diffractometer	operational
D3	single-crystal diffractometer	operational
D4 (50% with IN1)	liquids diffractometer	operational
D7	diffuse-scattering spectrometer	operational
D9	single-crystal diffractometer	operational
D10	single-crystal diffractometer	operational
D11	small-angle scattering diffractometer	operational
D16	small momentum-transfer diffractometer	operational
D17	reflectometer	operational
D19	single-crystal diffractometer	operational
D20	powder diffractometer	operational
D22	small-angle scattering diffractometer	operational
IN1 (50% with D4)	three-axis spectrometer	operational
IN4	time-of-flight spectrometer	operational
IN5	time-of-flight spectrometer	operational
IN6	time-of-flight spectrometer	operational
IN8	three-axis spectrometer	operational
IN10	backscattering spectrometer	operational
IN11	spin-echo spectrometer	operational
IN14	three-axis spectrometer	operational
IN16	backscattering spectrometer	operational
IN20	three-axis spectrometer	operational
PF1	neutron beam for fundamental physics	operational
PF2	ultracold neutron source for fundamental physics	operational
PN1	fission product mass-spectrometer	operational
PN3	gamma-ray spectrometer	operational
SALSA	strain analyser for engineering application	operational
VIVALDI	thermal neutron Laue diffractometer	operational

CRG instruments

ADAM	reflectometer	CRG-B operational
BRISP	Brillouin spectrometer	CRG-B commissioning
CRYO EDM	installation for the search of the neutron electric dipole moment	CRG-C operational
D1B	powder diffractometer	CRG-A operational
D15	single-crystal diffractometer	CRG-B operational
D23	single-crystal diffractometer	CRG-B operational
IN12	three-axis spectrometer	CRG-B operational
IN13	backscattering spectrometer	CRG-A operational
IN22	three-axis spectrometer	CRG-B operational
S18	interferometer	CRG-C operational

Jointly funded instruments

DB21 (50%)	single-crystal diffractometer	operational with EMBL
LADI (50%)	Laue diffractometer	operational with EMBL
IN15	spin-echo spectrometer	operational with FZ Jülich and HMI Berlin

Test and characterisation beams

CT1, CT2	detector test facilities
OrientExpress	Laue diffractometer
T3	neutron optics test facility
T13A, C	monochromator test facility
T17	cold neutron test facility
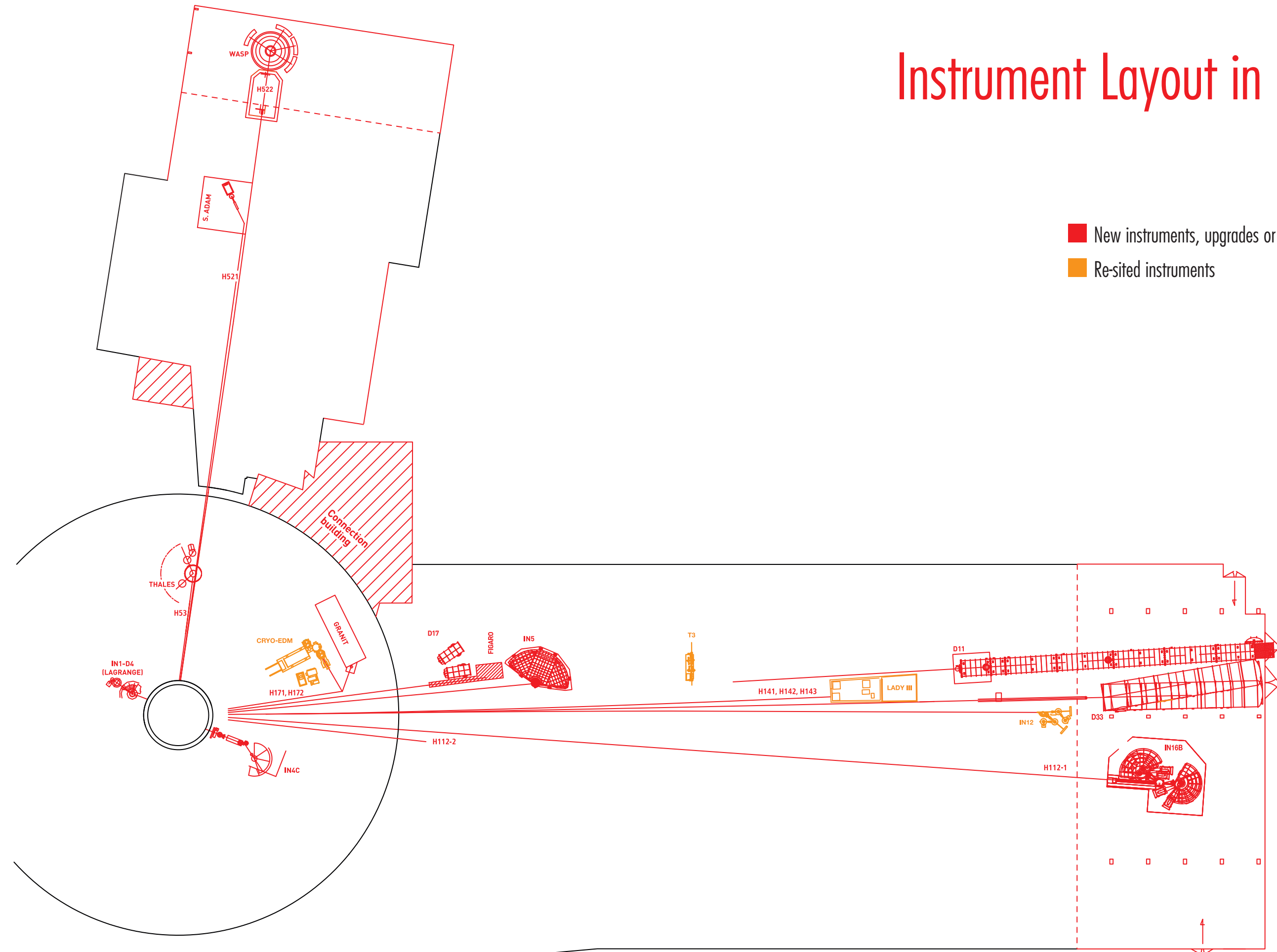
Neutron guide hall
ILL 22

Reactor hall
Inclined guide H4

Reactor hall ILL 5
Experimental level (C)

Reactor operational level (D)

Neutron guide hall - ILL 7
Vercors side (WEST)

Neutron guide hall - ILL 7
Chartreuse side (EAST)
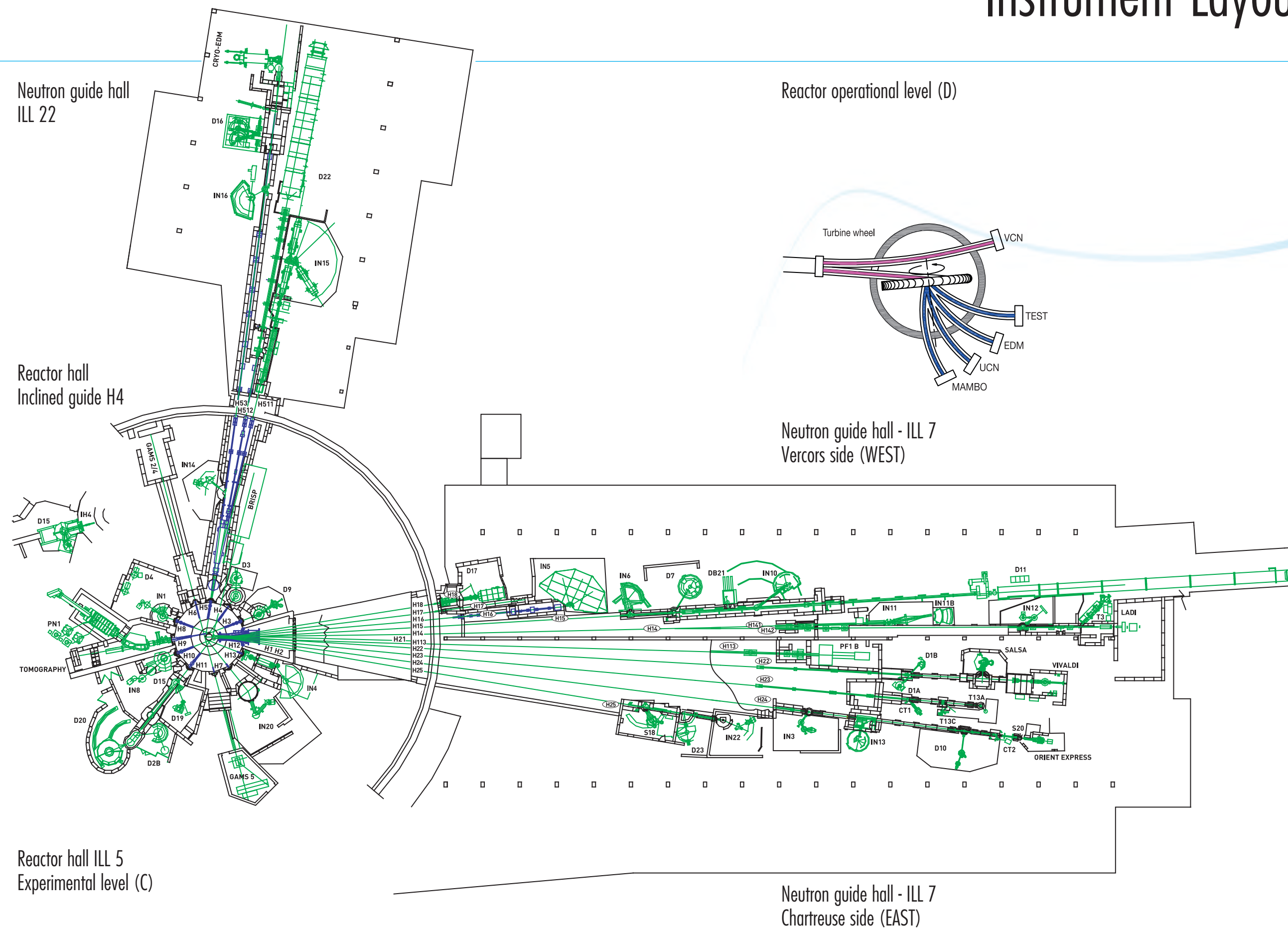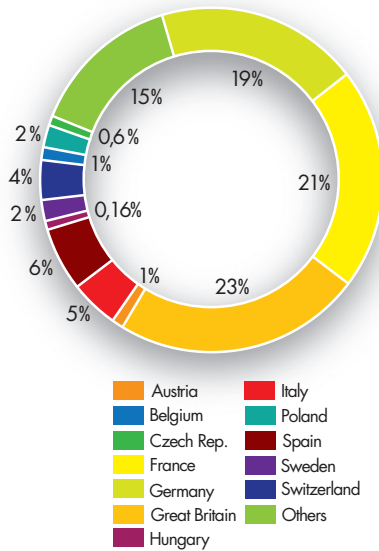
Figure 1: National affiliation of ILL users during 2007.

Legend:
- Austria
- Belgium
- Czech Rep.
- France
- Germany
- Great Britain
- Hungary
- Italy
- Poland
- Spain
- Sweden
- Switzerland
- Others

The ILL User Community

The ILL welcomed 1280 users in 2007, including 284 from France, 238 from Germany and 312 from the UK (*figure 1*). Many of our visitors were received more than once (for a total of 1944 visits).

We value feedback from our users as an indicator of how well our facility is fulfilling their needs and to initiate actions when this is not the case.

Instruments

The instrumental facilities at the ILL are shown in the schematic diagram on page 99.
Besides the 27 ILL instruments, there are 10 CRG-instruments, which are operated by external Collaborating Research Groups. There are currently three different categories of CRG instruments.

- CRG-A in which the external group leases an instrument owned by the ILL. They have 50% of the beamtime at their disposal and for the remaining 50% they support ILL's scientific user programme.
- The CRG-B category owns their instrument and retains 70% of the available beamtime, supporting the ILL programme for the other 30%.
- Finally, CRG-C instruments are used full time for specific research programmes by the external group, which has exclusive use of the beam.

DB21, LADI and IN15 have a special status, since they are joint ventures of the ILL with other laboratories: in the case of DB21 and LADI with EMBL and for IN15 with FZ Jülich and HMI Berlin.

The list of instruments as of December 2007 is summarised below (CRG instruments are marked with an asterisk *):
- powder diffractometers: D1A, D1B*, D2B, D20, SALSA
- liquids diffractometer: D4
- polarised neutron diffractometers: D3, D23*
- single-crystal diffractometers: D9, D10, D15*
- large scale structures diffractometers: D19, DB21, LADI, VIVALDI
- small angle scattering: D11, D22
- low momentum-transfer diffractometer: D16
- reflectometers: ADAM*, D17
- diffuse scattering and polarisation analysis spectrometer: D7
- three-axis spectrometers: IN1, IN3, IN8, IN12*, IN14, IN20, IN22*
- time-of-flight spectrometers: BRISP*, IN4, IN5, IN6,
- backscattering and spin-echo spectrometers: IN10, IN11, IN13*, IN15, IN16
- nuclear physics instruments: PN1, PN3, Cryo-EDM
- fundamental physics instruments: PF1, PF2

The interferometer S18 and Cryo-EDM are CRG-C instruments and are not available as a 'user' instrument. However, some beamtime on S18 is made available for prototype tests of USANS. Details of the instruments can be found on the web at http://www.ill.eu/instruments-support/instruments-groups/.
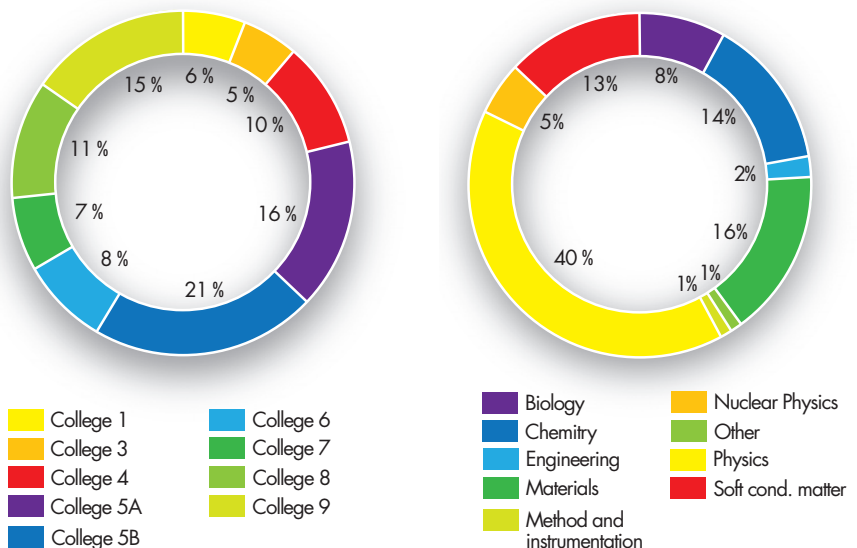
Figure 2: Beamtime allocation in 2007: distribution amongst the different research areas and colleges.

- College 1
- College 3
- College 4
- College 5A
- College 5B
- College 6
- College 7
- College 8
- College 9

- Biology
- Chemitry
- Engineering
- Materials
- Method and instrumentation
- Nuclear Physics
- Other
- Physics
- Soft cond. matter

Beamtime allocation & utilisation for 2007

Overall, the Subcommittees of the Scientific Council examined 1109 proposals requesting 8431 days for 2007, out of which 811 proposals received beamtime, allocating 4573 days of beamtime on the different instruments.

The distribution of beamtime for these experiments amongst the different research areas and colleges is shown in *figure 2*.

The distribution of beamtime requested and allocated amongst the different countries is shown in *Table 1*. In 2007, the member countries of the ILL were: France, Germany, UK, Austria, Belgium, the Czech Republic, Hungary, Italy, Poland, Spain, Sweden and Switzerland

In calculating the statistics of beamtime per country, shown in *Table 1a*, the attribution is based on the location of the laboratory of the proposers, not their individual nationality.

For a proposal involving laboratories from more than one member country, the total number of days is divided amongst the collaborating countries, and weighted by the number of people for each country. Local contacts are not counted as proposers except when they are members of the research team.

In *Table 1b*, the beamtime requested by and allocated to ILL, ESRF and EMBL is amongst the member countries according to their financial contributions to the institutes. In this same table, when a proposal involves collaboration with a non-member country, the allocated time is attributed entirely to the collaborating member country (or countries), and weighted by the number of people for each member country. Proposals for which all proposers are from non-member countries therefore do not appear in this table.

Table 1a: Distribution amongst the different countries of beamtime requested and allocated in 2007 during the Subcommittees of the Scientific Council.

Table 1b: Distribution amongst the Associate and scientific-member countries of beamtime requested and allocated in 2007 during the Subcommittees of the Scientific Council.
* Russia was member country only for the November 2006 round (allocation first two cycles in 2007).

All countries		Before national balance			After national balance	
Country	Requested days	Requested in %	Allocated days	Allocated in %	Allocated days	Allocated in %
AR	7.92	0.04	3.67	0.08	3.67	0.08
AT	39.13	0.46	25.71	0.53	25.71	0.54
AU	45.14	0.54	24.23	0.50	24.23	0.51
BE	44.07	0.52	25.28	0.52	25.28	0.53
BG	30.33	0.36	2.00	0.04	2.00	0.04
BR	9.10	0.11	3.10	0.06	3.10	0.06
BY	2.40	0.03	1.60	0.03	1.60	0.03
CA	20.30	0.24	14.80	0.30	14.80	0.31
CH	172.60	2.05	137.20	2.81	137.20	2.86
CN	10.02	0.12	6.27	0.13	6.27	0.13
CZ	37.94	0.45	36.19	0.74	36.19	0.75
DE	1168.58	13.86	649.60	13.30	659.27	13.75
DK	21.88	0.26	19.82	0.41	19.82	0.41
EG	7.50	0.09	0.00	0.00	0.00	0.00
EMBL*	17.00	0.20	12.40	0.25	12.40	0.26
ES	384.06	4.56	203.13	4.16	189.78	3.96
ESRF*	19.45	0.23	9.93	0.20	9.93	0.21
FI	5.00	0.06	4.30	0.09	4.30	0.09
FR	1317.06	15.62	756.91	15.50	764.51	15.94
GB	1750.00	20.76	1076.70	22.04	1080.90	22.54
GR	23.25	0.28	18.33	0.38	18.33	0.38
HU	29.42	0.35	8.75	0.18	8.75	0.18
IE	11.67	0.14	9.33	0.19	9.33	0.19
IL	4.76	0.06	6.19	0.13	6.19	0.13
ILL*	1330.87	15.78	818.58	16.76	817.66	17.05
IN	19.08	0.23	9.50	0.19	9.50	0.20
IT	486.57	5.77	241.97	4.95	207.75	4.33
JP	107.72	1.28	47.89	0.98	47.89	1.00
KR	3.97	0.05	1.97	0.04	1.97	0.04
LV	46.67	0.55	22.67	0.46	22.67	0.47
NL	35.17	0.42	22.00	0.45	22.00	0.46
NO	8.19	0.10	7.09	0.15	7.09	0.15
NZ	8.57	0.10	7.29	0.15	7.29	0.15
PL	146.02	1.73	65.17	1.33	67.17	1.40
PT	21.55	0.26	17.51	0.36	17.51	0.37
RO	14.00	0.17	0.00	0.00	0.00	0.00
RU	495.04	5.87	280.39	5.74	217.95	4.54
SA	1.00	0.01	0.50	0.01	0.50	0.01
SE	112.45	1.33	67.70	1.39	67.70	1.41
SG	0.86	0.01	0.86	0.02	0.86	0.02
TN	3.67	0.04	2.23	0.05	2.23	0.05
UA	29.07	0.34	14.53	0.30	14.53	0.30
US	372.18	4.41	197.87	4.05	198.87	4.15
ZA	10.33	0.12	3.50	0.07	3.50	0.07
Total	**8431.58**	**100.00**	**4884.67**	**100.00**	**4795.42**	**100.00**

* often in collaboration with other research groups

Member countries only				
Country	Requested days	Requested in %	Allocated days	Allocated in %
AT	67.96	0.83	43.44	0.91
BE	53.96	0.66	32.21	0.67
CH	245.37	2.99	186.21	3.90
CZ	53.58	0.65	48.81	1.02
DE	1778.49	21.68	1027.95	21.52
ES	485.04	5.91	269.38	5.64
FR	1942.56	23.69	1139.56	23.86
GB	2323.69	28.33	1428.32	29.90
HU	37.54	0.46	13.86	0.29
IT	598.02	7.29	288.59	6.04
PL	159.70	1.95	72.09	1.51
RUS*	324.55	3.96	144.75	3.03
SE	131.10	1.60	81.50	1.71
Total	**8201.58**	**100.00**	**4776.66**	**100.00**

Experimental and user programme
Beamtime allocation

A more complete view is given in **Table 2**. Request and allocation of beamtime – as well as the number of scheduled experiments – refer to standard submissions to the subcommittee meetings. The effective number of days given to our users takes into account also Director's Discretion Time (DDT) and CRG time for CRG instruments.

The instruments D4 and IN1 share a beam. Note that PF2 consisted of 4 different set-ups (MAM, TES, UCN, VCN) allowing several experiments to run simultaneously. Normally, for official statistics the total number of days requested and allocated is averaged by a factor 4.

Instrument	Requested days	Allocated days*	Number of scheduled experiments	Days available **	Days used for users***	Days lost	Days for commissioning /test/training	Days for internal research	EASY (hours
ADAM	101	55	10	180	180	0	0	0	-
BRISP	84	20	2	180	150	2	25	3	-
D10	267	173	24	180	160	4	10	6	-
D11	268	146	68	180	145	7	26	2	-
D15	11	54	8	180	141	6	19	14	-
D16	127	104	17	154	90	42	12	10	-
D17	310	150	44	180	141	4	28	7	-
D19	117	93	13	180	70	53	57	0	-
D1A	87	100	36	180	127	2	10	41	24
D1B	154	91	33	180	169	2	3	6	-
D20	297	120	55	180	152	5	11	12	-
D22	472	144	54	180	135	10	30	5	-
D23	108	67	8	180	158	12	10	0	-
D2B	277	138	66	180	150	2	19	9	27
D3	280	146	16	180	145	7	18	10	-
D4	179	73	20	105	74	19	12	0	-
D7	302	162	27	180	140	3	35	2	-
D9	297	125	17	180	126	20	28	6	-
DB21	14	14	1	35	3	9	23	0	-
IN1	123	60	10	78	62	9	7	0	-
IN10	155	153	20	180	129	1	26	24	-
IN11	277	145	18	180	140	11	20	9	-
IN12	68	39	6	180	166	6	8	0	-
IN13	211	79	13	180	137	6	14	23	-
IN14	253	151	20	180	140	21	9	10	-
IN15	112	67	9	180	137	16	27	0	-
IN16	422	150	28	180	150	8	16	6	-
IN20	183	145	19	180	138	14	19	9	-
IN22	108	58	8	180	170	5	5	0	-
IN4	180	129	26	180	111	18	28	23	-
IN5	352	154	39	180	166	3	7	4	-
IN6	253	149	33	180	161	3	13	3	-
IN8	183	137	20	180	133	2	39	6	-
LADI	123	99	11	180	41	2	113	24	-
PF1B	449	250	6	180	144	0	36	0	-
PF2/4****	245	194	8	210	151	0	35	24	-
PN1	274	56	10	180	111	34	35	0	-
PN3	345	114	9	180	72	28	60	0	-
SALSA	180	140	31	180	128	8	21	23	-
VIVALDI	148	129	30	180	138	17	22	3	-
Total (days)	**8431**	**4573**	**893**	**6862**	**5181**	**421**	**936**	**324**	
Percentage of the total available beamtime				**75%**	**6%**	**14%**	**5%**		

Table 2: Beamtime request/allocation by instrument. CRG instruments are in blue.

* 'days allocated' refers to only those days reviewed by the subcommittees (i.e., excluding CRG time for CRGs)

** 'available days' refers to the days of reactor operation in 2007 (see p.207)

*** 'days used' refers to the total number of days delivered to users (i.e., including CRG days for CRGs and DDT)

***** PF2 consists of 4 different set-ups where several experiments are running simultaneously

Instrument performances

NEUTRONS
FOR SCIENCE

Instrument performance

Table 2 also gives a summary of instrument performance for 2007. For each cycle, a record is kept of any time lost from the total available beamtime and the reasons for the lost time are analysed for all the instruments. The table gives a global summary for the year.

Overall 5181 days were made available to our users in 2007 on ILL and CRG instruments, which represents about 75% of the total days of operation. 324 days were used by ILL scientists to carry out their own scientific research. About 14% of the total beamtime available on the ILL instruments is allowed for tests, calibrations, scheduling flexibility, recuperation of minor breakdowns. Beam days delivered for science in 2007 amount to 5505 (used for users or for internal research).

A total of 893 experiments were scheduled. During 2007 the reactor operated for 4.0 cycles, representing 180 effective days of neutrons because of various minor reactor shut-downs (*see § Reactor Operation, p.207*).

In 2007, 421 out of 6862 days were lost due to various malfunctions, which represent about 6% of the total available beamtime. The breakdown by reasons for beamtime losses is shown in **figure 4**.

Use of ILL beamtime

- Users
- Losses
- Test/Commissioning
- Internal time

Reasons for beamtime losses
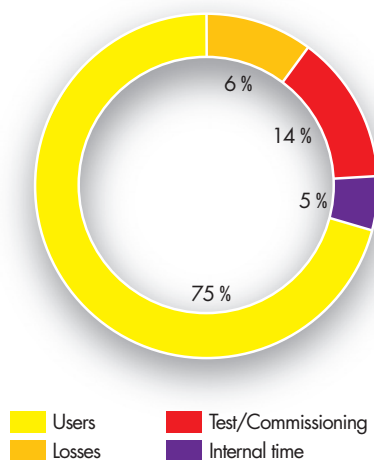
- Sample Env.
- Electrical
- Computing
- Detectors
- Mechanical
- Users
- Others
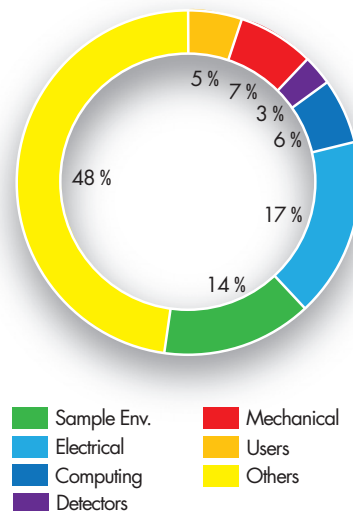
Detailed comments on the larger beamtime losses (20 days or more) are as follows:

- D19 lost one cycle because of major problems with the monochromator;
- D16 restart had to be postponed because of the planning of major works of neighbouring instruments;
- IN14 lost nine days for various crashes of VME electronics and suffered from other minor breakdowns;
- PN1 lost two weeks because of a failure of new high tension generators.
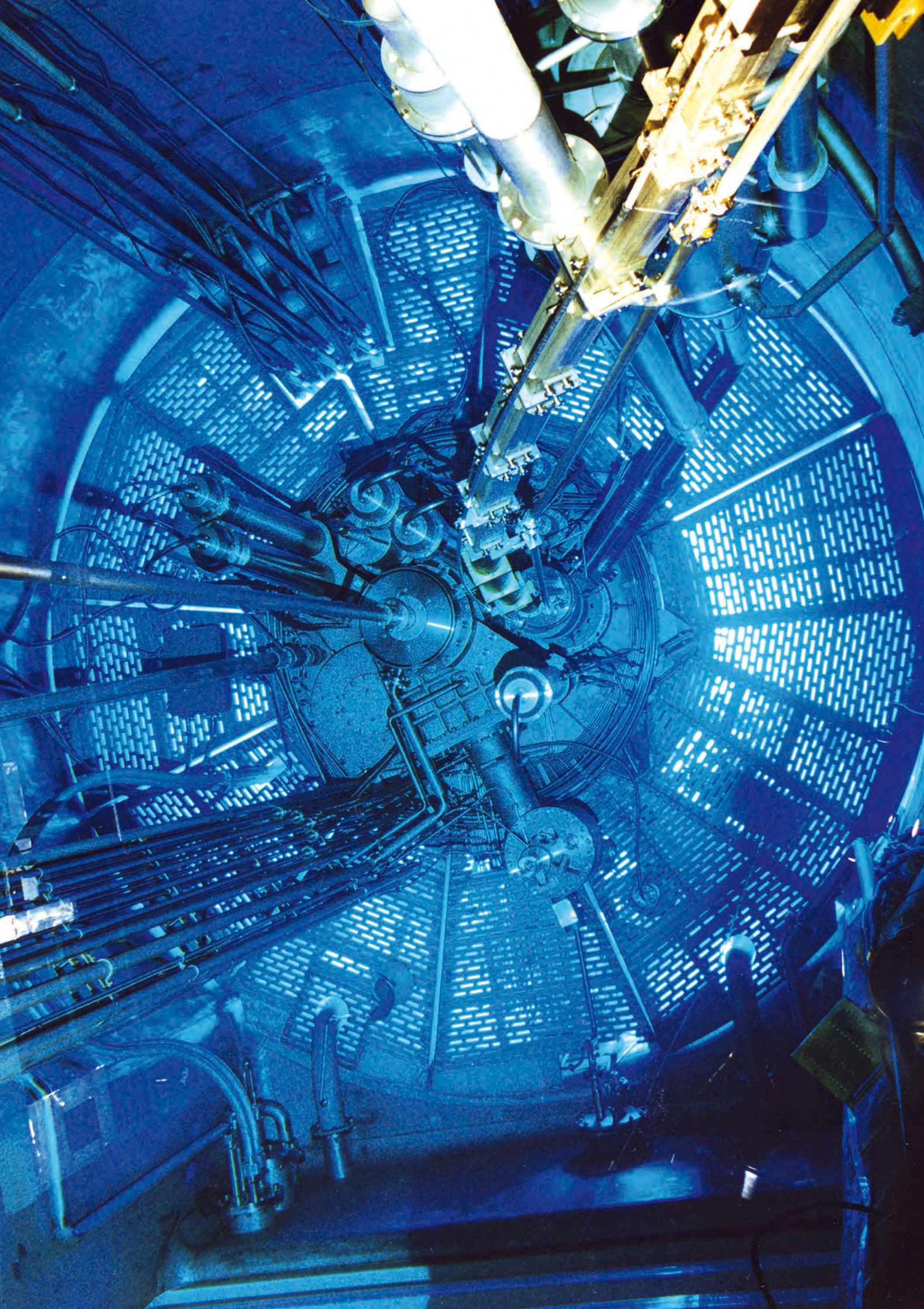
Reactor operation

The ILL's neutrons are generated by its high-flux reactor

The ILL's reactor produces the most intense neutron flux in the world
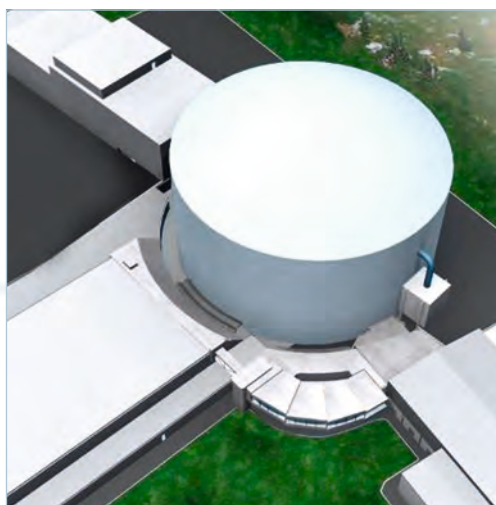
This reactor was refurbished between 1993 and 1995 and produces the most intense neutron flux in the world: 1.5×10^{15} neutrons per second per cm^2, with a thermal power of 58.3 MW.

The reactor operates 50-day cycles, with each cycle of operation followed by a shutdown period during which the fuel element is changed and a number of checks are carried out. Occasional longer shutdowns allow for equipment maintenance.
There are normally 4 reactor cycles per year, supplying 200 days of neutron flux for scientific use.

As part of the ILL's determination to guarantee the safety and reliability of its facilities over future years, the Reactor Division runs a 'key reactor components programme', the aim of which is to ensure the development and replacement as necessary of the essential main components of the reactor. The current plans under this programme cover the period up to 2016.
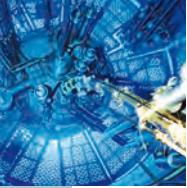
The four reactor cycles scheduled in 2007 provided for 184 days of scientific activity. Whilst the first two cycles ran perfectly, fission gas levels rose unacceptably during the third cycle. The reactor was therefore shut down and the fuel element removed. This resulted in a 24% loss in capacity. The fourth cycle was also interrupted on three occasions, following problems with the silt content of the water from the Drac river. Studies are now being conducted on the reasons for this change in water quality. The fourth cycle was extended by 2 days to compensate for the stoppages.

Cycle no.	Start of cycle	End of cycle	Actual operating days/Scheduled days	Equivalent Full Power Days scheduled	Unscheduled shutdowns
146	20.02.07	11.04.07	50/50	46.2/46.6	0
147	24.04.07	13.06.07	50/50	45.9/45.6	0
148	28.08.07	05.10.07	36.5/50	32/45.6	1
149	30.10.07	21.12.07	47.5/50	43.6/45.6	3
TOTAL			**184/200 (92%)**	**168/182**	**4**

Figure 1: View of the separation between the reactor building and one of the guide halls.

The end of the Refit Programme

Following the safety authorities' 10-year safety review of the high-flux reactor in May 2002, the ILL set out on a wide-ranging programme to upgrade and reinforce its nuclear installations. One of the main aims of this Refit Programme was the guarantee of compliance with recent changes in seismic regulations.

As a consequence between 2002 and 2007 a huge amount of renovation work was accomplished, particularly with regard to the ILL's ability to withstand an earthquake.
This included a major reinforcement of the reactor building and the associated facilities:

- new operational and command-control systems to ensure reactor shutdown in the event of an earthquake
- a new water circuit to feed the reactor tank and canal, now considered leak-tight in the event of an earthquake
- the removal of 1500 tons of concrete structures within the reactor building
- the separation from the reactor of the guide halls and the reinforcement of the main office building (**see figure 1**)
- new spent fuel racks
- the non-destructive examination of the heavy water pipe welds (with no signs of defect or ageing detected).

The Refit is now practically completed and the final review was held at the ILL on 11 October 2007. Ten ILL members of staff were affected to the programme and ten others were involved from external companies; the final budget, including these staff costs, turned out at approximately 30M€. Congratulations to all those who contributed so efficiently to a particularly delicate exercise, which should now ensure that the ILL is safe to operate until the year 2030.

Apart from the Refit work the main operations accomplished in 2007 were the following :

- comprehensive maintenance programme to guarantee the reliability and availability of the reactor
- preparation of the transfer of environmental monitoring activities to the ILL
- key Reactor Components Programme:
  - new 20kV electricity supply
  - ultrasonic testing of the primary circuit pipes
  - reinforcement of the emergency water circuits
  - renewal of the control of the nuclear ventilation
  - new up-to-date nucleonic studies…

ILL operations in 2007 generated waste and effluents within the regulatory limits applicable to our installation:

Evacuation of radioactive waste	Quantity
Decay bin (60 l)*	0
5 m³ pre-concreted crate (low and intermediate level waste)	0
5 m³ crate (low and intermediate level waste)	3
200 l drums of incineratable low-level waste	40
HDPE drums 120 l (low-level waste)	39

Waste stocked in these decay bins is still quite active and requires several years of interim storage before meeting ANDRA's specifications for processing as intermediate-level waste.

Gaseous effluents	Released in 2007
Rare gas (TBq)	1.1
Tritium (TBq)	11
Gaseous halogen and aerosols (TBq)	0.000017

Liquid effluents	Released in 2007
Activation products, except tritium (GBq)	0.48
Tritium (TBq)	0.53

The reactor chimney resistance in case of seism was also tested.

ILL Chronicle 2007

Founded on 19 January 1967 by the signing of a convention between the governments of the French Republic and the Federal Republic of Germany, the ILL celebrates its 40th anniversary.	**17 January**
Meeting of an instrument subcommittee to discuss the proposed high flux diffractometer DRACULA.	**1 February**
Meeting of an instrument subcommittee to discuss the status of the IN16B project.	**2 February**
Outdoor meeting of ILL management and ILL's Heads of Service.	**9 February**
Science on Stage Festival.	**2-6 April**
ILL and ESRF welcome Commissioner Janez Potočnik.	**5 April**
ILL PhD students Clip session.	**13 April**
Arrival of Oliver Zimmer to succeed Hans Börner as the new Head of Nuclear and Particle Physics group.	**15 April**
Meeting of the ILL Scientific Council and its Subcommittees.	**17-20 April**
Meeting of the Subcommittee on Administrative Questions (SAQ).	**26-27 April**
Meeting of the Steering Committee.	**14-15 June**
ILL invites its staff members and their families to an Open Day.	**16 June**
Signing of the new contract between the Swedish Research Council and the ILL.	**1 July**
Kick-off of the second phase ('M1') of the ILL Millennium Programme.	**10 July**
A symposium marks the retirement of Hans Börner, Nuclear and Particle Physics group leader.	**27 August**
Visit of Mr Pascal Couchepin, Vice-president of the Swiss Confederation and Head of the Federal Department of Home Affairs.	**10 September**
Visit of the Audit Commission.	**10-14 September**
Following a leak on the helium circuit of the cold source's compressor, the reactor was automatically shut down. It was restarted on 13 September.	**12 September**
Christian Vettier leaves the ILL after 8 years as the Head of Science Division.	**20 September**
Outdoor meeting of ILL management and ILL's Heads of Service.	**21 September**
Welcome to Dr. José Luis Martinez, new Deputy Director and Head of the Project and Techniques Division. Andrew Harrison becomes the new Head of Science Division.	**1 October**
First meeting of the newly installed Project Management Committee for a discussion of the new instrument and infrastructure projects of the M1 phase.	**1 October**
The reactor had to be shut down 12 days before schedule due to a minor defect in the fuel element.	**5 October**
French Science Festival week: the ILL and the ESRF manned a common exhibition stand in the centre of Grenoble.	**5-7 October**
Final Groupe Permanent visit.	**11 October**
Meeting of experts on small-angle neutron scattering to discuss the design of ILL's 3rd SANS instrument D33.	**19 October**
Meeting of the Subcommittee on Administrative Questions (SAQ).	**25-26 October**
Meeting of the ILL Scientific Council and its Subcommittees.	**6-9 November**
A workshop is organised in Madrid to celebrate the 20th Anniversary of Spain becoming a scientific member of the ILL.	**28 November**
Meeting of the Steering Committee.	**29-30 November**
NOMAD review.	**12-13 December**

Workshops and events

Workshops in which ILL was a major player in 2007

Celebration of the ILL's 40th anniversary (17 January)

40 YEARS JAHRE ANS

NEUTRONS FOR SCIENCE

International Workshop on Advanced Laue Diffraction (23-27 January)
M.H. Lemée-Cailleau and G. McIntyre (ILL),
D. Bourgeois (IBS), A. Cousson (LLB) and Q. Kong (ESRF)

International Workshop on Dynamics of Molecules and Materials (31 January - 2 February)
A. Ivanov and M. Johnson (ILL), S. Parker (ISIS)

Science on Stage 2 (2-6 April)
ILL and ESRF communication teams

D7 Millennium project meeting (26-27 April)
P. Deen, A. Murani, R. Stewart and K. Andersen (ILL)

4th Italian Neutron School of the Italian Society of Neutron Spectroscopy (14-17 September)

Celebration of ILL's 40th anniversary (17 January)

The ILL has firmly established itself as a pioneer in neutron science. This year the Institute celebrated its 40th anniversary and yet remains in the prime of youth! With its 40 years of experience the Institute can boast not only a most successful past but also the prospect of a splendid future. A lot has happened at the ILL since the 10-year Millennium Programme was first launched in 2001. The result is that our instruments can deliver eight times as much high-quality data as they did in 1999. Today, our principal ambition is to keep the ILL at the forefront of neutron science for the next 15 years.

The celebration of ILL's 40th anniversary, held on 17 January, was attended by more than 500 people, among whom we were pleased to welcome 160 external guests and 90 former employees of the Institute. Judging by the positive feedback we received from many external guests and the positive press coverage, the event can be considered as a great success for the ILL.

International Workshop on Advanced Laue Diffraction

LAUE 2007 was attended by about 90 scientists from all over the world. The aim of the workshop was to offer to a very diverse community of scientists, state-of-the-art experimental methods and hands-on experience of data-analysis for exploration, using single-crystal Laue diffraction, of the crystalline structure of complex materials in extreme cases. Examples of these are very small samples (biological materials, complex chemical structures…), radiation-sensitive samples, extreme conditions (very low temperatures, very high pressure), and time-resolved studies up to the femtosecond limit. This workshop provided the occasion to create a new community of scientists bringing together the various neutron and X-ray groups working with Laue diffraction. The success of this workshop can be judged by the unanimous desire for a follow-up workshop in 2009, most likely to be organised in Chicago.

http://www.ill.fr/fileadmin/users_files/Other_Sites/laue2007/Laue2007.html

Second edition of Science on Stage

A society which claims to be a leader in today's world must be equipped with leaders in science. The ILL and ESRF successfully organised the second edition of the 'Science on Stage' festival, which gathered about 500 science teachers from 27 European countries.
Science on Stage is organised by the seven members of the EIROforum (see p.116) with the goal of stimulating young people's awareness of and interest in science and technology, by increasing the quality and attractiveness of science lessons in school. The festival programme offered teachers a unique opportunity to exchange teaching materials and ideas, through the combination of a science teaching fair, on-stage activities and parallel sessions.
This year for the first time the festival programme included a Round Table discussion on 'Euopean science education in the age of the knowledged society'. Amonsgt the participants of the round table, we were honoured to welcome M. Janez Potočnik (European Commissioner for Science and Research) and M. Vittorio Prodi (European Parliament).

http://www.ill.fr/fileadmin/users_files/Other_Sites/scienceonstage2007/index.html

International Workshop on Dynamics of Molecules and Materials

The DMM2007 workshop – jointly organised by the ILL and ISIS, and attended by more than 75 scientists – aimed to highlight the experimental facilities and computational resources existing for the study of the dynamics of atomic groups or molecules that compose materials. This is key information for the understanding and, ultimately, controlling atomic bonding and properties of condensed matter. The important outcome of this successful event was a clear message from the user community that the efforts on developments and improvement of the experimental base for neutron research should be continued and accented. Ongoing development and modernisation of existing instruments (such as TOSCA at ISIS, VISION at SNS, IN1- BeFilter at ILL) were strongly supported during the workshop's round table.

http://www.ill.fr/news-events/events/past-events/dmm/

D7 Millennium project meeting (26-27 April)

The aim of the workshop was to celebrate the completion of the upgrade of the D7 diffuse scattering spectrometer as part of the ILL Millennium Programme. As a result of this upgrade, D7 is now 90 times more sensitive than it was in 2001. We were very fortunate to have amongst us around 35 users from both past and present to encourage the users of the future. Our honoured speaker was Otto Schärpf, builder of the original polarised D7, and chief architect of the methodology of polarisation analysis on multi-detector instruments using XYZ polarisation analysis.

The workshop was enthusiastically received by both the former and current user community. The unique possibilities afforded by the new D7 – to measure both static and dynamic magnetic short-range correlations with full polarisation analysis on a multi-detector spectrometer – were highlighted during the meeting. The variety and quality of the science presented bodes well for the future of D7 which, with almost 2 orders of magnitude increase in count-rate, has now come of age.

http://www.ill.fr/fileadmin/users_files/Other_Sites/D7/D7%20workshop/Home.html

4th Italian Neutron School of the Italian Society of Neutron Spectroscopy

The 4th edition of the Italian Neutron School, organised by the Italian Society of Neutron Spectroscopy (SISN) focused this year on Inelastic Neutron Scattering in Liquids and Disordered Systems. The school combined a theoretical session (from 10 to 12 September in Sestri Levante, Italy) and an experimental session (from 14 to 20 September at the ILL). The practical session at the ILL was attended by 20 Italian students, who were split up between 3 different instruments, the two Italian CRGs, IN13 and BRISP, together with the test triple-axis instrument IN3. They were able to perform real experiments and discover the beauty of neutron spectroscopy, which the theoretical session in Sestri Levante had previously encouraged. The enthusiastic young experimenters spent night and day both measuring spectra on the instruments and making data analysis. The outcome of their thoughtful work was presented at a conclusive seminar session.

The celebration of the 40th anniversary of the ILL (17 January).

Visit of the Commissioner Janez Potočnik (5 April).

Visit of the Vice-President of the
Swiss Confederation (10 September).

The Refit Management Committee (RMC) team.

Celebration of the 20th anniversary of Spain's partnership.

1, 2, 3: Christian Vettier leaves the ILL after eight years as the Head of the Science Division.

Open day

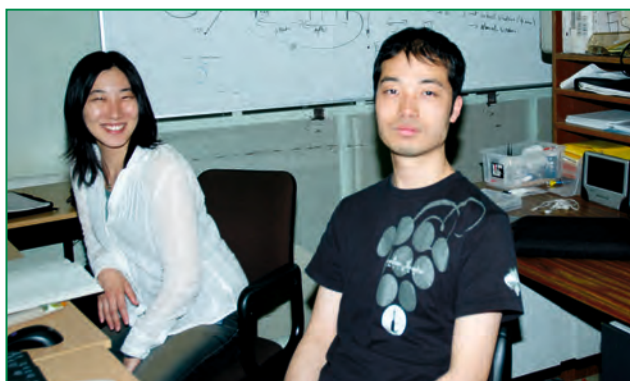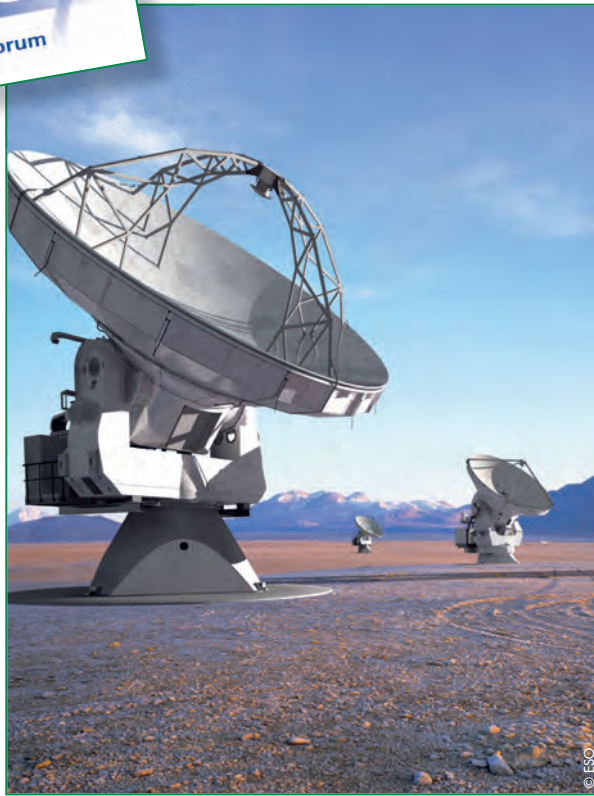## French science festival

Open day / French science festival
Happy users at ILL

Happy users at ILL

EIROforum: serving European science

Science is a team effort and to progress, it often needs special and large facilities, some of which require resources beyond the means of any single country. Europe has a great history of scientific endeavour, and since the early 1950s, a number of intergovernmental research organisations have been established to fulfil the needs of Europe's scientists.

EIROforum (*http://www.eiroforum.org/*) is a partnership of Europe's seven largest intergovernmental research organisations, and the ILL is one of them.

The seven EIROforum members are:

CERN - European Organisation for Nuclear Research
EFDA - European Fusion Development Agreement
EMBL - European Molecular Biology Laboratory
ESA - European Space Agency
ESO - European Southern Observatory
ESRF - European Synchrotron Radiation Facility
ILL - Institut Laue-Langevin

In EIROforum, these organisations pursue joint initiatives, combine resources, and share best practices. Collaboration between the seven members is contributing positively to the development of the European Research Area. Joint initiatives have already resulted in an important impact in the areas of Outreach and Education.

Another important achievement, is the publishing (4 times a year) of the European journal Science in School (*http://www.scienceinschool.org/*), which promotes inspiring science teaching.
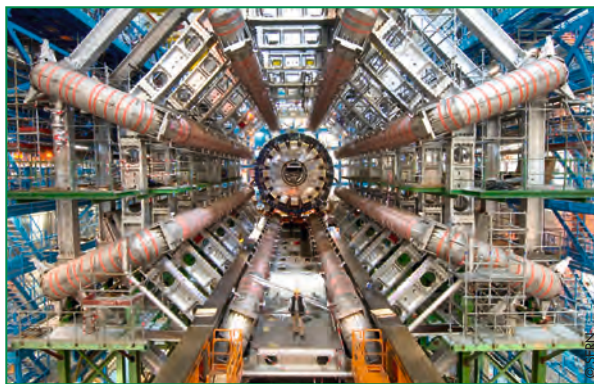
Science on Stage

In the framework of EIROforum, the ESRF and the ILL jointly organised this year the second edition of the Science on Stage festival (http://www.scienceonstage.net/).
Science on Stage involve thousands of European science teachers in a joint effort to raise interest in science and technology studies.

This second edition was held in Grenoble (2-7 April 2007) and gathered about 500 science teachers from 27 European countries who took part in this unique European event, which showcased the very best of today's science education and very inspiring experiments.
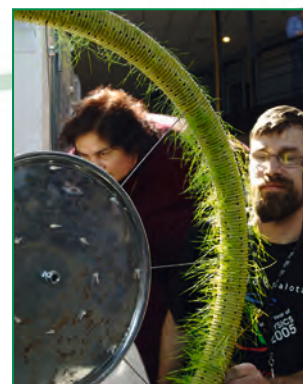
8 Administrative matters

Human Resources

For the Human Resources Service, 2007 was a year of intense collective bargaining and was also marked by the introduction of new electronic workflow applications. During the course of the year, three important agreements were signed with the trade unions.

Firstly, the new early retirement conditions negotiated for shift workers will provide a more equitable solution for the different categories of staff involved and will protect the Institute from financial risk. The second agreement was negotiated in response to new legislation on supplementary health insurance. As of 2008 subscription to ILL's health insurance scheme will be compulsory for all staff, allowing the Institute to benefit from an exemption to certain social security contributions. The third agreement covers the ILL's time-saving accounts. It will improve the management of the time saved on these accounts and reduce the associated financial risks.

The new workflow applications introduced in 2007 will help to streamline the management of staff travel and staff absences. The new systems should speed up the reimbursement of travel expenses and simplify the administrative procedures involved in the authorisation and recording of staff absences.

Major efforts were also made in 2007 to improve the balance of nationalities in the workforce. This included a recruitment drive abroad and the stepping-up of language training, following the introduction of the new ILL language policy encouraging the use of English as ILL's preferred working language.

Finally, a timetable was drawn up at the end of the year for the renegotiation in 2008 of some points of the ILL Collective Agreement. The aim is to provide the ILL with a modern collective agreement in line with the expectations and image of a world-leading international research institute.

Finance and Purchasing

On 1st July 2007 the Purchasing Service was merged with the Economic and Financial Service (which already managed some of ILL's commercial transactions). The new Finance and Purchasing Service thus created will provide a more efficient service to ILL's staff and users, and will facilitate relations with suppliers.

Prior to this merger, the ILL and ESRF stores also merged to form a joint stores on 1st February 2007. The new structure now offers a more economic procurement, a wider range of stock to the staff of both institutes and a more efficient delivery system for users.

The Finance team had to deal with a number of major challenges in 2007: the introduction of new accounting procedures for the recording for fixed assets, the implementation of new financial and procurement software, and in particular changes to ILL's auditing procedures, with the decision to bring in the firm KPMG as external auditors to assist with the audit of the 2007 accounts. The service also assisted with the inventory of the nuclear installations and the operation to re-evaluate the cost of decommissioning. The service's Customs group was also strengthened in 2007.

As part of a drive to improve competitivity in purchasing and ensure that the Institute has access to the best commercial offers available, the Purchasing team undertook an overhaul of the ILL's purchase procedures. Staff are also working to improve the distribution of procurement and the associated economic benefits across the ILL member countries.

The ILL continues to cooperate closely with the ESRF on purchasing matters. For instance, the two institutes returned to a regulated price for electricity in 2007, a move which has generated considerable savings.

In 2007 the main fuel cycle contracts were renegotiated with the traditional suppliers (AREVA TN and CERCA). New agreements were also signed, with ANDRA in particular, in the framework of the CEA Grenoble's denuclearisation operation.

Building and Site Maintenance

In 2007 the Building and Site Maintenance Service was involved in a number of major projects. Most noteworthy were the civil engineering work required for the installation of the instrument FIGARO and the beamline exit port for GRANIT, the biological shielding of instruments D11 and D16B, the installation of the new neutron guides H113 and H17, the launch of the work on the ILL 7-ILL 22 liaison building, the implementation of the third phase of the seismic refit programme, the refurbishment of the grounds in front of the ILL office building, and the start of work to create a Controlled Area (for radiation protection purposes) in the experimental halls ILL 7 and ILL 22.

Translation

The translation office continues to translate a wide variety of documents into and out of the Institute's three official languages – English, French and German. The office's work includes the translation of technical specifications, safety notices and presentations, employment contracts, vacancy notices, financial documents, and administrative notes, as well as brochures and leaflets aimed at the general public. Major annual projects include the translation of preparatory documents for meetings of the ILL's statutory bodies (SAQ, Steering Committee and Audit Commission) and the provision of interpreting services for these meetings. The office is also asked to proofread scientific papers prior to their submission for publication.

Administrative matters

Administration Division

The ILL's Administration Division comprises three separate services covering the following areas: human resources, finance and purchasing, and building and site maintenance.

The division also provides translation services and administrative and legal support. Steps are currently being taken throughout the division to improve task and personnel management through the creation of a quality-oriented culture.
This includes the introduction of IT-based information systems and tools to streamline administrative controls and procedures.
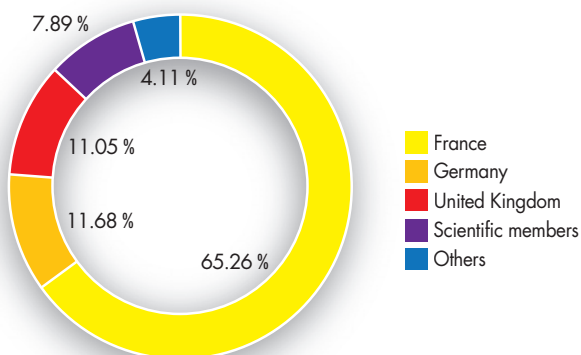
Staff

- 475 people including 67 experimentalists in the scientific sector and 22.5 thesis students.
- 310 French, 55.5 German, 52.5 British, 37.5 Scientific member countries and 19.5 others

Staff numbers on 31/12/07		%
France	310	65.26
Germany	55.5	11.68
United Kingdom	52.5	11.05
Scientific members	37.5	7.89
Other	19.5	4.11
Total	**475**	**100**

7.89 %
4.11 %
11.05 %
11.68 %
65.26 %

- France
- Germany
- United Kingdom
- Scientific members
- Others

Budget 2007 (excluding taxes)

Income	M€	%
Income from Associates	58.5	79.05
Income from Scientific members	13.3	17.97
Own income	2.2	2.97
Total	**74**	**100**
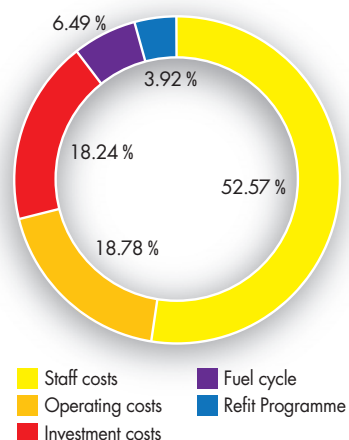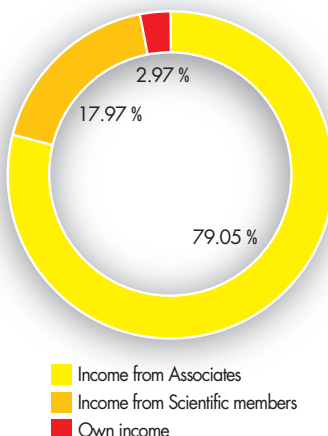
Expenditure	M€	%
Staff cost	38.9	52.57
Operating cost	13.9	18.78
Investment cost	13.5	18.24
Fuel cycle	4.8	6.49
Refit Programme	2.9	3.92
Total	**74**	**100**

2.97 %
17.97 %
79.05 %

- Income from Associates
- Income from Scientific members
- Own income

6.49 %
3.92 %
18.24 %
18.78 %
52.57 %

- Staff costs
- Operating costs
- Investment costs
- Fuel cycle
- Refit Programme

Distribution of ILL purchases
(excluding taxes)

Purchases	M€	%
France	19.8	78.23
Germany	2.28	9.01
United Kingdom	1.05	4.15
Scientific members	0.66	2.61
Other	1.52	6.01
Total	**25,31**	**100**

2.61 %
6.01 %
4.15 %
9.01 %
78.23 %

- France
- Germany
- United Kingdom
- Scientific members
- Others
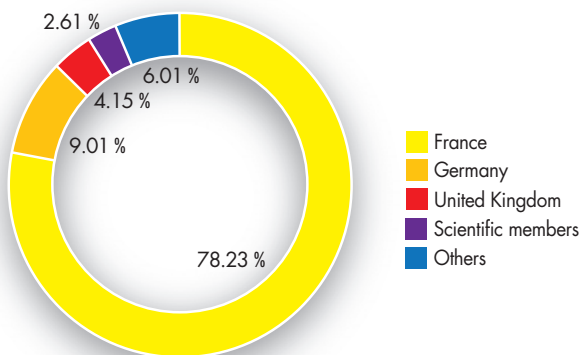
Facts and figures

Name
Institut Max von Laue - Paul Langevin (ILL)

Founded
17 January 1967. International Convention (renewal)
signed until 31 December 2013.

Associates
France
Commissariat à l'Energie Atomique (CEA)
Centre National de la Recherche Scientifique (CNRS)

Germany
Forschungszentrum Jülich (FZJ)

United Kingdom
Science & Technology Facilities
Council (STFC)

Countries with Scientific membership

Spain
Ministerio de Educación y Ciencia (MEC)

Switzerland
Bundesamt für Bildung und Wissenschaft

Italy
Istituto Nazionale per la Fisica della Materia (INFM)
Consiglio Nazionale delle Ricerche (CNR)

CENI (Central European Neutron Initiative)
Consortium, composed of:
 - Austria: Österreichische Akademie der
 Wissenschaften
 - Czech Republic: Charles University of Prague

Hungary
Research Institute for Solid State Physics and Optics
affiliated to the Budapest Neutron Centre (BNC-RISP)

Sweden
Swedish Research Council (SRC)

Belgium
Belgian Federal Science Policy Office (BELSPO)

Poland
The Henryk Niewodniczański Institute of Nuclear
Physics (Polish Academy of Sciences)

**Supervisory
and Advisory Bodies**

- Steering Committee, meeting twice a year
- Subcommittee on Administrative Questions,
 meeting twice a year
- Audit Commission, meeting once a year
- Scientific Council with 9 Subcommittees,
 meeting twice a year

Reactor
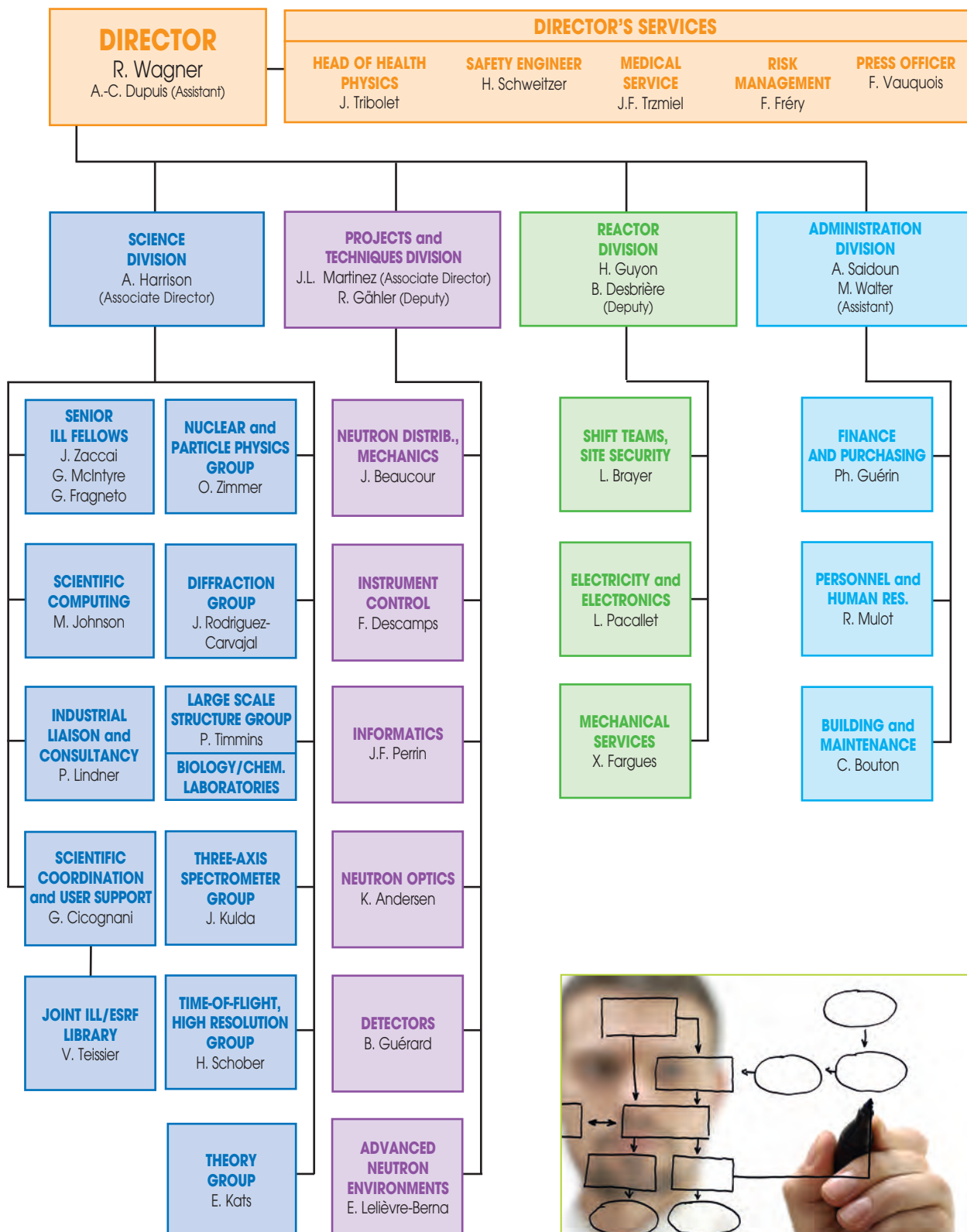- 58 MW, running 4 cycles in 2007
 (with cycles of 50 days)

Experimental Programme
- 893 experiments (allocated by subcommittees)
 on 27 ILL-funded and 10 CRG instruments
- 1280 visitors coming from 36 countries
- 1109 proposals submitted and 811 accepted

9

Organisation chart - December 2007

DIRECTOR	DIRECTOR'S SERVICES				
DIRECTOR R. Wagner A.-C. Dupuis (Assistant)	**HEAD OF HEALTH PHYSICS** J. Tribolet	**SAFETY ENGINEER** H. Schweitzer	**MEDICAL SERVICE** J.F. Trzmiel	**RISK MANAGEMENT** F. Fréry	**PRESS OFFICER** F. Vauquois

SCIENCE DIVISION
A. Harrison
(Associate Director)

PROJECTS and TECHNIQUES DIVISION
J.L. Martinez (Associate Director)
R. Gähler (Deputy)

REACTOR DIVISION
H. Guyon
B. Desbrière
(Deputy)

ADMINISTRATION DIVISION
A. Saidoun
M. Walter
(Assistant)

SENIOR ILL FELLOWS
J. Zaccai
G. McIntyre
G. Fragneto

NUCLEAR and PARTICLE PHYSICS GROUP
O. Zimmer

NEUTRON DISTRIB., MECHANICS
J. Beaucour

SHIFT TEAMS, SITE SECURITY
L. Brayer

FINANCE AND PURCHASING
Ph. Guérin

SCIENTIFIC COMPUTING
M. Johnson

DIFFRACTION GROUP
J. Rodriguez-Carvajal

INSTRUMENT CONTROL
F. Descamps

ELECTRICITY and ELECTRONICS
L. Pacallet

PERSONNEL and HUMAN RES.
R. Mulot

INDUSTRIAL LIAISON and CONSULTANCY
P. Lindner

LARGE SCALE STRUCTURE GROUP
P. Timmins

BIOLOGY/CHEM. LABORATORIES

INFORMATICS
J.F. Perrin

MECHANICAL SERVICES
X. Fargues

BUILDING and MAINTENANCE
C. Bouton

SCIENTIFIC COORDINATION and USER SUPPORT
G. Cicognani

THREE-AXIS SPECTROMETER GROUP
J. Kulda

NEUTRON OPTICS
K. Andersen

JOINT ILL/ESRF LIBRARY
V. Teissier

TIME-OF-FLIGHT, HIGH RESOLUTION GROUP
H. Schober

DETECTORS
B. Guérard

THEORY GROUP
E. Kats

ADVANCED NEUTRON ENVIRONMENTS
E. Lelièvre-Berna

Facts and figures

Publications

**In 2007,
the ILL received notice of
562 publications by ILL staff
and users**

**The distribution
by subject is as follows:**

Applied physics, instrumentation and techniques	41
Theory	22
Nuclear and particle physics	41
Magnetic excitations	65
Crystallography	63
Magnetic structures	106
Liquids and glasses	75
Chemistry	51
Biology	37
Soft matter	61

Books

I.N. Serdyuk, N.R. Zaccai and J. Zaccai,
'Methods in molecular biophysics',
Cambridge University Press
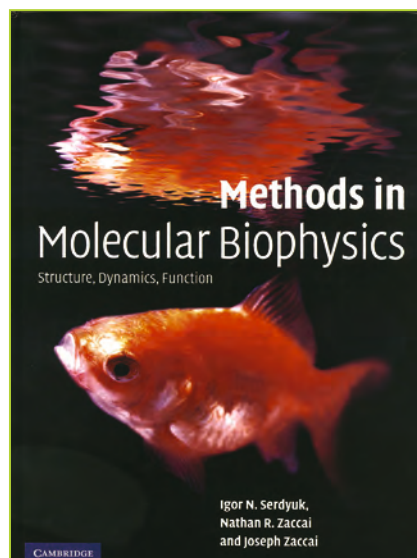
2007

ANNUAL REPORT 40th ANNIVERSARY - 1967/2007

40